Cost of energy optimisation of offshore wind turbine PMG drive trains based on uncertainty

Kerri Hart

A thesis submitted for the degree of Doctor of Philosophy

Centre for Doctoral Training in Wind Energy Systems
Department of Electronic and Electrical Engineering
University of Strathclyde

2019

Abstract

Offshore wind is a constantly evolving industry as the demand for clean renewable sources of energy continues to grow globally. The cost of energy (COE) is measure of the cost per unit of energy supplied by a provider over the lifetime of a project. Methods in which to reduce this cost are always a priority for parties involved in the design, installation and operation of a wind farm. This thesis explores the contribution of wind turbine drive train design and optimisation in the reduction of COE whilst providing a review of the most sensitive design parameters.

Chapters 1 and 2 provide the background to the COE calculation for offshore wind turbines and introduces some of the key issues with current models and challenges for creating reliable designs. Chapter 3 outlines the COE model methodology and introduces base case results for 4 different drive trains with permanent magnet generators (three geared designs and one direct drive topology without a gearbox). Chapter 4 provides an optimisation process based on a genetic algorithm to allow the design to be improved whilst considering several constraints. Chapter 5 looks at the optimised designs under different price input conditions to assess the impact on the COE. Chapter 6 introduces the concepts of *robust optimisation* and *optimisation under uncertainty* to account for price variability associated with material used in the drive train.

This thesis provides a novel approach to drive train optimisation whilst accounting for price uncertainty. The study highlights the key vulnerabilities for a design under material price fluctuations and presents design processes which include uncertainty and provide robust solutions for various drive train topologies.

The effect of drive train design and optimisation suggests that direct drive topologies (that do not have a gearbox) can offer the lowest COE solutions. This is primarily due to the increase in reliability achieved by eradicating the failures associated with wind turbine gearboxes. This result supports current trends observed in large offshore wind turbines where many of the installed >6MW machines are direct drive permanent magnet generators. Additionally, a well-designed drive train has the potential to reduce the COE by up to 15% as discussed in this thesis.

Acknowledgements

A special thank you goes to my first supervisor, Dr Alasdair McDonald, who has guided me the whole way through and none of this would have been possible without him. I have learned so much from Alasdair and I will always be grateful for his effort and support in helping me to help achieve my goals.

I am very grateful to the other students in the CDT who have made my time at the University enjoyable and memorable and I have made some lifelong friendships in the process. I would like to thank my family and friends who have supported me along the way and encouraged me through the most challenging times.

Finally, I want to thank my partner Marc, who has been there for me from day one of the PhD and helped me though all my difficulties I have faced over the years and always encouraged me to do my best. I would not be where I am today without him.

Table of contents

Nomenclature

A	Cross-sectional area
A_{Cus}	Copper conductor cross-sectional area
A_g	Arrangement constant
A_{gbs}	Gearbox surface area
B	Magnetic flux density
$\hat{B}_g$	Fundamental space harmonic
B_0	Flux density
B_g	Air gap flux density
B_{rm}	Remnant magnet flux density
b	Circumferential beam width
b_{sav}	Average slot width
b_w	Contact face width
b_s	Slot width
b_{so}	Slot opening width
b_t	Tooth width
C	Scale parameter
C_p	Power coefficient/aerodynamic efficiency
C_p	Elastic coefficient
D_{si}	Inner stator bore diameter
d	Axial beam width
d	Operating pitch diameter of pinion
d_m	Mean bearing diameter
E	Electromotive force
E_p	Stator winding induced no-load voltage
F	Facewidth
F	Force
F_a	Axial bearing load
f_0	angular frequency
f_0	Bearing dip factor

f_1	Coefficient of friction
f_2	Bearing design and lubrication factor
f_3 , f_4	Bearing seal factors
f_m	Mesh coefficient of friction
g_{eff}	Effective air gap
g	Air gap
g	Airgap of the generator
H_s	Recess approach sliding ratio
H_t	Recess end sliding ratio
h_s	Height of the generator stator teeth/slot height
h_{sy}	Height of the generator stator yoke
h_s	Stator teeth height
h_{sy}	Stator yoke height
h_y	Yoke height
h_{y0}	Extra yoke height due to deflection
I	Current
I	Pitting resistance geometry factor
J	Bending strength geometry factor
K	Load intensity
k_C	Carter factor
k_W	Winding factor
k_d	Winding distribution factor
k_{sfil}	Slot fill factor
k	*S*hape parameter
ℓ	lenth
l_m	Magnet length in the direction of magnetisation
l_s	Stack length
I_g	Grid side converter current
I_{gm}	Grid side converter maximum current
I_r	Yoke cross-section second moment of area
I_s	Generator side converter current

I_{sm}	Generator side converter maximum current
I_y	Axial arm second moment of area
I_z	Circumferential second moment of area
L_{sm}	Magnetizing inductance
l_{Cus}	Copper conductor length
l_{ar}	Arm radial length
l_b	Radial beam length
l_m	Magnet length
l_s	Stack length
M	Mesh mechanical advantage
M_0	Load independent frictional moment
M_1	Bearing load dependent torque
M_2	Axial load moment of friction
M_3	Sealed bearing addition frictional moment
m	Number of phases
m_{str}	Mass of structure
m_t	Transverse tooth module
N_s	Number of phase winding turns
N_{cp}	Conductors per phase (turns per phase)
N_{spp}	Number of slots per pole per phase
n	Rotational speed
n_1	Pinion rotational speed
n_{ar}	Number of arms
n_{rated}	Rated rotational speed
P	Maximum available power
P_1	Bearing dynamic load
P_A	Input power
P_{Bi}	Individual bearing total power loss
P_{Fe}	Specific iron losses
P_{Fe0h}	Hysteresis loss per unit mass
P_{Fe0e}	Eddy current loss per unit mass
P_{GWi}	Gear winding and churning losses

$P_{Gearbox\ loss}$ Gearbox losses

P_L Load dependant losses

P_{Mi} Mesh power losses

P_N Non-load dependant losses

P_P Individual oil pump power

P_Q Heat dissipation losses

P_S Individual oil seal losses

P_T Gear thermal rating

P_V Power input losses

P_W Gear winding and oil churning losses

P_{WB} Bearing winding and oil churning losses

P_{WBi} Individual bearing power loss

P_{conv} Converter loss

P_{convm} Converter dissipation losses

P_d Transverse diametral pitch

P_{rated} Wind turbine power

p Number of poles/pole pairs

q_r Mean normal radial stress

q Number of conductors per slot

q Number of conductors

R Outer radius

R_s Phase resistance

r Rotor radius

r Rotor radius

r_m Generator stator outer radius

r_{o1} Pinion outside radius

r_{o2} Gear outside radius

r_r Top magnet stator radius

r_{si} Inner stator bore radius

r_{w1} Pinion operating pinch radius

r_{w2} Gear operating pinch radius

r_m Radius of outer part of generator stator

τ_s Slot pitch

ω_m Mechanical angular frequency

ω_m Rotor angular speed

μ_{rm} Relative recoil permeability of the magnets

σ Shear stress

τ_p Pole pitch

τ_s Slot pitch

ω Rotational speed

Φ Magnetic flux

η Unit efficiency

θ Pitch angle

λ Tip speed ratio

μ_0 Permeability of free space

μ_r Permeability of material

ν Kinematic oil viscosity

ρ Air density

χ Optimum aspect ratio

List of Abbreviations

AEP = annual energy production in MWh

AOM = annual operations and maintenance cost in €/year

BOP = balance of plant

COE = cost of energy in €/MWh (€/megawatt-hour)

EMF = electromotive force

FCR = fixed charge rate in %

ICC = initial capital cost in €

List of Figures

List of Tables

Chapter 1 Introduction

1.1 Introduction to the cost of energy for offshore wind

Offshore wind energy is becoming increasingly prevalent as the demand for reliable, renewable energy sources continues to increase. Compared with onshore wind farm development, issues such as turbine size and noise production are much less of a concern offshore, and combined with excellent wind resources, offshore wind energy is becoming very attractive to developers on a global scale. However, the harsh sea environment poses several issues and limitations during the construction and operation of wind farms. Weather windows can be unpredictable and often too short to carry out significant repairs and so reliability is very important to limit the down time of an offshore wind turbine. Installation and wind turbine foundation costs are very high for offshore wind. The use of fewer, larger wind turbines (>5 MW) are now widespread industry practice for offshore wind in order to reduce the number of installations required and minimise the overall project cost.

As with any design, understanding the key cost drivers and further areas of improvement are always in the forefront of its development. For wind turbine drive trains, the scope for optimising the design is vast. With so many types of electrical machines available and speed options, choosing the right design for a particular application will always be challenging. A unit of measure used in the energy sector for describing the cost of electricity is known as Cost of Energy (COE). It is typically presented as a cost per unit of energy generated and can provide key information as to how expensive electricity generation technologies are over their lifetimes. Minimising the COE is the most important aspect of any energy generation project and is particularly challenging for offshore wind energy. The UK government has already surpassed its target of reducing the COE for offshore wind to £100/MWh [1] and with continued improvements in technology, offshore wind is now one of the most attractive forms of renewable energy generation. Renewable energy sources of electricity, including solar and biogas are becoming much more cost competitive compared with conventional fuel methods. The COE values for renewable generation are in the lower end of the fossil fuel cost range, as discussed in a study by the

Fraunhofer Institute for Solar Energy Systems ISE [2], which helps to drive further investments in clean energy generation projects.

Cost of Energy (COE) can be split up into 3 main categories:

- Initial capital costs – this covers all component and installation costs of the complete system including infrastructure and transport costs

- Annual energy production – this is the output of the wind turbine after all losses are taken into consideration and includes the days of the year that the wind turbine was operational

- Reliability and maintenance – this takes into account the failures of components, the cost to repair and any other maintenance costs.

To obtain the most suitable COE values for the lifetime of the project, having a thorough understanding of each of these 3 main categories is crucial. The wind turbine drive train contributes to all three categories. It is a significant part of the wind turbine topology as it is the interface between the turbine rotor and the grid. The drive train components convert the energy in the wind into electricity and can have numerous topologies, unlike the rest of the wind turbine (tower and rotor etc.) that are fairly homogenous.

Figure 1.1 illustrates state of the art drive train designs for modern wind turbines. Drive trains are tending towards using permanent magnet synchronous generators with fully rated converters to maximise the system efficiency and reliability [3]. Drive train design can have a significant effect on the COE as issues such as low efficiency, poor reliability and high capital costs can negatively impact the overall project cost.

This thesis aims to deliver a comprehensive analysis of the cost of energy for offshore wind turbines, whilst focusing on the design of the drive train. The wind turbines studied are all permanent magnet generator designs and their performance in terms of COE is scrutinized under a number of different design specifications and cases. The work undertaken in this thesis will attempt to include detailed drive train design in the cost of energy optimisation process. Although the values and assumptions used in this thesis are mainly based on academic knowledge and information from the public domain, some discussions with industrial partners have assisted in the process.
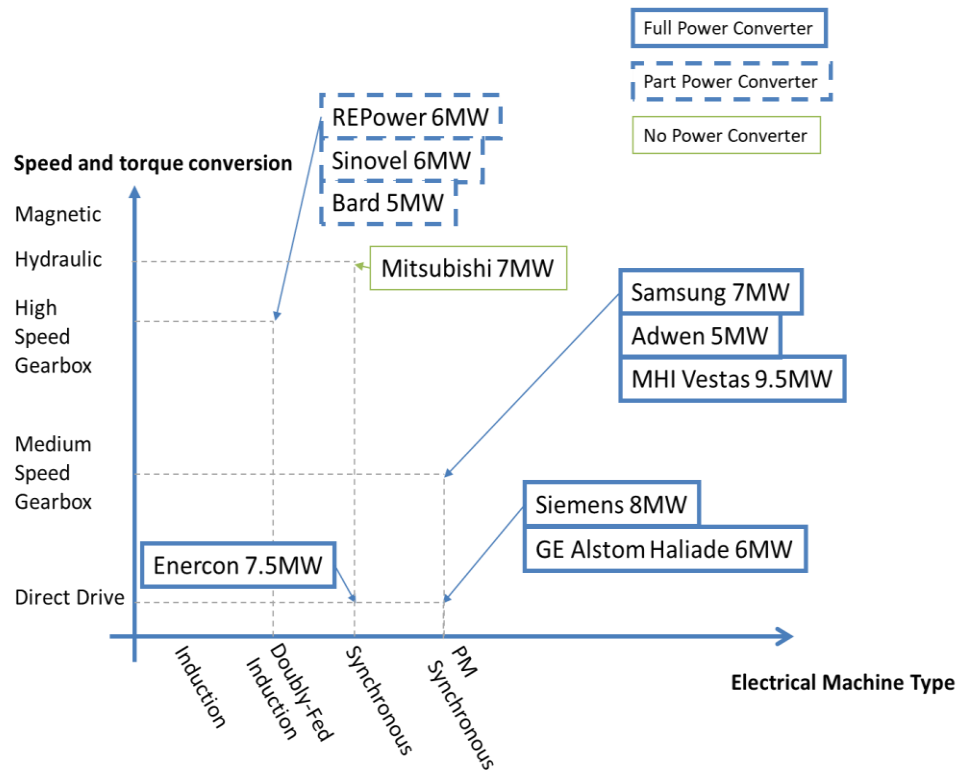
Figure 1.1 Electrical machine type and drive train choice for high power state of the art wind turbines. Taken from [4].

All wind turbine designs discussed in this thesis are modern 3-bladed, upwind, variable-speed, pitch regulated devices such as those shown in Figure 1.2.

Figure 1.2 Wind turbines photograph. Taken by author.

1.2 Offshore Wind and Turbine Challenges

Wind speeds across land are inherently lower than at sea due to the land's surface roughness which creates friction and slows down the moving air as well as creating turbulence. At sea, the surface is comparatively flat and so wind speeds are highest in offshore areas which provide the ideal conditions for wind turbines [5]. Average wind speeds in offshore locations can be around 12 m/s compared with onshore locations that would often rarely see average wind speeds greater than 9 m/s [6].

There are however, huge challenges to be overcome when planning and installing offshore turbines. The harsh sea environment means that the weather dictates the installation and maintenance of the turbines. Installation requires that both the wind speed and wave height to be below specific levels in order for the vessels and cranes to be able to operate safely [7]. If a scheduled installation or repair is unable to go ahead due to high winds, then this can be extremely costly to the owner. Having lightweight and easy to assemble/disassemble parts would be preferential but not always possible as generators/gearboxes can be heavy and complex [8].

Installing large offshore wind farms involves expensive transportation and procedures. The location of the wind farm and the type of seabed are major components in the planning and costing of wind farm installations. As with any offshore installation, wind turbines require vessels, cranes, highly trained personnel and specialist equipment [9].

Day rates of vessels used in offshore installation are very expensive (e.g. in excess of £100,000 per day [10]). Therefore, appropriate planning and methods are essential in assessing the duration of installation and evaluation of risk and uncertainties which may lead to delays and increased cost. Understanding site conditions and seasonal weather predictions will aid in the decision process for scheduling and limiting installations [11].

1.3 Modern offshore wind turbines

Wind turbines extract power in the wind by converting kinetic energy into pressure energy at the rotor plane. The use of an electrical generator then allows the rotational energy of the turbine shaft to be harvested as electrical energy and then utilised through the transmission and distribution system to provide power to the end consumer.

Wind turbines consist of a tower, blades, hub and nacelle. The nacelle houses the interior workings of the wind energy conversion system which is known as the drive train. The actual configuration of the drive train varies depending on the technology and the turbine manufacturer. Most modern offshore wind turbines are pitch regulated, variable speed designs – these turbines use pitch control above rated wind speed, and also use generator torque control over the whole operating range of the turbine to allow for variable speed operation of the machine.

1.4 Drive trains

Typically wind turbine nacelles consist of a gearbox and a medium or high-speed generator and a power electronic converter. Wind turbine gearboxes have finite lifetimes which are often much less than the expected lifetime of the turbine [12]. Gearboxes tend to require replacement at least once during the operational life of the wind turbine [13]. It can be assumed that the failure rate of gearboxes increases with an increasing number of gearbox stages [12]. As a result, many manufacturers are exploring ways in which to remove or replace the gearbox by adopting direct drive methods or altering the technology used to increase the shaft speed such as hydraulic and magnetic gearing options.

1.4.1 Generators for wind turbines

Generators for wind turbines, since around 2005, have been redeveloped and enhanced by manufacturers in order to comply with grid requirements for fault ride-through [14]. Many of the latest systems use brushless generators and fully rated converters. Until around 1998, most wind turbine manufacturers built constant speed

wind turbines with a three-stage gearbox, a standard squirrel-cage induction generator directly grid connected, and an output power below 1.5 MW [14]. These older machines are susceptible to instability issues and may have minimum working voltages which would limit their ability to support fault ride-through. Since then, more complicated variable speed wind turbines have emerged as manufacturers strive to optimise their designs and increase their efficiencies as well are providing more robust fault ride-through capabilities.

A study by H. Polinder in 2011 in [14], describes an overview of wind turbine generator systems and their recent trends. The study provides an insight into various types of wind turbine generator systems being used today and their benefits as well as highlighting some of the issues experienced by such designs. Until recently, constant speed systems were considered to have the lowest cost, size and weight compared with direct drive systems that were considered expensive, large and heavy. Siemens and Enercon, however, have shown that optimised direct drive designs have a weight comparable to geared systems.

The cost of power electronics has decreased significantly from over a decade ago making a brushless alternative to a typical DFIG more attractive as it can improve grid-fault ride-through capabilities. Advantages of a brushless generator system with gearbox and fully rated converter include:

- A less complex grid-fault ride-through capability,
- The use of more simple control methods,
- Can be used in both 50 Hz and 60 Hz grids,
- Brushless system so it has reduced maintenance and increased reliability making it attractive for offshore purposes.

Some disadvantages of a brushless system include:

- The requirement of a larger, more expensive converter (100% of rated power as opposed to a rating of 25% which is typical of standard DFIG machines),
- Higher converter losses due to all power generated being processed by the converter.

1.4.2 Direct Drive

Direct drive wind turbines are based on a direct coupling of the rotor and the generator. By eliminating the gearbox from wind turbines, failures associated with gearboxes are no longer an issue. This method results in the generator operating at the same speed as the rotor of the wind turbine. Direct drive wind turbines require large diameter generators to match the high torque created by the rotor and therefore can be heavy and expensive. Transportation and installation issues may also be an issue for such large generator designs.

1.4.3 Permanent Magnets

The use of permanent magnets in place of conventional excitation methods of a wound rotor allows more efficient designs to be produced. According to the literature [15][16], the demand for high-performing NdFeB (Neodymium Iron Boron) permanent magnets and their doped elements, such as Dysprosium will increase.
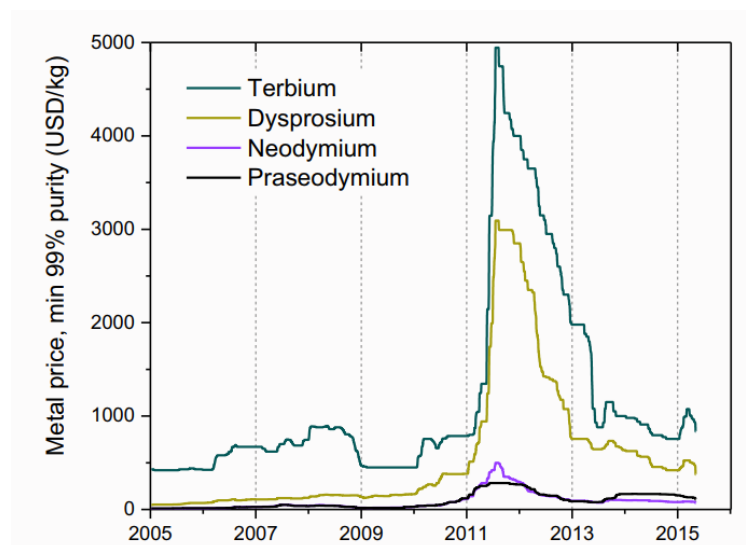
Figure 1.3 Prices of magnetic material over 10 year period. Taken from [15].

China holds the monopoly in terms of rare earth metal resource and production. With continued supply and demand issues as well as economic instability, the price of these materials is subject to high fluctuations. Figure 1.3 shows the huge price rise in

magnetic material between 2011 and 2012 during the volatile period of disputes with China.

Therefore, the availability of magnet production relies heavily on intercontinental relationships. This could render projects infeasible if another price rise similar to that of 2011 was to happen again.

1.5 Reliability of wind turbines

The operations and maintenance (O&M) of wind turbines is based primarily on the reliability of the components [9]. It is important to understand the failure modes and the implications of particular designs. This will allow suitable lifetime cost estimates to be calculated in order to create a successful project. Wind turbines are still within relative infancy compared with other electricity generation methods such as coal power plants. Therefore, there is limited information available regarding long term reliability of wind turbines. Understanding the causes of failures and the most vulnerable parts of the system will aid in the designing and maintenance of wind turbines. The following sections outline some of the key reliability issues associated with wind turbine drive trains.

1.5.1 Failure modes of the drive train

As with any engineering project, understanding the failure modes and the lifetime of the components will allow correct maintenance and repair schedules to be determined. The failure modes of an offshore wind turbine are outlined by Luengo [17], Shipurkar [18] and Alewine [19] who each present a breakdown of each subsystem of the wind turbine into its main components and failure modes.

As this thesis focuses on the drive train design, only the failure modes associated with the generator and gearbox will be focused on.

```
┌─────────────────────┐              ┌─────────────────────┐
│  Gearbox Failure    │              │  Generator Failure  │
└─────────────────────┘              └─────────────────────┘
```
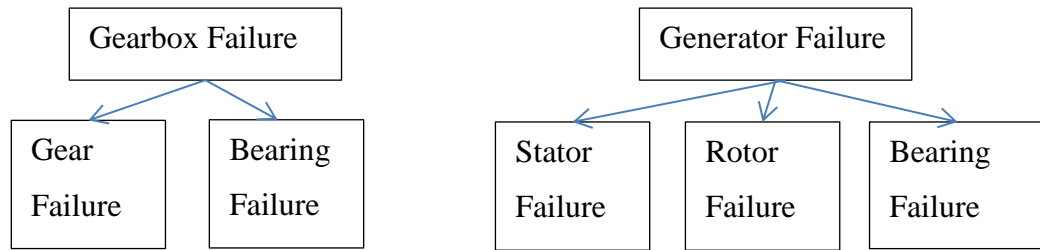
Figure 1.4 Diagram of the main components of gearbox and generator failures.

Figure 1.4 shows a simplified breakdown of the key gearbox and generator failures. By breaking up the failure modes of the gearbox and generator, a design specific failure analysis can be conducted.

1.5.2 Generator failures

There are many reasons for parts of a generator to fail, some only create minor issues whereas other severe problems could destroy the machine completely. The root causes of generator failures are outlined in [20] which can typically be issues such as end winding looseness, contamination and poor workmanship. These issues can lead to failure mechanisms such as:

- Slot bar vibration
- Vibration sparking
- Partial discharge – end windings
- Partial discharge – slots
- Local over-heating

These problems can then result in failure mode of varying degree of severity such as:

- Electrical connection failure
- Foreign object damage
- Over-flux damage

More details regarding generator failures, and particularly winding issues, are described in [19] and [21]. There are key aspects that can affect the lifetime of components, some of which [21] are shown below:

1. Design of the windings
2. Quality of winding manufacturing process and materials
3. Operating environment of the machine
4. Past maintenance

Insulation thickness, operating voltage and temperature all play a part in the lifetime of the machine components. From a designer's perspective, appropriate cooling, winding and slot wedge quality, and protective measures are vital to ensure longevity of the product.

1.5.3 Gearbox failures

High-speed wind turbine systems typically have a gearbox as the interface between the rotor and the generator. These gearboxes are subject to high levels of vibrations associated with the rotor and drive train and so have limited life expectancies. The typical issues and types of failures seen in gearboxes include [22]:

- Macropitting
- Cracks
- Scuffing
- Corrosion
- Contamination (oil)
- Foam (oil)

Careful design consideration by expert engineers can help reduce the risk of failures and early detection methods would also play an important role in the maintenance of wind turbine gearboxes.

1.6 Research Question

There are major studies on wind turbine drive trains for offshore wind energy by authors such as Polinder [23][24][25], Hui Li [26][27] and Bywaters [28]. Multiple configurations are discussed in these publications ranging from large direct drive options to drive trains that comprise of six separate small generators. The designs have pros and cons and finding a "one size fits all" solution doesn't seem to be leading towards any conclusions. Noting the current industrial trend to use permanent magnet synchronous generators with fully rated converters, the following question arises:

"What is the best drive train design for a large offshore wind turbine with a permanent magnet generator in terms of cost of energy?"

This broad question seems to require a rather specific answer. The work undertaken in this thesis attempts to answer such a question whilst respecting a large degree of cost uncertainty in the process of the design. Throughout the thesis, the "goal" of finding the "best" design develops into a more detailed analysis of probabilities, uncertainties, compromise and justification of various designs. There cannot simply be one solution, but a number of probable solutions suited to various conditions.

1.6.1 Novelty of Research

Although the cost of energy for wind turbines is a significant area of research, the design optimisation based on subassemblies and components of the drivetrain has very few studies and literature available. The work in this thesis covers a number of areas where published work is limited such as:

- Design and comparison of 4 different speed classes of permanent magnet generators which includes a direct drive and 3 different geared designs
- Optimisation and sensitivity analysis based on material cost probabilities
- Design specific failure rate estimation based on component dimensions
- Optimisation under uncertainty of the drive train
- The generator and gearbox are optimised concurrently in order to obtain the most suitable operating speed and dimensions in terms of cost and reliability

Manufacturers have their own in-house methodologies for designing drive train topologies, but this information is not publicly available. By creating a model that allows several drive train types to be compared and discussed, this thesis will help some of the key decision drivers for manufacturers to be more understood. This work will not only serve as an aid to manufacturers but will also benefit developers from a turbine procurement perspective, where important decisions regarding future proofing the technology will become much more important. Material price fluctuations and supply chain uncertainty have the potential to restrict the accessibility of some designs and so careful consideration of the drive train type is very important for offshore wind development.

1.6.2 Industrial Engagement

Throughout the process of developing the models used in this thesis, guidance and advice was provided from various engagements with industrial partners. These included site visits and discussions with the engineering team at Siemens in Brande, Denmark, Magnomatics in Sheffield, UK, Artemis (MHI) in Edinburgh, UK and SSE in Glasgow, UK. These engagements provided support and advice during the creation of the optimisation models which is relevant to current industrial practices and formed part of the early stages of validation.

1.6.3 Layout of the Thesis

The thesis consists of seven chapters with Chapters 1 and 2 detailing the research question and literature review. Chapter 3 describes the method for modelling the cost of energy of wind turbines with different drive trains and presents base case results for each and discusses the significance of each of the solutions. Chapter 4 develops an optimisation technique using a genetic algorithm and these models to explore various outcomes in the design space with fixed cost inputs. It also presents an independent variable sensitivity analysis to identify the key cost drivers in the design optimisation process. Chapter 5 presents a detailed sensitivity analysis of each of the optimised designs from Chapter 4, taking into account the probability distributions of

material prices and Monte Carlo sampling methods. Chapter 6 presents an optimisation under uncertainty methodology where the objective function was altered to account for the uncertainty of the input material costs. Chapter 6 also presents robust optimisation cases which represent real-life considerations and project feasibility. Chapter 7 concludes the results of all the models and analysis of the designs. Figure 1.5 shows the 4 results chapters divided into their respective content focus.

	No Optimisation	Optimisation
No Uncertainty	Chapter 3	Chapter 4
Uncertainty	Chapter 5	Chapter 4 Chapter 6

Figure 1.5 Diagram illustrating the contents of the results chapters in this thesis.

A master flow chart of the thesis modelling progression throughout the chapters is also presented in Figure 1.6 below.

Base Case Loss and COE Model

(Chapter 3)

- Generator Loss equations
- Gearbox loss equations
- Failure rates and downtime
- Weibull distribution
- Cost assumptions and calculations

Optimisation model and sensitivity to independent variables

(Chapter 4)

- Use of genetic algorithm to optimise design process
- Air gap radius and gear ratio sensitivity analysis

Optimised results sensitivity to external parameter variation

(Chapter 5)

- Generator/gearbox major replacement scenario
- Material price variation and the effects on COE
- Statistical probability of prices and Monte Carlo sampling

Optimisation under uncertainty and robust optimisation with addition design constraints

(Chapter 6)

- Including cost uncertainty input and Monte Carlo Sampling
- Robust optimisation and additional model objectives
- Alternative magnetic material scenario

Figure 1.6 Master flow chart of thesis optimisation approach for each chapter.

1.7 References for Chapter 1

[1]   RenewableUK, "Offshore wind on target to become lowest-cost, large scale clean energy source." [Online]. Available: https://www.renewableuk.com/news/327446/. [Accessed: 01-Jul-2019].

[2]   C. Kost, "Levelized cost of electricity renewable energy technologies." Fraunhofer ISE, Report, 2018.

[3]   C.-Y. Hsiao, S.-N. Yeh, and J.-C. Hwang, "Design of High Performance Permanent-Magnet Synchronous Wind Generators," *Energies*, vol. 7, no. 11, pp. 7105–7124, 2014.

[4]   J. Carroll, "Cost of energy modelling and reduction opportunities for offshore wind turbines," PhD Thesis, University of Strathclyde, 2016.

[5]   E. Hau, *Wind Energy: Fundamentals, Technologies, Applications, Economics*, 2nd ed. Springer Berlin, 2006.

[6]   4coffshore, "Global Offshore Wind Speeds Rankings." [Online]. Available: https://www.4coffshore.com/windfarms/windspeeds.aspx.

[7]   L. Castro-Santos, A. Filgueira-Vizoso, I. Lamas-Galdo, and L. Carral-Couce, "Methodology to calculate the installation costs of offshore wind farms located in deep waters," *J. Clean. Prod.*, vol. 170, pp. 1124–1135, 2018.

[8]   I. F. A. Vis and E. Ursavas, "Assessment approaches to logistics for offshore wind energy installation," *Sustain. Energy Technol. Assessments*, 2016.

[9]   Tavner, *Offshore Wind Turbines: Reliability, availability and maintenance.* 2013.

[10]   Y. Dalgic, I. Lazakis, and O. Turan, "Vessel charter rate estimation for offshore wind O&M activities," in *Developments in Maritime Transportation and Exploitation of Sea Resources*, 2013.

[11]   C. A. Irawan, D. Ouelhadj, D. Jones, M. Stålhane, and I. B. Sperstad, "Optimisation of maintenance routing and scheduling for offshore wind farms," *Eur. J. Oper. Res.*, 2017.

[12]   K. Smolders and H. Long, "Reliability analysis and prediction of wind turbine gearboxes," in *European Wind Energy Conference*, 2010.

[13]   S. Alshibani and V. G. Agelidis, "Issues regarding cost estimation of

permanent magnet synchronous generators for mega-watt level wind turbines," *2011 IEEE Int. Electr. Mach. Drives Conf.*, pp. 1629–1634, May 2011.

[14] H. Polinder, "Overview of and trends in wind turbine generator systems," *2011 IEEE Power Energy Soc. Gen. Meet.*, pp. 1–8, Jul. 2011.

[15] C. C. Pavel *et al.*, "Substitution strategies for reducing the use of rare earths in wind turbines," *Resour. Policy*, vol. 52, no. May, pp. 349–357, 2017.

[16] J. Griffiths and S. Easton, *Marine Estate Research Report, Use of rare earth metals in offshore windfarms*. 2011.

[17] M. M. Luengo and A. Kolios, "Failure mode identification and end of life scenarios of offshore wind turbines: A review," *Energies*, vol. 8, no. 8, pp. 8339–8354, 2015.

[18] U. Shipurkar, K. Ma, H. Polinder, F. Blaabjerg, and J. A. Ferreira, "A review of failure mechanisms in wind turbine generator systems," *2015 17th Eur. Conf. Power Electron. Appl. (EPE'15 ECCE-Europe)*, pp. 1–10, 2015.

[19] K. Alewine and W. Chen, "A review of electrical winding failures in wind turbine generators," *IEEE Electrical Insulation Magazine*, vol. 28, no. 4. pp. 8–13, 2012.

[20] P. E. C. V. Maughan, "Root-cause diagnostics of generator service failures," *Conf. Rec. 2004 IEEE Int. Symp. Electr. Insul.*, no. September, pp. 154–162, 2004.

[21] G. C. Stone, E. A. Boulter, I. Culbert, and H. Dhirani, *Electrical insulation for rotating machines : design, evaluation, aging, testing, and repair*. 2004.

[22] S. Sheng, "Gearbox Typical Failure Modes , Detection and Mitigation Methods," *NREL/PR-5000-60982*, 2014.

[23] H. Polinder, F. F. A. Van Der Pijl, G. J. De Vilder, and P. J. Tavner, "Comparison of direct-drive and geared generator concepts for wind turbines," *IEEE Trans. Energy Convers.*, vol. 21, no. 3, pp. 725–733, 2006.

[24] H. Polinder, J. A. Ferreira, B. B. Jensen, A. B. Abrahamsen, K. Atallah, and R. A. McMahon, "Trends in wind turbine generator systems," *IEEE J. Emerg. Sel. Top. Power Electron.*, vol. 1, no. 3, pp. 174–185, 2013.

[25] H. Polinder, "Optimization of Multibrid Permanent-Magnet Wind Generator

Systems," *IEEE Trans. Energy Convers.*, vol. 24, no. 1, pp. 82–92, Mar. 2009.

[26]   H. Li and Z. Chen, "Design optimization and evaluation of different wind generator systems," *Electr. Mach. Syst. 2008. ICEMS 2008. Int. Conf.*, pp. 2396–2401, 2009.

[27]   Y. Xue, L. Han, H. Li, and L. Xie, "Optimal Design and Comparison of Different PM Synchronous Generator Systems for Wind Turbines," pp. 2448–2453.

[28]   G. Bywaters, V. John, J. Lynch, P. Mattila, G. Norton, and J. Stowell, "WindPACT Drive Train Alternative Design Study Report," *Natl. Renew. Energy Lab. Tech. Rep.*, 2005.

Chapter 2 Literature Review

There are many existing studies on cost of energy and wind turbine drive train design. This chapter will review the literature in the context of the research question presented in the Introduction chapter (i.e. "What is the best drive train design for a large offshore wind turbine with a permanent magnet generator in terms of cost of energy?"). In so doing the major works looking at offshore wind cost of energy models will be examined and important papers on state of the art and novel drive train designs and their potential impact on cost of energy will be reviewed.

This chapter begins with a description of cost of energy (COE) studies and their limitations, followed by generator and gearbox considerations. The chapter also looks at current work on wind turbine failure rates and repairs and how some methods can be adapted in this thesis to include design specific failure rate inputs. The chapter concludes with a summary of the key issues that will be addressed in this thesis based on existing studies and their limitations in order to create a comprehensive drive train model.

2.1 Cost of energy

The original motivation for creating a detailed COE model was based on an NREL study by Bywaters [1] and work by H. Polinder [2]. The NREL report is a comprehensive study on modern wind turbine drive train design and includes aspects of COE modelling. However, it does not provide details for offshore wind turbine design, nor does it include an uncertainty analysis. It is not clear to the extent the design process has been optimised and so as a design tool, it has limitations.

The Polinder study [2] presents a comparison of doubly-fed induction generators and synchronous generators with various topologies for a 3MW onshore wind turbine. This paper is the key reference paper for the generator loss modelling presented in this thesis. Some key findings from the study were that using permanent magnet synchronous generators produced the highest energy yield and that a direct drive topology with a permanent magnet generator could be the best option due to not having a gearbox or issues associated with brushes/slip rings. It is also suggested

that the use of a fully rated converter would mitigate issues from voltage disturbances from grid faults. However, the paper describes that reliability and availability needed more work. Therefore, it seemed that using permanent magnets as an excitation source and a fully rated converter could provide the reliable and efficient wind turbine system needed for offshore installations. With a more detailed reliability and availability calculation, improved analysis of the benefits of such configurations can be investigated. Additionally, amending the assumptions to include offshore wind considerations will make the model suitable for offshore wind farm COE analysis. The Polinder study presented its cost results in terms of annual energy yield/total cost. This method does not allow for complete project cost analysis and design improvement based on lifetime to be explored and so this provided scope for an alternative COE approach. The gearbox model is also simplistic and not related to operating speed and dimensions and so limits the optimisation process of the geared designs. Therefore, there is scope for improving the model optimisation process.

Other studies [3][4][5] provided useful insights into the COE estimation process but similarly do not have detailed drive train design considerations. Understanding the challenges when calculating the COE will allow steps to creating a fully comprehensive model to be developed.

2.1.1 Challenges with COE models

The cost of energy, COE, for offshore wind is challenging in terms of estimating and predicting lifetime costs of wind farms. There have been several publications dedicated to estimating these costs based on various scaling techniques and some historical data [6],[7],[4]. NREL (National Renewable Energy Laboratory) have produced technical papers [8],[9], detailing the estimated costs of wind turbines. The NREL studies provide an appropriate level of detail that is suitable to produce design-specific models for wind turbines and so form a key basis for the development of the model used in this thesis. A significant observation when regarding these documents is that the cost models are not dependant on the drive train type or drive train specifics. This is particularly crucial when estimating

operations and maintenance (O&M) costs as various failure rate specifications will apply to different designs and so will influence the overall COE. Figure 2.1 illustrates some key parameter sensitivities against a baseline from [9].

When estimating the initial capital costs for the wind turbine, considering the detailed design and dimensions of the drive train could provide valuable additional information for decision making processes. Trading-off between upfront cost and reliability could potentially save a considerable amount of money over the lifetime of the wind farm. In order to understand the implications of such an analysis, detailed optimisation models would provide an insight into the steps that could help reduce the COE of offshore wind energy.
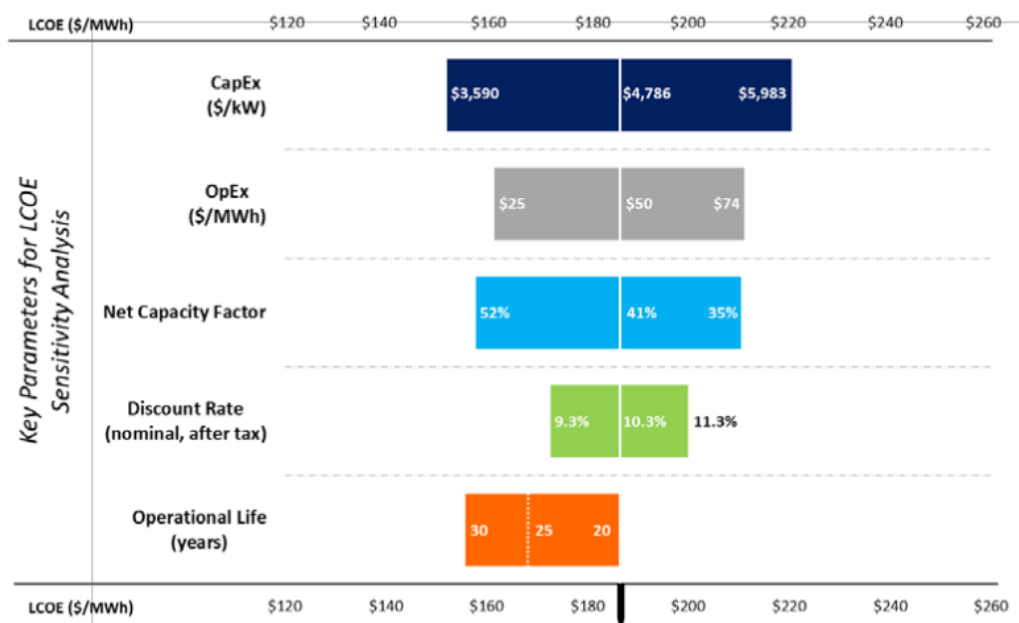
Figure 2.1: Key sensitivity analysis parameters for fixed-bottom offshore wind LCOE from [9].

A cost of energy review by NREL that includes offshore wind energy is detailed in [9]. The typical contributions to initial capital cost (ICC) for offshore wind are represented in Figure 2.2. The cost of the wind turbine accounts for almost a 1/3 of the overall capital cost and so it is clear that achieving an efficient and preferably low cost design will offer the best solution in keeping the COE as low as possible. The paper describes the challenges with material costs and turbines prices being driven by foreign exchange rate movements.
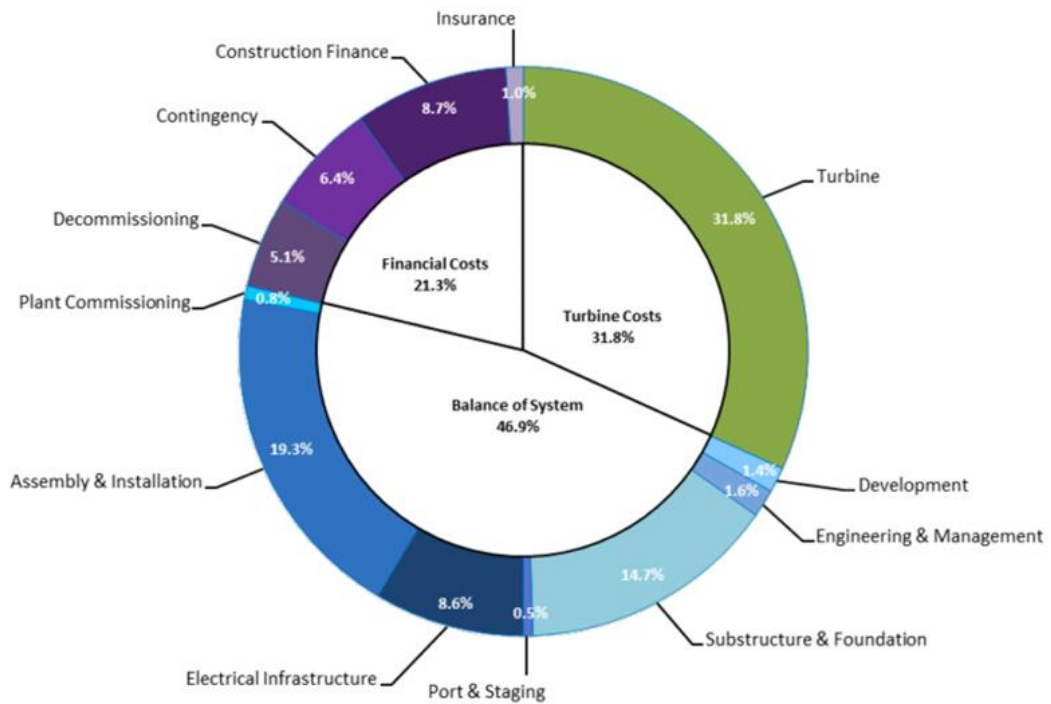
Figure 2.2 Capital cost for fixed-bottom offshore wind turbine. From [9].
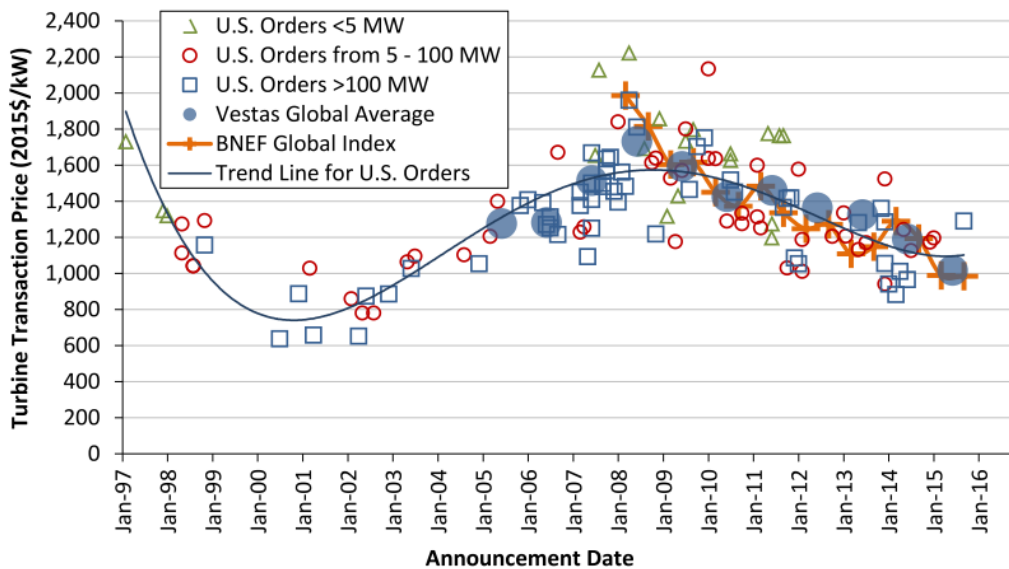
Figure 2.3 Wind turbine price over time. Taken from [9].

The cost of wind turbines since 2009 has been decreasing (Figure 2.3) which is mostly due to the improvement in technology and competitive market. The drivers of the fluctuations in prices are suggested to be based on labour costs, warranty provisions and profit margins [9]. There is continued scope for further price

reduction in the ICC of the wind turbine and so provides additional motivation for design based optimisation of the drive train.

2.1.2 Contract for difference (CFD)

The UK government transitioned from the Renewable Obligation (RO) to Contract for Difference (CfD) in 2017. The new CfD regime introduced a new competitive approach to the development of offshore wind sites allowing winning bidders for each project to obtain a contract for a fixed price of energy generate by that project [10]. The CfD auction saw the cost of energy for new offshore wind farm fall by 50% making it one of the cheapest forms of new power in the UK. Record lows of £57.50/MWh have already been seen with two offshore wind projects as part of the CfD scheme. The Department for Business, Energy and Industrial Strategy (BEIS) expects wholesale power prices to average £53/MWh in the period from 2023 to 2035, covering the bulk of their 15-year contract period [11]. Many costs associated with offshore wind farms such as substations and export systems are no longer part of the capital expenditure of the project (as turbines can be connected to existing infrastructure installed in earlier phases or the turbines are directly connected to the grid, typically using 66 kV HVDC) and so costs are driven ever lower as more efficient cost effective wind turbines are installed. For the purposes of consistency with the models in this thesis, the additional costs of building a substation and other BOP (balance of plant) contributions remain part of the model and so COE for the results in this thesis will be higher than current market estimates.

2.2 Wind turbine topologies

Variable-speed is becoming standard for large wind turbines, both on and offshore, as loads associated with fixed-speed machines are reduced and the turbine has the ability to comply with Grid Code requirements. A doubly fed induction generator (DFIG) wind turbine, such as the example shown in Figure 2.4, uses a wound-rotor induction generator with slip rings [12]. The slip rings allow current to pass through the rotor windings and variable speed operation is achieved by injecting a

controllable voltage into the rotor at slip frequency. The rotor winding is fed through a variable-frequency power converter, typically based on two AC/DC IGBT-based voltage source converters (VSCs) which are linked by a DC bus [13]. The power converter enables the variable-speed operation of the turbine due to the network electrical frequency being decoupled from the rotor mechanical frequency.

The rotor of a DFIG wind turbine can absorb power from the grid depending on the rotational speed of the generator. If the generator operates above synchronous speed, power will be delivered from the rotor through the converters to the network, and for below synchronous speed operation, power will be absorbed by the rotor from the network through the converters.
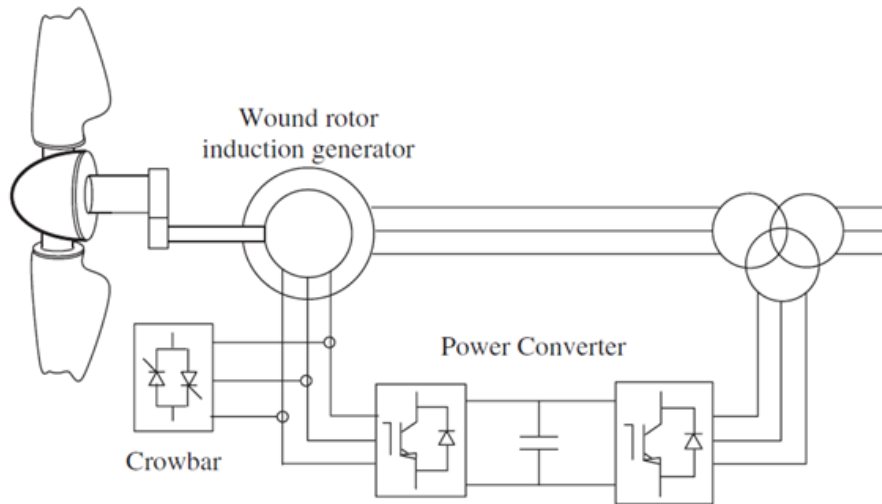
Figure 2.4 – Configuration of a typical DFIG wind turbine with a crowbar which is used to protect the generator and converters from over-current, and to limit the voltage [13].
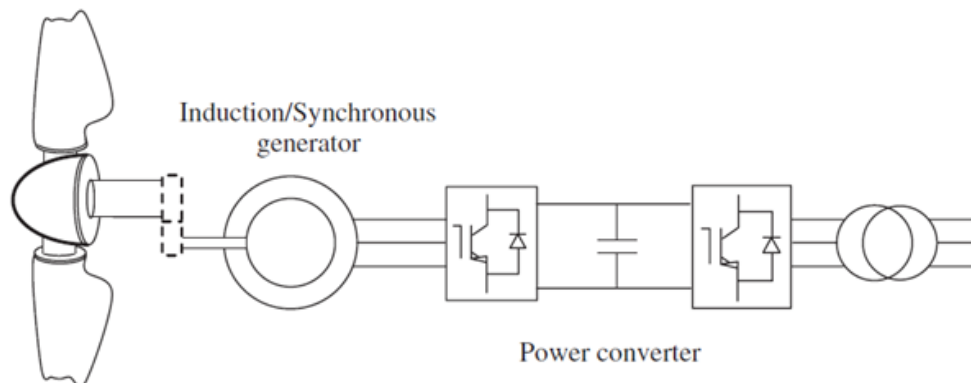
Figure 2.5 – Configuration of a fully rated converter-connected wind turbine (dashed section illustrates direct drive or gearbox options [13].

Fully rated converter (FRC) wind turbines (shown in Figure 2.5) offer a high level of control through the use of power converters [14]. The configuration of FRC wind turbines can differ significantly between models, as the turbines can use a wide range of generator types and may or may not have a gearbox. Since the power converters offer an interface wind turbine and the network, the operation of the generator is effectively isolated from the grid. This means that the electrical frequency of the generator can vary as wind speed changes, yet the grid frequency remains unchanged, and the machines is able to operate at a variable speed [13].

The control strategy for the generator operation and power flow is dependent on the type of power converter configuration used in the system. The network-side converter can be arranged to maintain a constant DC bus voltage with torque applied to the generator which is controlled by the generator-side converter. Each converter can independently generate or absorb reactive power. The torque applied to the generator can also be controlled by the network-side converter [13].

2.3 Wind turbine drive trains

A study by H. Polinder [15] looks at the trends of wind turbine generators over the years and the latest emerging technology. The paper asks a number of questions and describes some key factors regarding the cost minimisation objectives of developing wind turbine concepts and they are as follows:

1. Capital expenditures are important, but not decisive, because operational expenditures also have to be considered.
2. What is the best generator over time as material cost varies over time? There are uncertainties over these price developments and their influences on decisions.
3. What is the best generator system for a location for a specific wind profile?
4. The efficiency of the system is important, but not decisive as a system with a lower efficiency and lower COE would be preferential.

Considering these 4 aspects of generator design creates an opportunity for a detailed sensitivity analysis in order to answer some of the questions. Polinder [15] concludes

that there is no convergence to a single best wind turbine generator system, but a large variety of designs which can be seen coming on the market.

2.3.1 Current state of the art drive trains

There are many alternative drive train configurations to the conventional gearbox and electrically excited generator configurations that are becoming increasingly competitive in the aim of reducing the cost of energy and creating reliable, efficient technology. This section outlines some examples of the next generation of alternative drive trains.

2.3.1.1 Superconducting generator

Superconducting generators can produce much higher power densities in the windings than conventional electrical generators and various studies are focusing on the development of these generators for offshore wind applications [16][17]. A study by J. Wang et. al. [18] compares two 12 MW nine-phase superconducting synchronous generators with different armature winding arrangements. Multiphase generators are used to reduce the current and voltage stress of the switching devices used in the full-power converters. Other advantages of a multiphase generator include lower torque ripples and higher fault tolerance.

The study by J. Wang presents a traditional radial flux topology with an inner rotor, illustrated in Figure 2.6. Copper field windings in traditional synchronous generators are replaced with superconducting coils and a cryostat to maintain constant low temperatures for superconductivity.
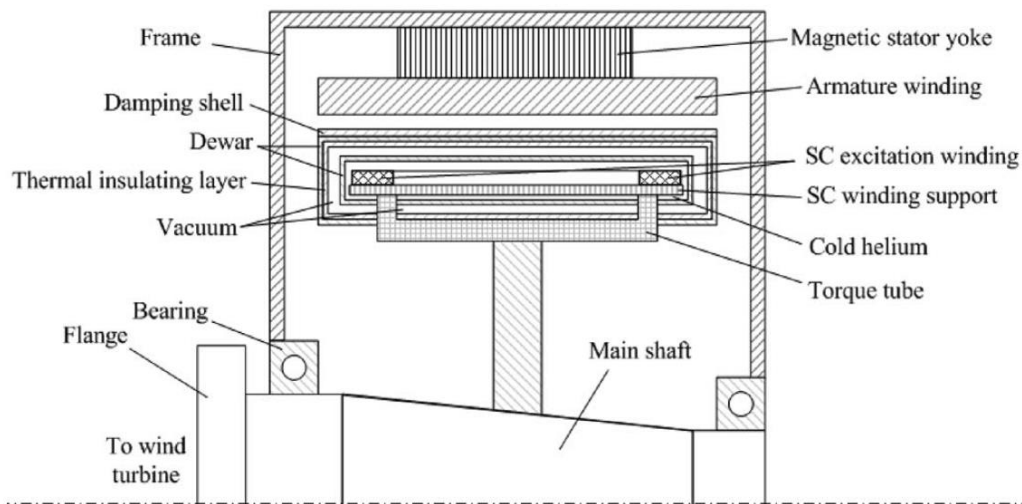
Figure 2.6 – Design specifications of superconducting generator for wind large turbines and its schematic [18].

The rated speed of the generator is 9 rpm (same as the turbine rotor) meaning that 13 MNm of torque should be transferred to the generator.

2.3.2 Hydraulic Drivetrains

The use of hydraulics to control the torque of the wind turbine is becoming an increasingly developed technology with the potential to replace conventional gearboxes. Work completed by Jose Cidras and Camilo Carrillo from the University of Vigo in Spain [19] presents a model in which the prime mover of an energy conversion system is controlled via hydrostatic transmission. This will allow the generator to operate at a constant speed and so keep a constant frequency. The paper focuses on modelling and simulating a Shaft Coupled Generator (SCG) and has laboratory based experimental results in order to verify the results. The results presented show a good agreement between the experimental data and the simulated results, indicating that the tool is useful in the design stages of hydraulic transmission based systems.

The hydrostatic transmission is attained through the use of a hydrostatic pump and a hydrostatic motor connected by pressure lines forming a closed circuit. The pumps have variable displacement volume so that the flown volume per revolution can be changed and so the rotational speed between the pump and the motor can be modified (Artemis Digital Displacement® Technology – owned by

Mitsubishi Heavy Industries [20] utilises this control and has been demonstrated in the MWT 167H/7.0 (formerly the SeaAngel)). This paper describes the displacement control using Electrohydraulic Stroke Control installed on the pump.
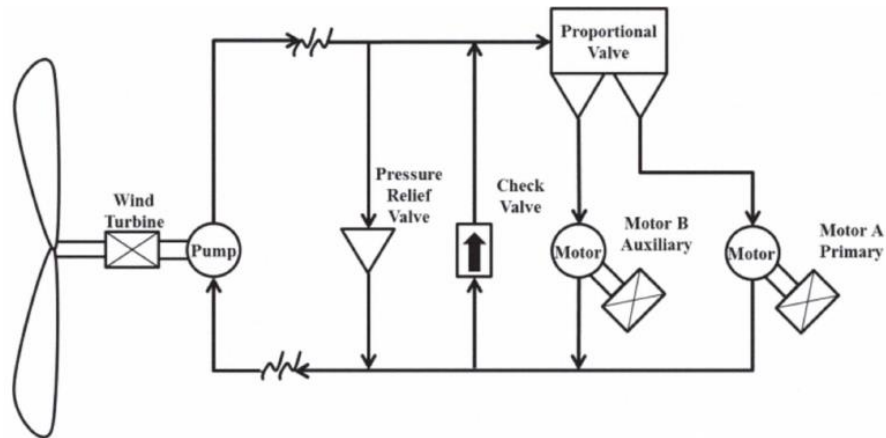
Figure 2.7 Schematic of hydraulic transmission system of a wind turbine [21].

Further studies on hydraulics for wind turbines include work by Sina Hamzehlouia and Afshin Izadian [21]. Their work involved the development of a mathematical model of a hydraulic wind power transmission system. Hydraulic transmission uses the hydraulic pump to convert the mechanical input energy into pressurized fluid. Hydraulic hoses and steel pipes are used to transfer the harvested energy to the hydraulic motors.

2.3.3 Magnetic Drivetrains

Magnetic gears use magnets to transmit torque between an input and an output shaft without physical contact between them. Advances in magnetic gears have resulted in their torque transmission capability becoming competitive to that of mechanical gears whilst providing significant operational advantages [22]. A combination of a magnetic gear and an electrical machine creates a "pseudo" direct drive system capable of producing high torque densities.

A study by K. Atallah et. al. [23] from the University of Sheffield investigates a "pseudo" direct drive machine which combines a magnetic gear and

electrical machines both magnetically and mechanically. A cross section of the machine is shown in Figure 2.8.
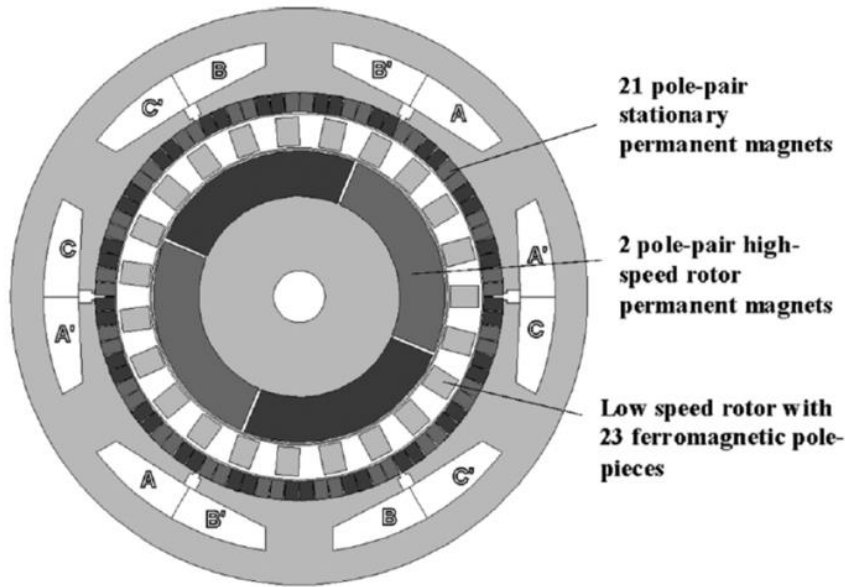
Figure 2.8 Radial (left) and axial (right) cross section of "pseudo" direct drive machine [23].

In order that a constant torque is transmitted between the components in the system, the relationship between the number of pole-pairs and pole-pieces must follow the equation below:

$$p_i + p_o = n_p \tag{2.1}$$

where p_i is the number of pole-pairs on the inner permanent magnet array (in Figure 2.8 this is indicated as 2 pole-pairs located on the high speed rotor), p_o is the number of pole-pairs on the outer permanent magnet array (in Figure 2.8 this is indicated as 21 pole-pairs fixed on the stationary outer ring), and n_p is the number of ferro-magnetic pole-pieces on the intermediate annular component which is the modulating component (in Figure 2.8 this is indicated as 23 pole-pieces) [24].

Speeds of the different components in the gear are related by the following equation:

$$p_i \omega_i + p_o \omega_o = n_p \omega_p \tag{2.2}$$

where ω_i is the speed of the inner permanent magnet array, ω_o is the speed of the outer permanent magnet array, and ω_p is the speed of the modulating component.

The UK company, Magnomatics® has developed magnetic gearing technology which, according to simulation, has the capability of transmitting toque density of the order of 50-150 kNm/m³ comparable to that of two and three stage helical gearboxes [25]. Their design incorporates the magnetic gear technology with a brushless permanent magnet generator. Three main components of the design are as follows:

1. Outer stator, comprising a lamination pack with copper windings, and stationary outer magnets.

2. Inner permanent magnet array rotating at high speed with no external mechanical connection.

3. Intermediate annular component, the modulating rotor with ferro-magnetic pole-pieces, rotating at low speed and connected to the input shaft of the generator.

Magnomatics® are currently involved in projects to bring this technology into wind [26] and marine [27] applications which can potentially provide efficient and reliable alternatives to conventional drive trains.

2.3.4 Permanent magnet generators

The use of permanent magnets in wind turbines has both benefits and disadvantages. It provides efficient designs with high energy yield, yet the price of magnets is very volatile and so PMGs can be considered a risky development.

Many authors have investigated the design of permanent magnet generators over the past few decades including Gruars [28], Spooner [29], Dubois [30][31], Bumby [32] and Muljadi [33]. Although for smaller machines, a study by Spooner [29], presents the use of buried ferrite magnets to reduce costs associated with rare-earth magnets and a modular design. The use of a modular arrangement benefits the assembly process as it avoids the need to bring together two large components with large magnetic fields present. This benefit was further explored by Muljadi [33] where the use of permanent magnets and a modular arrangement is combined with

torus formed winding to enable ease of assembly. Benefits of the design include the ability to replace a failed module quickly or even bypass the module to minimise turbine downtime. The paper does not consider the COE for such designs but does highlight a number of advantages to using such a design such as the enhanced repair processes that can be achieved. It does not quantify the failure rates and repair time savings, so a more detailed approached could be applied to improve the conclusions of the generator benefits and limitations.

Bumby [32] described the benefits of using trapezoidal magnets and coils for an air-cored axial flux , namely that it can provide a compact design as the active area of the generator is decoupled from its diameter. The paper looks at a 2.5 kW vertical axis wind turbine and even though it provides a useful design for small machines, it does not indicate how the design would scale for high power wind turbines or include an analysis of a horizontal axis wind turbine.

2.3.5 "Multibrid" technology

Introducing a geared stage to a PMG will allow smaller generator diameters to be used and so can offer a solution to the issue with high capital cost associated with a direct drive option [2]. Work by Li, Chen and Polinder [34], investigates the optimisation of a PMG including "multibrid" technology that integrates the generator, gearbox, main shaft and bearing into a common housing. Some limitations of this method include the gearbox weight and cost estimates. The gearbox weight is estimated with a weight factor that is calculated using gear ratios and torque. It does not consider the dimensions of the gearbox or details such as the number of teeth and face width. The losses are also assumed to be 1.5 % of the power for a single-stage and so there is no design specific dependence for the gearbox that would allow a number of variations to be produced.

2.3.6 Direct drive generators and structural challenges

The benefits of using a direct drive system in place of a high-speed generator include the removal of the gearbox and increased efficiency. There are many challenges

faced with creating large direct drive generators. This includes trying to create a lightweight, yet structurally sound supportive structure that is able to withstand the high torque produced by the generator.

Dubois [30] offered a detailed analysis of direct drive generators based on torque density and a cost/Nm. The paper is based on the analysis and cost of the active materials only and does not include a structural cost or a lifetime COE analysis that would be essential for wind farm cost modelling.

Work by Grauers [28] offers a cost estimate of the generator structure C_{str} based on the length and diameter of a reference structure so that:

$$C_{str} = \frac{c_{str}}{2}\left[\left(\frac{d_{se}}{d_{ref}}\right)^a + \left(\frac{l_{tot}}{l_{ref}}\right)^a\right] \qquad (2.3)$$

where c_{str}, d_{ref} and l_{ref} are the cost, diameter and length of a reference structure respectively, a is a constant set at 3 and d_{se} and l_{tot} are the diameter and length of the generator. This method requires a reference cost and also does not indicate any structural information such as forces and deflection which would be dependent on torque/operating speed. An alternative method of designing a structure would help improve this cost estimate method and link directly to the design of the generator and its operating strategy.

A study by A. Zavvos, A.S. McDonald and M. Mueller in [35] investigates minimising the structural mass of a direct drive generator using an analytical and finite element analysis optimisation technique. The variables used in the optimisation process are shown in Figure 2.9. The effect on the structural mass of the generator for various structural dimensions was calculated whilst maintaining the structure's aspect ratio of the length being half the radius. Although the support structure of the generator is not the focus of the work in this thesis, the sizing was based on similar principles and a deflection model which is explained in more detail in Chapter 3. Work by McDonald focuses on detailed structural analysis of various direct drive topologies [36].
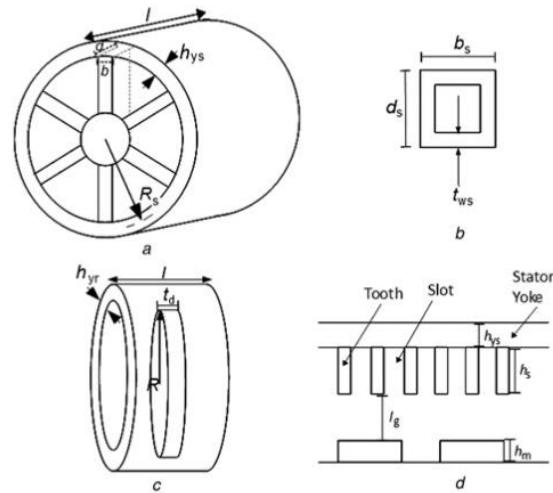
Figure 2.9 – Diagram illustrating the dimensions of the variables used to optimise the structure of each of the generators studied in [35].

An example of a mainstream direct drive wind turbine with a permanent magnet generator is the Siemens SWT-6.0-154 where details can be seen in Table 2.1.

Table 2.1 Details of the Siemens 6MW direct drive wind turbine.

Specification	Data
Manufacturer and Model	Siemens SWT-6.0-154
Rated Power	6 MW
Cut in wind speed	3 m/s
Rated wind speed	12 m/s
Cut out wind speed	25 m/s
Diameter of rotor	154 m
Generator type	Synchronous, Permanent magnet
Generator power	6 MW
Generator rated speed	11 rpm
Output voltage	690 V

The Siemens SWT-6.0-154 is a well-established direct drive wind turbine for use in the offshore environment and so provided the inspirations for modelling PMG with both geared and a direct drive power trains in order to assess the benefits of the removal if the gearbox. There are higher power machines available such as Siemens

SG 8.0-167 DD and SWT-7.0-154, but for the purposes of comparison and for mainstream power ratings for offshore, this thesis will only focus of 6 MW ratings.

Due to limiting factors such as weight and logistics, a reasonable design constraint for direct drive generator could include a maximum total weight of <100 t and a maximum external diameter of 8 m [37]. Although there are other possible sizes and weights, this limit takes into account the capabilities of transport and lifting equipment in most cases.

2.4 Gearbox loss and sizing methods

Gearbox losses are mechanical losses resulting from the speed conversion of the low speed shaft of the wind turbine rotor to the high-speed shaft of the generator. They are primarily due to tooth contact losses and viscous oil losses [38][39]. A basic approximation of gearbox losses assumes a viscous loss of 1% of rated power per stage [38]. Higher speed gearboxes allow smaller generators to be used and so by allowing a variety of design to be produced, a greater range of possible designs can be analysed to assess the benefits and limitation of each.

Gearbox efficiency η_{gear} can therefore be modelled using the following equation:

$$\eta_{gear} = \frac{P_m - (0.01)qP_{mR}}{P_m} \times 100 \qquad (2.4)$$

where P_m is the turbine power, q is the number of gearbox stages, and P_{mR} is the rated power of the wind turbine [38]. Figure 2.10 shows a graph of gearbox efficiencies for a single, two and three stages gearbox based on equation (2.4).
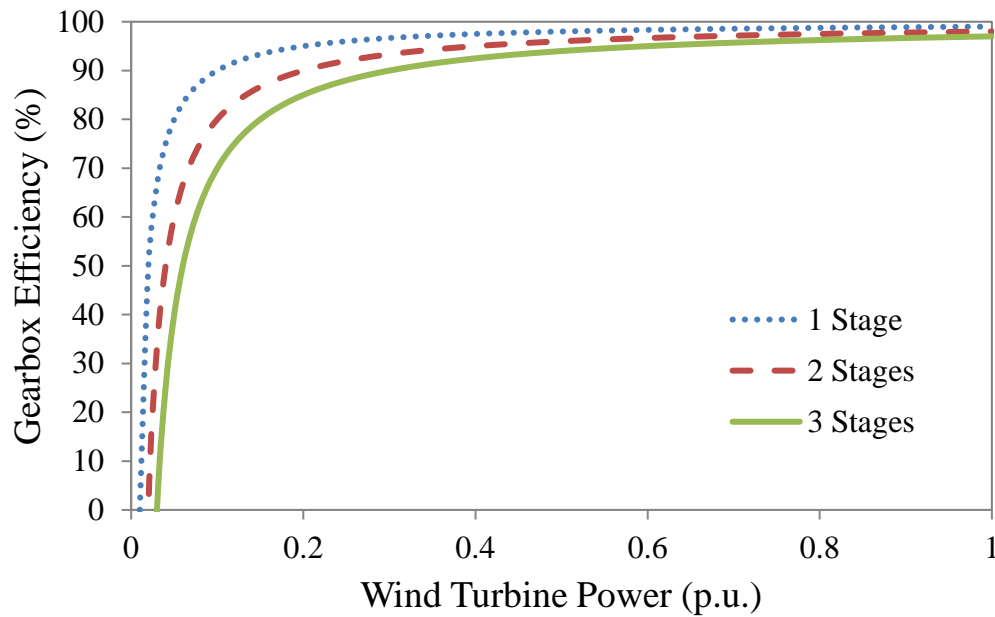
Figure 2.10 – Graph of gearbox efficiency for a single, two and three stage gearbox.

Despite being a crude approximation, this method of gearbox efficiency estimation serves well for basic wind turbine loss modelling calculations. However, for a more design specific loss estimate, a more robust loss calculation method is required. Chapters 3 and 4 outline a much more substantial method of calculating losses that also includes a number of stress limiting factors which allow complete gearbox systems to be designed. This will vastly improve the loss and cost estimates of the system as it will depend on the sizing and operational speed of the gearbox and not a simple "one size fits all" assumption.

2.5 Failure rates and repair costs

Failure rates and repair costs for offshore wind energy are not currently available for a full lifetime assessment due to its infancy in mainstream operation. This is even more limited for permanent magnet generators (PMGs) which are still a new and developing technology. Efforts have been made in publications such as [40],[41],[42] to provide estimates of failure rates, reliability and associated costs for various wind farm models. Some work by Carroll [43],[44] has involved adjusting some already

available failure data for onshore wind turbines into values that can be assumed for an offshore environment.

Most literature (e.g. Tavner, Spinato, Faulstich) focuses on failure rates and downtime of each "lumped" component of the entire wind turbine such as "generator", "gearbox", "yaw" and "hydraulic system". Specific component details and failure modes of each of these parts is not provided. In order to create a design-specific based failure rate analysis, the specific failure modes associated with the drive train have to be identified and quantified in order to represent the most vulnerable and expensive problems that can occur within each section of the drive train.

2.5.1 Failure rates based on drive train types

As this study involves as a direct comparison between geared and direct drive designs, it is important to use suitable estimates to reflect the design differences of these two drive trains.

A detailed study by M. D. Reder [40] provides some data that distinguishes between the failure rates of DFIG and Synchronous generator based wind turbines. The geared designs are all DFIG so for direct comparison with PMGs it can only provide a basic level of comparison. It provides useful information about the complete system failure rates for wind turbines greater than 1 MW rated power. These failure rates are shown in Figure 2.11 and Figure 2.12 below.
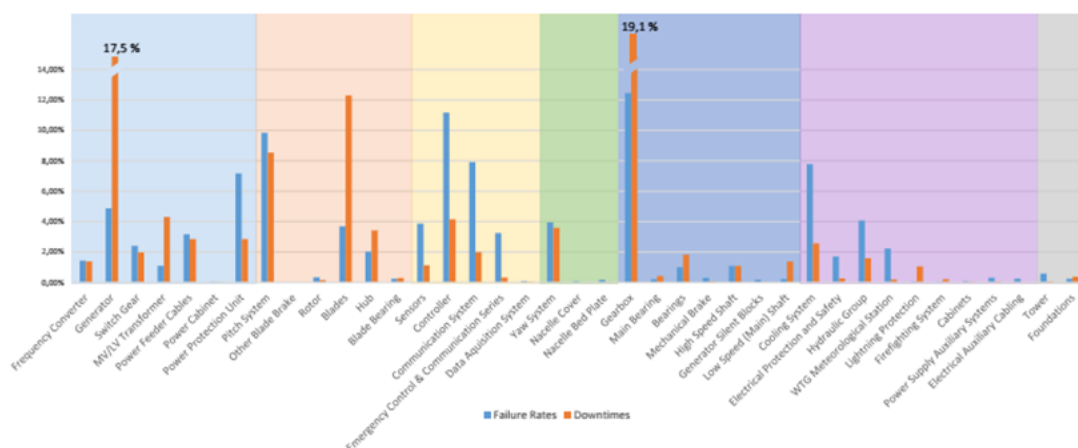
Figure 2.11 Normalised failure rates and downtimes for geared wind turbines >1MW. Taken from [40].
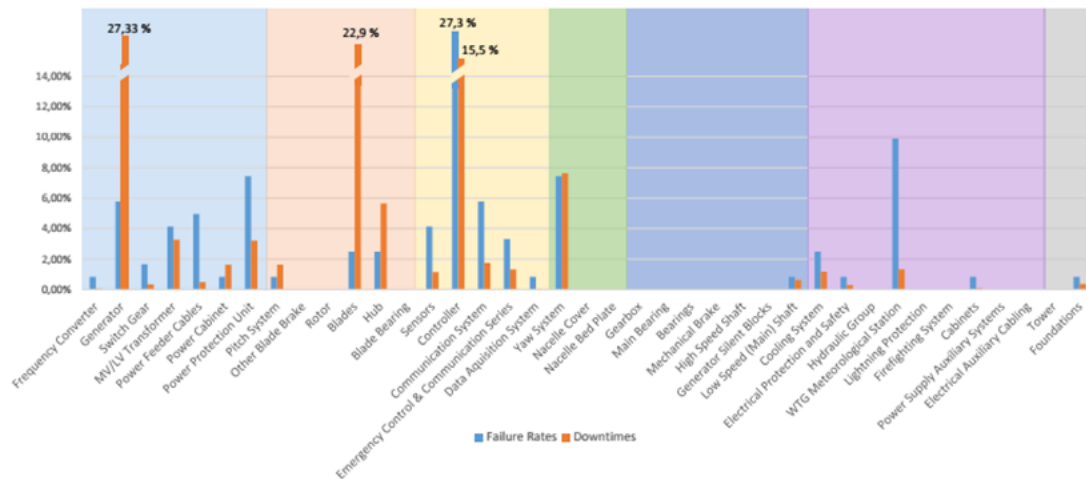
Figure 2.12 Normalised failure rates and downtimes for direct drive wind turbines. Taken from [40].

A study by T. M. Delorm [45] offers a comparison of failure rates of wind turbine sub-assemblies for both geared and direct drive wind turbines with permanent magnet generators in an offshore environment with drive train types shown in Figure 2.13. This paper presents data for industrial onshore wind turbine technologies that are adjusted for the offshore environment.

Concept type	Drive train architecture	Example manufacturers	Example turbine models	Example powers (MW)
Type 1	Three-stage gearbox with IG and fully rated converter	Siemens	SWT-3.6-107	3.60
			SWT-3.6-120	3.60
			SWT-3.6-130	4.00
Type 2	Three-stage gearbox with DFIG and partially rated converter	Vestas	V90-3.0	3.00
		Senvion	5M	5.00
			6.2M126	6.15
			6.2M152	6.15
Type 3	One- or two-stage gearbox with PMG and fully rated converter	Vestas	V112-3.3	3.30
			V164-8.0MW	8.00
		Areva	M5000-116	5.00
			M5000-135	5.00
Type 4	PMG direct drive with fully rated converter	Nordex	N150 6000	6.0
Type 5	PMG direct drive with two fully rated active redundant converters	New product	–	6.0

IG: induction generator; DFIG: doubly fed induction generator; PMG: permanent magnet generator.

Figure 2.13 Examples of drive train types. Taken from [45].

It can be seen from Figure 2.13 that turbines from the Type 3 and Type 4 category such as the Areva M5000-135 and Nordex N150 6000 have drive trains with the same topology type as those that will be considered in this thesis. The results from [45] provide the closest estimate for modelling specifically PMGs for offshore wind

turbines and so values from this paper were used as base case values to create design specific failure rates. The details are outlined in Chapter 3.
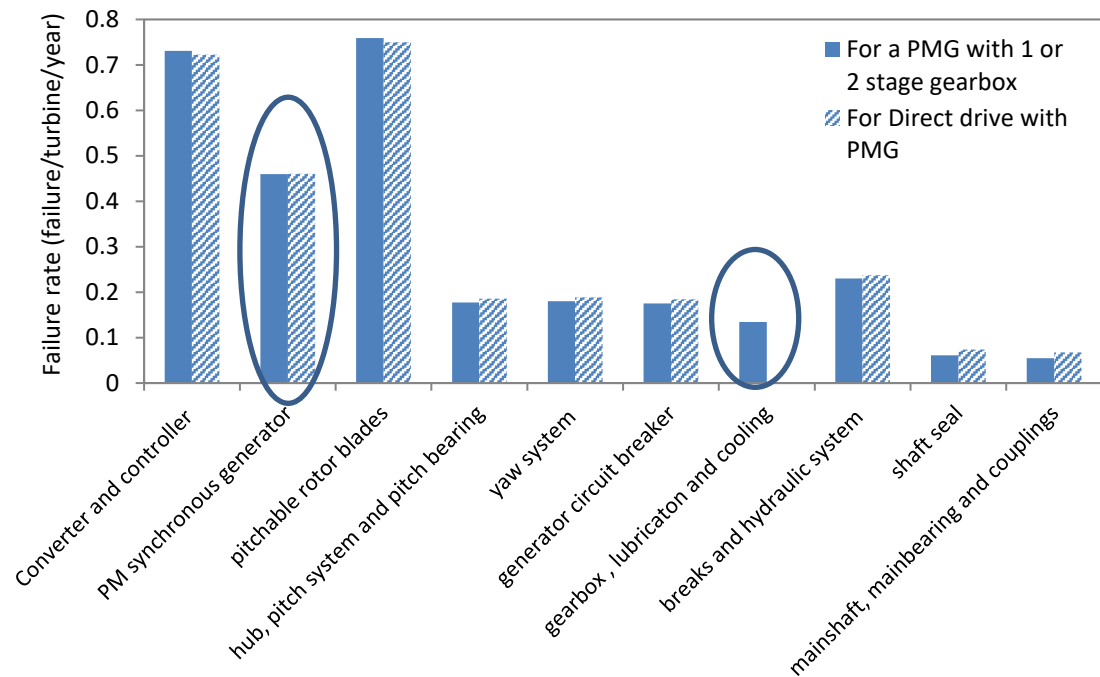
Figure 2.14 Summaries the failure rate differences between geared and direct drive PMG drive trains and highlights the generator and gearbox that make up the main part of the modelling. Adapted from [45].

From Figure 2.14, it is clear that failures associated with the controller and the rotor are the most significant, but since this thesis focuses only on drive train designs, the failures associated with the rest of the wind turbines are kept constant. Looking at only the gearbox and generator from Figure 2.14, the failure rate values here can be used as base case values and altered with the design.

Table 2.2 Base assumptions taken from [45] to be used in Chapter 3.

	Failure rates for offshore wind (failure/turbine/year)	
	Geared PMG wind turbine	Direct drive PMG wind turbine
Generator	0.46	0.46
Gearbox, lubrication and cooling	0.134	-
All other sub-assemblies	2.368	2.410
Total system failure rate	2.962	2.87

From Table 2.2 the generator failure rates appear to be constant between geared and direct drive PMG with the geared design to be assumed mainly single stage gearbox. The values currently do no distinguish between 1, 2 and 3 stage gearbox variations, nor do they include any design specific failure rate dependencies. Therefore, further adaptation is required in order to obtain failure rates that reflect certain design considerations. Details of the method to adapt these values to a more appropriate representation of the generator dimensions are outlined in Chapter 3.

2.5.2 Repair costs and downtime

A study by Carroll [44] looks at associating a failure with a cost and repair time. The method breaks up the failure type into repair options which are minor repair, major repair and major replacement.

	Minor Repair	Major Repair	Major Replacement
DFIG	0.091	0.030	0.002
PMG	0.074	0.002	0.000
PRC	0.069	0.037	0.001
FRC	0.440	0.139	0.014
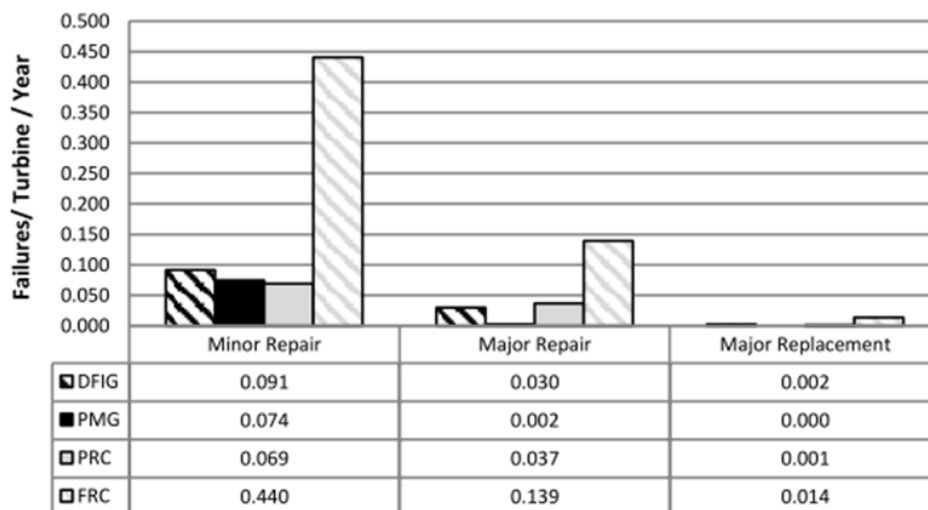
Figure 2.15 Failures per turbine per year for each failure type of generator and converter types. Taken from [44].

A comparison by Carroll [44] of failures rates of a doubly-fed induction generator (DFIG), and permanent magnet generator (PMG), a partially rated converter (PRC) and a fully rated converter (FRC) are shown in Figure 2.15. It can be seen that there are no major replacements for the PMG which is based on a limited data set and so it is possible for a complete generator replacement to occur, but it is not part of the

base case in this study. A sensitivity to include a major replacement is presented in Chapter 4 to assess the financial implications.

Carroll's work also includes a detailed analysis of repair time and technician requirements that provide a comprehensive model for complete repair costs under a number of different scenarios. The values used in parts of the models are based on various assumptions due to the limited data for certain topologies but offers suitable estimates that can be applied to all drive train types. For example, the repair times and number of technicians required for each failure type are assumed the same across all drive train types. This assumption is maintained in this thesis too as the difference between failures for each drive train is based on the dimensions of the drive train itself. Therefore, various overall O&M costs are represented by drive train dimensions and so can be considered design specific.

2.6 Leading offshore wind turbine manufacturers

Most current large wind turbines consist of permanent magnet generators for offshore wind installations. The following 4 examples show the leading manufacturer's current portfolio of high-power offshore wind turbines:

- MHI Vestas are paving the way for high power offshore wind with their V164-9.5 MW™ wind turbine rated at 9.5 MW. The turbine consists of a permanent magnet generator with medium-speed drive train with a strengthened gearbox.

- The Siemens Gamesa SG 8.0-167 DD wind turbine is high power direct drive turbine exclusively for offshore. It has a permanent magnet generator with a power rating of 8 MW.

- The Haliade 150-6MW by GE Renewable Energy is a 6MW offshore wind turbine that utilises its Pure Torque technology which is based on optimised torque pathways through the frame rather than through the drive train. This method provides improved reliability.

- The Goldwind GW 154/6.7MW offshore wind turbine is another direct drive wind turbine with permanent magnet generator (Goldwind's PMDD turbine technology).

Therefore, it is apparent that the use of permanent magnet generators are becoming more widespread compared to other generator types for modern large offshore turbines. The reliability and efficiency improvements are the key drivers in keeping maintenance costs down for the harsh sea environment.

2.7 Summary of Chapter 2

This chapter outlined various studies that cover the complete range of COE evaluation for offshore wind turbines focusing primarily on the drive train. It was clear from work by Polinder, Carrol, Tavner, Spinato and Faulstich, that despite having detailed analysis of particular aspects of wind energy cost and reliability, no complete method for drive train design-based optimisation exists when calculating COE.

It can be concluded that to collate a number of methods into one model and create a number of reasonable assumptions, a more comprehensive drive train design model can be developed. The main aspects to include in the models for this thesis can be summarized as follows:

1. To include a detailed gearbox model that includes dimensions and stress calculations compared with the commonly used "one size fits all" approached from the discussed literature. This approach will allow variations between gearbox and generator to be explored and a larger design space to be adopted.

2. To have failure rates based on the drive train topology with design specific values. The failure rate data from the discussed literature is based on large data sets from a number of different wind turbines from various environments: there is no way to tell which value corresponds to a specific drive train topology and design. Including a failure rate that is linked with features such as generator diameter, will allow models to be constrained beyond simply initial capital cost and will look into the long term implications such a design in terms of maintenance.

3. To include an optimisation process that covers material price fluctuations and uncertainty whilst incorporating the above 2 aspects. This will allow the

detailed model to be fully analysed for various cost assumptions which will cover most likelihoods of material prices that may pose risks to the project.

Based on the current offshore PMG wind turbines market and major manufacturers design trends, the analysis of PMGs in terms of uncertainty is extremely important for keeping the COE as low as possible. This thesis aims to provide answers and a sensitivity analysis for PMGs with different drive train designs and really create a starting point for a comprehensive design based COE model that not only considers costs, but detailed reliability analysis.

2.8 References for Chapter 2

[1]   G. Bywaters, V. John, J. Lynch, P. Mattila, G. Norton, and J. Stowell, "WindPACT Drive Train Alternative Design Study Report," *National Renewable Energy Lab. (NREL) Technical Report*. 2005.

[2]   H. Polinder, F. F. A. Van Der Pijl, G. J. De Vilder, and P. J. Tavner, "Comparison of direct-drive and geared generator concepts for wind turbines," *IEEE Trans. Energy Convers.*, vol. 21, no. 3, pp. 725–733, 2006.

[3]   S. Alshibani, V. G. Agelidis, and R. Dutta, "Lifetime cost assessment of permanent magnet synchronous generators for mw level wind turbines," *IEEE Trans. Sustain. Energy*, vol. 5, no. 1, pp. 10–17, 2014.

[4]   D.-M. Valcan, P. C. Kjar, L. Helle, S. Sahukari, M. Haj-Maharsi, and S. Singh, "Cost of energy assessment methodology for offshore AC and DC wind power plants," *2012 13th Int. Conf. Optim. Electr. Electron. Equip.*, pp. 919–928, May 2012.

[5]   K. Hart, A. McDonald, H. Polinder, E. Corr, and J. Carroll, "Improved cost of energy comparison of permanent magnet generators for large offshore wind turbines," *EWEA Conf. Proc.*, 2014.

[6]   K. Cory and P. Schwabe, "Wind Levelized Cost of Energy : A Comparison of Technical and Financing Input Variables Wind Levelized," *Tech. Rep.*, vol. NREL/TP-6A, no. October, 2009.

[7]   P. Heptonstall, R. Gross, P. Greenacre, and T. Cockerill, "The cost of offshore wind: Understanding the past and projecting the future," *Energy Policy*, vol. 41, pp. 815–821, Feb. 2012.

[8]   L. Fingersh, M. Hand, and A. Laxson, "Wind Turbine Design Cost and Scaling Model," *Tech. Rep.*, vol. 29, no. December, pp. 1–43, 2006.

[9]   C. Mone, M. Hand, M. Bolinger, J. Rand, D. Heimiller, and J. Ho, "2015 Cost of Wind Energy Review NREL/TP-6A20-66861," 2015.

[10]   Oxford Institute for Energy Studies, "Auctions for allocation of offshore wind

contracts for difference in the UK," *OIES Pap. EL 33*, 2019.

[11]   "Analysis: UK auction reveals offshore wind cheaper than new gas, Carbon Brief." [Online]. Available: https://www.carbonbrief.org/analysis-uk-auction-offshore-wind-cheaper-than-new-gas. [Accessed: 26-Aug-2018].

[12]   H. Li and Z. Chen, "Design optimization and evaluation of different wind generator systems," *Electr. Mach. Syst. 2008. ICEMS 2008. Int. Conf.*, pp. 2396–2401, 2009.

[13]   O. Anaya-Lara, N. Jenkins, and J. Ekanayake, *Wind energy generation: modelling and control*. ISBN: 978-0-470-71433-1, Wiley, 2011.

[14]   G. Ramtharan, A. Arulampalam, J. B. Ekanayake, F. M. Hughes, and N. Jenkins, "Fault ride through of fully rated converter wind turbines with AC and DC transmission systems," *IET Renew. Power Gener.*, 2009.

[15]   H. Polinder, J. A. Ferreira, B. B. Jensen, A. B. Abrahamsen, K. Atallah, and R. A. McMahon, "Trends in wind turbine generator systems," *IEEE J. Emerg. Sel. Top. Power Electron.*, vol. 1, no. 3, pp. 174–185, 2013.

[16]   O. Keysan and M. A. Mueller, "A transverse flux high-temperature superconducting generator topology for large direct drive wind turbines," in *Physics Procedia*, 2012.

[17]   O. Keysan and M. A. Mueller, "Superconducting generators for renewable energy applications," 2012.

[18]   J. Wang, R. Qu, and Y. Liu, "Comparison study of superconducting generators with multiphase armature windings for large-scale direct-drive wind turbines," *IEEE Trans. Appl. Supercond.*, vol. 23, no. 3, 2013.

[19]   J. Cidrás and C. Carrillo, "Regulation of synchronous generators by means of hydrostatic transmissions," *IEEE Trans. Power Syst.*, vol. 15, pp. 771–778, 2000.

[20]   Windpower Engineering, "OEM begins test on what could be 7 MW hydraulic drive train," 2013. [Online]. Available: https://www.windpowerengineering.com/design/oem-begins-test-on-what-could-be-7-mw-hydraulic-drive-train/.

[21]   S. Hamzehlouia and A. Izadian, "Modeling of hydraulic wind power transfers," in *2012 IEEE Power and Energy Conference at Illinois, PECI 2012*, 2012, pp. 1–6.

[22]   P. M. Tlali, R. J. Wang, and S. Gerber, "Magnetic gear technologies: A review," in *Proceedings - 2014 International Conference on Electrical Machines, ICEM 2014*, 2014.

[23]   K. Atallah, J. Rens, S. Mezani, and D. Howe, "A novel 'pseudo' direct-drive brushless permanent magnet machine," in *IEEE Transactions on Magnetics*, 2008, vol. 44, no. 11 PART 2, pp. 4349–4352.

[24]   J. Häfner, B. Jacobson, and ABB, "Proactive Hybrid HVDC Breakers - A key innovation for reliable HVDC grids," *Electr. power Syst. Futur. Integr. supergrids microgrids Int. Symp. Bol. , Italy*, 2011.

[25] P. Jamieson, *Innovation in wind turbine design*. John Wiley & Sons Ltd, 2011.

[26] OffshoreWIND.biz, "Norvento Begins Testing New Offshore Wind Turbine Prototype," 2019. [Online]. Available: https://www.offshorewind.biz/2019/03/19/norvento-begins-testing-new-offshore-wind-turbine-prototype/.

[27] Business Up North, "Sheffield-Based Magnomatics Making Waves With Marine Turbine Project," 2018. [Online]. Available: https://www.businessupnorth.co.uk/sheffield-based-magnomatics-making-waves-marine-turbine-project/.

[28] A. Grauers, "Design of Direct-driven Permanent-magnet Generators for Wind Turbines," *Thesis, Chalmers University of Technology*. 1996.

[29] E. Spooner and A. Williamson, "Modular, permanent-magnet wind-turbine generators," *IAS '96. Conf. Rec. 1996 IEEE Ind. Appl. Conf. Thirty-First IAS Annu. Meet.*, vol. 1, pp. 497–502, 1996.

[30] M. R. Dubois, H. Polinder, and J. A. Ferreira, "Comparison of generator topologies for direct-drive wind turbines," *Conf. Pap.*, 2000.

[31] M. Dubois, "Optimized permanent magnet generator topologies for direct-drive wind turbines," *Conference Paper*. 2004.

[32] J. R. Bumby, N. Stannard, J. Dominy, and N. McLeod, "A permanent magnet generator for small scale wind and water turbines," *2008 18th Int. Conf. Electr. Mach.*, no. 1, pp. 1–6, 2008.

[33] E. Muljadi, C. P. Butterfield, and Y. H. Wan, "Axial-flux modular permanent-magnet generator with a toroidal winding for wind-turbine applications," *IEEE Trans. Ind. Appl.*, vol. 35, no. 4, pp. 831–836, 1999.

[34] H. Polinder, "Optimization of Multibrid Permanent-Magnet Wind Generator Systems," *IEEE Trans. Energy Convers.*, vol. 24, no. 1, pp. 82–92, Mar. 2009.

[35] M. Mueller, A. Zavvos, and A. McDonald, "Optimisation tools for large permanent magnet generators for direct drive wind turbines," *IET Renew. Power Gener.*, vol. 7, no. 2, pp. 163–171, Mar. 2013.

[36] A. S. Mcdonald, "Structural analysis of low speed, high torque electrical generators for direct drive renewable energy converters," PhD Thesis University of Edinburgh, 2008.

[37] R. Scott Semken *et al.*, "Direct-drive permanent magnet generators for high-power wind turbines: benefits and limiting factors," *IET Renew. Power Gener.*, vol. 6, no. 1, p. 1, 2012.

[38] S. M. Muyeen, *Wind Energy Conversion Systems*. London: Springer London, 2012.

[39] P. M. T. Marques, C. M. C. G. Fernandes, R. C. Martins, and J. H. O. Seabra, "Efficiency of a gearbox lubricated with wind turbine gear oils," *Tribol. Int.*, 2014.

[40] M. D. Reder, E. Gonzalez, and J. J. Melero, "Wind Turbine Failures - Tackling current Problems in Failure Data Analysis," *J. Phys. Conf. Ser.*, vol.

753, no. 7, 2016.

[41]   M. N. Scheu, A. Kolios, T. Fischer, and F. Brennan, "Influence of statistical uncertainty of component reliability estimations on offshore wind farm availability," *Reliab. Eng. Syst. Saf.*, vol. 168, no. May, pp. 28–39, 2017.

[42]   F. Spinato, P. J. Tavner, G. J. W. van Bussel, and E. Koutoulakos, "Reliability of wind turbine subassemblies," *IET Renew. Power Gener.*, vol. 3, no. 4, p. 387, 2009.

[43]   J. Carroll, A. McDonald, and D. McMillan, "Failure rate, repair time and unscheduled O&M cost analysis of offshore wind turbines," *Wind Energy*, vol. 19, no. 6, pp. 1107–1119, 2016.

[44]   J. Carroll, "Cost of energy modelling and reduction opportunities for offshore wind turbines," PhD Thesis, University of Strathclyde, 2016.

[45]   T. M. Delorm, Y. Lu, A. Christou, and P. McCluskey, "Comparisons of offshore wind turbine reliability," *Proc. Inst. Mech. Eng. Part O J. Risk Reliab.*, vol. 230, no. 3, pp. 251–264, 2016.

Chapter 3 Cost of Energy Modelling and Base Case

This chapter introduces and develops models for assessing the annual energy production, capital costs and operational and maintenance costs for different drive train designs in offshore wind turbines. This information is brought together in a lifetime cost per MWh of energy produced metric. This is a fair means of comparison between competing designs and represents the design goal of the end consumer.

Common features of the different drive trains and the baseline wind turbine are presented alongside models of losses, costs and downtime which vary with a number of drive train independent design variables. These models are a mixture of established and new models in the context of offshore wind (i.e. gearbox loss modelling, gearbox cost modelling, drive train O&M costs and availability modelling) which fill some of the gaps identified in Chapter 2. The cost of energy for four different baseline drive trains is calculated using these models setting up the rest of the thesis where uncertainty in and optimisation of the drive train is explored further.

3.1 Cost of Energy Equation

The calculation of the COE for wind is described in various publications such as the detailed breakdown shown in [1],[2][3] and [4]. The key variables used in this thesis are suitably represented in equation (3.1) and so this calculation was used for all designs throughout the presented models.

$$COE = \frac{(FCR \times ICC) + AOM}{AEP} \qquad (3.1)$$

where,

COE = cost of energy in €/MWh (€/megawatt-hour)

FCR = fixed charge rate in % (which allows for the inclusion of additional financial costs such as interest on debt and money set aside each year)

ICC = initial capital cost in €

AOM = annual operations and maintenance cost in €/year

AEP = annual energy production in MWh

The COE equation is further illustrated in Figure 3.1 which presents a flow chart of the main elements that calculate the cost of energy.
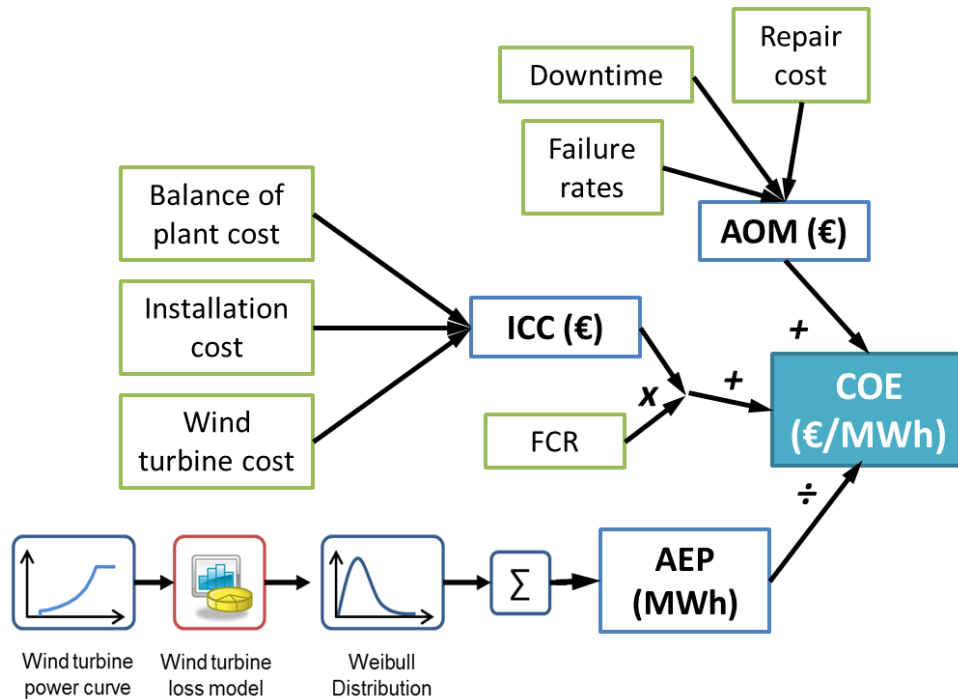
Figure 3.1 Flow chart of the COE equation.

3.2 Annual Energy Production (AEP)

The electricity generated by a wind turbine over one year is known as Annual Energy Production (AEP). Maximising this yield is a key component in the design of wind turbines. This section outlines the process of extracting energy from the wind and the subsequent losses experienced within the drive train.

3.2.1 Wind Turbine Aerodynamics and wind resource

Wind turbines extract power in the wind by converting kinetic energy into pressure energy at the rotor plane. The maximum available power in the wind [5] is given by the following:

$$P = \frac{1}{2}\rho\pi r^2 v^3 \tag{3.2}$$

where, ρ is the air density, r is the rotor radius and v is the wind speed.

The power output from a wind turbine is given by:

$$P = \frac{1}{2}\rho\pi r^2 v^3 C_p \tag{3.3}$$

where C_p is the power coefficient (or aerodynamic efficiency where curves can be seen in Figure 3.2) which is a function of tip speed ratio λ and pitch angle θ. However, the fundamental limit of the power that can be extracted from a wind turbine is governed by the Betz limit in which the power coefficient has a maximum value of 16/27 or 0.593. This means that at maximum efficiency, the energy extracted will not exceed 59% of the available energy in the wind. In reality, turbines typically have power coefficients in the range of 0.35 to 0.45.
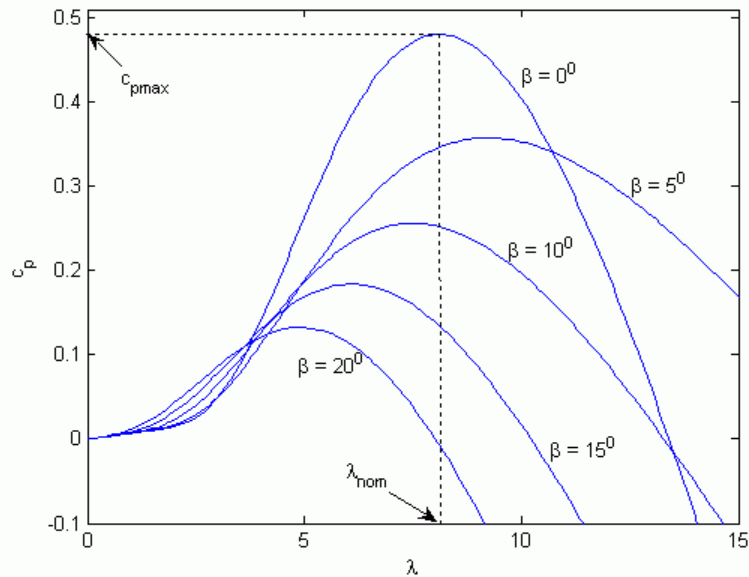
Figure 3.2 $C_p - \lambda$ curves for different pitch angles β. Taken from Matlab documentation [6].

Turbines experience torque on the blades which is given by the power, P divided by the rotational speed, ω of the rotor as follows:

$$T = \frac{P}{\omega} \tag{3.4}$$

and the rotor speed, ω is related to the wind speed through the tip-speed ratio:

$$\lambda = \frac{\omega r}{v} \tag{3.5}$$

From here we get the following relationship for torque:

$$T = \frac{1}{2\lambda} \rho \pi r^3 v^2 C_p \qquad (3.6)$$

Variable speed operation for a wind turbine allows maximum energy to be extracted from the wind by maintaining the maximum power coefficient throughout the operation range.

The torque-speed diagram in Figure 3.3 illustrates an example of maximum C_p tracking and pitch regulated control at rated speed. Above rated wind speed, the operating speed is maintained by generator torque control.
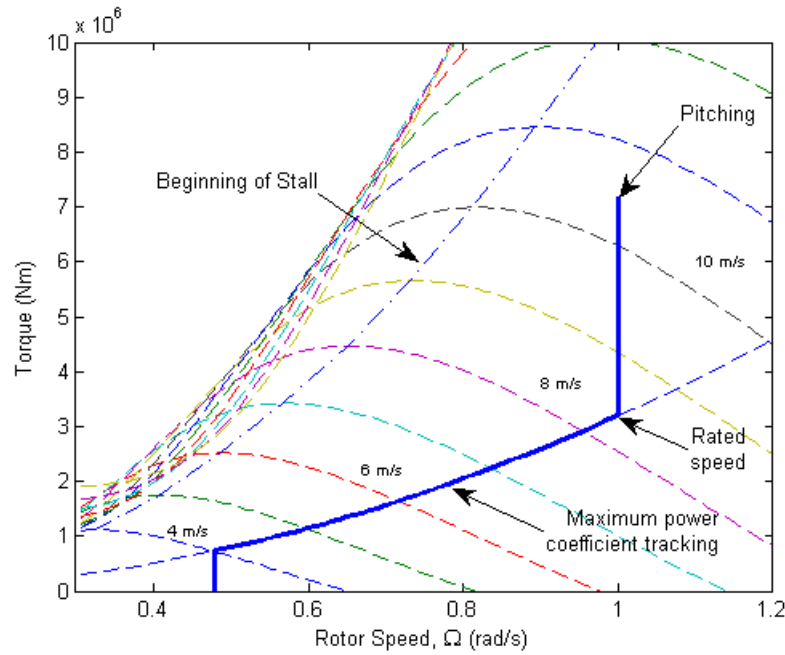
Figure 3.3 Example operating regime showing the torque speed relationship with C_p tracking and pitch control for a variable speed wind turbine (created by author).

The Weibull distribution $p(v)$ can be used to describe the variation in wind speed and is given in equation (3.7) below:

$$p(v) = \frac{k}{C} \left(\frac{v}{C}\right)^{k-1} \exp\left[-\left(\frac{v}{C}\right)^{k}\right] \qquad (3.7)$$

where k is the shape parameter, C is the scale parameter, and v is the wind speed. This distribution offers a suitable fit for wind speeds for various wind sites throughout a year and is a widely accepted method of estimating wind site characteristics.

The annual energy production (AEP) is calculated based on the Weibull probability distribution:

$$AEP = 8760 \int_{v_\text{i}}^{v_\text{c}} P_\text{grid}(v)p(v)dv \qquad (3.8)$$

where v_i is the cut-in wind speed, v_c is the cut-out wind speed if the turbine and 8760 represents the number of hours in a year. The cut-in wind speed is the minimum operating wind speed for turbine operation (Figure 3.4 shows a cut-in speed of 4 m/s) and a cut-out speed is the maximum safe wind speed for operation (typically around 25 m/s).
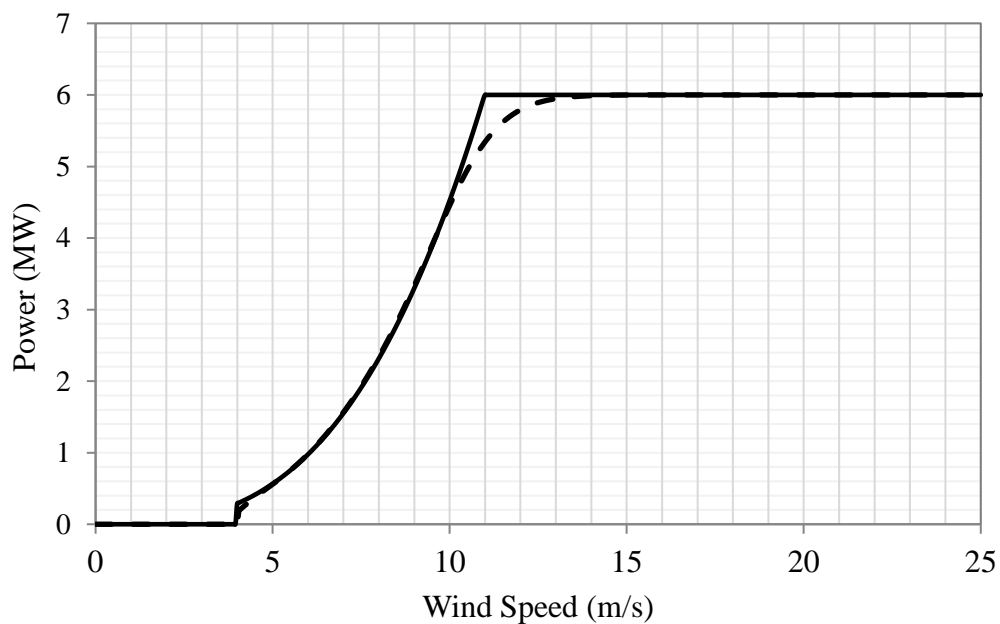
Figure 3.4 Example ideal power curve (solid line) and actual power curve (dashed line) for a 6MW wind turbine.

3.3 Electrical Generator Theory

Having discussed the process of extracting energy from the wind and controlling the operating speed of the wind turbine, the next step in producing electricity from the wind turbine is to use an electrical generator.

Electrical generators produce an electromotive force (e.m.f.) in a coil or conductor through Faraday's Law of Induction. This results from the relative motion

between a magnetic flux and an electrical conductor. In order to generate electrical power, the induced e.m.f. must exist in a closed circuit where current flows.

The magnetic flux density, $\boldsymbol{B}$ (Wb/m^2) is related to the magnetic field intensity by the permeability, μ of the material in which the field is occurring:

$$\boldsymbol{B} = \mu\boldsymbol{H} \tag{3.9}$$

where $\mu=\mu_0\mu_r$ is the permeability (Wb/A-m) made up of the permeability of free space, μ_0 which has a value of $4\pi\times10^{-7}$ Wb/A-m, and the dimensionless relative permeability of the material, μ_r. Magnetic flux Φ (Wb) is the integral of the product of the magnetic field flux density and the cross-sectional area A through which it is directed:

$$\Phi = \int \boldsymbol{B} \cdot d\boldsymbol{A} \tag{3.10}$$

A changing magnetic field induces an electromotive force (EMF), E in a conductor within the field which is described by Faraday's Law of Induction:

$$E = -\frac{d\Phi}{dt} \tag{3.11}$$

A coil in a changing magnetic field with have an EMF induced in it that is proportional to the number of turns, N so that:

$$E = -\frac{d(N\Phi)}{dt} \tag{3.12}$$

A current flowing in a conductor in the presence of a magnetic field will induce a force on the conductor, which is the principle of motors. For generators, a conductor which is forced to move through a magnetic field will have a current induced in it. The force $d\boldsymbol{F}$ in a conductor of incremental length $d\ell$ is given by:

$$d\boldsymbol{F} = Id\ell \times d\boldsymbol{B} \tag{3.13}$$

The windings of an electrical generator introduce resistance into the circuit and so voltage drop is observed.

Details of the magnetic circuit parameters and design considerations for an electrical generator are presented in 3.4.1

3.3.1 Synchronous Generator

A synchronous generator is an AC rotating machine in which its speed (under steady state operation) is proportional to the frequency of the current in the stator. The magnetic field created by the current in the stator rotates at the same speed as the magnetic field created by either the field current on the rotor for wound motor machines or the magnetic field from the permanent magnets for permanent magnet machines. These machines rotate at synchronous speed and so are known as synchronous generators.

Reactive power generated by a synchronous machine can be controlled by changing the magnitude of the rotor field current which is an attractive property for maintaining power system stability.

The relationship between electrical angle and the rotor mechanical angle is proportional to the number of poles, P so that:

$$\theta = \frac{P}{2}\theta_m \tag{3.14}$$

where θ is the electrical angle and θ_m is the rotor rotational angle in radians, and by taking the derivative of each side we get:

$$\omega = \frac{P}{2}\omega_m \tag{3.15}$$

where ω is the electrical angular frequency in electrical radians per second and ω_m is the mechanical angular frequency in radians per second. These equations are linked to the motional emf discussed at the beginning of section 3.3 which ultimately result in the generation of electrical output from a rotational mechanical input.

The stator of a synchronous machine consists of a laminated electrical steel core and a three-phase winding which is made up of coils. The dimensions and arrangement of these generator parts are directly related to the losses which are discussed in greater detail in the following sections.

3.4 Drive Train Loss Modelling

This thesis focuses on the COE of offshore wind based on the drive train design and so only the losses in the drive train are modelled depending on dimensions – all other losses are assumed constant regardless of the drive train topology. Whilst cognisant that other factors such as the structural requirements for the tower and foundation would be linked to variables such as drive train mass, these impacts where not considered as part of the scope.

3.4.1 Generator loss modelling

Modelling the losses in the generator is based on steady state equations for this study. They comprise of copper and iron losses arising from the magnetic field and current carriers. The dimensions of each part of the generator topology are calculated to obtain accurate steady state losses for that particular design. The following equations are used to set up the generator dimensions in order to provide input to the generator loss equations which were taken from work by Polinder [7]. Figure 3.5 illustrates the dimensions of a cross section of a single pole pair and the slots for the full pitching winding arrangement used in the models.
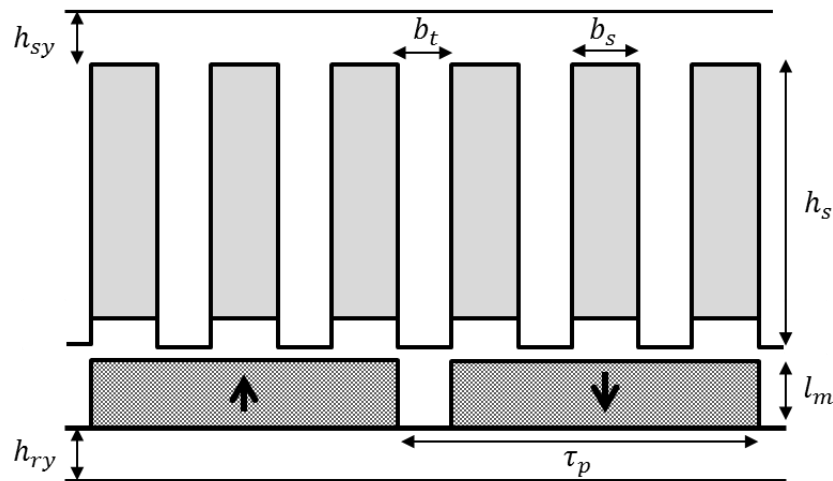
Figure 3.5 Dimensions of a section of permanent magnet generator showing one pole pair (magnets) with full pitch winding arrangement (showing 6 slots and 6 teeth for stator windings). The labelled dimensions are further discussed in the following text. Adapted from [7].

The radius of the outer part of the generator stator is given by:

$$r_m = r_{si} + h_{sy} + h_s \tag{3.16}$$

where, r_{si} is the radius of the inner stator bore, h_{sy} is the height of the stator yoke, and h_s is the height of the stator teeth. Figure 3.5 depicts these dimensions. The radius of the stator at the top of the magnets can be shown as:

$$r_r = r_{si} - g \tag{3.17}$$

where g is the air gap. The slot pitch is calculated as follows:

$$\tau_s = \frac{\pi r_{si}}{mqp} \tag{3.18}$$

where p is the number of poles, q is the number of conductors per slot and m is the number of phases. The slot pitch can also be given by:

$$\tau_s = \frac{\pi D_{si}}{S_n} \tag{3.19}$$

with D_{si} being the diameter of the inner stator bore and S_n being the number of slots. The number of conductors per phase is shown as:

$$N_{cp} = N_{spp}pq \tag{3.20}$$

with N_{spp} being the number of slots per pole per phase. Slot width, b_s is found using the following equation:

$$b_s = b_{sts}\tau_s \tag{3.21}$$

where b_{sts} is the slot width to slot pitch ratio. The width of a stator tooth, b_t is then found as:

$$b_t = \tau_s - b_s \tag{3.22}$$

Flux density always decreases across the slot opening and so an expression must be used in order to obtain a suitable flux density calculation of the air gap. The following equations are largely taken from the work by Polinder [7]. To account for the variation in flux across the slots and stator teeth, the Carter Factor, k_C [8] is used.

$$k_C = \frac{\tau_s}{\tau_s - g_1 \gamma} \tag{3.23}$$

$$g_1 = g + \frac{l_m}{\mu_{rm}} \tag{3.24}$$

$$\gamma = \frac{4}{\pi}\left(\frac{b_{so}}{2g_1}\tan^{-1}\left(\frac{b_{so}}{2g_1}\right) - \ln\sqrt{1 + \left(\frac{b_{so}}{2g_1}\right)^2}\right) \tag{3.25}$$

where l_m is the magnet length in the direction of magnetisation and μ_{rm} is the relative permeability of the magnets. For Neodymium Iron Boron (NdFeB) magnets the relative permeability is ~1.05 [8]. In this model the slot opening width b_{so} is assumed to be equal to the slot width b_s and does not account for tooth edge profile.

Using the Carter Factor, the effect of the slotting of the machine can now be represented as an effective air gap g_{eff}. An estimate of the effective air gap is given by

$$g_{eff} = k_C\left(g + \frac{l_m}{\mu_{rm}}\right) \tag{3.26}$$

with g being the physical air gap.

The total flux in rotating electrical machines consists of a main flux and the components of flux leakage [8]. The air gap flux linkage corresponds to the magnetizing inductance and the flux leakage corresponds to a leakage inductance. The magnetic equivalent circuit is shown in Figure 3.6.
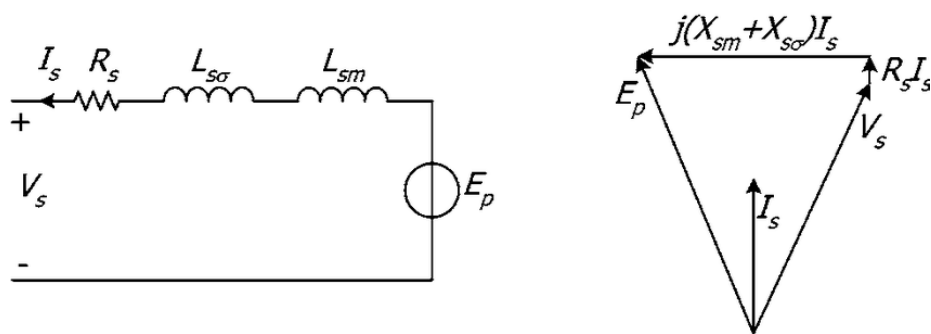
Figure 3.6 Equivalent circuit and phasor diagram for the permanent magnet synchronous generator. Taken from [7].

The magnetizing inductance is given by:

$$L_{sm} = \frac{6\mu_0 l_s r_s (k_W N_s)^2}{p^2 g_{eff} \pi} \tag{3.27}$$

Where l_s is the stack length, r_s is the stator radius, N_s is the number of turns of the phase winding, p is the number of pole pairs, and k_W is the winding factor. The layout of the generator is shown in Figure 3.7.
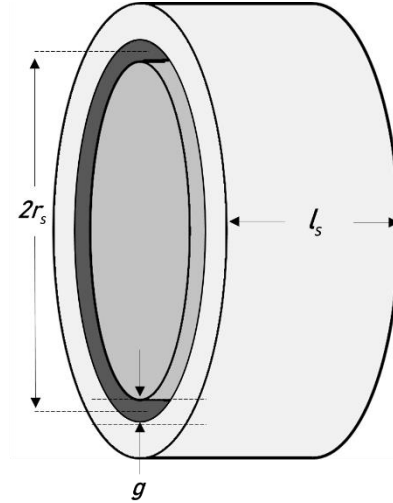
Figure 3.7 Illustration of the radius, stack length and airgap of a PMG.

The fundamental space harmonic of the magnet flux density resulting from the magnets can be calculated as:

$$\hat{B}_g = \frac{l_m}{\mu_{rm} g_{eff}} B_{rm} \frac{4}{\pi} \sin\left(\frac{\pi b_p}{2\tau_p}\right) \tag{3.28}$$

where B_{rm} is the remanent flux density of the magnets.

The distribution factor for the windings is given by:

$$k_d = \frac{\sin\left(\pi/6\right)}{q \sin\left(\pi/6\right)} \tag{3.29}$$

The no-load voltage induced in the stator windings by the flux density is given by,

$$E_p = \sqrt{2} k_w N_s \omega_m r_s l_s \hat{B}_g \tag{3.30}$$

with ω_m being the angular speed of the rotor.

The phase resistance is used to calculate the copper losses and is given by,

$$R_s = \frac{\rho_{Cu} l_{Cus}}{A_{Cus}} \tag{3.31}$$

where ρ_{Cu} is the resistivity of copper, l_{Cus} is the length of the copper conductor of the phase winding and A_{Cus} is the cross-sectional area of the conductor. The length of the conductor is estimated as,

$$l_{Cus} = N_s\left(2l_s + 4\tau_p\right) \tag{3.32}$$

The cross-sectional area is estimated as

$$A_{Cus} = \frac{pqk_{sfil}b_{sav}h_s}{N_s} \tag{3.33}$$

where q is the number of slots per pole per phase, k_{sfil} is the slot fill factor which is set at 60 %, b_{sav} is the average slot width and h_s is the height of the slot.

The specific iron losses are calculated using,

$$P_{Fe} = 2P_{Fe0h}\left(\frac{f_e}{f_0}\right)\left(\frac{\hat{B}_{Fe}}{\hat{B}_0}\right)^2 + 2P_{Fe0e}\left(\frac{f_e}{f_0}\right)^2\left(\frac{\hat{B}_{Fe}}{\hat{B}_0}\right)^2 \tag{3.34}$$

where P_{Fe0h} is the hysteresis loss per unit mass at angular frequency f_0 and flux density B_0, f_e is the frequency of the field in the iron, and P_{Fe0e} is the eddy current loss per unit mass.

3.4.2 Gearbox loss modelling

Gearbox losses and maintenance requirements play significant roles in the cost of energy (COE) of wind turbines. Modelling the expected losses in the design stages of wind turbine drivetrains can provide estimations on the wind turbine performance and cost. Gearbox losses are typically approximated based on an assumption of 1% viscous losses per gearbox stage Polinder [7] assumed $x = 3\%$ for a 3-stage gearbox and $x=1.5\%$ for a single-stage gearbox and scaled the loss using a ratio of actual rotational speed (n) to rated rotational speed (n_{rated}). P_{rated} is the wind turbine power.

$$P_{Gearbox\ loss}(n) = xP_{rated}\frac{n}{n_{rated}} \tag{3.35}$$

This approach offers estimated losses that are linear with rotational speed – does not consider load dependant losses or the topology of the gearbox itself. Therefore, a method of modelling load dependant gearbox losses specific to gearbox

configurations and ratios will provide a more accurate account of the likely transmission losses of wind turbine gearboxes.

An International Organisation for Standardisation Technical Report (ISO/TR 14179-1) titled "Gears – Thermal capacity – Part 1: Rating gear drives with thermal equilibrium at 95 °C sump temperature" [9] provides detailed power loss equations for gears. The losses calculated in the following gear and bearing loss sections are all based on the calculations from this ISO document. The report utilizes an analytical heat balance model to calculate the transmittable power for a single or multiple stage gear drive. The loading through the gearbox is calculated for each component and when planetary gear sets ae used, the distribution of torque is equal across all planets. The detailed losses for individual gearbox components are discussed in the following sections.

Maintaining an acceptable temperature in the oil sump of a gear drive is essential for the life of the gear system. Therefore, gear mechanical and thermal ratings must be carefully selected to ensure the longevity of the gearing. The thermal rating is based on the condition that the losses, P_V at input power are equal to the heat dissipation, P_Q such that:

$$P_Q = P_V \tag{3.36}$$

The heat generation in a gear drive, P_V is the sum of load dependent losses, P_L and non-load dependent losses, P_N and is given by:

$$P_V = P_L + P_N \tag{3.37}$$

The load dependent losses, P_L is a function of input power, P_A:

$$P_L = f(P_A) \tag{3.38}$$

Therefore, the basic heat equation is obtained as follows:

$$P_Q - P_N - f(P_A) = 0 \tag{3.39}$$

The unit efficiency can then be calculated as shown:

$$\eta = 100 - \frac{P_L + P_N}{P_A} \times 100 \tag{3.40}$$

So the thermal rating of the gear can be calculated using the following equation:

$$P_T = \frac{P_Q}{1 - \frac{\eta}{100}} \tag{3.41}$$

The heat generated in a gear drive is calculated as the sum of the load dependent losses, P_L and the non-load dependent losses, P_N.

The load dependant losses are comprised of the sum of all the individual gear mesh losses, P_M and the sum of all the individual bearing losses, P_B as shown in the below equation:

$$P_L = \sum P_B + \sum P_M \tag{3.42}$$

The non-load dependant losses are comprised of the sum of the individual oil seal losses, P_S, the sum of the individual windage and oil churning losses for the gears, P_W and bearings, P_{WB}, and the sum of the individual oil pump powers, P_P.

$$P_N = \sum P_S + \sum P_W + \sum P_{WB} + \sum P_P \tag{3.43}$$

3.4.2.1 Mesh power loss for spur and helical gears

An example profile of gear tooth geometry is shown in Figure 3.8.
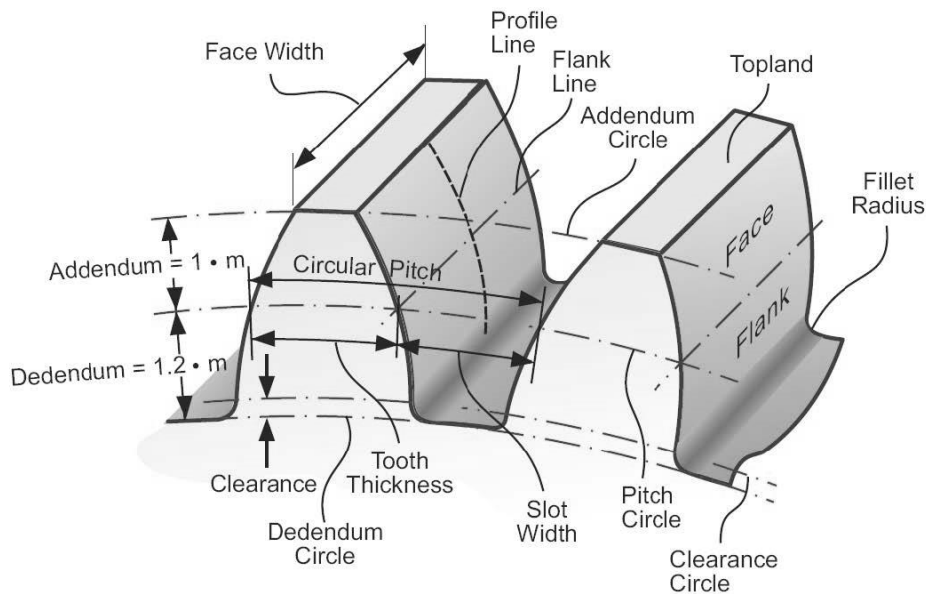
Figure 3.8 Gear tooth profile example. Taken from [10].

Mesh losses [9] are calculated as a function of the mechanics of tooth action and the coefficient of friction and is shown in the following equation:

$$P_{Mi} = \frac{(f_m T_1 n_1 \cos^2 \beta_w)}{9549M} \tag{3.44}$$

The mesh power loss, P_{Mi} has the units of kW. f_m is the mesh coefficient of friction, T_1 is the pinion torque in Nm, n_1 is the pinion rotational speed in rpm, β_w is the operating helix angle in degrees and M is the mesh mechanical advantage which can be calculated using the equation:

$$M = \frac{2 \cos \alpha_w (H_s + H_t)}{H_s^2 + H_t^2} \tag{3.45}$$

where α_w is the transverse operating pressure angle in degrees. H_s and H_t are the sliding ratios at the start of approach and the end of recess respectively and are both given in the following two equations:

$$H_s = (u + 1)\left[\left(\frac{r_{o2}^2}{r_{w2}^2} - \cos^2 \alpha_w\right)^{0.5} - \sin\alpha_w\right] \tag{3.46}$$

$$H_t = \left(\frac{u + 1}{u}\right)\left[\left(\frac{r_{o1}^2}{r_{w1}^2} - \cos^2 \alpha_w\right)^{0.5} - \sin\alpha_w\right] \tag{3.47}$$

where u is the gear ratio, r_{o2} is the gear outside radius (mm), r_{w2} is the gear operating pitch radius in (mm), r_{o1} is the pinion outside radius (mm), and r_{w1} is the pinion operating pitch radius in (mm). The gear ratio is calculated by dividing the number of gear teeth z_2 by the number of pinion teeth z_1 as shown below:

$$u = \frac{z_2}{z_1} \tag{3.48}$$

The load intensity K is given by the following equation:

$$K = \frac{1000T_1(z_1 + z_2)}{2b_w(r_{w1})^2 z_2} \tag{3.49}$$

where b_w is the face width in contact (mm). The mesh coefficient f_m can be calculated using the following equation if the pitch line velocity V is 2 ms^{-1}< $V \leq 25$ ms^{-1} and the K-factor is 1.4 N/mm^2< $K \leq 14$ N/mm^2:

$$f_m = \frac{v^j K^g}{C_1 V^h} \tag{3.50}$$

where v is the kinematic oil viscosity at operating sump temperature, in centistokes (square mm per second), and the constants are as follows: $j = -0.223$, $g = -0.4$, $h = 0.7$, and $C_1 = 3.239$.

3.4.2.2 Gear windage and churning power loss

Gear windage loss [9] arises from the fluid drag experienced by the gear moving in air or air-oil mist. An approximation for the roughness factor for the tooth surface power loss calculation is given by the equation:

$$R_f = 7.93 - \frac{4.648}{m_t} \tag{3.51}$$

where m_t is the transverse tooth module. Gear windage and churning losses, P_{GWi}, are calculated using three components: Losses associated with a smooth outside diameter (using equation (3.51)), such as the outside diameter of a shaft losses associated with smooth sides of a disc, such as the faces of a gear (using equation (3.52)), and the losses associated with tooth surfaces, such as the outside diameter of a gear or pinion (using equation (3.53)).

$$P_{GWi} = \frac{7.37 f_g v n^3 D^{4.7} L}{A_g 10^{26}} \tag{3.52}$$

$$P_{GWi} = \frac{1.474 f_g v n^3 D^{5.7}}{A_g 10^{26}} \tag{3.53}$$

$$P_{GWi} = \frac{7.37 f_g v n^3 D^{4.7} F \left(\frac{R_f}{\sqrt{tan\beta}} \right)}{A_g 10^{26}} \tag{3.54}$$

A_g is the arrangement constant which is set at 0.2.

3.4.2.3 Bearing power loss

The bearing dimensions are scaled from the dimensions given in [11] according to the radius of the gears for simplicity. These values are used in the following equations to provide bearing loss estimate that are linked to the design parameters.

Radially loaded bearings

The bearing load dependent torque M_1 (Nm) is given as shown below [9]:

$$M_1 = \frac{f_1(P_1)^a(d_m)^b}{1000} \tag{3.55}$$

Where f_1 is the coefficient of friction, P_1 is the bearing dynamic load (N), a and b are exponents specific to the bearing type, and d_m is the bearing mean diameter (mm) which can be calculated using:

$$d_m = \frac{d_i + d_o}{2} \tag{3.56}$$

Axially loaded cylindrical roller bearings

For cylindrical roller bearings that have to support an additional axial load, an additional frication moment M_2 (Nm) must be included which depends on the axial load [9]:

$$M_2 = \frac{f_2 F_a d_m}{1000} \tag{3.57}$$

where f_2 is a factor depending on bearing design and lubrication, F_a is the axial bearing load (N). So the total power loss for an individual bearing can be calculated using:

$$P_{Bi} = \frac{(M_1 + M_2)n}{9549} \tag{3.58}$$

with n being the bearing rotational speed in revolution per minute.

Bearing windage and churning power loss

The load-independent frictional moment for the bearing M_0 is calculated as follows :
If $vn < 2000$

$$M_0 = 1.6 \times 10^{-8} f_0 d_m^3 \tag{3.59}$$

If $vn \geq 2000$

$$M_0 = 10^{-10} f_0 (vn)^{2/3} d_m^3 \tag{3.60}$$

where f_0 is the bearing dip factor. For sealed bearings and additional frictional moment for the seal M_3 can be calculated:

$$M_3 = \frac{\left(\left(\frac{d_m}{f_3}\right)^2 + f_4\right)}{1000} \tag{3.61}$$

Where f_3 and f_4 are bearing seal factors. The power loss for each bearing can then be calculated as shown in the equation below:

$$P_{WBi} = \frac{(M_0 + M_3)n}{9549} \tag{3.62}$$

3.4.2.4 Gearbox oil specifications

The oils used in gearboxes are selected based on the teeth meshing characteristics, operating speeds and temperatures. Detailed studies of oil for gearboxes are given in the literature [12][13][14] and it can be assumed that a mineral oil of suitable kinematic viscosity and operating temperature range would be selected for the designs considered in this thesis.
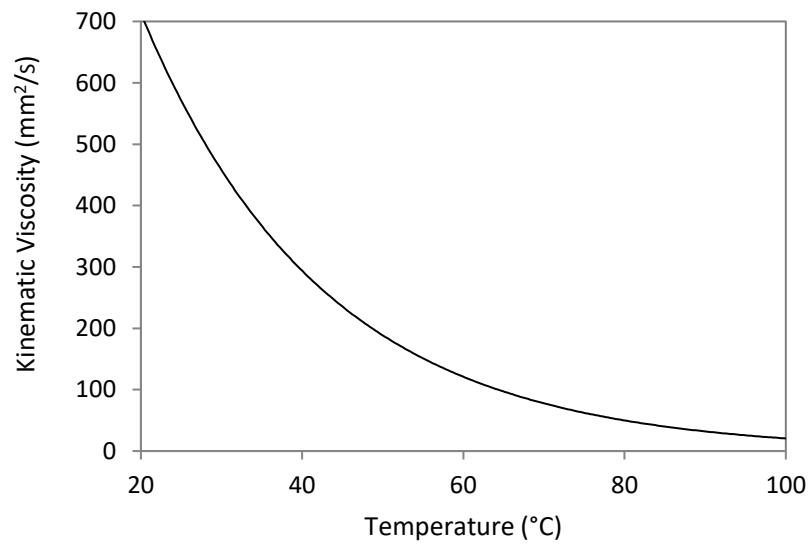
Figure 3.9 Example of a typical kinematic oil viscosity with temperature curve.
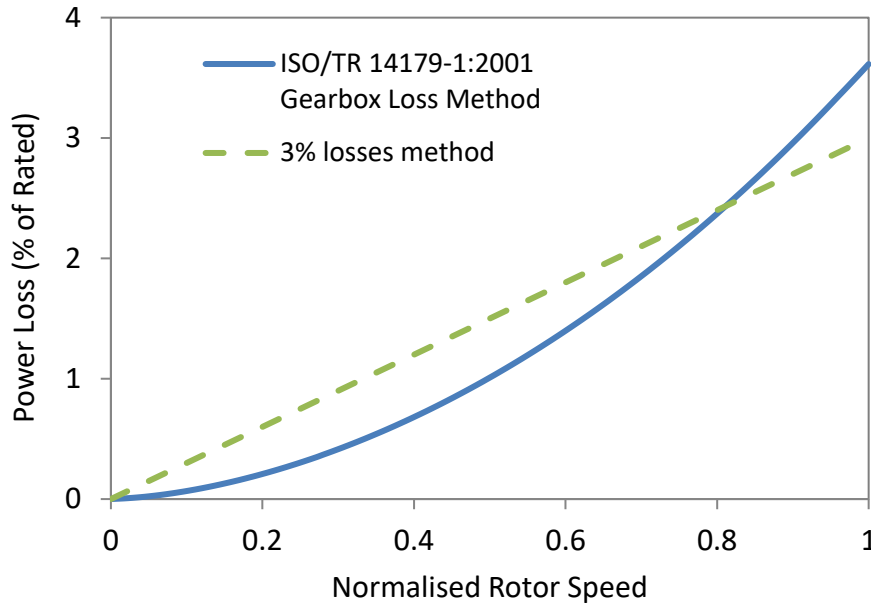
Figure 3.10 Comparison of the standard gearbox loss calculation method based on 3% rated with the improved ISO method for a 3-stage gearbox.

Benefits of using the ISO method for calculating gearbox include that lower losses associated with below rated operation are represented more accurately (as shown in Figure 3.10) and the losses are directly linked to the design, from dimensions and operating speed to temperature and oil viscosity. Therefore, it is a much more detailed representation of a gearbox and so can form part of a more detailed design.

3.4.3 Converter loss modelling

Having an interface between the generator and the grid connection allows the outputs the meet the grid requirements. A back-to-back voltage source is used and the loss calculations are taken from Polinder et.al. [7] such that losses are given by:

$$P_{conv} = \frac{(P_{convm})}{31}\left(1 + 10\frac{I_s}{I_{sm}} + 5\frac{I_s^2}{I_{sm}^2} + 10\frac{I_g}{I_{gm}} + 5\frac{I_g^2}{I_{gm}^2}\right) \tag{3.63}$$

where P_{convm} is the dissipation in the converter at rated power which is assumed to be 3% of the rated power of the converter. I_s is current in the generator side converter, I_{sm} is the maximum current of the generator side converter, I_g is the current in the grid side converter, and I_{gm} is the maximum current in the grid side converter.

3.5 Initial Capital Cost (ICC)

Cost assumptions used throughout the models are based mostly on the estimates presented in [1] and all costs are converted into Euros (based on the relevant year) and appropriate conversions are used to account for inflation. This NREL study provides an appropriate level of detail that is suitable to produce design-specific cost assumptions for wind turbines and so forms a key basis for the development of some of the costs used in this thesis.

Due to limiting factors such as weight and logistics, a reasonable design constraint for direct drive generator would include a maximum total weight of <100 t and a maximum external diameter of 8 m [15]. This has been applied to the models to maintain designs that would be currently viable for production and transportation.

3.5.1 Cost of the Generator Active Materials

The cost of the generator active materials is based on the mass of permanent magnets, copper and iron and their associate cost/kg. As a base case a cost of 60 €/kg is assumed for the NdFeB permanent magnets, 15 €/kg for the copper windings, 3 €/kg for the steel laminations, 2 €/kg for structural steel and 7 €/kg for structural aluminium. The costs are based on current price estimations from recent market activity. The masses of the active materials are all calculated from the dimensions described in Section 3.4.1. The masses of the structural material are calculated as described in the following section.

3.5.2 Cost of the generator structure

The generator structure cost is based on a structural model developed by McDonald and Bhuiyan [16]. A study by McDonald [17] presents detailed structural analysis which has been simplified for this thesis. Although the structural model was implemented in this work, the focus of the thesis is on the active materials in the generator. Therefore, the structural section in the model was not further developed as part of the optimisation process later described in the thesis. It provided a suitable estimate for the sizing of the support structure for the active parts of the generator.

The structure is designed using radial, axial and tangential deflection models and a support arm based construction [17]. Based on the model from [18], the rotor deflection is allowed to deflect radially into air-gap by 5% of the air-gap length, the tangential deflection is 1% of the air-gap and the structure is allowed to deflect axially by 0.2% of the air-gap. The mean normal radial stress is given by:

$$q_r = \frac{B_g^2 w}{2\mu_0 \tau_p} \tag{3.64}$$

where B_g is the air gap flux density, w represents the width of the magnet [18]. The radial deflection mid-way between two arms is calculated by:

$$u = \frac{q_r R^2}{Y h_y}\left(1 + \frac{R^3}{I_r}\alpha\right) \tag{3.65}$$

where R is the outer radius of the structure, Y is the Young's modulus of the structural material, h_y is the height of the yoke, I_r is the second moment of area for the yoke cross-section and α is a function of the dimensions and number of arms [18]. For the tangential direction, the deflection z is given by:

$$z = \frac{T_{max} l_{ar}^3}{12 Y I_z} \tag{3.66}$$

where T_{max} is the maximum generator torque, l_{ar} is the radial length of the arms and I_z is the second moment of area of the arms in the circumferential direction [18]. The axial deflection component is given by:

$$y = \frac{W l_b^3}{12 Y I_y} + \frac{w l_{ar}^4}{24 Y I_y} \tag{3.67}$$

where W represents the weight of the permanent magnets, the copper windings, iron, aluminium of other materials that make up the back iron weight, l_b is the radial length of the beam, w is the weight component of the arms and I_y is the second moment of area of the structural arms in the axial direction [18]. Once the deflection components are found, appropriate dimensions are calculated to fulfil the allowable deflection constraints and so the mass of the structure can be calculated directly from the dimensions such that:

$$m_{str} = \rho\left[2\pi R h_{y0} l_s + n_{ar} l_{ar}\left(bd - (b - 2t_a)(d - 2t_a)\right)\right] \tag{3.68}$$

where ρ is the density of the material, h_{y0} is the extra yoke height due to deflection, n_{ar} is the number of arms, b and d are the average beam widths in the circumferential and axial direction respectively, and t_a is the wall thickness of beam [18]. From the mass, a cost per kg is applied to the material type and the cost of the structure can be calculated.

3.5.3 Cost of the Gearbox

The gearbox and bearings are costed based on their masses and assumed cost per kg of material. The bearings are also assumed to have a cost per kg based on the dimensions. In order to obtain a design specific cost estimate, a tooth machining, carburizing and hardening cost was assumed to be €25 per kg (estimated based on in-house knowledge and literature [19]). Therefore, with the total weight of the teeth calculated based on their dimensions, a reasonable estimate can be concluded for the hardening treatment of the gears. Combining the teeth cost with the total mass and bearing cost, a reasonable, design-based gearbox cost can be obtained. All assumptions used throughout this model can be altered to more accurate values if further information is known by the user. Basic cost assumptions are also made for the casing and other cost factors such as lubricant. These additional assumptions are held constant throughout the models.

3.5.4 Other Capital Costs

The power converter cost is estimated from the rating of the wind turbine using [1],

$$Converter\ Cost = Machine\ Rating \times 79 \qquad (3.69)$$

in which the cost is in US dollars and the machine rating is in kW. The mass of the converter is not calculated as the work does not look at the effect of top head mass or other mass related considerations and so a cost estimate is sufficient for the model.

Since the model is implemented for an offshore wind turbine, a marinization cost is applied to account for the additional treatment of components which is required in order for it to withstand operation in a marine environment. This has been

assumed as an additional percentage of the total wind turbine cost and tower cost and estimated as 13.5% [1].

$$Marinization\ cost = 13.5\%\ of\ turbine\ and\ tower\ cost \qquad (3.70)$$

Balance of plant (BOP) has been estimated as 37% [20] of the overall initial capital cost of the wind farm. With the wind turbine being estimated as 33% of the overall development cost, then BOP can be calculated as,

$$BOP = \frac{37}{33} \times Total\ cost\ of\ wind\ turbine \qquad (3.71)$$

Installation costs and other costs such as planning and consent make up the other remaining 30% and so can be estimated as

$$Installation = \frac{30}{70} \times (Total\ cost\ of\ wind\ turbine + BOP) \qquad (3.72)$$

Although it is a crude estimate, it serves its purpose a suitable assumption as the focus of the analysis is on the wind turbine drive train.

3.6 Operations and Maintenance Costs

A commonly used annual operations and maintenance (AOM) cost is taken as $0.02/kWh from [1] such that a basic AOM estimate can be calculated as

$$AOM = 0.02 \times AEP \qquad (3.73)$$

with AEP being annual energy production in kWh and AOM having the units of 2003 US dollars. This crude method is not useful as it makes no differentiation regarding the drive train type or any reliability considerations of the wind turbine. Therefore, a new approach was taken to improve this estimate.

A purpose of the models presented in this thesis is to create design specific operations and maintenance (O&M) costs based on the drive train components as discussed in Chapter 2. A more robust method would be to associate a failure rate with each of the drive train sub assembly components that are linked to known failure modes.

3.7 Improved O&M cost methodology

A study by Carroll titled "Cost of energy modelling and reduction opportunities for offshore wind turbines" [21] focuses on a reliability analysis of wind turbines using various databases and repair strategy scenarios to provide a comprehensive review of the effects on cost of energy. By using several of the numbers and assumptions from this study, cost of repair and downtimes can be linked to the design specifications in order to achieve a design based O&M cost. The following sections outline the procedure to obtain a design specific availability value for each drive train.

For the purposes of modelling the O&M cost, and in this case it will also be referred to as AOM (annual operations and maintenance) depending on the context, the procedure has been split into 8 levels:

1. The failure categories were identified such that they comprise

    - Minor repair – this corresponds to a small part replacement and typically would use a crew transfer vehicle (CTV) or helicopter transfer if applicable and only use local craning method such as nacelle cranes.

    - Major repair – this would require most extensive work to items such as the gearbox, blades and electrical components where the wind turbine would likely be out of commission for several days. The work would typically use CTVs and utilise the on-board craning methods

    - Major replacement – this involves the complete removal of significant components such as the whole generator and would require jack-up vessels and a full maintenance crew. From failure to successful repair can be many days and so major replacements are costly to the project.

2. The failure modes were defined such that they can be identified as the following:

    - Generator failures

    - Gearbox failures

    - Rest of wind turbine failures

3. The failure categories were designated a downtime per failure for each failure in order to calculate the availability of the wind turbine and the cost to repair.

4. Each failure mode and category was assigned a staff cost to repair.

5. Each failure mode and category was assigned a repair cost.

6. Each failure mode and category was assigned a transport cost for repair.

7. A failure rate was identified for each failure mode so that failure rate was linked directly to dimensions. For example, a large generator with more windings will experience a higher number of failures compared with a smaller generator. Similarly, a large gearbox will experience higher loads and will be subject to a higher level of fatigue and bearing failure.

8. A total cost for AOM is produced for each specific design that takes into account design specific failures and downtimes.

This approach is unique and never been done before and so it provides a significantly improved methodology for estimating the repair costs and downtime associated with PMG drive trains. The following sections outline the details of the 8 point process for calculating AOM.

3.7.1 Downtime and Availability

To obtain an appropriate availability figures based on the maintenance of the offshore wind turbine, a downtime per failure type will allow each failure category to be associated with a duration of unavailability – this will cover the onset of the failure (the commencement of the downtime), the transportation time for the technicians and the time to complete the repair in order to re-establish full wind turbine operation. Taking example figures from [21] for a downtime and repair time scenario for a site located 10 km from shore (values shown in Table 3.1), and failure rate examples also provided in [21], a downtime/failure can be calculated for each drive train design which are shown in Table 3.2.

Table 3.1 Down time example (total hours for each failure category)

	Drive train type			
	Direct Drive	1 Stage Geared	2 Stage Geared	3 Stage Geared
Gearbox Down Time Example				
Minor Repair	19.5	18.3	17.2	16
Major Repair	3.1	3.0	2.8	2.7
Major Replacement	12	9.8	7.5	5.9
Gearbox Down Time Example				
Minor Repair	0	10.1	11.7	13.3
Major Repair	0	11.3	19.5	27.7
Major Replacement	0	27.6	51.7	75.8
All other parts down time including converter	374			
Minor Repair	227			
Major Repair	73			
Major Replacement	74			

Table 3.2 Downtime/failure (hours) for each failure category

	Drive train type			
	Direct Drive	1 Stage Geared	2 Stage Geared	3 Stage Geared
Generator Downtime per failure (h/failure)				
Minor Repair	36	36	36	37
Major Repair	103	106	108	104
Major Replacement	1333	1158	938	738
Gearbox Downtime per failure (h/failure)				
Minor Repair	0	57	38	31
Major Repair	0	628	650	660
Major Replacement	0	1104	1231	1285
All other parts down time/ failure	157.9			

The downtime per failure value allows both the availability and the repair time and cost to be calculated. The values for all other parts are used consistently with each of the designs as the focus of the work is on drive train analysis only and the other parts of the wind turbine are assumed identical regardless of the drive train type.

3.7.2 Repair and Technician Cost for Generator and Gearbox

The repair time and the cost of repair are based on the cost of materials and the technician costs for the repair work. This includes values for both the gearbox and generator and the contributions of a minor repair, minor replacement and major replacement for each. Each repair job has a number of technicians required, the number of hours to complete the repair and assumed hourly rates of the technicians to estimate the overall cost of the staff that would carry repairs. The cost of repaired or replaced parts are also calculated based on values from [21] that are normalised against a complete replacement cost of the entire generator or gearbox system.

Table 3.3 Repair cost assumption applied to the models

Repair time (h)		
	Generator	Gearbox
Minor	6.5	7.9
Major repair	24.3	21.9
Major replacement	81.1	231
Average number of technicians		
	Generator	Gearbox
Minor	2.2	2.2
Major repair	2.7	3.2
Major replacement	7.9	17.2
Technician hours per failure type (h)		
	Generator	Gearbox
Minor	14	17
Major repair	66	70
Major replacement	641	3970
Scaled repair cost (euro)		
	Generator	Gearbox
Minor	0.0027	0.0021
Major repair	0.058	0.042
Major replacement	1	1

3.7.3 Transport Costs

The cost of the vessels and transport used for each type of repair has also been estimated based on values from [21]. These values are a result from an analysis of databases of many different wind turbines and represented as a transport cost per

MWh of energy produced. The EWEA offshore statistics report [22] states that the average annual energy output of an offshore wind turbine is 10,242 MWh, so this value, along with the failure rates given by [21], was used to convert the transport cost per MWh to a transport cost per failure. This meant that the transport cost can now be linked directly to the design based on the failure assumptions. The following values were used for each of the drive train design per failure.

Table 3.4 Transport cost per failure for each drive train

Cost in Euros	PMG DD	PMG 1G	PMG 2G	PMG 3G
Transport Cost per failure	8,330	13,980	15,230	16,450

These transport costs are applied to the entire wind turbine system including non-drive train related failures.

3.7.4 Reliability and Failure Rate Assumptions

There is not enough data in existence or available to access for the failures in a permanent magnet generator for offshore wind turbine. Therefore, using a number of assumptions and available information from wind turbine reliability studies [23][24][25], a simple approach can be implemented to estimate the failure rates and costs of repair. This also applies to the gearbox and so the following sections outline some of the assumptions made to link failure rate to design.

3.7.4.1 Permanent magnet generator failure rates

A straightforward method to obtain failure estimates for PMGs could be to use the available figures for DFIGs and remove the slip ring failures and any other failures that are mitigated with the use of permanent magnet excitation. This means that as an overall percentage of failure contributions, the other components will have slightly greater contributions to the overall split of failures. Figure 3.11 shows the simplified version of permanent magnet generator failure components which was adapted from [26].
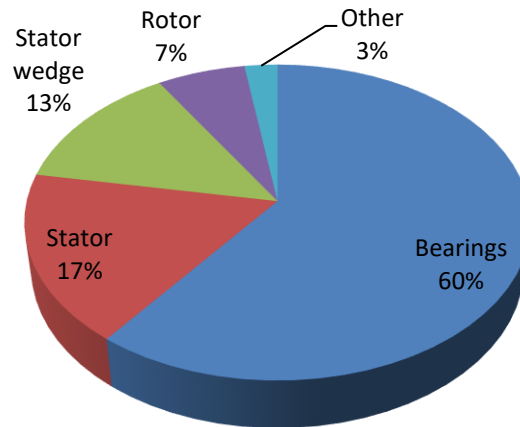
Figure 3.11 Failure components of a PMG adapted from [26].

Due to the removal of components associated with electrically excited generators such as brushes/slip rings, the contribution of failures associated with the PMG can be assumed as shown in the following table.

Table 3.5 Failure rate contribution assumptions for a PMG

Failure components	Failure rate contribution %
Bearings	60.4
Stator	17.4
Stator wedge	13.4
Rotor	6.4
Other	2.4
Total	100

From Carroll's study [21] there is a list of failure rates for PMGs which are split into generator, gearbox, converter and the rest of the turbines as shown in Figure 3.12. This offers a reasonable starting point in which to link failure rates to designs.
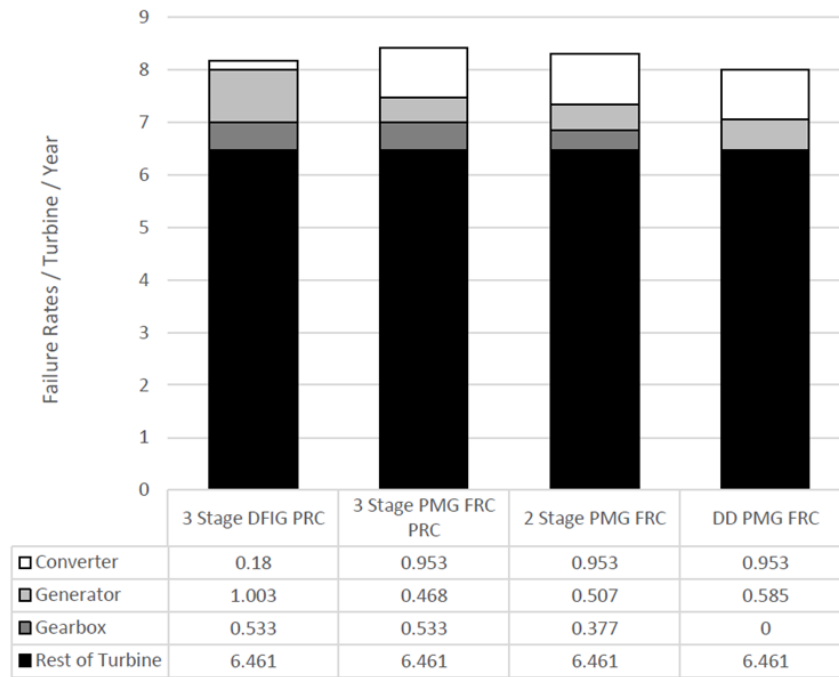
Figure 3.12 Failure rate of wind turbines with different drive train types (taken from [21]).

The values for the DD PMG, the 2 Stage PMG and the 3 Stage PMG from Figure 3.12 were taken and used to calcuate values for a 1 Stage PMG (the relationship is a straight line). The values were converted to be consistant with the assumptions [25] being created for this study such that the new values can be given as:

Table 3.6 Baseline generator failure rates for each drive train type

New baseline failure rates			
PMG 3G	PMG 2G	PMG 1G	PMG DD
0.394	0.427	0.460	0.493

The values in Table 3.6 were then linked to basic dimension assumptions relevant for a 6 MW wind turbine based on scaling values from [7] and adjusting for offshore wind conditions. The failure rates were linked to the surface areas of each generator type based on the basic dimension assumptions. Data does not exist for failure rates linked to surface area and validating such a method is not possible at this stage. The failure rates are based on a limited database of wind tubines with an average rating much lower than 6MW. It is therefore, unlikley to be accurate and only serves as an

initial assumption in the process of developing a detailed dimensional relationship with failure rate. Despite being a crude estimate it provides a useful method to add a trend between surface area and failure rate. The resulting trendline is shown in Figure 3.13 where it is concluded that a reasonable estimate for generator failure rate can be given by

$$\lambda_{PMG} = 0.0011A_{gs} + 0.404 \tag{3.74}$$
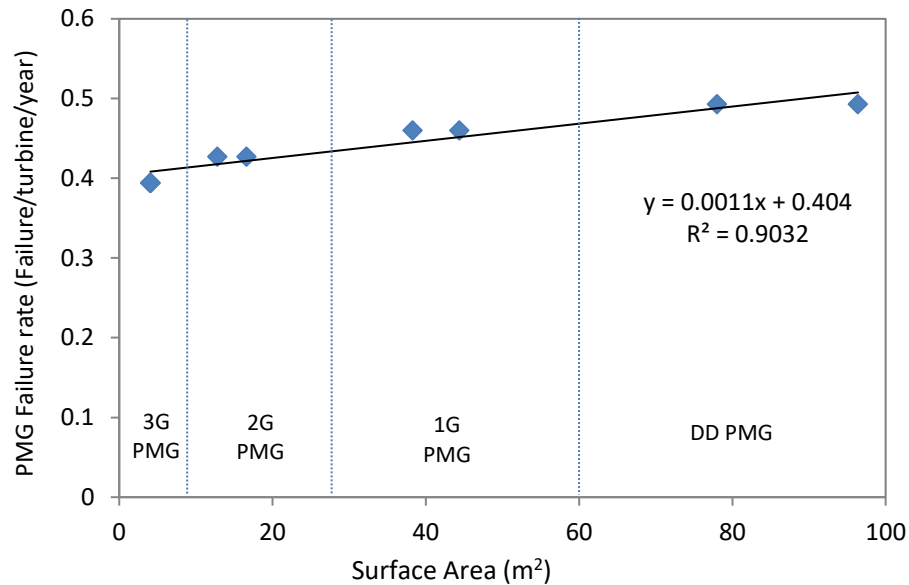
Figure 3.13 Assumed relationship between generator surface area and failure rates for a PMG.

The typical surface area ranges for each drive train type are assumed and can be seen in Figure 3.13 (e.g. surface areas above 60 m^2 represent a direct drive generator of around 6 MW rating).

3.7.4.2 Gearbox failure rates

Reliability studies for gearboxes are outlined in various literature such as [27] and [28]. A reference gearbox is described in [11] which also illustrated a fatigue vulnerability diagram as shown in Figure 3.14. This diagram is useful to identify the areas of the gearbox most likely to fail. It can be seen from the red and orange colour mapping, that the bearings are the most vulnerable part of the gearbox and

particularly so for the high-speed section. A gearbox review [11] outlines the failure rate contributions for a gearbox to create a picture of the most vulnerable sections. The values from [27] were adapted to follow the 2 planetary and 1 parallel gear stage topology being considering for this thesis. The altered chart can be seen in Figure 3.15 that also shows that the bearing contributes the most to the failures of the system.
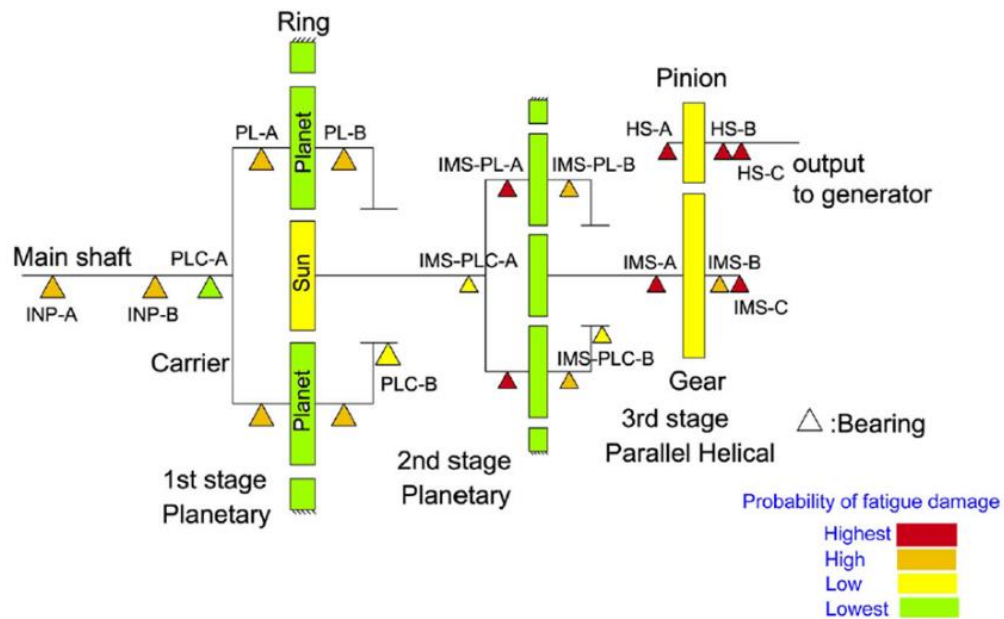
Figure 3.14 Gearbox vulnerability diagram for 2 planetary stages and one parallel gear stage (taken from [11]).

By taking the values for overall gearbox failure rates scaled from [21] and combining it with the distribution shown in Figure 3.15, a complete set of component level failure rates can be produced as a base case 3-stage gearbox. The method assumed each additional gear stage holds the same failure rates despite subject to additional operating forces (i.e. the failure rates for a single stage are the same as the failure rates of the first stage of a 3-stage gearbox).
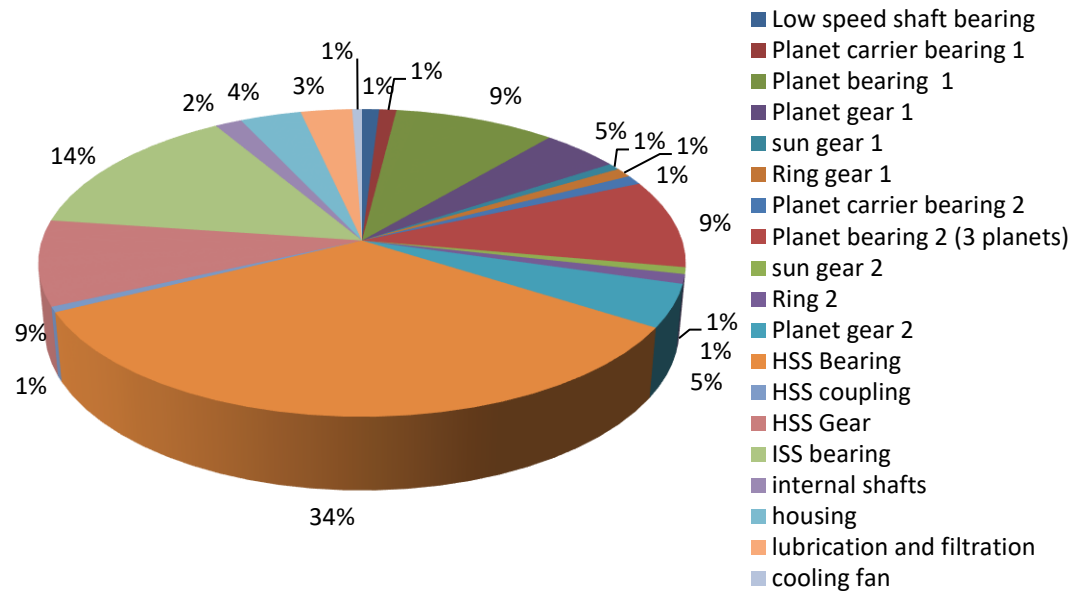
Figure 3.15 Failure rate contribution for 3-stage gearbox adapted to 2 planetary stages and 1 parallel stage.

Table 3.7 Failure rate example for components of a gearbox and their % contributions to overall failure rate

Failure component	3 Stage		2 Stage		Single Stage	
	%	Failure/ turbine/year	%	Failure/ turbine/year	%	Failure/ turbine/year
Low Speed Shaft Bearing	0.987	0.011	4.816	0.011	8.379	0.011
Planet Carrier Bearing 1	0.987	0.011	4.816	0.011	8.379	0.011
Planet Bearing 1	9.302	0.022	13.131	0.022	16.695	0.022
Planet Gear 1	4.510	0.016	8.339	0.016	11.903	0.016
Sun Gear 1	0.705	0.011	4.534	0.011	8.097	0.011
Ring Gear 1	0.987	0.011	4.816	0.011	8.379	0.011
Planet Carrier Bearing 2	0.987	0.011	4.816	0.011	-	-
Planet Bearing 2 (3 Planets)	9.302	0.031	13.131	0.031	-	-
Sun Gear 2	0.705	0.011	4.534	0.011	-	-
Ring 2	0.987	0.011	4.816	0.011	-	-
Planet Gear 2	4.510	0.019	8.339	0.019	-	-
HSS Bearing	33.686	0.383	-	-	-	-
HSS Coupling	0.564	0.006	-	-	-	-
HSS Gear	8.950	0.102	-	-	-	-
ISS Bearing	14.235	0.162	-	-	-	-
Internal Shafts	1.550	0.012	5.379	0.012	8.943	0.012
Housing	3.524	0.015	7.353	0.015	10.916	0.015
Lubrication And Filtration	2.960	0.014	6.789	0.014	10.352	0.014
Cooling Fan	0.564	0.011	4.393	0.011	7.956	0.011
Total	**100**	**0.871**	**100**	**0.217**	**100**	**0.134**

The details of the gearbox component failure rates example shown in Table 3.7 can be very useful if known by manufacturers. For the purposes of the baseline models, the overall gearbox failure rate is estimated in a similar manner to the generator failure rate: being based on surface area which is described in more detail in the following section.

3.7.5 Gearbox Design Assumptions and Constraints

The geared designs had additional constraints that were implemented to ensure the dimensions of the gearbox meet maximum stress requirements. The contact stress was limited to 160,000 lb/in^2 and the bending stress was limited to 50,000 lb/in^2 chosen from values given in [29] and other gear tooth geometry was estimated based on the values in [30]. It was assumed that the steel would undergo appropriate heat treatment for hardening and so suitable values were used that would represent typical gear steel. Contact stress is calculated by:

$$s_c = C_p \sqrt{\frac{W_t}{dFI}} \qquad (3.75)$$

where C_p is the elastic coefficient in $(lb/in^2)^{0.5}$, W_t is the transmitted tangential load in lb, d is the operating pitch diameter of the pinion in inches, F is the facewidth in inches and I is the geometry factor for pitting resistance (assumed 0.11 based on values from [30]). The bending stress is calculated using:

$$s_c = \frac{W_t P_d}{FJ} \qquad (3.76)$$

where P_d is the transverse diametral pitch in (inches)$^{-1}$, J is the geometry factor for bending strength (assumed 0.4 based on values from [30])

The maximum face width to pinion pitch diameter ratio was limited to 1.25 as described in [31]. The geared designs also have a minimum and maximum number of planets depending on the gear ratio also found in [31]. The constraints for the number of planets are defined as:

- 5 planets for ratios of 1:4
- 4 planets for ratios between 1:4.05 and 1:6
- 3 planets for ratios between 1:6.05 and 1:13

For the purposes of the models used in this study, failure rates that are also linked with dimensions would allow a design specific consideration to be made in terms of reliability. Similarly, to the procedure used for the generator, the failure rates were linked to appropriate dimensions and plotted against surface area (Figure 3.16) to obtain the following relationship for gearbox failure rate:

$$\lambda_{gb} = 0.0005 A_{gbs}{}^2 - 0.0407 A_{gbs} + 0.9386 \qquad (3.77)$$

where A_{gbs} is the surface area of the gearbox which comprises the gears and bearings.
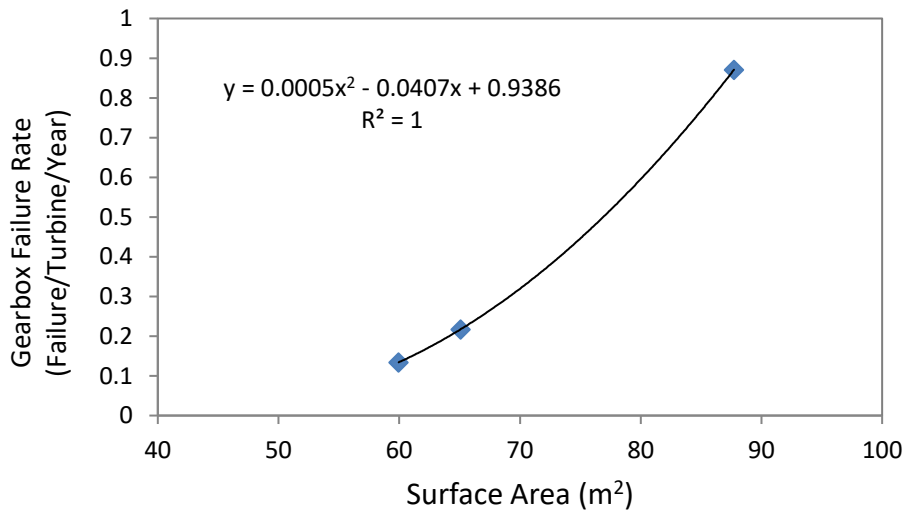
Figure 3.16 Gearbox failure rate relationship with surface area assumption.

As with the generator failure rate assumptions outlined in Chapter 3, the crude surface area-based failure rate offers a reasonable starting point in linking the design with its reliability. The calculation of surface area considers the gears, pinions and their teeth, and all the bearing dimensions and so covers the size of the complete system. The failure rate does not yet consider the operating speed of the gearbox, but this factor is considered in Chapter 4 as part of a design analysis.

3.7.6 Other Repair and Technician Costs

Other repair costs and technician costs for the rest of the wind turbine were included and kept constant regardless of the drive train dimensions and specifications as they

are not specifically related to the drive train. The following table outlines the set values for each drive train for these additional repair and technician costs.

Table 3.8 Repair and staff costs for all other parts

Costs in Euros	PMG DD	PMG 1G	PMG 2G	PMG 3G
Repair cost per failure (all other parts)	2,050	1,090	1,700	2,300
Staff cost per failure (all other parts)	1,900	1,870	1,970	2,080

The values were taken from work by Carroll [21] at an assumed distance of 10 km from the shore.

3.7.7 Final failure rates for each topology

The failure rates are given in Table 3.9 for the generator, gearbox and the rest of the wind turbine for each of the drive train topologies. The generator failure rate is linked to the surface area A_s of the generator as described in Section 3.7.4.1.

Table 3.9 Base failure rate assumptions

	Drive train type			
	Direct Drive	1 Stage Geared	2 Stage Geared	3 Stage Geared
Generator Failure Rate (total)	$0.001*A_s+0.4$			
Minor Repair (%)	97.4%			
Major Repair (%)	2.6%			
Major Replacement (%)	0			
Gearbox Failure Rate (total)	0	~0.134	~0.217	~0.871
Minor Repair (%)	0	26.2%		
Major Repair (%)	0	6.5%		
Major Replacement (%)	0	67.3%		
All other parts failure rate	2.37	2.37	2.37	2.37

From Carroll [21] a failure with a total repair material cost of less than €1,000 is considered a minor repair, between €1,000 and €10,000 a major repair and above €10,000 a major replacement.

3.8 Base Case Results

The costs of the generator configurations are based on the mass of materials used in each generator and material cost in Table 3.10. Other costs such as the cost of the converter are scaled with an inflation rate of 2.4% p.a. [32] to be in accordance with the present day value. Inflation in recent years perhaps does not reflect the assumed value, but for the purposes of model consistency it was kept constant and still allows appropriate comparisons to be made as they were not integral parts of the model.

Table 3.10 Input data for wind turbine model.

Wind Turbine Characteristics	
Rated Grid Power (MW)	6
Rotor Diameter (m)	140
Rated Wind Speed (m/s)	11
Rated Speed (rpm)	10.5
Optimum Tip Speed Ratio	8
Maximum Aerodynamic Efficiency (%)	48
Mass density of air (kg/m^3)	1.225
Generator Material Characteristics	
Slot filling factor k_{sfil}	0.6
Remnant flux density of magnets B_{rm} (T)	1.2
Recoil permeability of the magnets μ_{rm}	1.06
Resistivity of copper at 120°C ρ_{Cu} ($\mu\Omega$m)	0.025
Eddy-current losses in laminations at 1.5 T, 50 Hz P_{Fe0h} (W/kg)	0.5
Hysteresis losses in laminations at 1.5 T and 50 Hz P_{Fe0h} (W/kg)	2
Loss Modelling	
Maximum losses in a 6 MW VSI P_{convm} (kW)	180
Cost Modelling	
Laminations cost (€/kg)	3
Structural steel cost (€/kg)	2
Structural aluminium cost (€/kg)	7
Copper cost (€/kg)	15
Permanent magnet cost (€/kg)	60
Rest of wind turbine cost (k€)	4000

The power curve and Weibull distribution of the turbine are shown in. The cut-in wind speed is 4 m/s and the cut-out wind speed is 25 m/s with a rated power of 6 MW being attained at a wind speed of 11 m/s. The parameters for the Weibull

distribution are based on a hypothetical location in the North Sea with a mean wind speed of around 8.0 m/s, a scale parameter of 8.2 and a shape parameter of 1.7.
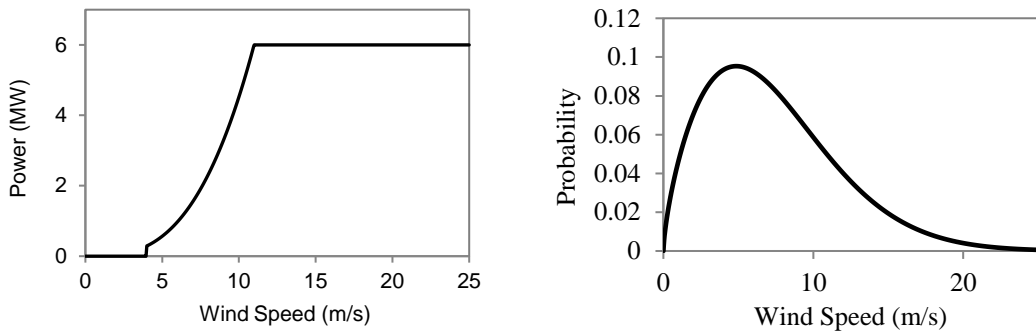
Figure 3.17 Power curve and Weibull distribution as a function of wind speed.

The results for all four designs are presented in Table 3.11. The design of the generators parameters is based on the torque scaling of the generators previously studied in [7] with some costs based on [33], [34] and [20]. Torque is the product of force F and radial distance r ($T=Fr$) where force can also be written in terms of shear stress σ and area A ($F=\sigma A$). By considering the generator area to be the equivalent to the surface area of a cylinder ($A=\pi l_s d$), the equation for torque can be written as:

$$T = \frac{\sigma \pi d^2 l_s}{2}$$
(3.8.1)

where d is the diameter of the generator and l_s is the stack length.

The optimum aspect ratio [15] of the generator which equals length divided by diameter ($\chi=l_s/d$) can be calculated using the equation:

$$\chi = \left(\frac{\pi}{4p}\right)p^{1/2}$$
(3.8.2)

where p is the number of pole pairs. In the case of the DD PMG, the number of pole pairs chosen was 100 as this maintained a generator frequency of 20 Hz. This implies that an optimum aspect ratio would be 0.09. However, the generator would require a diameter >10 m to achieve such a ratio and so carries unnecessary high project risk in terms of cost and logistics. Therefore, a maximum diameter of 10 m was imposed on the DD PMG. The sizing of the generators were based on maintaining similar pole dimensions used for the 3 MW machine [7]. The gear ratios were also kept to similar values to those studied in [7], but with dimensions in keeping with those assumed in

the reference gearbox of [11] with contact and bending stress considerations as discussed in section 3.7.5.

Table 3.11 Base case design specifications and performance for the 4 drive trains.

	DD PMG	PMG 1G	PMG 2G	PMG 3G
Generator Specifications				
Generator speed (rpm)	10.5	72.5	375.8	1152.4
Gearbox ratio	-	1:6.9	1:35.7	1:105.4
Stator radius r_s (m)	3.5	2.5	1.02	0.67
Stack length l_s (m)	1.5	0.8	0.51	0.6
Number of pole pairs p	100	60	20	6
Air gap g (mm)	7	5	2.04	1
Stator slot width b_{ss} (mm)	16.5	19.6	21.2	37.7
Stator tooth width b_{st} (mm)	20.2	24.0	25.9	46.1
Stator slot height h_{ss} (mm)	80	80	80	80
Stator yoke height h_{sy} (mm)	40	40	40	40
Rotor yoke height h_{ry} (mm)	40	40	40	40
Magnet height l_m (mm)	15	15	15	15
Magnet width b_p (mm)	70	83	90	160
Generator Parameters				
Main inductance L_m (mH)	9.01	0.93	0.39	0.18
Stator leakage inductance $L_{s\sigma}$ (mH)	10.73	0.72	0.22	0.03
Stator resistance R_s (mΩ)	186.87	14.54	4.57	0.86
Generator Material Weight (ton)				
Iron	31.7	12.1	3.2	2.5
Copper	6.8	3.0	1.0	1.0
PM	3.8	1.1	0.3	0.2
Total	42.3	16.2	4.5	3.7
Cost (kEuro)				
Generator active material	422.4	146.9	41.0	34.7
Generator construction	67.3	8.8	1.7	0.8
Gearbox	0	412	477	307
Generator system cost	490	568	519	342
Converter	762	762	762	762
Other wind turbine parts	4108	4108	4108	4108
Total cost of wind turbine	6083	6172	6117	5916
Annual Energy				
Copper losses (MWh)	920	198	273	71
Iron losses (MWh)	97	219	135	333
Converter losses (MWh)	614	670	734	678
Gearbox losses (MWh)	0	284	448	832
Availability (%)	95.5	94.2	93.1	86.2
Total losses (MWh)	1631	1093	1152	1099
Energy yield (GWh)	19.46	19.59	19.13	17.56
Cost of Energy				
ICC (kEuro)	18434	18704	18537	17927
AOM (kEuro)	34.7	92.6	156.0	309.5
FCR	0.116	0.116	0.116	0.116
COE (Euro/MWh)	111.47	115.28	120.37	135.88

From the initial results presented in Table 3.11 (which were calculated in MATLAB [6]), both the PMG DD and the PMG 1G offer the lowest COE at just over 111.47 €/MWh and 115.28 €/MWh respectively. The PMG 3G is very high in comparison with a COE of 135.88 €/MWh and with these current assumptions would not provide a cost-effective design. The following sections details the loss mechanisms and costs for each of the designs.

3.8.1 PMG DD

Overall this drivetrain gave the lowest COE in the baseline study. The Siemens SWT-6.0 150 and Alstom Haliade turbines – although very different machines – fit into this category. Results from the MATLAB model for the DDPMG are shown in Figure 3.18 and Table 3.11. The results shown include the wind turbine power curve, the system efficiency and losses. The significant losses in the system result from high copper losses. This is due to the requirement that in order to produce a high torque there is a large number of coils.
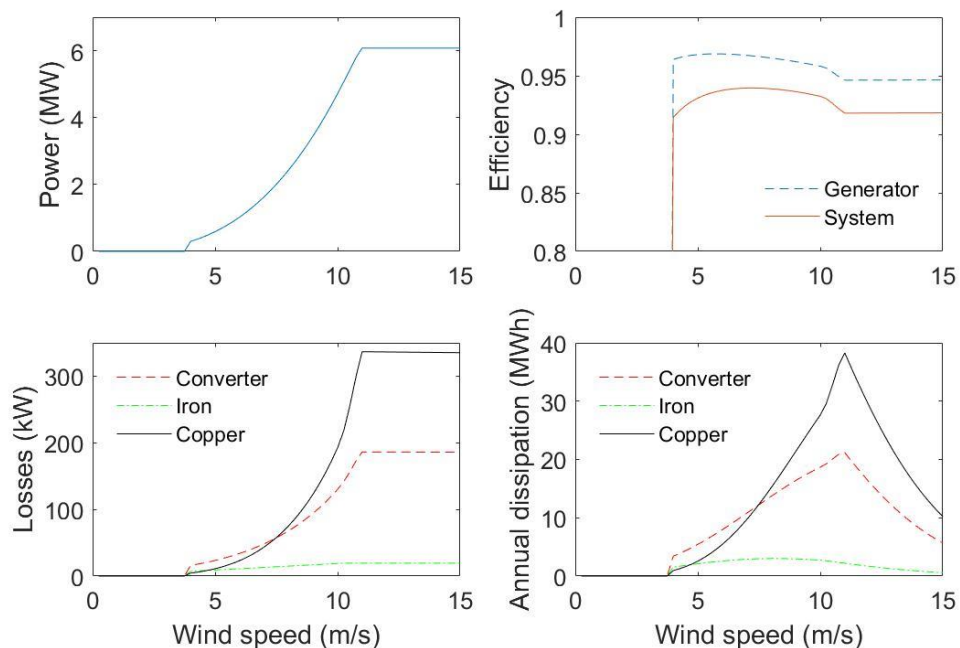
Figure 3.18 PMG DD Drivetrain Operation & Performance

3.8.2 PMG 1G

This drivetrain a similar but slightly higher COE than the direct-drive machine. Although it has a lower rating than the turbine discussed here, the AREVA M5000 would be a good exemplar of the single-stage PM generator drivetrain. Results are shown in Figure 3.19 and Table 3.11.

Because of its smaller torque rating the electrical machine is smaller and cheaper (in terms of materials and construction) than the direct-drive generator. The addition of the gearbox does make it more expensive (than the direct drive machine) from the view point of capital costs.

The real benefit of a PMG driven by a single-stage gearbox is the low losses with copper losses, iron losses and gearbox losses all being fairly balanced. Although there is a gearbox – which means that there are failures and downtime over and above the direct-drive machine – there are typically less electrical failures because the generator is smaller and has less windings that are prone to failures compared to larger generators. Offshore availability is lower compared to the direct-drive machine due to the increase in downtime from gearbox maintenance which is assumed to be the most significant contributor of downtime for geared topologies.
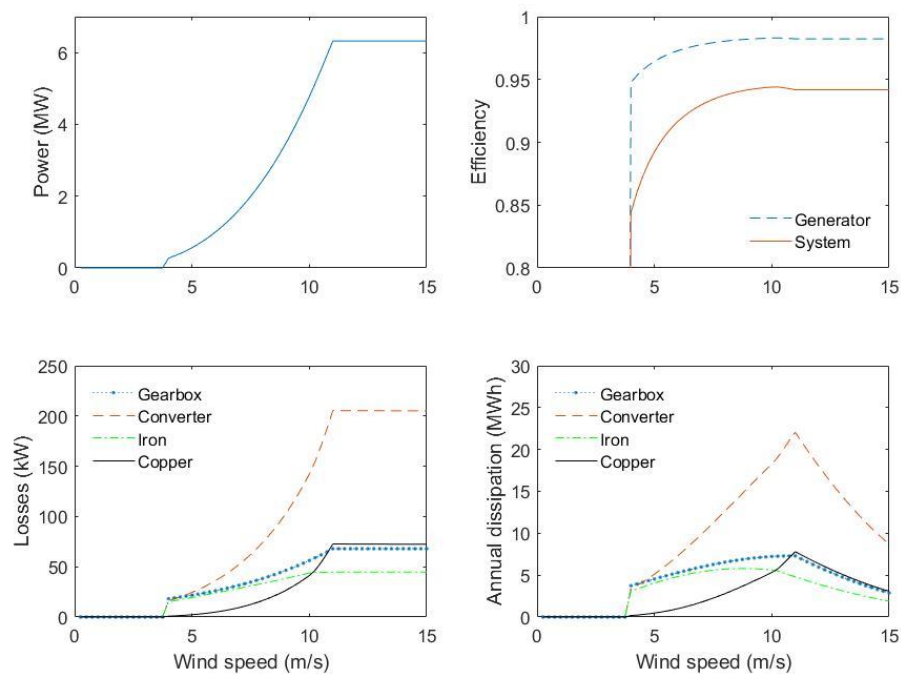
Figure 3.19 PMG 1G Drivetrain operation & performance.

3.8.3 PMG 2G

The Gamesa G128-5.0 MW and Samsung S7.0-171 turbines adopt a 2-stage gearbox with a permanent magnet generator. Results are shown in Figure 3.20 and Table 3.11.

Here the COE is higher than the direct-drive and PMG 1G. Overall losses and costs are higher than the drivetrains with slower generators; availability is worse because of the added failures in the gearbox when a second stage is added. The generator size is considerably smaller than the single-stage gearbox design and so has reduced losses in the stator. This lightweight generator would also be advantageous to developers during installation procedures. However, due to having a two-stage gearbox, the gearbox losses become more significant and the gearbox itself is larger and more expensive.
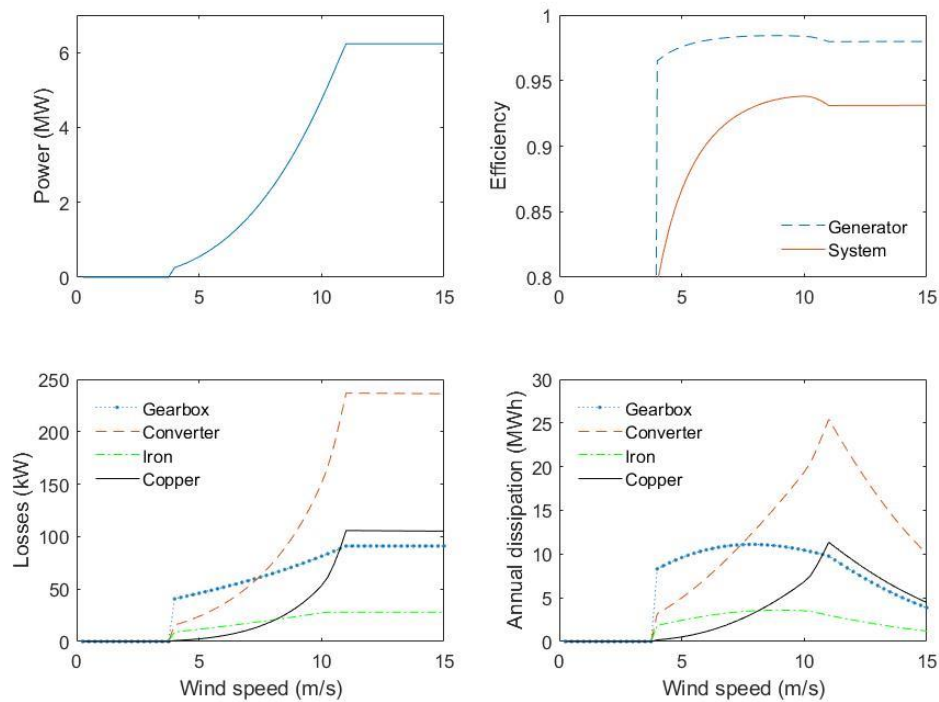
Figure 3.20 PMG 2G Drivetrain operation & performance.

3.8.4 PMG 3G

The PMG driven by a 3-stage gearbox has not yet been a popular choice in the offshore wind market, although the leading generator manufacturers such as ABB and the Switch have high speed PMGs in the 5-7 MW range. As one might expect, the generator is very compact, cheap and efficient. Unfortunately the increased losses, cost and downtime due to the additional gearbox stage give rise to a higher COE than all of the other drivetrains. Results from the MATLAB model for the PMG with a 3-stage gearbox are shown in Figure 3.21 and Table 3.11. It might be attractive should the cost of permanent magnets become very high as smaller generators would significantly offset the high ICC of the magnets.
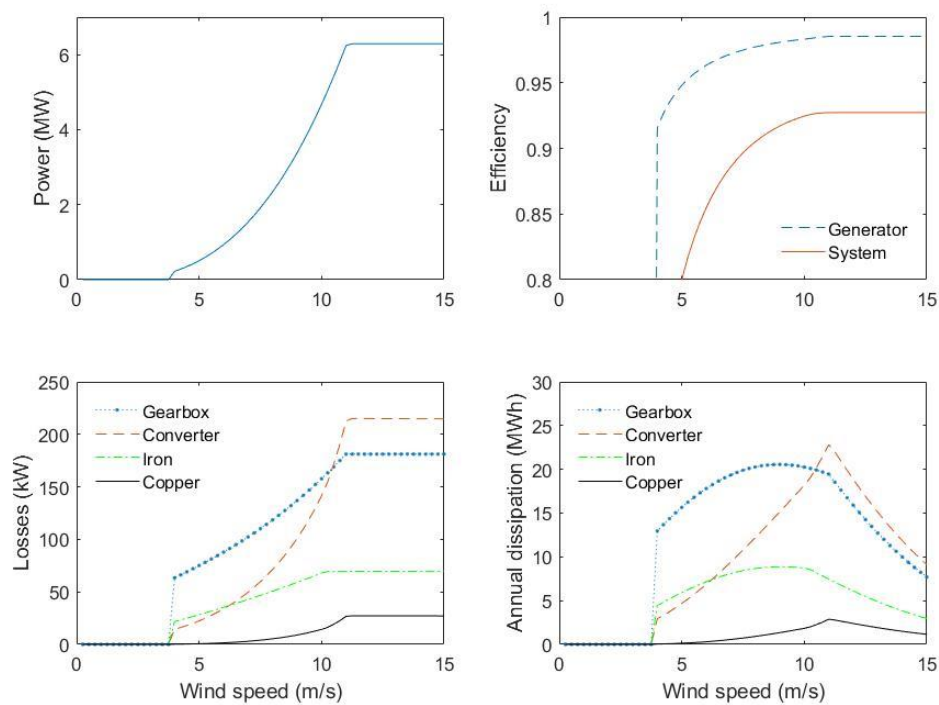
Figure 3.21 PMG 3G Drivetrain operation & performance

3.9 Summary of base case results

The base case results presented in this chapter offer and insight into the benefits and challenges of each drive train topology. The PMG DD and the PMG 1G appear to produce the lowest COE values when using basic assumptions. The PMG 3G suffers the poorest outcome in terms of COE due to issues with the reliability assumptions

for the topology. These outcomes are not yet optimised and some assumptions are still only basic such as sizing parameters. Therefore, in order to achieve more constrained, yet computationally optimised designs, a more detailed design process was adopted which is explained in detail in Chapter 4.

3.10 References for Chapter 3

[1]   L. Fingersh, M. Hand, and A. Laxson, "Wind Turbine Design Cost and Scaling Model," *NREL/TP-500-40566*, vol. 29, no. December, pp. 1–43, 2006.

[2]   K. Cory and P. Schwabe, "Wind Levelized Cost of Energy : A Comparison of Technical and Financing Input Variables Wind Levelized," *Tech. Rep.*, vol. NREL/TP-6A, no. October, 2009.

[3]   International Renewable Energy Agency, "Renewable Power Generation Costs in 2018," *International Renewable Energy Agency*. 2019.

[4]   C. Mone, M. Hand, M. Bolinger, J. Rand, D. Heimiller, and J. Ho, "2015 Cost of Wind Energy Review," *NREL/TP-6A20-66861*, no. May. 2015.

[5]   T. Burton, N. Jenkins, D. Sharpe, and E. Bossanyi, *Wind energy handbook*, 1st ed. John Wiley & Sons Ltd, 2001.

[6]   "Matlab software, version R2017a." .

[7]   H. Polinder, F. F. A. Van Der Pijl, G. J. De Vilder, and P. J. Tavner, "Comparison of direct-drive and geared generator concepts for wind turbines," *IEEE Trans. Energy Convers.*, vol. 21, no. 3, pp. 725–733, 2006.

[8]   J. Pyrhonen, T. Jokinen, and V. Hrabovcova, *Design of Rotating Electrical Machines*, 2nd ed. John Wiley & Sons Ltd, 2014.

[9]   British Standards Institute, "Gears — Thermal capacity — Part 1: Rating gear drives with thermal equilibrium at 95 °C sump temperature," *ISO*, vol. ISO/TR 141, 2001.

[10]   "The   Basics   of   Gear   Theory."   [Online].   Available: https://www.geartechnology.com/articles/0615/The_Basics_of_Gear_Theory/. [Accessed: 09-Sep-2018].

[11]   A. R. Nejad, "Development of a 5MW reference gearbox for offshore wind turbines," *Wind Energy*, vol. 17, 2016.

[12]   C. M. C. G. Fernandes, M. Hammami, R. C. Martins, and J. H. Seabra, "Power loss prediction: Application to a 2.5 MW wind turbine gearbox," *Proc. Inst. Mech. Eng. Part J J. Eng. Tribol.*, vol. 230, no. 8, pp. 983–995, 2016.

[13]   B.-R. Höhn, K. Michaelis, and M. Hinterstoißer, "Optimization of Gearbox Efficiency," *Gomabn*, vol. 48, no. 4, pp. 462–480, 2009.

[14]   D. E. P. Gonçalves, C. M. C. G. Fernandes, R. C. Martins, and J. H. O. Seabra, "Torque loss in a gearbox lubricated with wind turbine gear oils," *Lubr. Sci.*, vol. 25, no. 4, pp. 297–311, 2013.

[15]   R. Scott Semken *et al.*, "Direct-drive permanent magnet generators for high-power wind turbines: benefits and limiting factors," *IET Renew. Power Gener.*, vol. 6, no. 1, p. 1, 2012.

[16]   A. McDonald and N. Bhuiyan, "On the optimization of generators for offshore direct drive wind turbines," *IEEE Trans. Energy Convers.*, vol. 8969, no. c, pp. 1–1, 2016.

[17]   A. S. McDonald, "'Structural analysis of low speed, high torque electrical generators for direct-drive renewable energy converters,' Ph.D. dissertation, Dept. Eng. And Electron., Univ. Edinburgh, Edinburgh, Scotland," 2008.

[18]   A. McDonald and N. A. Bhuiyan, "On the Optimization of Generators for Offshore Direct Drive Wind Turbines," *IEEE Trans. Energy Convers.*, vol. 32, no. 1, pp. 348–358, 2017.

[19]   S. Midea, *Heat Treating: Including Steel Heat Treating in the New Millennium*, 1st ed. Asm Intl, 2000.

[20]   RAB, "Value breakdown for the offshore wind sector," Renewables Advisory Board, Report, 2010.

[21]   J. Carroll, "Cost of energy modelling and reduction opportunities for offshore wind turbines," PhD Thesis, University of Strathclyde, 2016.

[22]   EWEA, "The European offshore wind industry key 2015 trends and statistics," *Eur. Wind Energy Assoc.*, no. January, p. 31, 2015.

[23]   P. J. Tavner, J. Xiang, and F. Spinato, "Reliability analysis for wind turbines," *Wind Energy*, vol. 10, no. 1, pp. 1–18, Jan. 2007.

[24]   M. D. Reder, E. Gonzalez, and J. J. Melero, "Wind Turbine Failures -

Tackling current Problems in Failure Data Analysis," *J. Phys. Conf. Ser.*, vol. 753, no. 7, 2016.

[25]   T. M. Delorm, Y. Lu, A. Christou, and P. McCluskey, "Comparisons of offshore wind turbine reliability," *Proc. Inst. Mech. Eng. Part O J. Risk Reliab.*, vol. 230, no. 3, pp. 251–264, 2016.

[26]   U. Shipurkar, K. Ma, H. Polinder, F. Blaabjerg, and J. A. Ferreira, "A review of failure mechanisms in wind turbine generator systems," *2015 17th Eur. Conf. Power Electron. Appl. (EPE'15 ECCE-Europe)*, pp. 1–10, 2015.

[27]   L. Alhmoud and B. Wang, "A review of the state-of-the-art in wind-energy reliability analysis," *Renew. Sustain. Energy Rev.*, vol. 81, no. May 2017, pp. 1643–1651, 2018.

[28]   S. Sheng, "Wind Turbine Gearbox Condition Monitoring Round Robin Study – Vibration Analysis Wind Turbine Gearbox Condition Monitoring Round Robin Study – Vibration Analysis," *NREL/TP-5000-54530*, no. July, 2012.

[29]   American Gear Manufactures Association, "ANSI/AGMA 2001-D04 Fundamental Rating Factors and Calculation Metrhods for Involute Spur and Helical Gear Teeth," *ANSI/AGMA Stand. Ser.*, vol. 04, p. 66, 2004.

[30]   American Gear Manufacturers Association, "Geometry Factors for Determining the Pitting Resistance and Bending Strength of Spur, Helical and Herringbone Gear Teeth AGMA 908-B89," *ANSI/AGMA Stand. Ser.*, vol. 89, no. August, p. 79, 1989.

[31]   C. D. Schultz, "The Effect of Gearbox Architecture on Wind Turbine Enclosure Size Enclosure Size." American Gear Manufacturers Association, AGMA Technical Report, 2009.

[32]   "Trading Economics, Euro Area Inflation Rate. [Online] [Cited 20/7/12] http://www.tradingeconomics.com/euro-area/inflation-cpi." .

[33]   TCE, "A Guide to an Offshore Wind Farm," The Crown Estate, Report, 2010.

[34]   RenewableUK, "Offshore Wind: Forecasts of future costs and benefits," RenewableUK, Report, 2011.

Chapter 4 Permanent Magnet Generator Drive Train Optimisation

This chapter outlines the chosen optimisation method for the 4 drive train designs introduced in Chapter 3 and presents the initial optimised solutions. The aim of this chapter is to create a detailed constrained optimisation method for PMG based drive trains to reduce the COE and create feasible designs. Optimising for COE is an effective method for creating a design based on its lifetime operation and does not just depend on capital cost but looks at efficiency and reliability too. Minimising the COE of the design does require a lot of information about the rest of the system which is unaffected by the optimisation process and so leads to further challenges obtaining representative values.

The chapter begins with a breakdown of the key considerations and assumptions developed for the model. The assumptions include specific design constraints as well as cost estimates for calculating various contributions to the cost of energy (COE). The results from the optimisation of all 4 drive trains are presented and a sensitivity to design specifications for each concludes the chapter. Although this thesis focuses on PMG type drive trains to align with current industrial trends, the methodology can be applied to other powertrain types.

4.1 Optimisation methods

Optimisation involves finding the maximum or minimum of a function depending on its objective. Typically, in multi-variable functions, there may be local or global solutions and systems can deterministic or stochastic which include randomness or probability. Optimisation can be constrained by several conditions or free to locate optimum values (unconstrained). Depending on the mathematic problem, different optimisation methodologies will provide different levels of certainty and confidence in the outcome. Choosing an appropriate methodology for the optimisation problem depends on the requirements of the optimisation process. Some of the most widely used optimisation techniques in engineering and mathematics include interior-point

method, pattern search techniques, evolutionary algorithms, genetic algorithms and particle swarm optimisation [1][2].

The COE minimisation objective function that will be used in this analysis is a mixed integer problem (pole pairs and number of teeth for gear stages are integers) that includes a number of constraints and so requires a solver that can handle such problems. In addition, it is recognised that several outcomes can be produced for similar objective function results as the problem is multi-variable. Having an optimisation process that allows for key parameter sensitivities to be identified and for a high level of control over the constraints is required for this thesis.

4.2 Optimisation using Genetic Algorithm

Genetic algorithms offer an attractive optimisation process based on the evolution of variables within a population and allows several outcomes to be explored rather than converging to a single minimum. Genetical algorithms are used in many fields of engineering such as optimising water distribution systems [3], optimising energy efficiency in building designs [4] and for designing offshore wind electrical system optimisation processes [5]. Due to the flexibility in the uses of a genetic algorithm in terms of multiple solutions and its ability to handle mixed integer values, the genetic algorithm solver was selected as the optimisation method for this thesis.

The Genetic Algorithm toolbox in Matlab [6] was used as the optimisation process for each design case. MATLAB's genetic algorithm solver "ga" offers an efficient method with both linear and non-linear constraints and can handle mixed integer problems unlike the other optimisation method available in MATLAB [7]. Genetic algorithms allow various solutions to be identified which will provide useful analysis and a sensitivity study of the results.
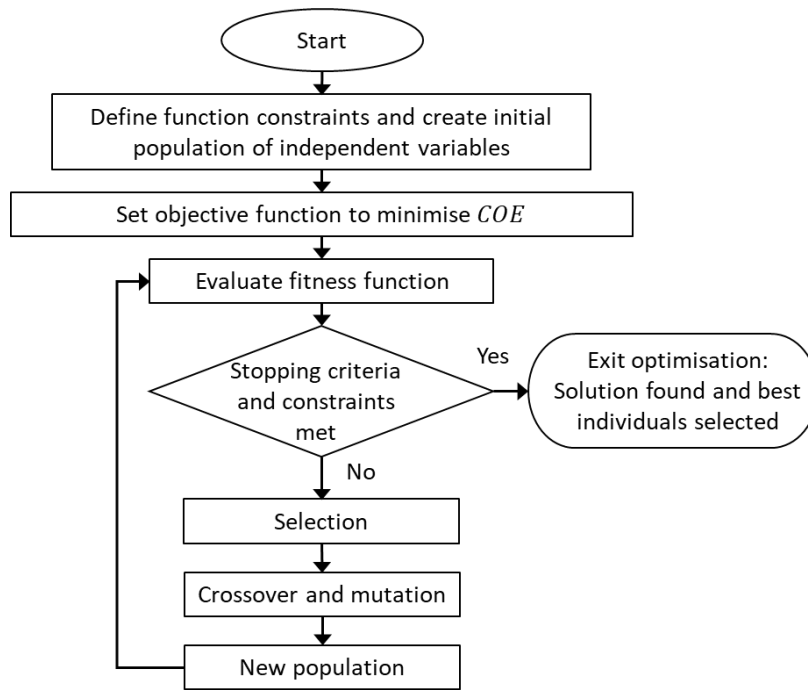
Figure 4.1 Flow chart of GA optimisation process.

The genetic algorithm (GA) computes the following steps [7] which are also presented as a flow chart in Figure 4.1:

1. A random initial population is created

2. A sequence of new populations is created. At each step the current generation individuals are used to create the next population. The following steps are performed to create the new population:

    a   Each member of the current population is scored by computing its fitness value. These values are called the raw fitness scores.

    b   The raw fitness scores are scaled to convert them into a more usable range of values. These scaled values are called expectation values.

    c   Members are selected, called parents, based on their expectation.

    d   Some individuals in the current population that have lower fitness are chosen as elite. These elite individuals are passed to the next population.

    e   Children are produced from the parents by either making random changes to a single parent, known as mutation, or by combining the vector entries of a pair of parents, known as crossover.

    f   The current population is replaced with the children to form the next generation.

3. The algorithm stops when one of the stopping criteria is met.

Each chosen independent variable used in the optimisation process was allocated lower and upper values that would provide feasible outcomes and the GA would identify a local minimum. Each iteration of the GA, results in different local minima so in to locate a global minimum, the population constraints would require restriction. Advantages of using a GA include reduced computational time as it has can be used in parallel and finds solutions quickly. A feature of using the GA producing is the ability to produce many different independent variable outcomes whilst minimising the COE. For example, two separate iterations could produce the same COE output, but with different independent variable values. An advantage of allowing a number of design options to be produced could be that technical experts would be able to judge the most suitable designs in terms of manufacturing and operational capabilities. Rather than producing just one definitive outcome, a number of outcomes would provide additional discussion and scrutiny opportunities that could assist in the manufacturing process.

4.2.1 Genetic Algorithm implementation challenges

A significant challenge when using a genetic algorithm methodology is the model sensitivity to the initial conditions and upper and lower parameter bounds. This requires prior knowledge of some unfeasibility issues that may result if inappropriate initial conditions are chosen which can be time consuming to rectify. Also, the stopping criteria may require several alterations to suit the type of optimisation required and the number of variables involved in the process which can also lead to some difficulties in implementing the model.

4.3 Design Considerations and Constraints

Each design had various constraints and assumptions applied to the models. Specific details of constraints for each design are described throughout this chapter. For consistency and comparability between each case, the random number selection of initial population was kept constant. The generator structure cost is based on a simplified cost model that includes deflection calculations (more detail in Chapter 3) and the overall cost is expected to be higher than presented. For the purposes of comparison, the additional cost not shown is assumed to be included in the "rest of the wind turbine" cost.

4.4 Direct drive generator

The design of the 6 MW direct drive generator was initially based on a study by Polinder [8] which was scaled up from a 3 MW to a 6 MW wind turbine.

The direct drive model has 8 different variables used in the optimisation which are as follows:

1. **The air gap radius of the generator, r_s**
   - ➢ This variable allows the diameter of the generator vary.
2. **The stack length of the generator, l_s**
   - ➢ This helps size the generator lengthwise and so dictates the volume of magnet, steel and copper.
3. **The number of pole pairs, p**
   - ➢ Varying this allows the optimal flux density profile to be obtained and is related to the size of the generator.
4. **The height of the magnet, h_m**
   - ➢ The height of the magnet is important to have sufficient flux crossing the air gap but is also expensive with larger magnets so having it as a variable will help optimise the design for cost.
5. **The magnet width to pole pitch ratio, τ_p**
   - ➢ This will help size the magnets in accordance with the pole pitch.

6. **The size of the air gap, g**

   ➤ The size of the air gap is a key part of the magnet circuit for the design with too large an air gap meaning flux cannot cross, and too small an air gap creates issues with assembly.

7. **The height of the slots, h_s**

   ➤ This helps size the stator slots and the volume of copper

8. **The slot width to pole pitch ratio, τ_s**

   ➤ The width of the slots in relation to the slot pitch is important so that the path of flux is optimised and for the slot teeth to be sufficiently thick for structural strength.

By choosing the above parameters as optimisation variables, the complete generator system can be determined such that COE is minimised for the particular conditions. The direct drive generator length to diameter ratio was limited such that $0.2 < l_s /2r_s < 0.27$ based on numbers from [9].

4.4.1 Optimised design for PMG DD

An optimised design for the PMG DD produced a COE of 109.98 €/MWh which is a saving of 1.49 €/MWh compared with the base case of Chapter 3.

The loss characteristics are shown in Figure 4.2. The most significant losses occur in the copper windings with a base loss of 300 kW at rated wind speed and above.
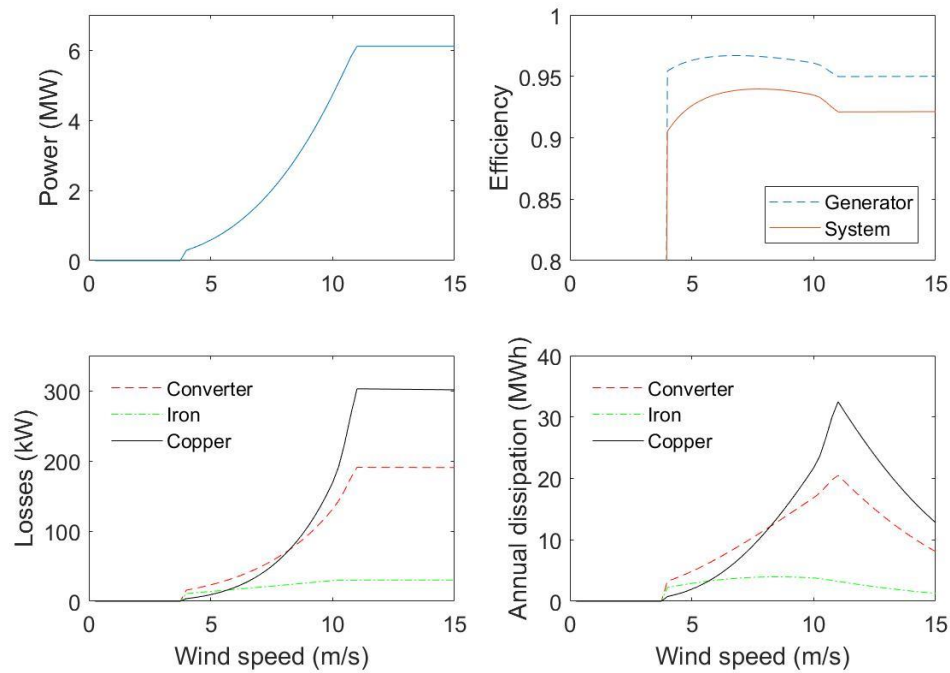
Figure 4.2 Efficiency and loss characteristics of the optimised PMG DD.

4.5 Single-stage gearbox and medium speed generator

The single-stage gearbox model has an additional 5 variables, along with the initial 8 generator design variables seen with the direct drive design, in order to optimise the gearbox. The gearbox is a planetary spur gear design with the following additional independent variables:

9. **The pitch diameter of the sun, D_{sun}**
10. **The number of teeth on the sun, z_{sun}**
11. **The number of teeth on the ring, z_{ring}**
12. **The number of teeth on each planet, z_{planet}**
13. **The face width of the gears, F_{gear}**

These additional 5 variables are enough to calculate the complete dimensions of the gearbox with a few additional assumptions such as the gear module is equal between gears and basic gear tooth profile assumptions. The number of planets is linked to the

gear ratio, so the optimisation process will decipher the best layout for the planetary stage gearbox that keeps the COE minimised.

4.5.1 Optimised design for PMG 1G

An optimised design for the PMG 1G produced a COE of 113.79 €/MWh which is a saving of 1.45 €/MWh compared with the base case of Chapter 3. The loss characteristics are shown in Figure 4.3.
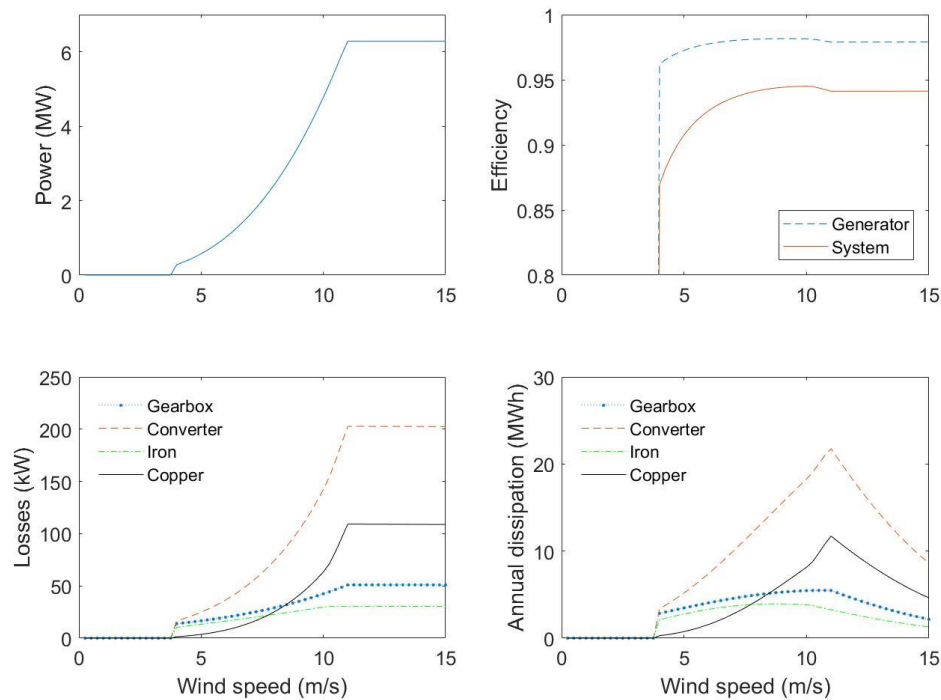

Figure 4.3 Efficiency and loss characteristics of the optimised PMG 1G.

Compared with the PMG DD, the copper losses for the PMG 1G are reduced due to the smaller generator size and gearbox losses are introduced. The converter contributes most significantly to the annual energy dissipation and is a set loss assumption between all drive trains and is proportional to the power rating of the wind turbine.

4.6 Two-stage gearbox and medium-high speed generator

The two-stage gearbox model also has a further 5 variables to include the second stage of the gearbox, so the total number of variables is 18. The 2nd gearbox stage is a

planetary spur gear design so that it is in keeping with current industrial trends [10][11][12]. The planetary gear type of the 1st stage remains the same as the single stage design, but its specifications will alter throughout the optimisation process along with the new secondary stage so that both stages optimise with each other. The 5 additional independent variables are as follows:

14. The pitch diameter of the second stage sun, D_{sun2}

15. The number of teeth on the second stage sun, z_{sun2}

16. The number of teeth on the second stage ring, z_{ring2}

17. The number of teeth on each planet of the second stage, $z_{planet2}$

18. The face width of the gears of the second stage, F_{gear2}

4.6.1 Optimised design for PMG 2G

An optimisation process allowed the gear ratio to vary between 1:15 and 1:40 to provide a higher degree of freedom to the model to determine the optimum design. Typical gearboxes with more than one stage have ratios between 1:20 and 1:120 as discussed in various literature [12][13]. An optimised design for the PMG 2G produced a COE of 117.74 €/MWh which is a saving of 2.63 €/MWh compared to the results in Chapter 3. The loss characteristics for the PMG 2G are shown in Figure 4.4.

The gearbox losses are more significant at lower wind speeds and so this is reflected in the reduced efficiency in the system at wind speeds below rated. Although at rated speed, copper losses are higher, the annual dissipation due to gearbox losses is higher than the losses associated with the generator. The benefits of having a reduced generator size are slightly offset by the increased gear losses.
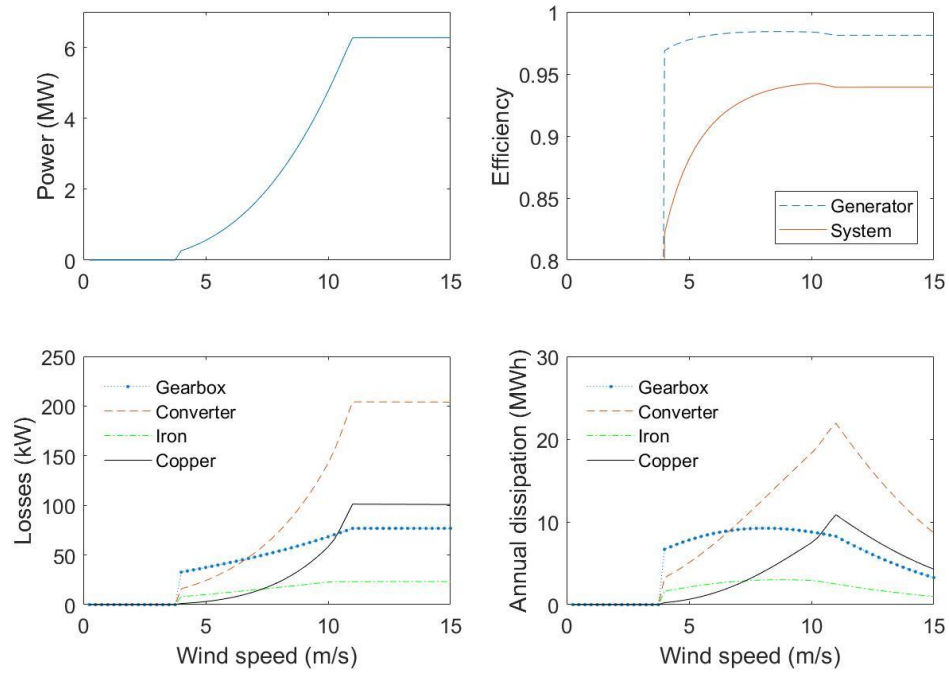
Figure 4.4 Efficiency and loss characteristics of the optimised PMG 2G.

4.7 Three-stage gearbox and medium-high speed generator

The three-stage gearbox model also has a further 4 variables to include the final third stage of the gearbox so the total number of variables is 22. The 3rd gearbox stage is a parallel helical gear design with a helix angle of 10 degrees and the additional variables are as follows:

19. The pitch diameter of the gear, D_{gear}

20. The number of teeth on the gear, z_{gear}

21. The number of teeth on the pinion, z_{pinion}

22. The face width of the gears for the third stage, F_{gear3}

4.7.1 Optimised design for PMG 3G

An optimised design for the PMG 3G produced a COE of 118.84 €/MWh which is a huge saving of 17.04 €/MWh (almost 15%) compared with the base case of Chapter 3.
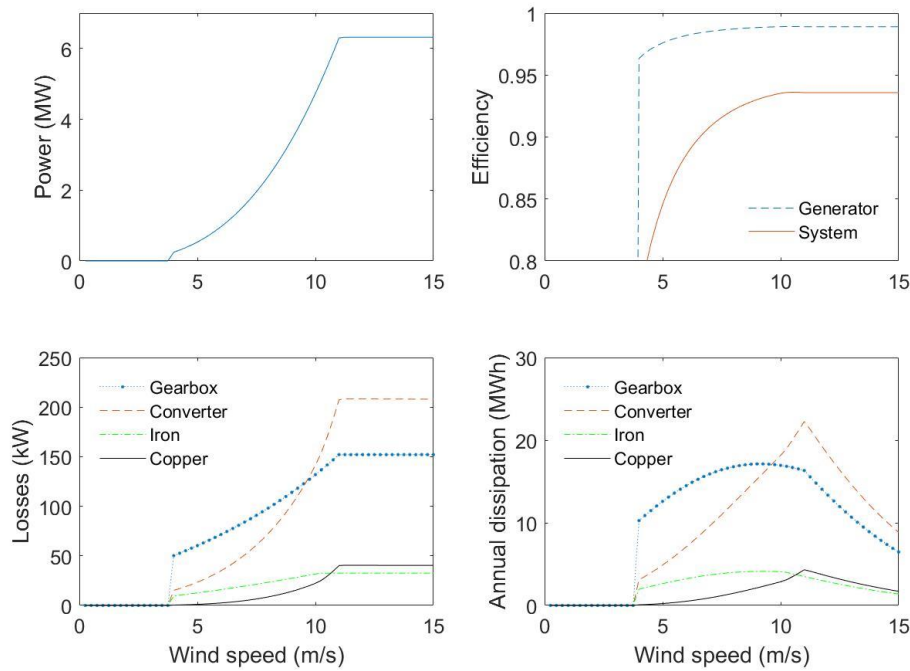
Figure 4.5 Efficiency and loss characteristics of the optimised PMG 3G.

This improved COE result implies that the gearbox loading constraints allow the best possible design for a 3-stage gearbox to be produced that satisfies a number of conditions and operation requirements.

The loss characteristics are shown in Figure 4.5. The losses associated with the gearbox have much more of an impact on the system efficiency, particularly at below rated wind speeds. The annual energy dissipation due to the gearbox is higher than the dissipation linked to the converter. Despite the additional gear stage, the overall COE for the PMG 3G is almost identical to the PMG 2G, with the 2-stage gearbox design offered a slight improvement. This suggests that there is little financial incentive between the two designs and that ultimately a decision would lie with manufacturers and developers that may require alternative objectives.

4.7.2 Optimised design comparison

The results shown in

Table 4.1 compares the 4 optimised designs.

Table 4.1 Optimised design for each drive train based on GA minimisation of COE

	DD PMG	PMG 1G	PMG 2G	PMG 3G
Generator Specifications				
Generator speed (rpm)	10.5	52.5	170.3	890.1
Gearbox ratio	-	1:5	1:16.2	1:84.8
Stator radius r_s (m)	4.04	2.61	1.19	0.43
Stack length l_s (m)	1.61	0.83	0.72	0.79
Number of pole pairs p	183	86	27	10
Air gap g (mm)	6.47	5.25	2.26	0.93
Magnet height l_m (mm)	12.36	17.12	25.40	28.81
Generator Material Weight (ton)				
Iron	30.4	8.4	4.0	1.4
Copper	8.0	2.5	1.2	0.4
PM	2.4	1.0	0.5	0.3
Total	40.8	11.9	5.7	2.0
Cost (kEuro)				
Generator active material	357.2	123.2	61.4	26.1
Generator construction	69.8	12.0	2.3	0.5
Gearbox	0	397	464	467
Generator system cost	427	532	527	494
Converter	762	762	762	762
Other wind turbine parts	4108	4108	4108	4108
Total cost of wind turbine	6012	6131	6126	6088
Annual Energy				
Copper losses (MWh)	820	260	268	152
Iron losses (MWh)	186	236	184	197
Converter losses (MWh)	614	669	684	667
Gearbox losses (MWh)	0	200	366	703
Availability (%)	95.5	94.4	93.8	93.4
Total losses (MWh)	1619	1169	1143	1031
Energy yield (GWh)	19.50	19.63	19.33	19.18
Cost of Energy				
ICC (kEuro)	18219	18580	18563	18448
AOM (kEuro)	34.9	81.7	126.8	142.7
FCR	0.116	0.116	0.116	0.116
COE (Euro/MWh)	109.98	113.79	117.74	118.84

The most significantly improved design compared with the base results of chapter 3 was the PMG 3G that had its COE reduced from 135.88 €/MWh to 118.4 €/MWh. The PMG 2G design has very similar results in terms of COE with a value of 117.74 €/MWh. Therefore, it can be concluded that there is very little financial difference in these two design options over the lifetime of the project if the assumptions hold true.

The PMG DD came out on top again with the lowest COE. It should be noted that because of the limited available data for PMG reliability, only major and minor

repair statistics are used and not major replacement. The impact of a major replacement of the generator is investigated in Chapter 5 to observe the influence on the COE.

The PMG 1G optimisation produced promising results and the COE reduced by 1.45 €/MWh compared with the base case in Chapter 3.

4.8 Optimisation sensitivity analysis

The optimised designs provided a useful insight into how the designs compare with one another whilst restricted by optimisation constraints. A key method in comparing the performance of each drive train against the others is to conduct a sensitivity to the design parameters. By varying the air gap radius independently for each generator and allowing the other parameters to be optimised for that set radius value, the design variations and COE output can be assessed. For the geared designs, the impact of redesigning the gearbox for alternative gear ratios could provide more a larger variety of solutions depending on manufacturing considerations. The following design parameters (which had the highest impact on the COE values) were independently varied between a specified range and the effect on the physical design dimensions and the COE were analysed:

- Generator air gap radius
- Gear ratio

4.8.1 Sensitivity to generator air gap radius

The generator air gap radius was the first independent variable to be studied in the simple sensitivity analysis. All 4 drive train designs were optimised again whilst holding the air gap radius constant for each iteration and varying its value through a range.

4.8.2 Direct drive design results

The radius was varied between 3.5 m and 5.5 m (even though a diameter of 10m would create its own logistical challenges, it was useful to observe the impact on the design). The COE results are shown in Figure 4.6 below.
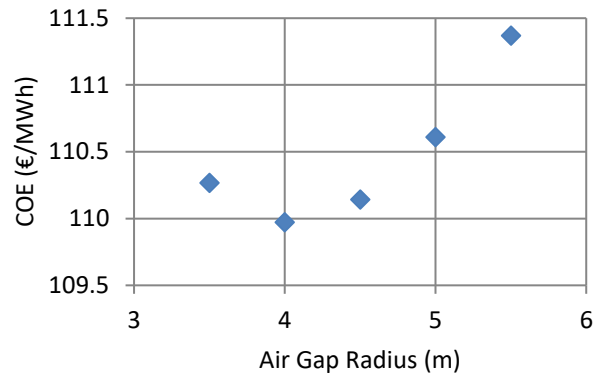
Figure 4.6 Cost of energy with varying generator radius between 3.5 and 5.5 m for the PMG DD drive train.

A cost of energy minimum of around 110 €/MWh is observed at 4 m when increasing the generator radius from 3.5 m to 5.5 m. With one of the main issues being transport and installation of very large diameter generator, the ultimate choice in diameter is dictated by the method used to install. It is possible to push diameters beyond a typical 6 m and this case a diameter of 8 m offers the most cost-effective design. A possible solution would be to manufacture the generator as a modular system which would assist in the installation process as separate lighter sections will be much easier to transports and can lifted with less expensive methods.
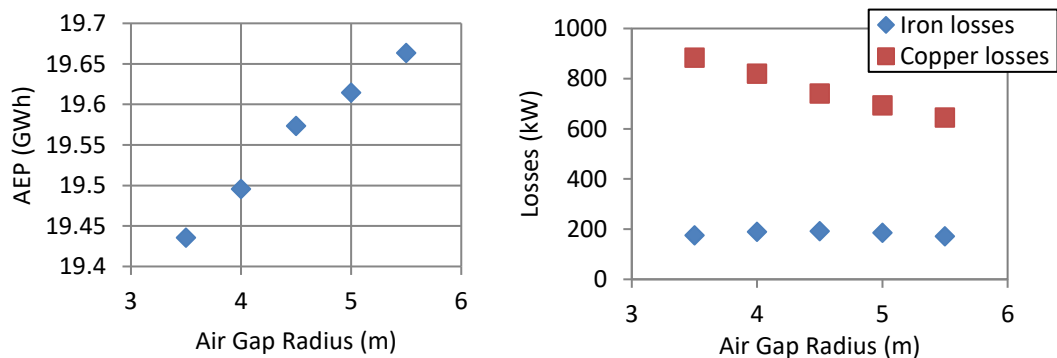
Figure 4.7 Annual energy production and losses with increasing generator radius for the PMG DD drive train.

The Joule losses are significantly reduced with increasing generator radius with more than 40% improvement in losses with the large radius. Iron losses are kept fairly constant although a very small increase is observed. With overall losses reduced and an improved generator efficiency obtained at higher radii, the energy produced also increased.
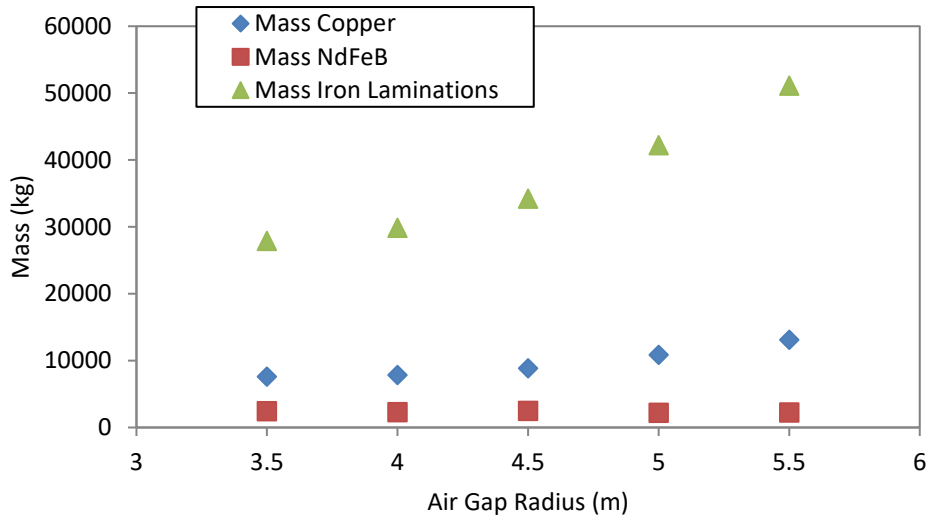
Figure 4.8 Mass increase in copper, permanent magnet and iron laminations with increasing generator radius for the PMG DD drive train.

The overall mass of magnets remains around 2300 kg across the range of air gap radius values which signifies the importance of keeping the volume of magnets as low as possible. Significant increases in weight are observed at higher radii in terms of iron laminations (82% increase in mass across the observed range of radii). However, compared with the price of the magnets and the copper, the cost of iron is overall low impact per kg. The optimiser tries to maintain a low volume of materials whilst maximising the dimensions

The generator structure cost (Figure 4.9) is only based on a simple cost per kg from a mass calculated using the method described in Chapter 3. The cost values may be slightly low compared to values from [8] but it can be assumed that the "rest of the wind turbine" cost covers any shortfall in terms of the complete structure cost.

As this method is kept constant throughout the model it serves as a suitable value for drive train comparison purposes.
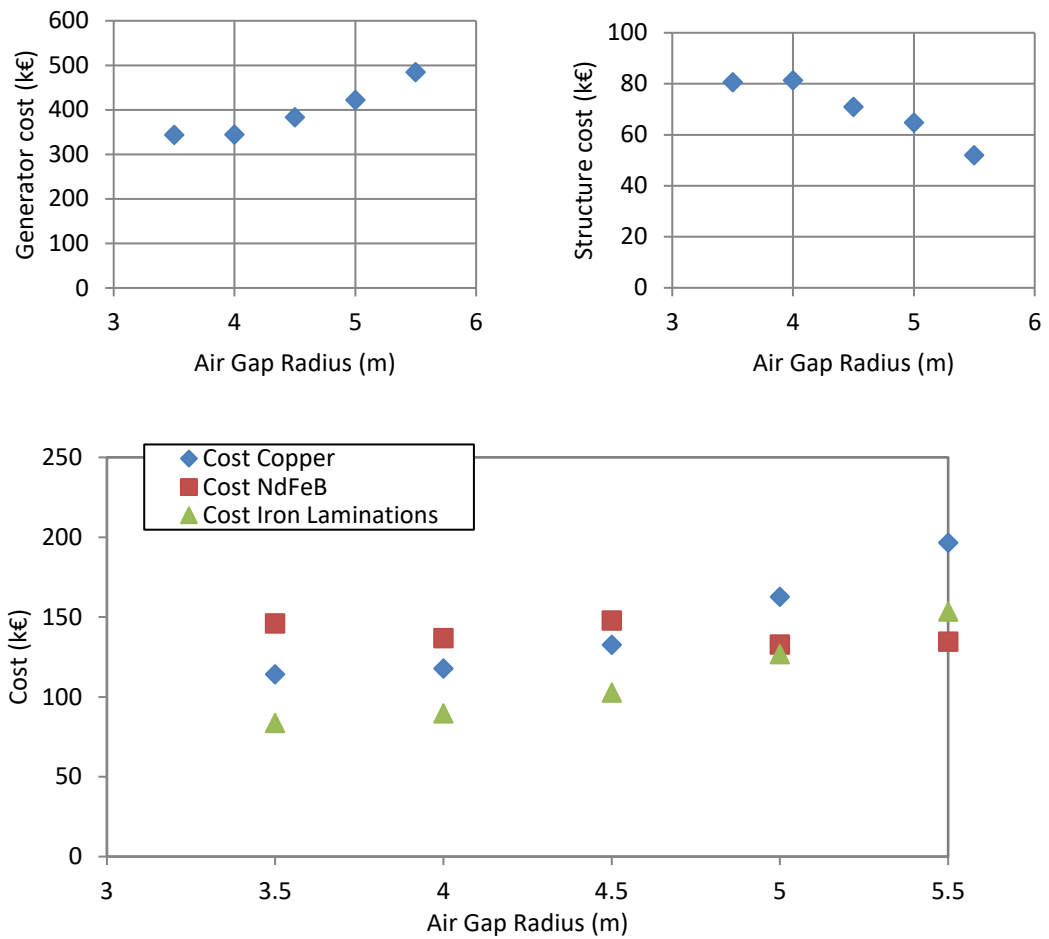
Figure 4.9 Generator active materials cost and structure cost with varying radius for the PMG DD drive train.
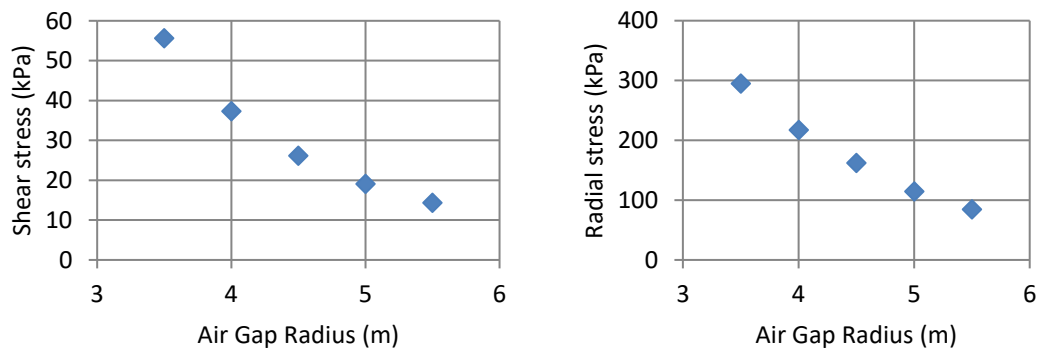
Figure 4.10 Shear stress and normal radial stress with increasing generator radius for the PMG DD drive train.

The shear stress decreases as the diameter increases and so the cost of the structure can also reduce as the volume of steel reduces. Reducing the magnitude of the magnetic circuit parameters allows the design to be kept within cost effective physical limits. When increasing the diameter of the generator, the stack length decreases as expected to maintain the $r_s^2 l_s$ relationship with torque and shear stress.

$$\sigma = \frac{\tau}{2\pi r_s^2 l_s} \tag{4.1}$$
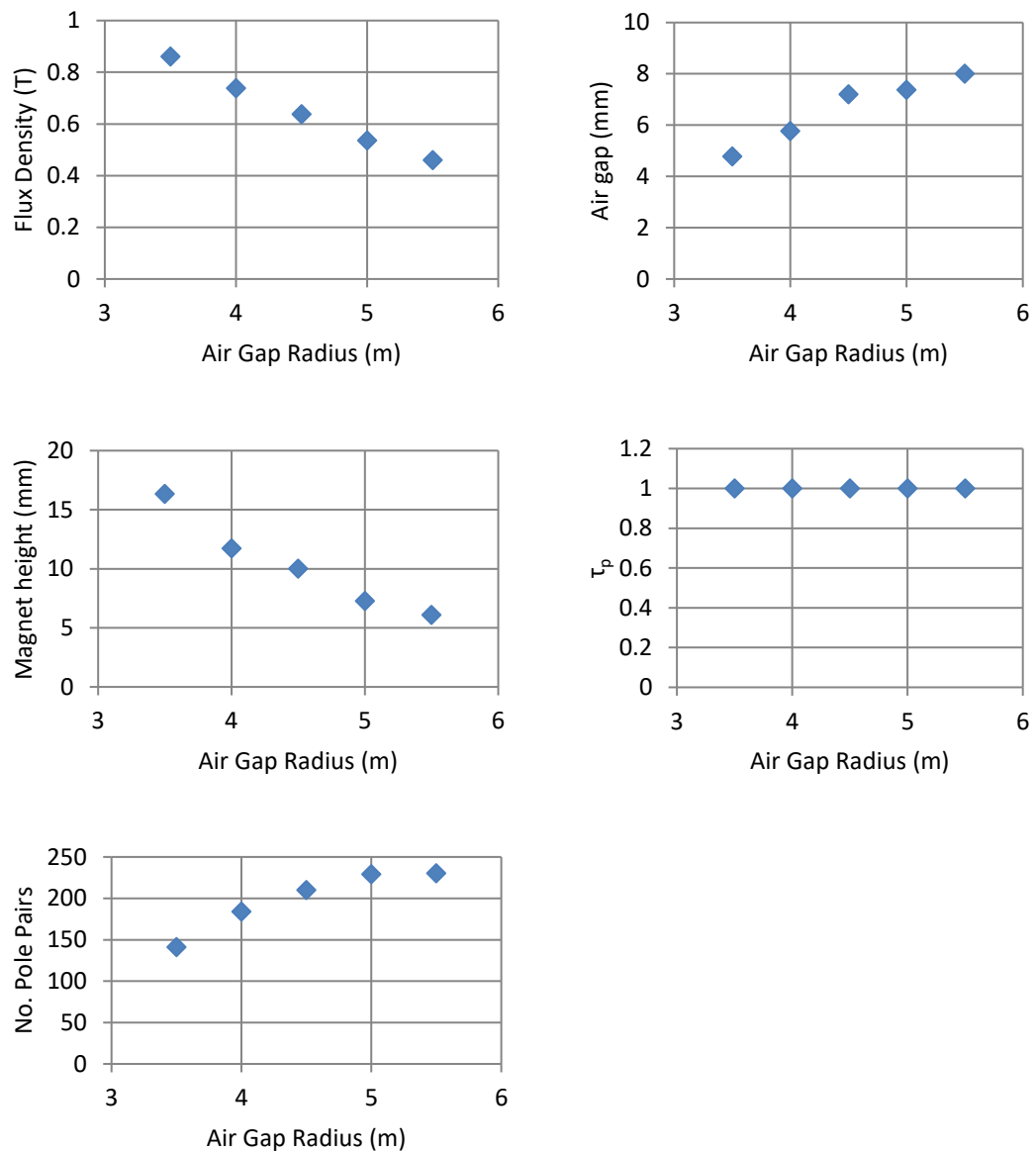
Figure 4.11 The effect of increasing the generator radius on the flux density, air gap width, magnet height, the magnet width to pole pitch ratio, and number of pole pairs for the PMG DD drive train.

It can be observed from Figure 4.11 that the magnet height has a maximum value of 16.4 mm at a generator radius of 3.5 m. The width of the magnets to the pole pitch ratio start to reduce after 4.5 m are reduced meaning that the magnets are further apart from each other despite the number of poles increasing. This implies a lower level of flux leakage as the poles themselves are smaller and flux lost to neighbouring magnets is reduced. There is a trade-off between the magnet height and the increasing air gap where the design becomes increasingly expensive and that the model forces the minimisation of the magnetic material to keep COE low and so compromises the magnetic circuit efficiency.

Air gap size has a "rule of thumb" of $2r/1000$. The graph below shows how the air gap size is chosen to be lower than the "rule of thumb" values. The air gap was free to vary $2r/1000 \pm 20$ %. As the radius increases, the air gap progressively gets further from the predicted value until at a 5 m radius, the air gap is optimised to be 9 mm rather than the predicted value of 10 mm. The optimiser tends to keep the air gap size as low as possible and still maintain a functioning value of flux density.
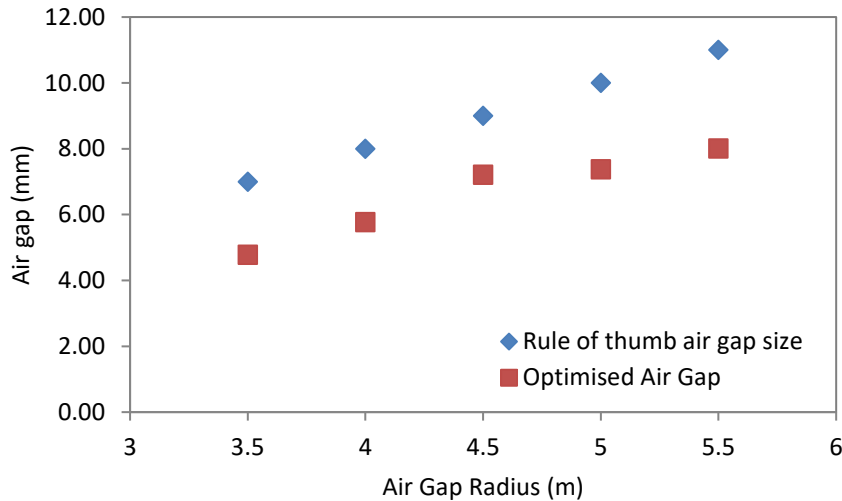
Figure 4.12 Optimised air gap in comparison with the predicted air gap for the PMG DD drive train.
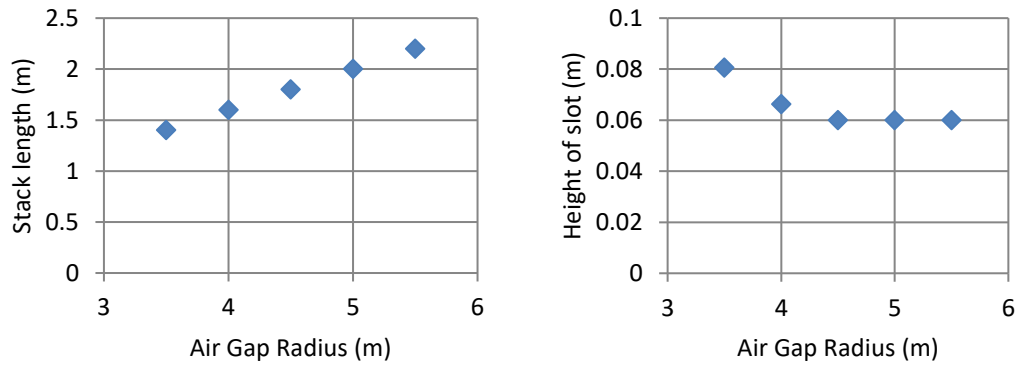
Figure 4.13 Stack length and height of slot with varying the air gap radius for the PMG DD drive train.

Since the optimisation is based on minimising the cost of energy over the lifetime of the turbine, the results may not present the most efficient design in terms of magnetic circuit and AEP, but focuses more on the reduction in cost. There tends to be a trade-off with efficiency and capital cost.

4.8.3 Single-stage gearbox PMG sensitivity results

The generator air gap radius was varied between 1.5 m and 3.5 m. The COE results are shown in Figure 4.6 below.
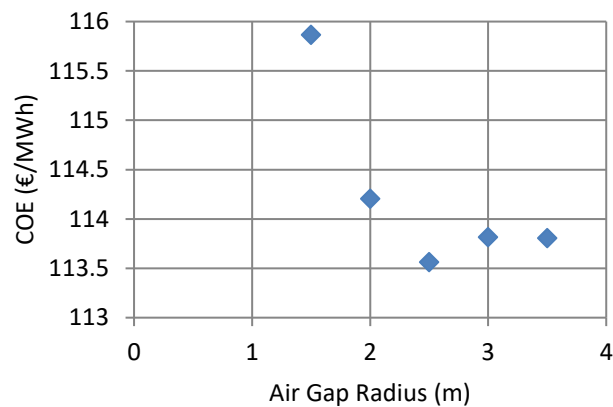
Figure 4.14 Cost of energy with varying generator radius between 1 and 3 m for the PMG 1G drive train.

The cost of energy reduces by 2.3 €/MWh when increasing the generator radius from 1 m to 2.5 m before increasing again as the radius tends towards 3.5 m. This is a

different result compared to the direct drive case as the addition of the gearbox creates further constraints on the optimum design dimensions. Very large radii add additional mass and so mitigate the benefit of using a gear stage in terms of cost.
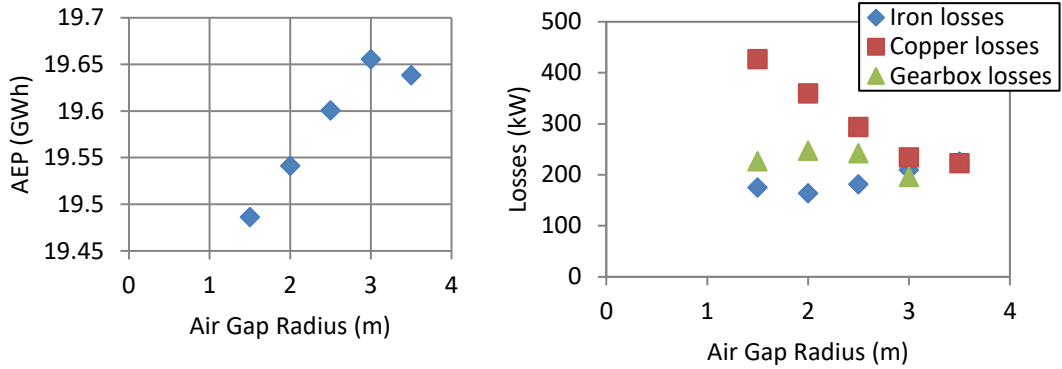
Figure 4.15 Annual energy production and losses with increasing generator radius for the PMG 1G drive train.

The Joule losses reduce with increasing generator radius whilst the iron losses slightly increase. The losses associated with the gearbox fluctuate as the radius increases as the design and dimensions of the gearbox vary to keep the COE as low as possible. The annual energy production reduces slightly from its maximum that was obtained at 3 m generator radius, and so reiterates how larger generator radii in the case of the PMG 1G does not improve the design.
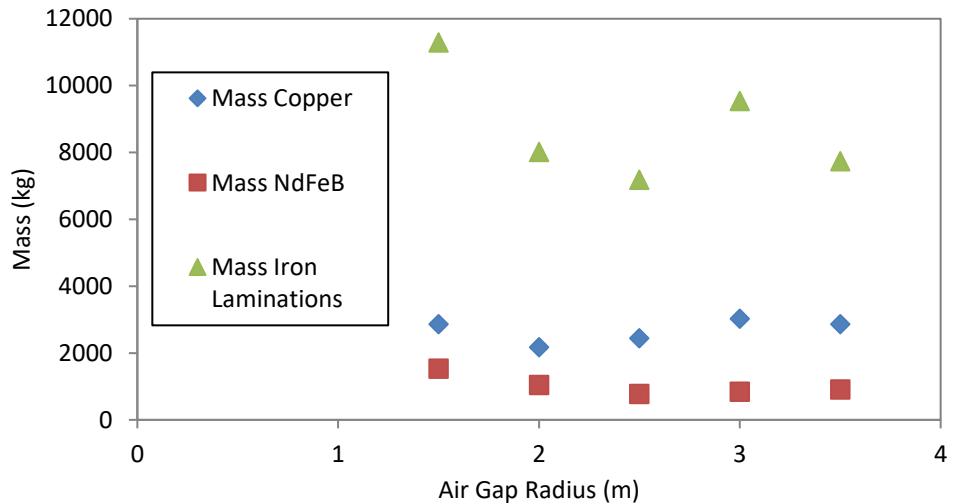
Figure 4.16 Mass reductions in copper, permanent magnet and iron laminations with increasing generator radius for the PMG 1G drive train.

In terms of the total mass of the active materials, a minimum is observed at a radius of 2.5 m. These are promising results for the PMG 1G as it allows much lighter designs to be produced and so will provide additional savings in terms of installation lifting equipment.
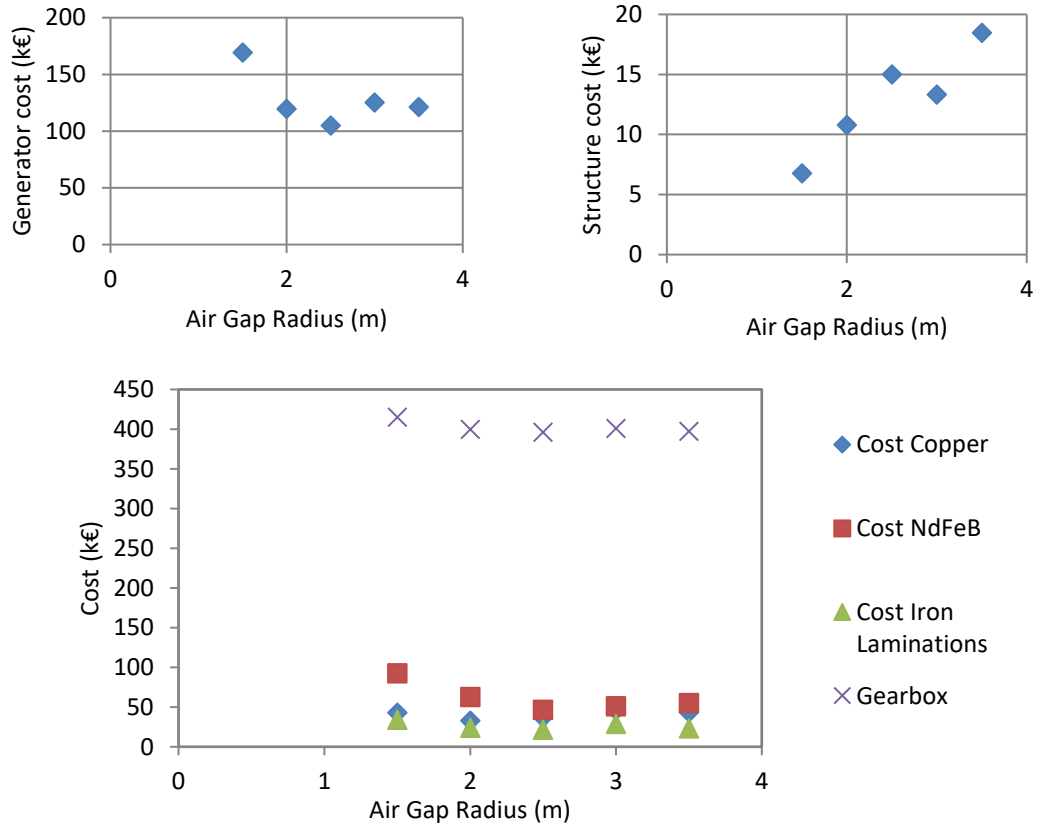
Figure 4.17 Generator active materials cost and structure cost with varying radius for the PMG 1G drive train.
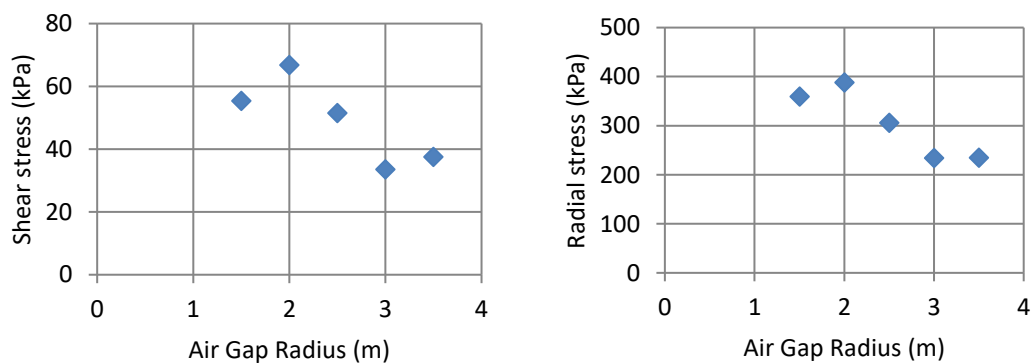
Figure 4.18 Shear stress and normal radial stress with increasing generator radius for the PMG 1G drive train.

Similarly, with the savings in weight, the savings in cost can be observed at around 2.5 m in Figure 4.17. The gearbox cost dominates the design and so compromise is made typically with the size of the generator. The flux density reduces as the radius increases and hence the shear stress is lowered.
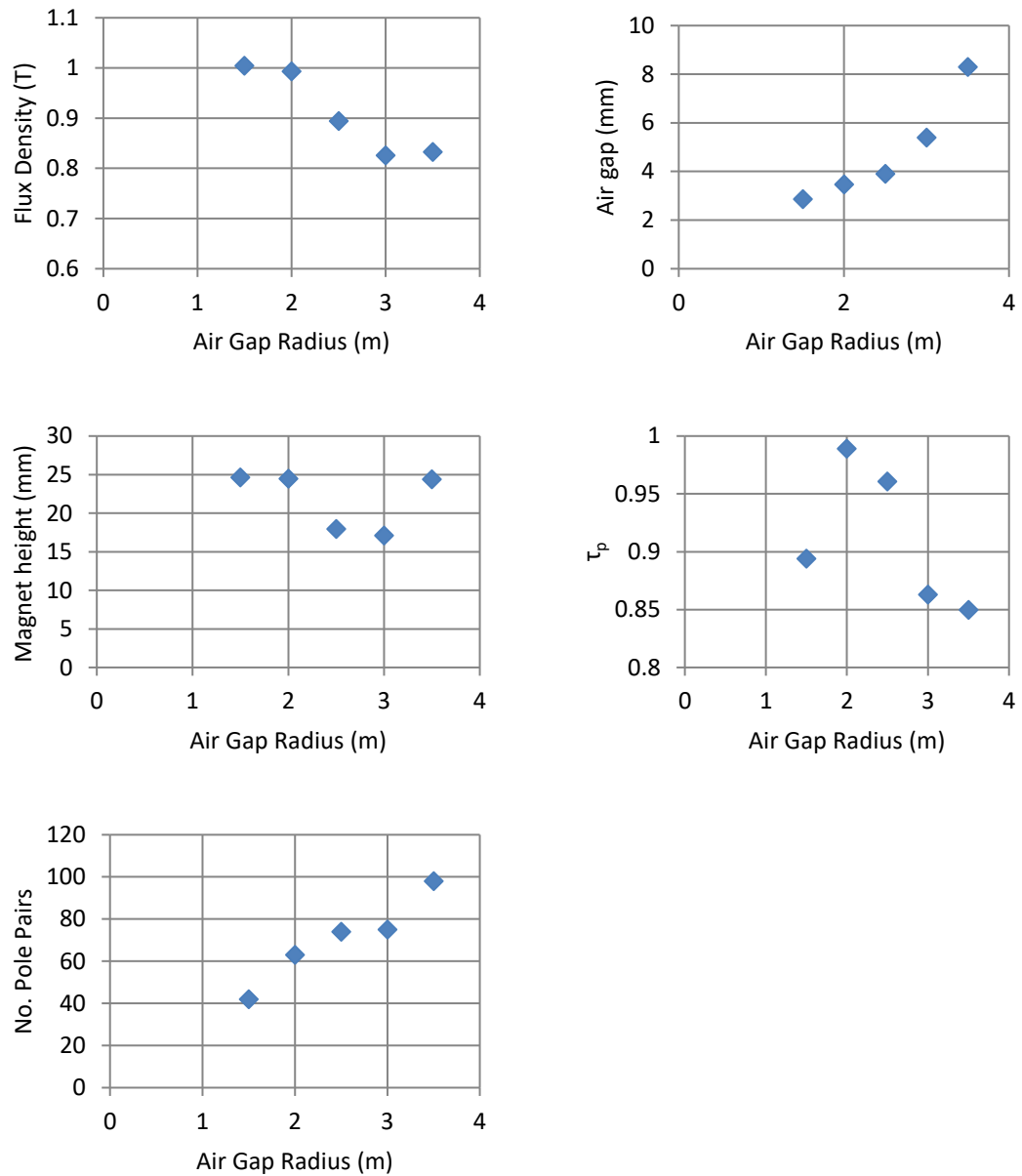
Figure 4.19 The effect of increasing the generator radius on the flux density, air gap width, magnet height, the magnet width to pole pitch ratio, and number of pole pairs for the PMG 1G drive train.

The number of pole pairs has a maximum value of 98 at 3.5 m as seen in Figure 4.19.
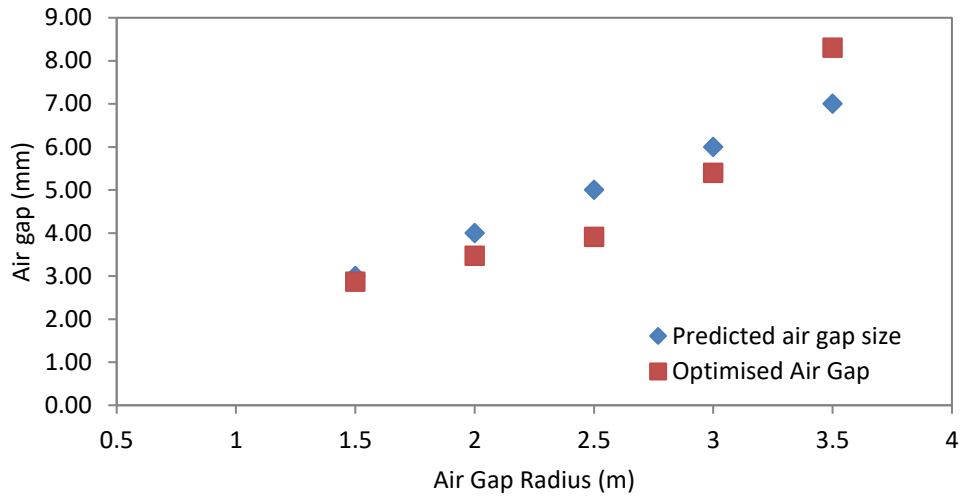
Figure 4.20 Optimised air gap in comparison with the predicted air gap for the PMG 1G drive train.

The air gap increases a lower rate than the predicted air gap as shown in Figure 4.20 as the radius increases. At 3.5 m radius, the air gap exceeds the predicted air gap of 7 mm by 1.3mm.
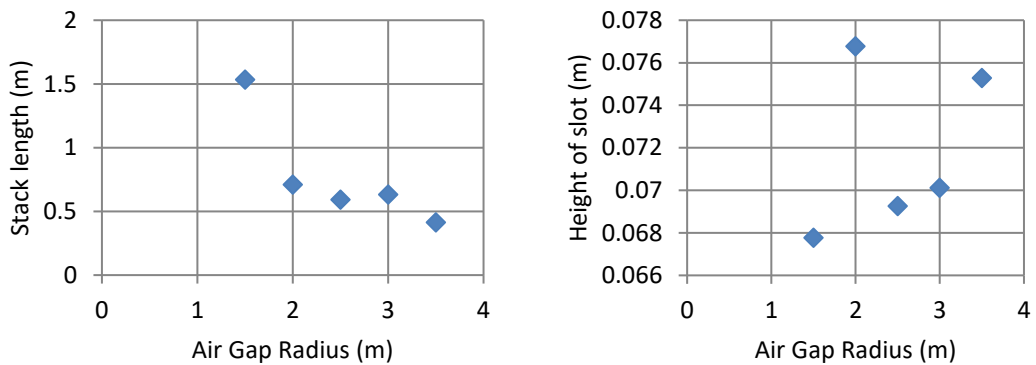
Figure 4.21 Stack length and height of slot with varying the air gap radius for the PMG 1G drive train.

The stack length of the generator reduces as expected as the radius increases to maintain its flux density in the air gap with minimised COE.

4.8.4 Two-stage gearbox PMG sensitivity results

The results for the sensitivity to the design variables for the PMG 2G are presented in the following sections. The radius of the PMG 2G was varied between 0.8 m and 1.8 m. The COE results are shown below.
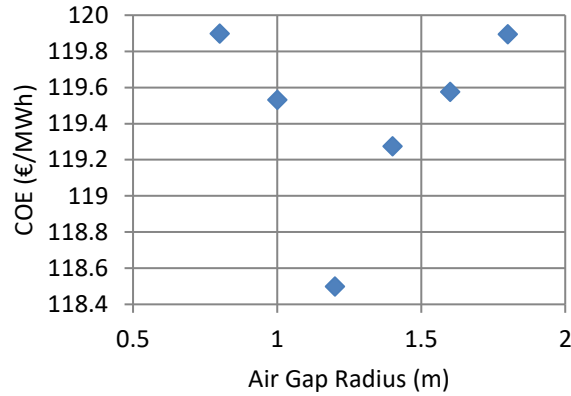
Figure 4.22 Cost of energy with varying generator radius between 0.55 and 0.85 m for the PMG 2G drive train.

The cost of energy has a minimum of 118.5 €/MWh at 1.2 m when increasing the generator radius from 0.8 m to 1.8 m. The benefit of operating at a higher speed is the reduced size of the generator, but in this case the use of 2 gear stages only adds additional capital and O&M costs which results in an overall higher COE.
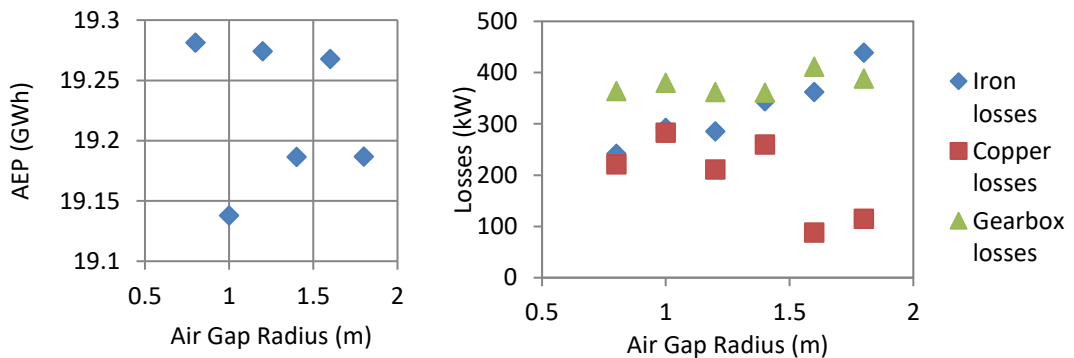
Figure 4.23 Annual energy production and losses with increasing generator radius for the PMG 2G drive train.

In terms of AEP as shown in Figure 4.23, there is no trend with increasing the air gap radius and so is not a key influence of the COE reduction factors when optimising for

the 2-stage gearbox topology. The Joule losses generally show a downwards trend as the air gap radius increases as opposed to the iron losses that increase over the range.

Looking at the mass comparison between the generator active materials as shown in Figure 4.24, the overall mass does not change much but the individual masses trade-off with one another to maintain a low cost as the radius increases.
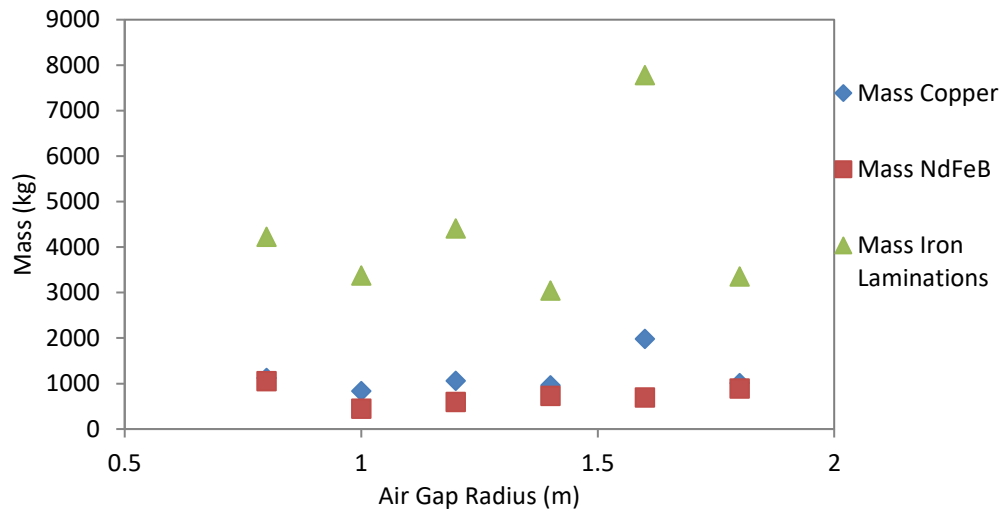
Figure 4.24 Mass variations in copper, permanent magnet and iron laminations with increasing generator radius for the PMG 2G drive train.

A cost comparison of the generator, structure and gearbox is shown in Figure 4.25. The structure cost fluctuates over the range to accommodate the change in generator dimensions and the generator cost varies within the range €50k to €95k. The cost of the gearbox dominates the overall drive train cost being almost 4 times the cost of the generator active materials.

The shear stress in greatly reduced as the radius increases due to the relationship with torque and length as shown in equation (4.1).
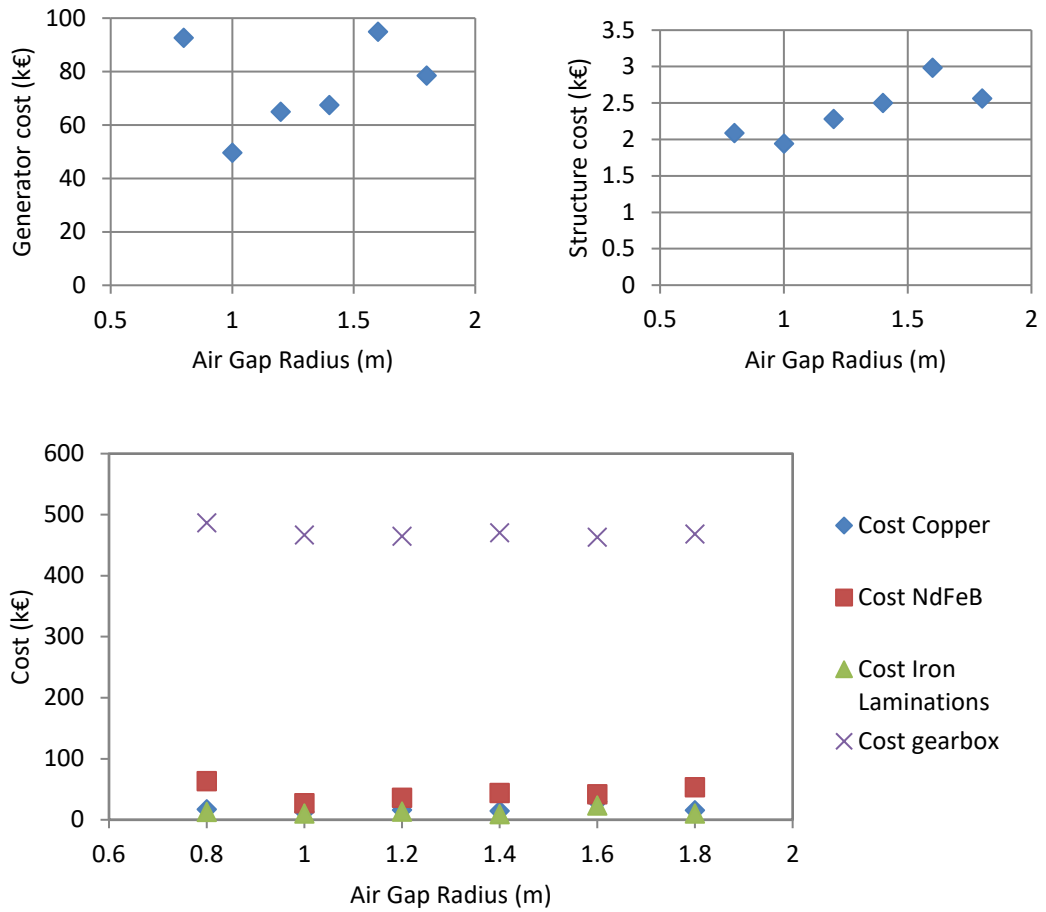
Figure 4.25 Generator active materials cost and structure cost with varying radius for the PMG 2G drive train.
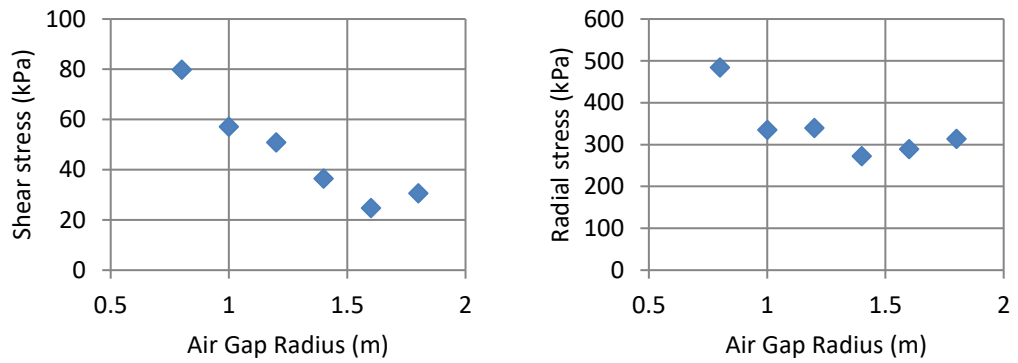
Figure 4.26 Shear stress and normal radial stress with increasing generator radius for the PMG 2G drive train.
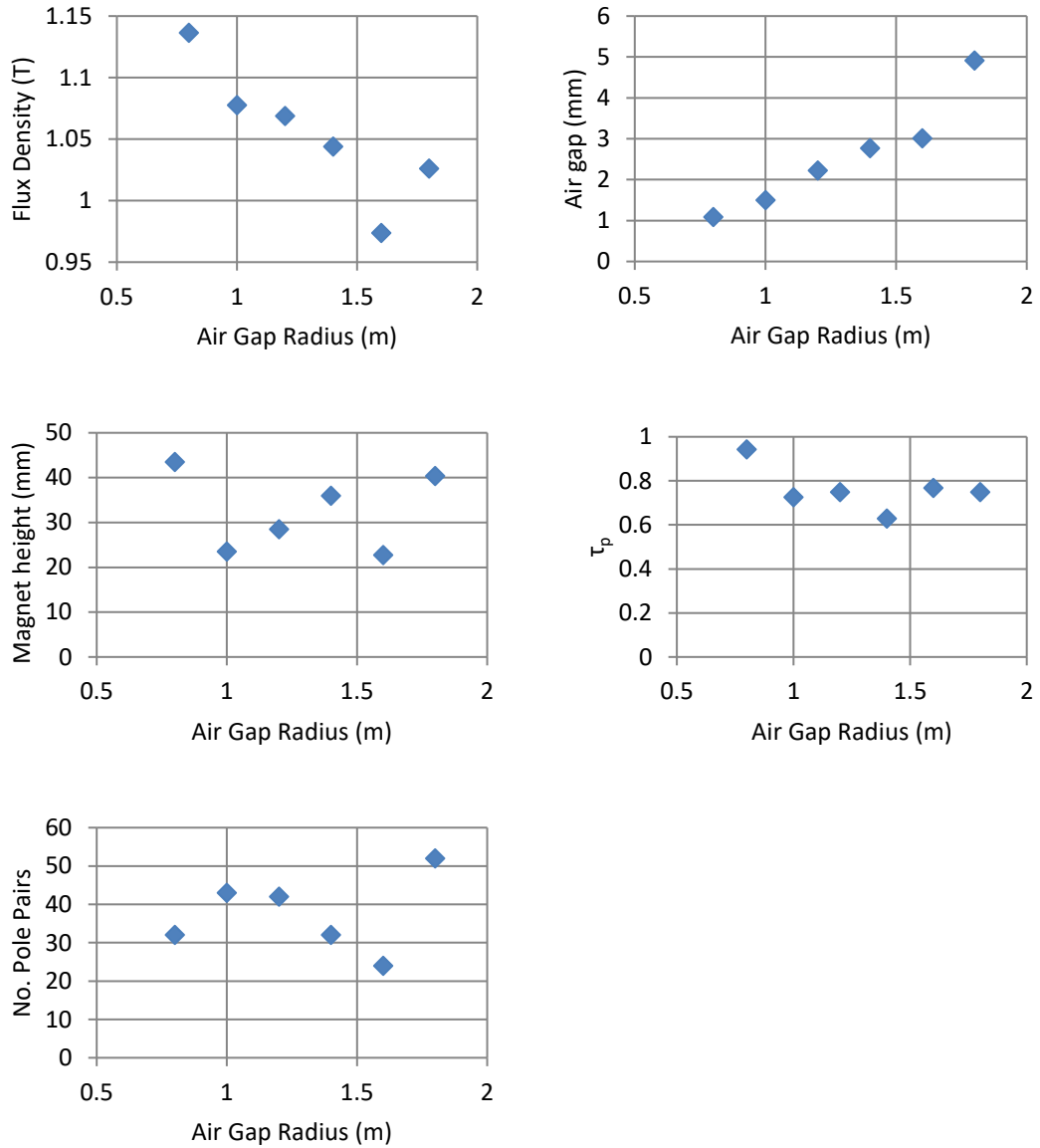
Figure 4.27 The effect of increasing the generator radius on the flux density, air gap width, magnet height, the magnet width to pole pitch ratio, and number of pole pairs for the PMG 2G drive train.

The flux density varies between 0.97 and 1.14 T as shown in Figure 4.27. The whole magnetic circuit parameters vary considerably as the generator radius increases including the number of pole pairs, the magnet height and the magnet width to pole pitch ratio. This highlights that the dimensions and layout of the magnets are not considered significant for this generator type. The dominance of the gearbox cost allows a variety of design options to be explored when regarding the generator which

would benefit some manufacturers that may have production limitations for the materials.
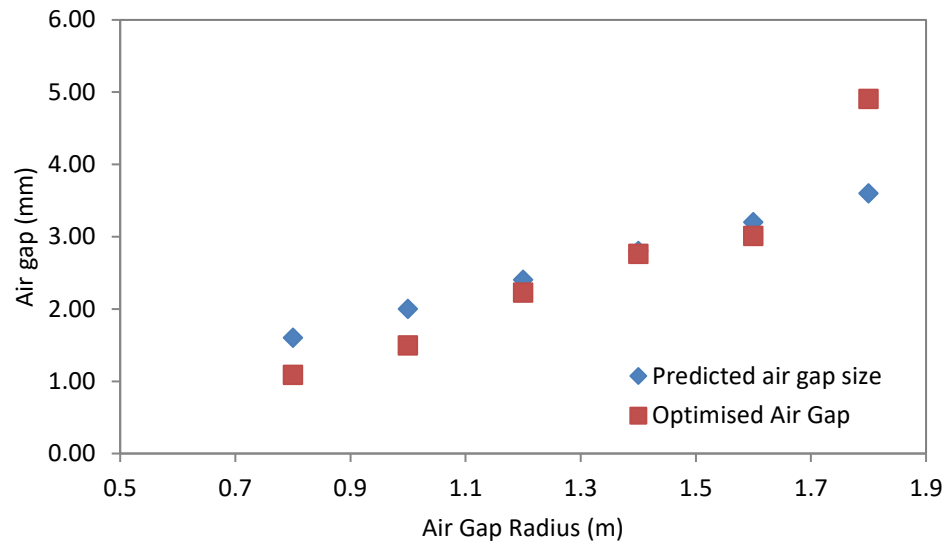
Figure 4.28 Optimised air gap in comparison with the predicted air gap for the PMG 2G drive train.

The optimised air gap increases at a changing rate compared to the predicted air gap as shown in Figure 4.28. The stack length is also at its lowest value of 0.54 m at a radius of 1.8 m which could offer benefits in terms of offering a compact design.
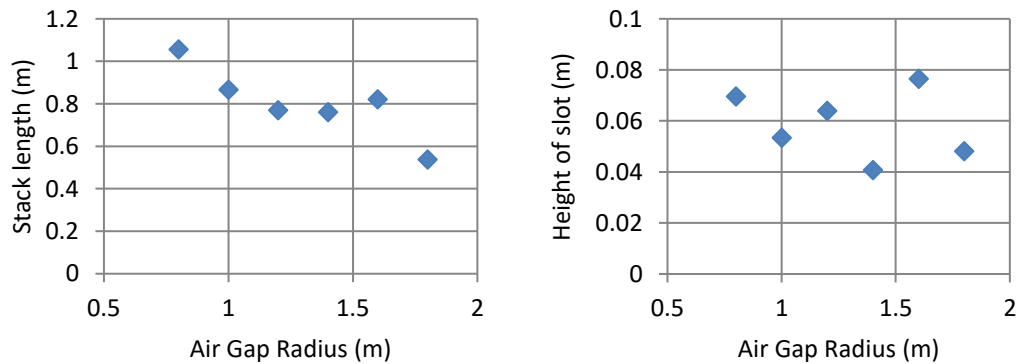
Figure 4.29 Stack length and height of slot with varying the air gap radius for the PMG 2G drive train.

4.8.5 Three-stage gearbox PMG sensitivity results

The optimisation sensitivity to the air gap radius for the PMG 3G is shown in the following sections. The radius was varied between 0.35 m and 0.6 m. The COE results are shown in Figure 4.30 below.
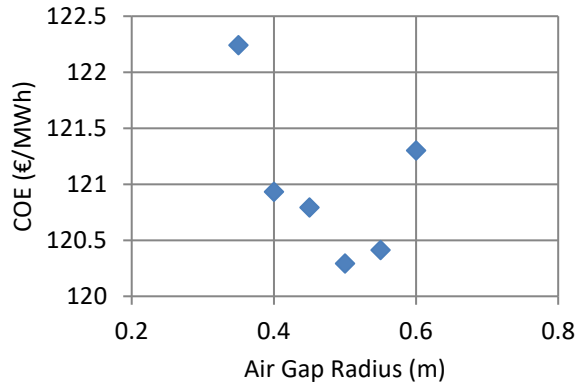
Figure 4.30 Cost of energy with varying generator radius between 0.35 and 0.6 m for the PMG 3G drive train.

The cost of energy has a minimum of 120.3 €/MWh at 0.5 m when increasing the generator radius from 0.35 m to 0.6 m. The PMG 3G has a large dependence on its gearbox topology to keep the COE low and increasing the radius only reduces the performance of the design. The annual energy production shown in Figure 4.31 also mirrors this as the wind turbine output drops when the generator radius is set to 0.6 m. The losses of the system are also shown in Figure 4.31 where is can be seen that the iron losses increase while the copper losses decrease with increasing the generator diameter.
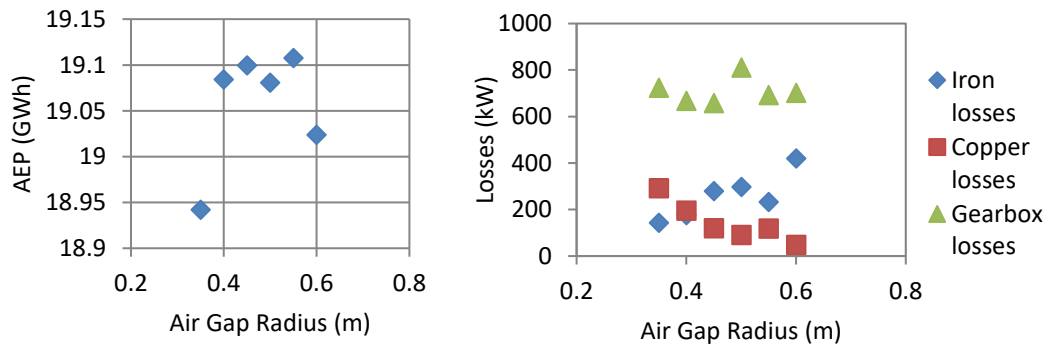
Figure 4.31 Annual energy production and losses with increasing generator radius for the PMG 3G drive train.

The masses of the active generator materials are shown in Figure 4.32 where it can be observed that the magnets and the copper mass doesn't increase significantly compared with the iron laminations. This highlights that there is not much benefit in increasing the amount of magnetic material in the generator when increasing the radius and so the larger mass results from adding more iron to create the larger design. There does not appear to be any cost benefit when increasing the radius for a high-speed generator beyond 0.5 m in this case.
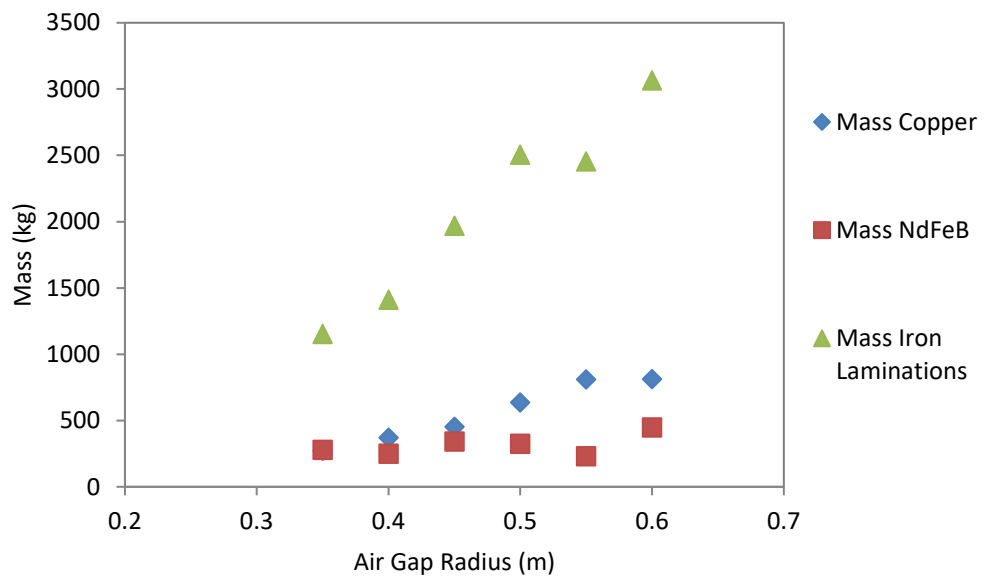
Figure 4.32 Mass reductions in copper, permanent magnet and iron laminations with increasing generator radius for the PMG 3G drive train.

The lowest generator cost occurs at a generator radius of 0.3 m which can be seen in Figure 4.33. The cost of the generator active materials are also shown where it can be seen that the cost of the magnets still dominates the overall material cost and that despite having a higher mass of iron, the iron cost is still relatively low as the generator radius increases. This also indicates that increasing the radius does not add enough benefit in terms of efficiency and overall COE.
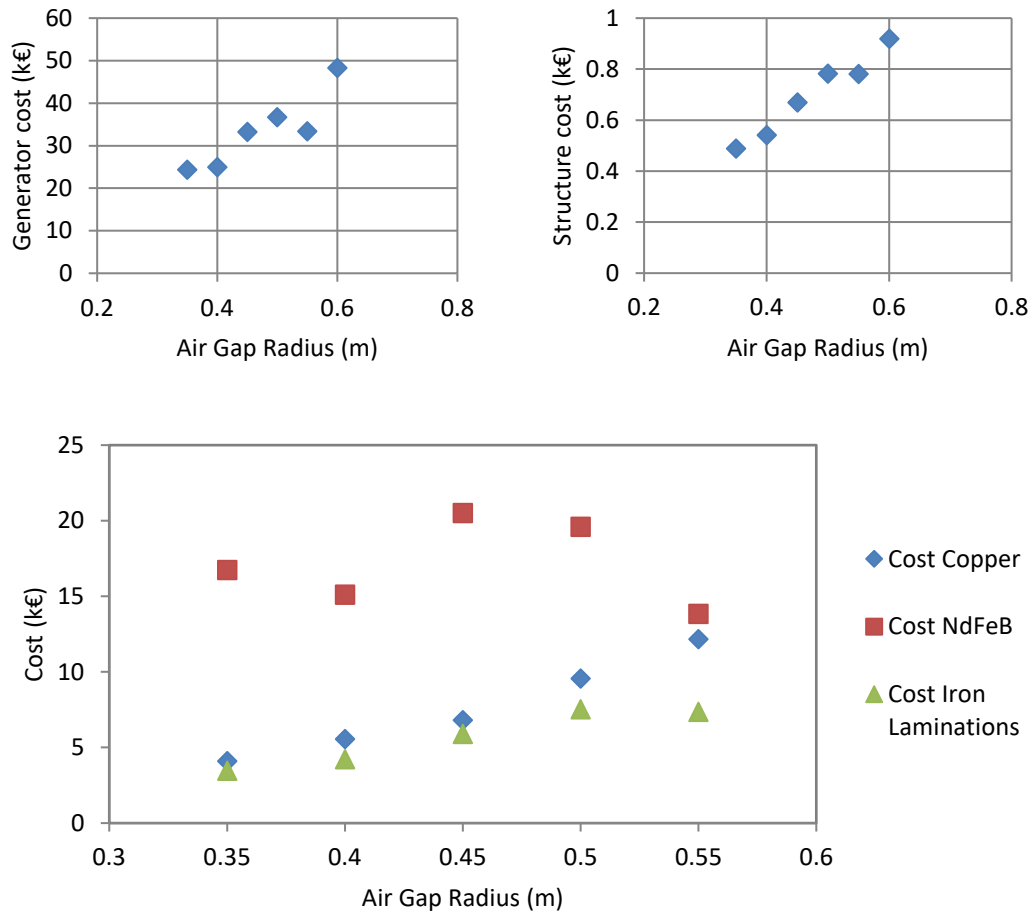
Figure 4.33 Generator active materials cost and structure cost with varying radius for the PMG 3G drive train.

The cost of the gearbox as the generator air gap radius increases in shown in Figure 4.34. The lowest gearbox cost of €481k is observed at 0.6 m generator radius which corresponds to a gear ratio around 1:81. This is the point where the gearbox has its lowest cost configuration but does not provide the lowest COE. For manufacturers with high-quality gearbox systems, a high-speed generator offers a promising solution as large savings can be achieved with cheaper and smaller generators. The use of permanent magnets is not as much of an issue regarding price volatility of rare earths, as there is a much lower volume compared with low and medium-speed options, and so PMG 3G designs could be considered less risk in terms of the material prices.
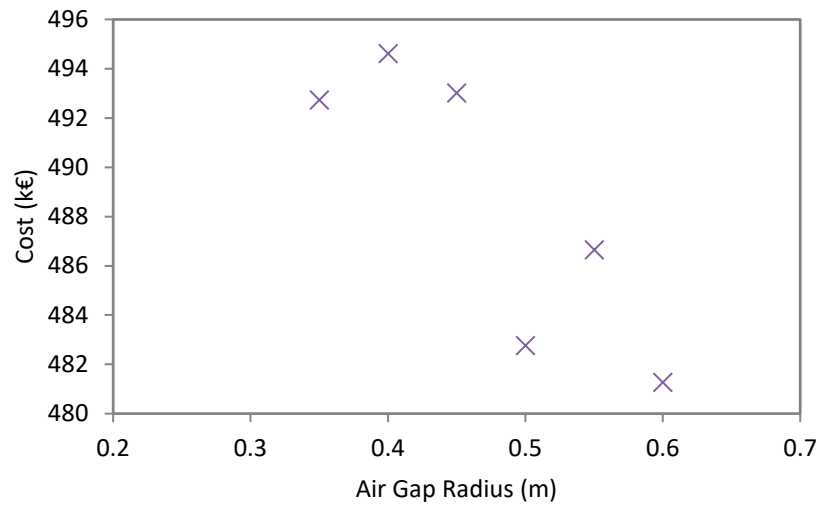
Figure 4.34 Gearbox cost when varying the generator radius for the PMG 3G drive train.

The stresses of the generator are shown in Figure 4.35 where it can be observed that the shear stress decreases as the radius increases.
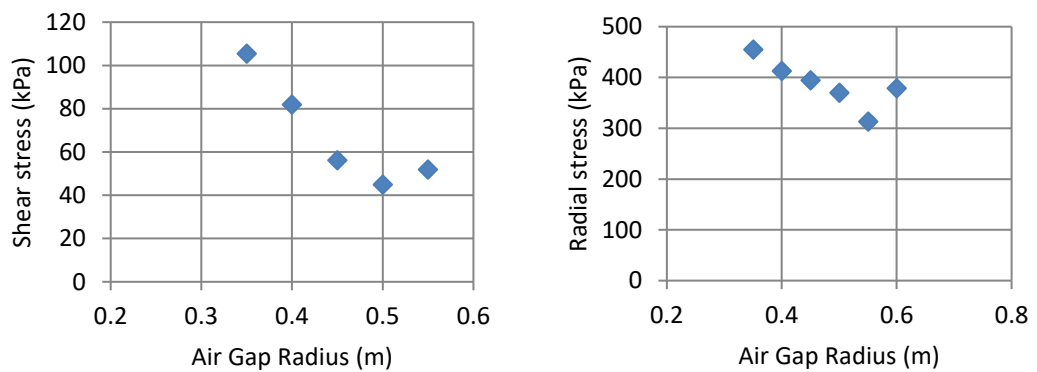
Figure 4.35 Shear stress and normal radial stress with increasing generator radius for the PMG 3G drive train.

The magnetic circuit parameters are shown in Figure 4.36.
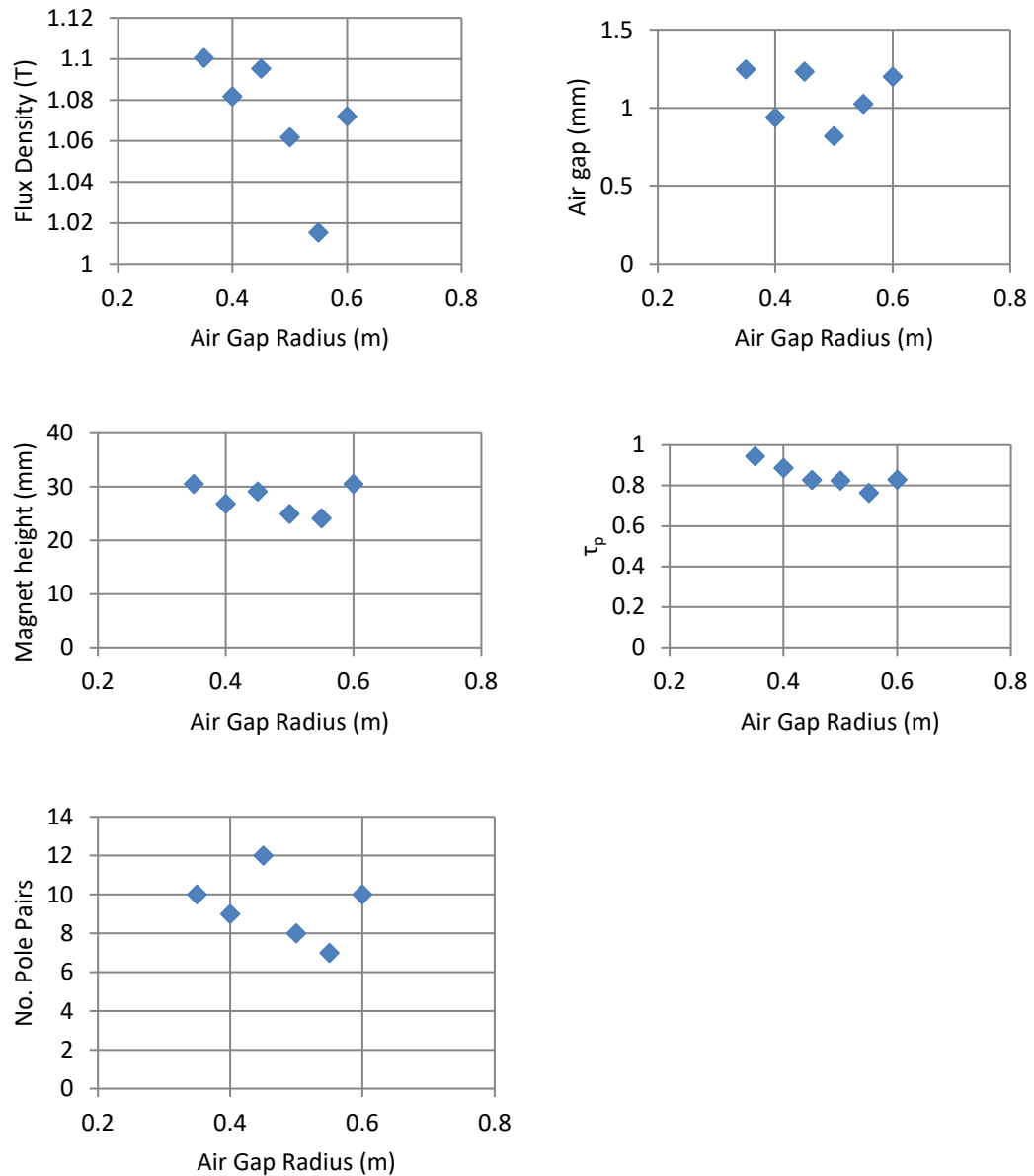
Figure 4.36 The effect of increasing the generator radius on the flux density, air gap width, magnet height, the magnet width to pole pitch ratio, number of pole pairs for the PMG 3G drive train.

The effect of increasing the generator radius shows a fluctuation in the magnet height and the number of pole pairs without any significant trend. This is a useful result for high-speed options as there is no strict requirements for the magnet circuit and so provides much more design flexibly. The PMG 3G is also relatively unaffected by magnet price fluctuation in terms of COE due to the higher degree of freedom in the magnet circuit design and the much lower volumes of magnets used.
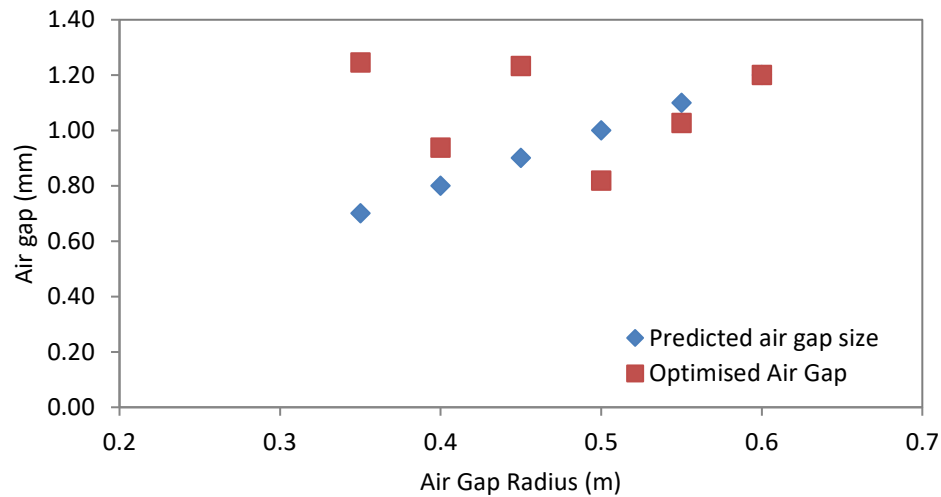
Figure 4.37 Optimised air gap in comparison with the predicted air gap for the PMG 3G drive train.

When designing small diameter generators, the air gap would expectedly be very small. The predicted air gap, which is estimated as 1/1000 of the diameter, would produce an air gap of 0.7 mm if the radius was 0.35 m which can be seen in Figure 4.37. Such a small air gap would be a manufacturing and a structural challenge which may not offer the best magnet circuit parameters. The optimisation process produces a much higher value for air gap, typically close to or above 1 mm across the range of radius values that were investigated which is shown in Figure 4.37. The air gap trend as the generator radius increases is completely opposite to the observed trend with the other 3 drive train options. The larger air gap paired with the higher magnet heights of the 3-stage gearbox drive train implies that the design options available for high speed generators are vast compared with the highly restricted design of the direct drive option. In this case, the increasing radius creates a trade-off for magnet mass and so the magnet size, pole pairs and air gap can all change to produce the required flux density.

The stack length and the slot height also change to accommodate the increase in radius as can be seen in Figure 4.38.
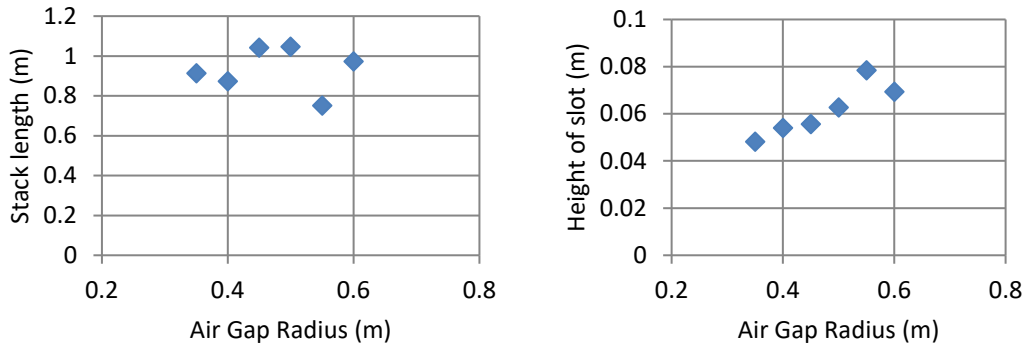
Figure 4.38 Stack length and height of slot with varying the air gap radius for the PMG 3G drive train.

4.8.6 Drive train comparison to air gap radius sensitivity

When the COE of each of the 4 drive trains are compared directly, as shown in Figure 4.39, it is clear that each presents a minimum in COE when varying the air gap radius. Air gap radii above and below these values results in less attractive designs as capital cost and efficiency trade off against each other. The progression to reducing the COE with the removal of each subsequent gear stage is also clear as the COE values progressively reduce towards the PMG DD topology.
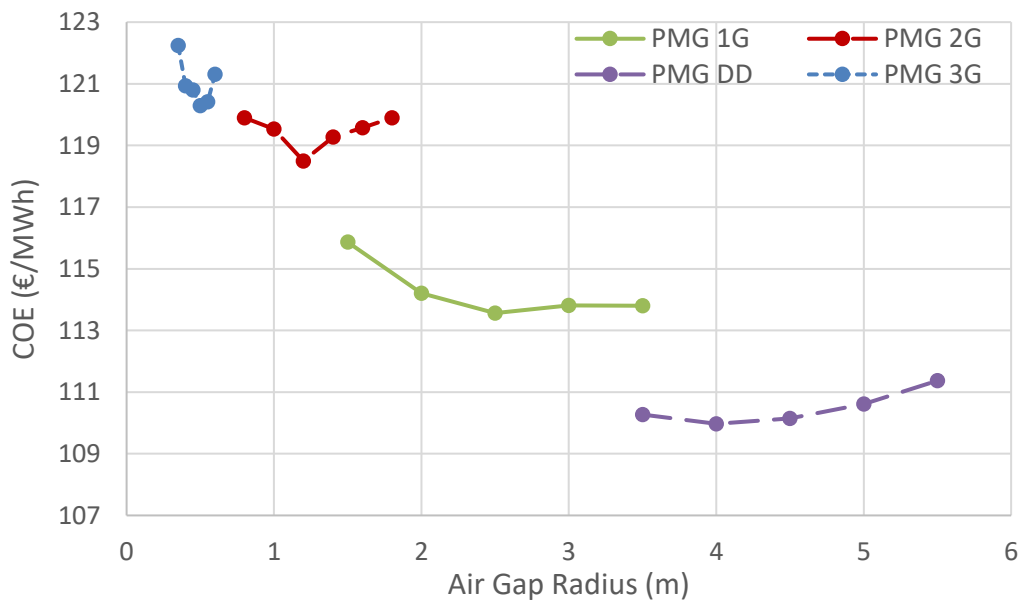
Figure 4.39 COE of the 4 drive trains when varying air gap radius.

4.8.7 Sensitivity to gear ratio

Selecting appropriate gear ratios for efficient and cost effective drive trains is very important as it directly affects the generator and gearbox specifications. The COE for varying the gear ratio for the PMG 1G, 2G and 3G drive trains is shown in Figure 4.40.
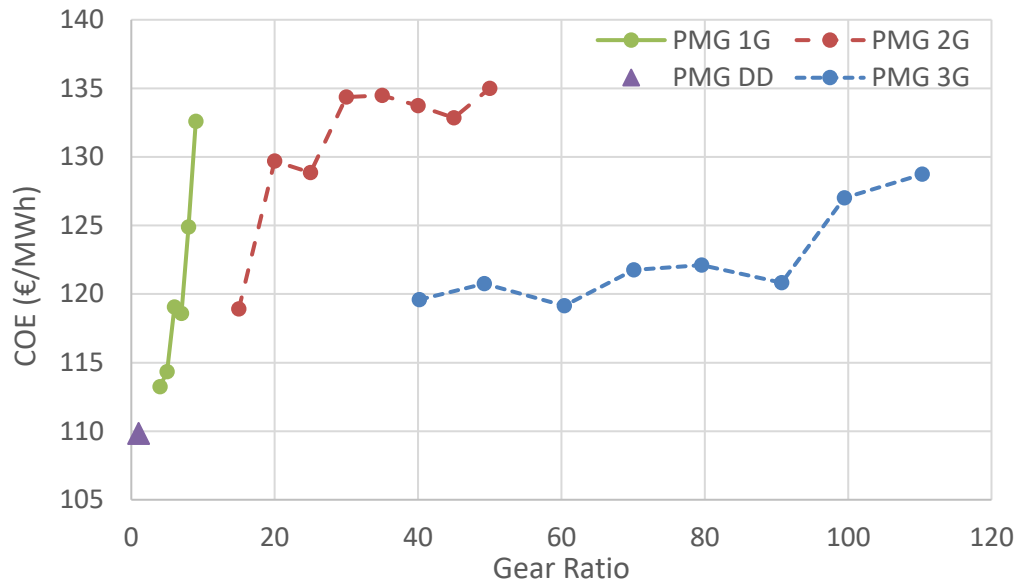
Figure 4.40 COE for 4 the drive trains against gear ratio.

The PMG 1G is highly sensitive to the gear ratio as the optimisation process tries to keep the ratio as low as possible. The lower the gear ratio, the lower the COE as the designs all tend towards being direct drive with a gear ratio of 1:1 highlighting how for this method of calculating the COE, a direct drive topology offers the best performance. This supports trends already observed in onshore wind turbines from [12] where more direct drive options are being in installed. The PMG 3G can be designed for several gear ratios and gearbox arrangements without affecting the COE significantly and so could be a preferential topology where component and manufacturing capabilities are restricted.

Having a closer look at the losses and masses of the drive train components when increasing the gear ratio will allow the reasons for the optimisation methods to converge towards a 1:1 ratio to be identified. The following sections investigate this for each of the 3 geared drive train designs.

4.8.7.1 Gear ratio sensitivity for PMG 1G

For the PMG 1G the losses in the generator and gearbox are shown in the figure below along with the active mass material changes.
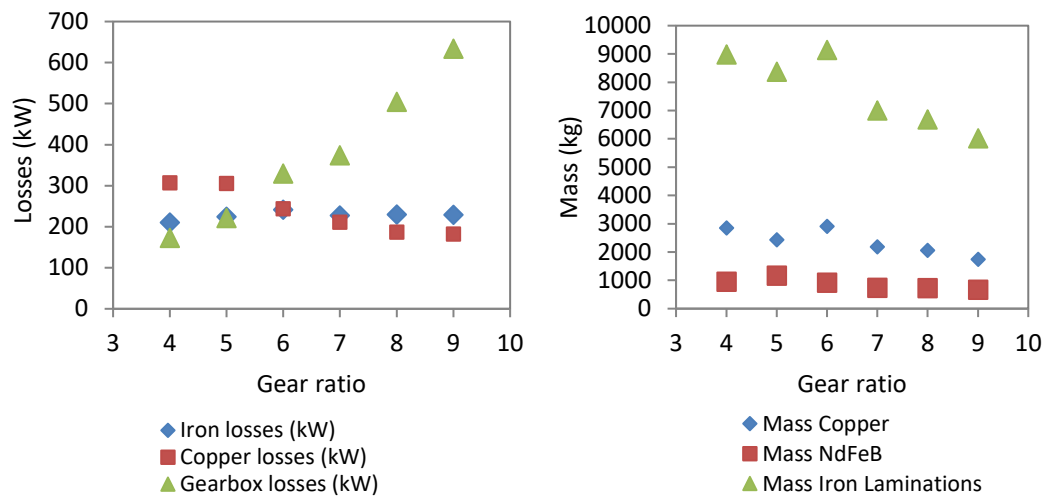

Figure 4.41 Losses and masses when increasing the gear ratio for the PMG 1G.

With a single stage gearbox, the gear ratio is altered by changing the number of gear teeth in the planetary gear set to allow the speed to change and changing the number of planets depending on the ratio. The corresponding diameter and facewidth changes too in order to meet the contact stress requirements. The losses in the gearbox are increased with increasing gear ratio due to the increasing size of the components and higher effects of meshing and churning losses, whereas the losses associated with the active generator materials decreases as smaller and more compact designs can be created that use less material. This is also highlighted by the reductions in mass observed in all generator materials as the gear ratio increases. The generator dimensions are shown in the following figure.
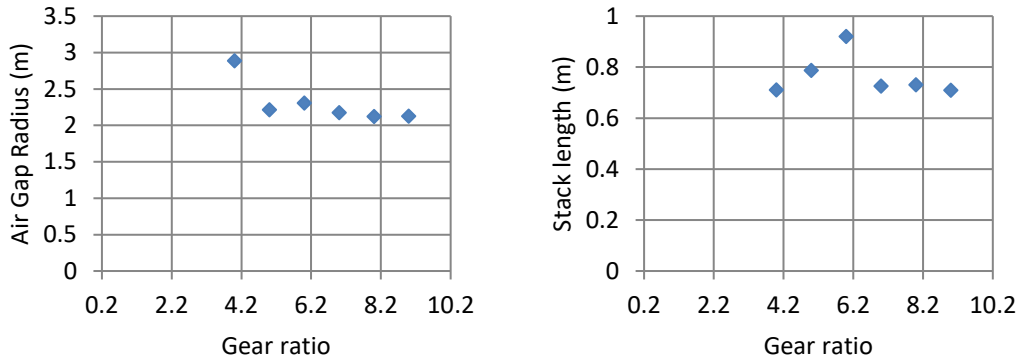
Figure 4.42 Air gap radius and stack length when increasing the gear ratio for the PMG 1G.

4.8.7.2 Gear ratio sensitivity for PMG2G

For the PMG 2G the losses in the generator and gearbox are shown in the figure below along with the active mass material changes.
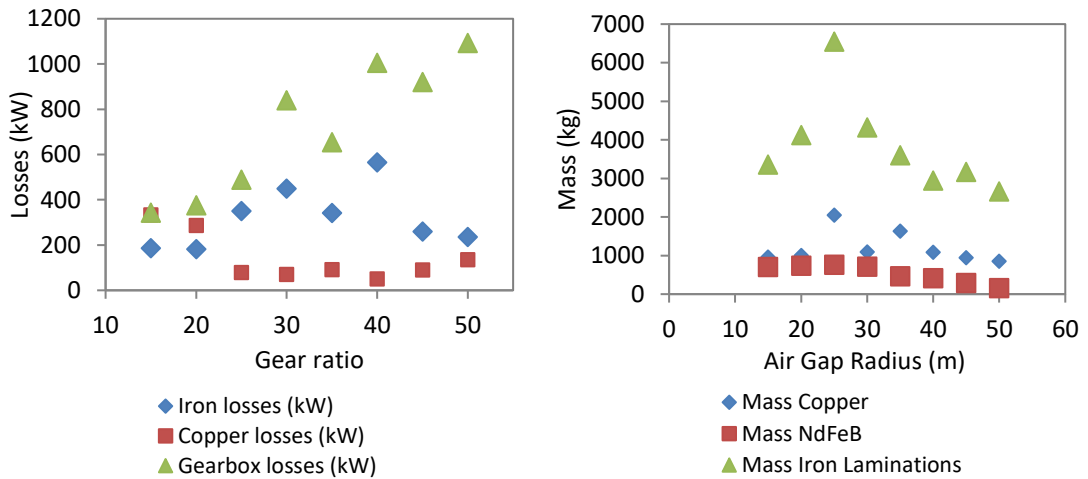

Figure 4.43 Losses and masses when increasing the gear ratio for the PMG 2G.

The losses associated with the gearbox increase significantly when increasing the gear ratio. At the same time there is some change in the losses based on the generator's active materials as the design progresses to accommodate the increasing speeds. However, these losses are roughly the same between the higher and lower operating speeds of the range with the most notable difference occurring in between (iron losses initially increasing while copper losses initially decreasing). The

corresponding changes in the generator radius and stack length can be observed in the following figure.
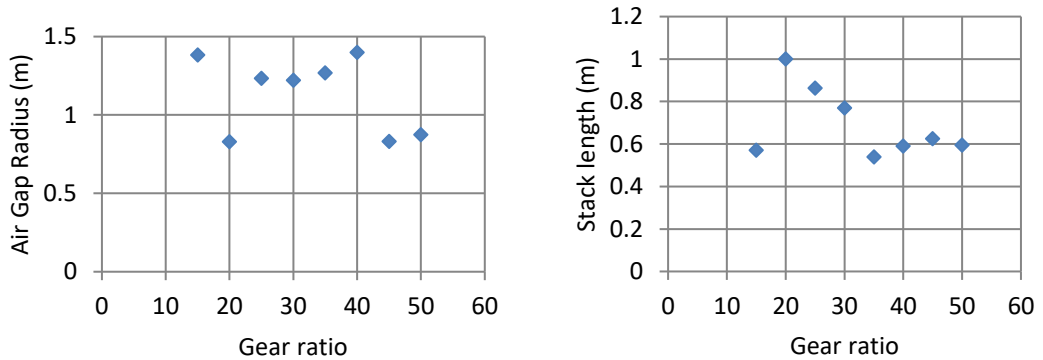
Figure 4.44 Air gap radius and stack length when increasing the gear ratio for the PMG 2G.

4.8.7.3 Gear ratio sensitivity for PMG3G

For the PMG 3G the losses in the generator and gearbox are shown in the figure below along with the active mass material changes.
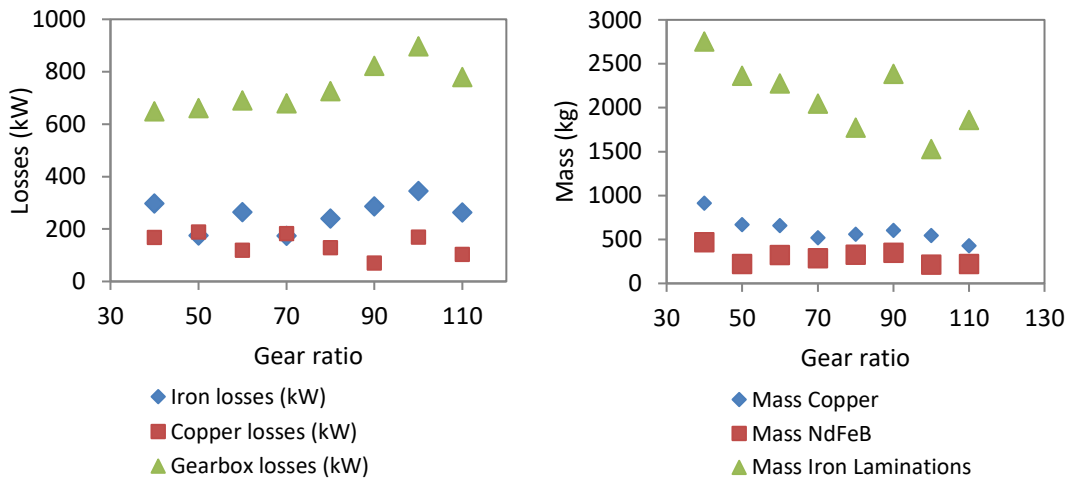
Figure 4.45 Losses and masses when increasing the gear ratio for the PMG 3G.

By increasing the operating speed of the generator with higher gear ratios, the dimensions can be reduced and so the overall generator mass reduced. Larger gearboxes that operate at high speeds produce higher losses compared to lower speed options which has an impact on the performance of the drive train. The reduction in

generator mass is achieved mainly by the radius reducing to by around half as can be seen in the following figure.
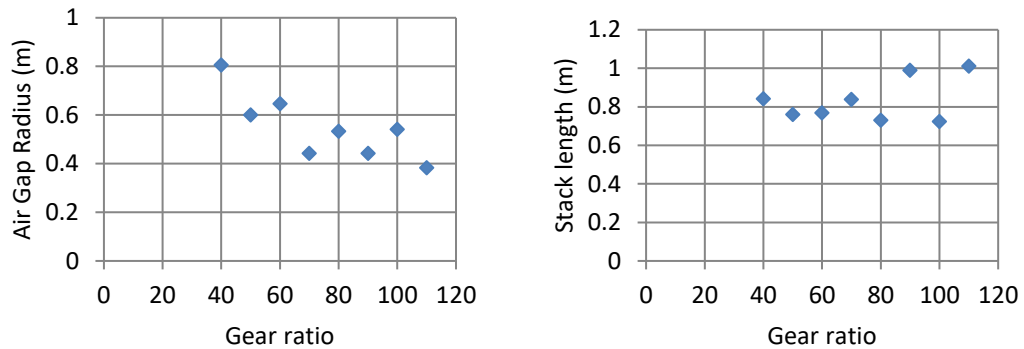
Figure 4.46 Air gap radius and stack length when increasing the gear ratio for the PMG 3G.

4.9 Discussion and comparison of COE optimisation models for PMG drivetrains

The optimised variables for each drive train from section 4.7.2 are shown in Table 4.2. Compared with the results of Chapter 3 that assumed some basic dimensions for the drive train, the process of optimisation produced COE results that represent a more consistent and appropriate design process that reflect several real-life conditions.

The direct drive design (PMG DD) outperformed the other geared designs in terms of COE with the current constraints and assumptions applied to models. This result is in line with current trends that are removing the gearbox from the drive train in order create more reliable and efficient wind turbines. An 8.08 m diameter, 1.61 m length and 183 pole pairs produce a design with a COE of 109.983 €/MWh and with the UK government's original target of a cost of £100/MWh (roughly 111 €/MWh at historical exchange rates) for offshore wind energy by 2020, this design is in keeping with the target.

The PMG 1G offered the best solution out of the geared drive trains with a COE of 113.79 €/MWh and both the PMG 2G and the PMG 3G offered designs with similar COE values at 117.74 €/MWh and 118.84 €/MWh, respectively.

Table 4.2 Summary of each optimised variable from each drive train

	PMG DD	PMG 1G	PMG 2G	PMG 3G
Cost of energy (€/MWh)	**109.98**	**113.79**	**117.74**	**118.84**
Air gap radius (m)	4.04	2.61	1.19	0.43
Stack Length (m)	1.61	0.83	0.72	0.79
Number of pole pairs	183.00	86	27	10
Magnet height (mm)	12.36	17.12	25.40	28.81
Magnet width to pole pitch ratio	1.00	0.90	0.78	0.91
Air gap (mm)	6.47	5.25	2.26	0.93
Height of slot (mm)	66.33	55.03	64.84	55.09
Ratio of slot width to pitch	0.55	0.55	0.53	0.50
1st stage sun pitch diameter (mm)	-	908	1046	1093
Number of 1st stage sun teeth	-	44	35	46
Number of 1st stage ring teeth	-	176	106	140
Number of 1st stage planet teeth	-	61	33	43
Facewidth 1st stage (mm)	-	798	787	727
2nd stage sun pitch diameter (mm)	-	-	673	702
Number of 2nd stage sun teeth	-	-	38	37
Number of 2nd stage ring teeth	-	-	115	139
Number of 2nd stage planet teeth	-	-	37	47
Facewidth 2nd stage (mm)	-	-	510	381
3rd stage gear pitch diameter (mm)	-	-	-	1473
Number of 3rd stage gear teeth	-	-	-	119
Number of 3rd stage pinion teeth	-	-	-	27
Facewidth 3rd stage (mm)	-	-	-	392

Modern day trends show that installations of direct drive PMGs are dominant for large offshore wind turbines and this is reflected in the optimisation results presented in this chapter. However, not all manufacturers use direct drive and this could be explained by the fact that changes in permanent magnet and copper price would have a significant impact on the price of a direct drive generator. Higher speed drive trains with a smaller generator will inherently have less exposure to cost uncertainty. Although high cost factors such as balance of plant impact significantly on the ICC of a wind farm, the drive train can contribute to overall lifetime savings if designed correctly. There are many uncertainties associated with all wind farm projects ranging from cost price fluctuations and wind profiles of the selected site, to the reliability and repair costs of the system over its years of operation. Chapter 5

focuses on a sensitivity analysis of the 4 optimised designs presented in this chapter in order to assess the impact of such uncertainties.

4.10 References

[1]   J. Kennedy, *Particle Swarm Optimization*. Encyclopedia of Machine Learning, Boston, MA: Springer, 2011.

[2]   C. A. Coello, "Multi-objective optimization," in *Handbook of Heuristics*, 2018.

[3]   M. Van Dijk, S. J. Van Vuuren, and J. E. Van Zyl, "Optimising water distribution systems using a weighted penalty in a genetic algorithm," *Water SA*, 2008.

[4]   W. Yu, B. Li, H. Jia, M. Zhang, and D. Wang, "Application of multi-objective genetic algorithm to optimize energy efficiency and thermal comfort in building design," *Energy Build.*, 2015.

[5]   M. Zhao, Z. Chen, and F. Blaabjerg, "Optimisation of electrical system for offshore wind farms via genetic algorithm," *IET Renew. Power Gener.*, 2009.

[6]   Matlab Software version R2017a, "Optimization Toolbox." 2017.

[7]   Mathworks, "Global Optimization Toolbox User's Guide for Matlab." User Guide, 2018.

[8]   H. Polinder, F. F. A. Van Der Pijl, G. J. De Vilder, and P. J. Tavner, "Comparison of direct-drive and geared generator concepts for wind turbines," *IEEE Trans. Energy Convers.*, vol. 21, no. 3, pp. 725–733, 2006.

[9]   L. Sethuraman, M. Maness, and K. Dykes, "Optimized Generator Designs for the DTU 10-MW Offshore Wind Turbine using *GeneratorSE*," *35th Wind Energy Symp.*, no. January, 2017.

[10]   C. D. Schultz, "The Effect of Gearbox Architecture on Wind Turbine Enclosure Size Enclosure Size." American Gear Manufacturers Association, AGMA Technical Report, 2009.

[11]   A. R. Nejad, "Development of a 5MW reference gearbox for offshore wind turbines," *Wind Energy*, vol. 17, 2016.

[12]   C. Vázquez-Hernández, J. Serrano-González, and G. Centeno, "A market-

based analysis on the main characteristics of gearboxes used in onshore wind turbines," *Energies*, vol. 10, no. 11, 2017.

[13]   S. Sheng and C. Broomfield, "'Wind Turbine Gearbox Condition Monitoring Round Robin Study – Vibration Analysis' NREL, Golden, Colorado, Report no. NREL/TP-5000-54530 (2012)."

Chapter 5 Sensitivity and Uncertainty Analysis for Optimised Designs

This chapter takes the 4 optimised designs from Chapter 4 and investigates the sensitivity of their COE to various assumptions and fixed input parameters. Initially this is a sensitivity analysis to single input parameter varying within pre-defined ranges. The chapter then goes onto to characterise the historic variability of material prices into probability distributions, and, combining with results from the preceding sensitivity analysis shows the resulting COE probability distributions of the four designs from Chapter 4. In order to look at the impact if uncertainty of multiple parameters simultaneously, a Monte Carlo approach is used to evaluate the four designs. This approach offers an effective statistical method in sampling uncertainty and is linked to real life historical price data. In the next chapter (Chapter 6), uncertainty will be included within the optimisation; in this chapter it is applied after the optimisation.

Another aspect of the analysis was to include a sensitivity to wind conditions and the failure rate assumptions. The following parameters were varied to simulate operation in an alternative wind site and for increased failure rate:

- Weibull Shape Parameter, k
- Weibull Scale Parameter, C
- Generator major replacement – one complete replacement over the lifetime.

The material costs are dictated by the fluctuations and volatility of the raw material prices, most significantly the rare earth materials used in the permanent magnets. The following material costs were varied to observe the COE dependence on the material price:

- Copper cost for the generator windings
- Permanent magnet cost (NdFeB)
- Iron laminations cost and structural steel cost

- Aluminium price for the generator supporting structure

Looking at all the above conditions for the optimised designs will allow the identification of the most critical considerations of the designs to be identified. The cost sensitivity only applies to the drive train and the cost of the materials that would make up the tower, blades and other wind turbine components are kept constant throughout.

This chapter begins with the optimised drive train designs undergoing a sensitivity to wind conditions to assess how the designs would be impacted if installed in various sites with varying wind profiles. The next part focuses on including a generator major replacement to investigate the impact of higher failure rates. The raw material costs are then subject to variations to assess how the drive trains would perform in terms of COE. The first step is to look at simple linear price changes for a direct comparison between each material and its impact on the cost of the projects. In order to obtain values that would represent the most likely cost scenario in reality, probability distributions were created based on real life historical data. These probabilistic values were varied independently for each material to observe the individual effects of cost fluctuations on each drive train. The final section looks sampling values from the probability distributions of each material using Monte Carlo methods to create a probabilistic COE result for each drive train.

5.1 Wind conditions and reliability assumptions sensitivity

Some turbines perform better in lower wind conditions than others depending on the topology and performance at low wind speeds. Wind turbines are divided into classes from 1 to 3 that represent the wind profile the turbine is designed for. Classes 2 and 3 are the most common classes of wind turbines that operate in average wind speed conditions of typically below 8.5 m/s. Class 1 turbines experience stronger winds and so design alterations to the blades, tower and supporting structures would be required to accommodate the high loads experienced by the wind turbine.

From a designer's perspective, optimising a wind turbine for a particular site condition could suggest that the performance would be comprised if installed in sites

with very different wind conditions. It is important to be able to quantify the loss or gain in performance of wind turbines for use in varying site conditions.
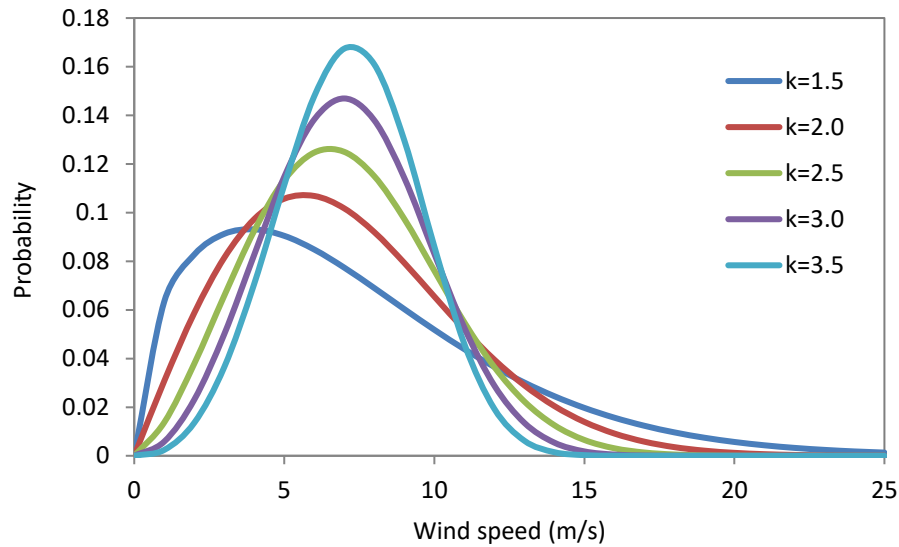
Figure 5.1 Probability of wind speed with varying shape parameter, k with the Weibull distribution.
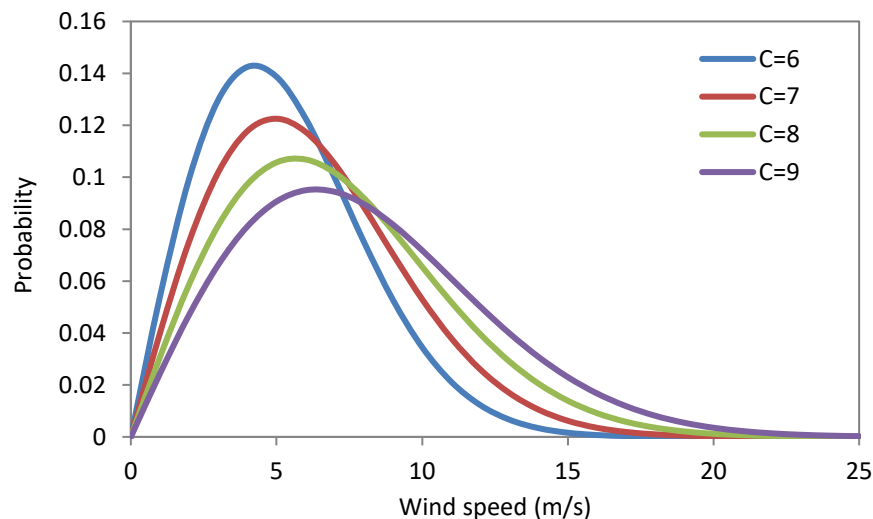
Figure 5.2 Probability of wind speed with varying scale parameter, C with the Weibull distribution.

In order to assess how the optimised designs perform with varying wind profiles, the shape parameter, k and scale parameter, C of the Weibull distribution were varied to allow each drive train to be analysed. Examples of how varying the shape parameter and scale parameter affects the wind speed probability are given in Figure 5.1 and Figure 5.2.

The specifications of the rotor, such as the size of the blades, were not altered during the sensitivity when varying the wind conditions profile. More detailed aerodynamic design considerations would assist in optimising the wind turbine further, but for the purposes of drive train analysis, all other wind turbine specifications were kept constant.

5.1.1 Shape parameter

The shape parameter of the Weibull distribution indicates the variability of the wind with low values corresponding to a larger range of wind speeds. High wind variability can create larger loading conditions on the rotor, but if average speeds are low enough, the wind turbine should not be subject to high winds too frequently throughout operation. For the each of the drive trains, varying the shape parameter affects the energy yield (AEP) and the overall COE as shown in Figure 5.3 and Figure 5.4 respectively.
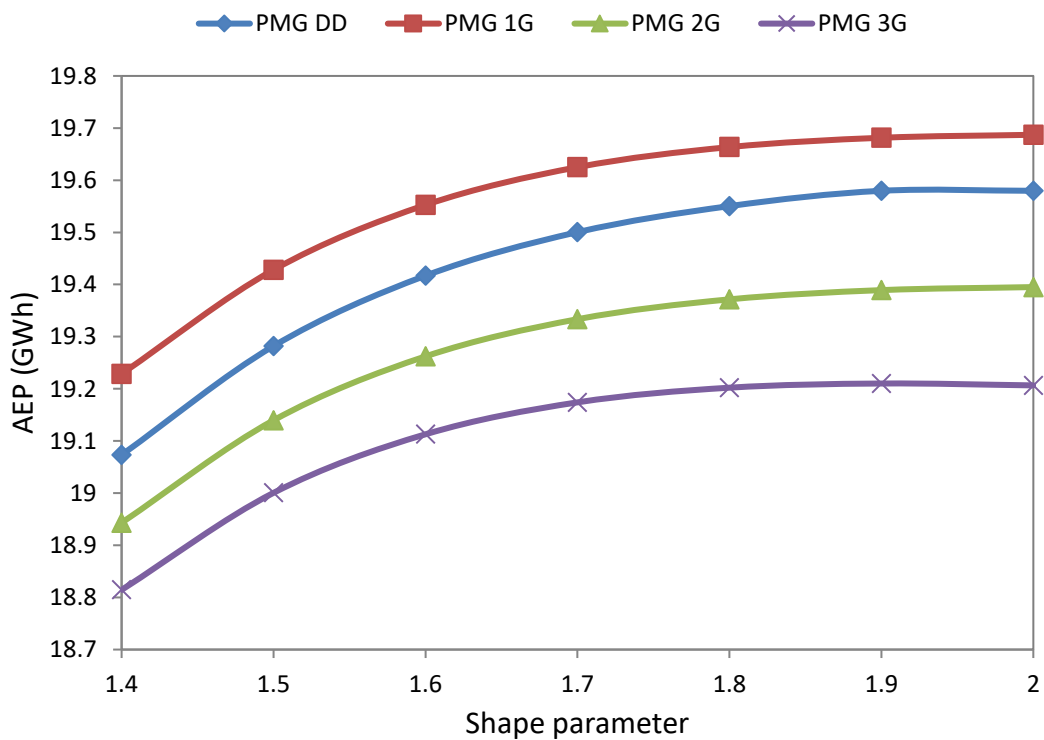
Figure 5.3 AEP sensitivity to Weibull shape parameter for the 4 drive trains.

For the drive trains, the AEP follows a logarithmic trend when increasing the shape parameter. The AEP increases with a steep gradient at the beginning of the range of

values before slowing down and tending towards a maximum value at the higher end of shape parameter. Likewise the same happens for reduction in COE where it can be seen that there is only a small decrease between shape parameter values over 1.8.
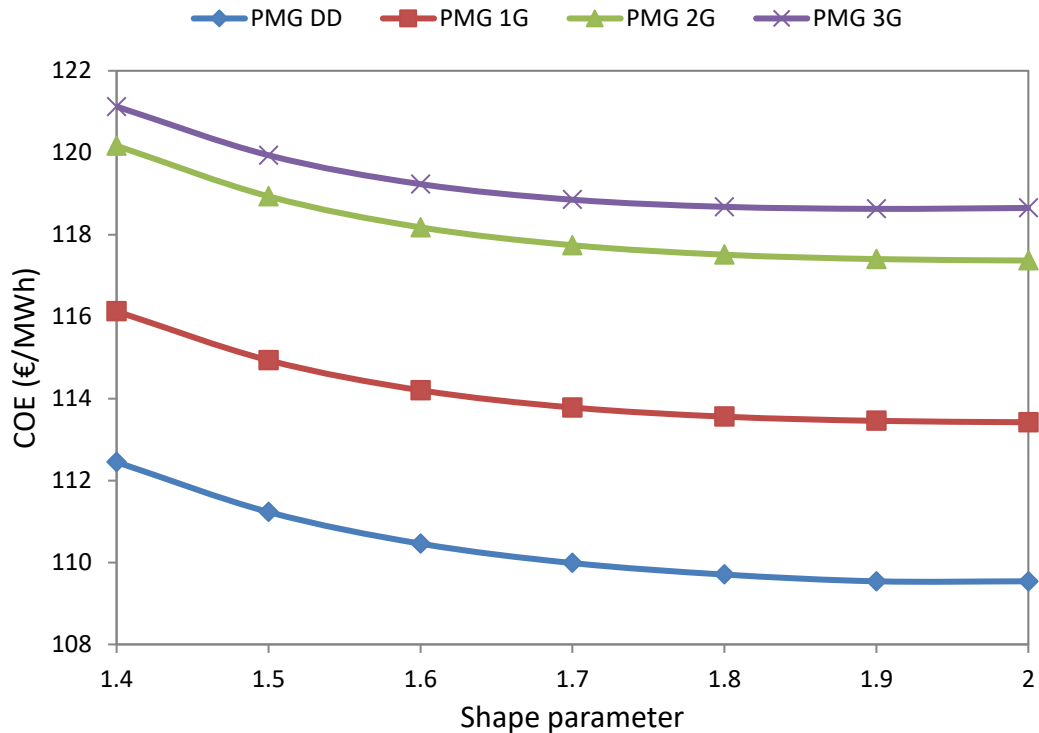
Figure 5.4 COE sensitivity to Weibull shape parameter for the 4 drive trains.

The PMG 1G produces the AEP out of the 4 drive trains whilst PMG DD offers the lowest COE. The effect on increasing the shape parameter for the PMG 3G shows tend to a plateau in AEP around 19.2 GWh at values above 1.8 as shown in Figure 5.3. Consequently, the COE also tends towards a plateau above a shape parameter at a cost of 118.7 €/MWh. This outcome suggests that for high variability wind speeds, having a high-speed generator and 3-stage gearbox could be more optimally suited to such conditions.

5.1.2 Scale parameter

The scale parameter represents the characteristic wind speed of the distribution and is proportional to the average wind speed. At higher wind speeds, there is more energy

available in the wind and so higher outputs can be achieved. The following graphs show the AEP and COE linear dependence on the scale parameter and the potential energy gain/saving that can be obtained in higher wind speed areas. The scale parameter was varied from 7.8 to 8.4 whilst the shape parameter was held constant at 1.7.
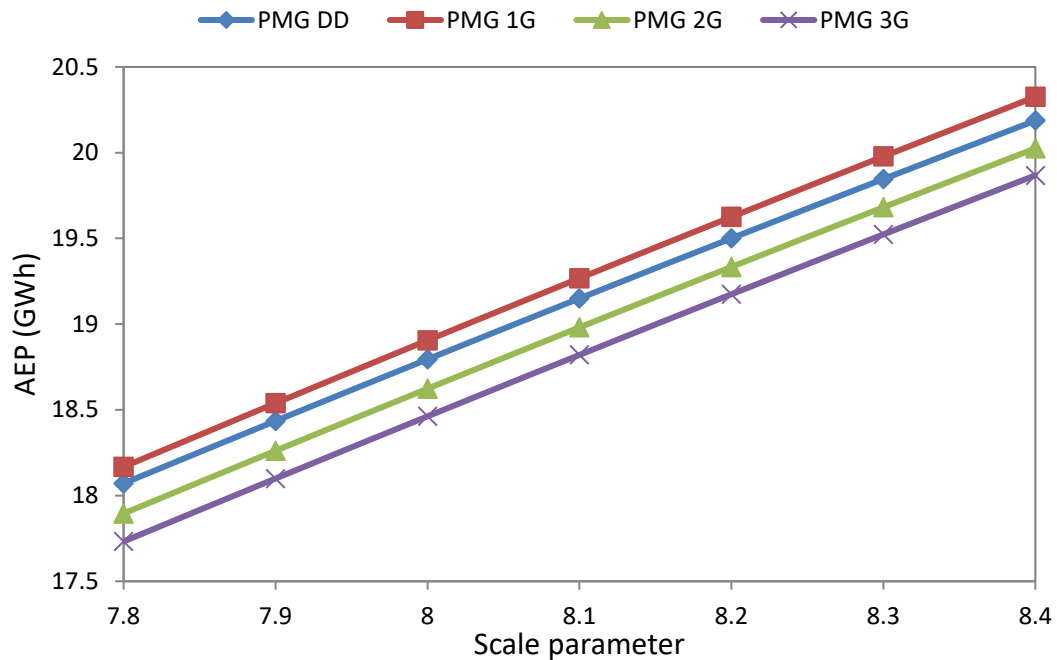
Figure 5.5 AEP sensitivity to Weibull scale parameter for all 4 drive trains.

The drive trains all present a potential COE reduction of over 10% when placed in an offshore environment with a scale parameter of 8.4 compared with 7.8 as shown in Figure 5.6. This corresponds to an AEP increase by 2.2 GWh. The high scale parameter may not represent a real case but for the purposes for performance comparison, it is clear that the winds conditions, and in particular the average wind speed, play a significant role in the performance of the drive trains.

The benefits of having higher average wind speeds on a site include the higher energy yield and subsequent reduced COE. With appropriate site selections and wind turbine class design, significant cost savings can be achieved with each drive train. The wind speed characteristics do not affect the relative COE for each drive train. Therefore, no particular drive train is best suited to specific conditions as each one has the same overall performance variation across the wind speed ranges.
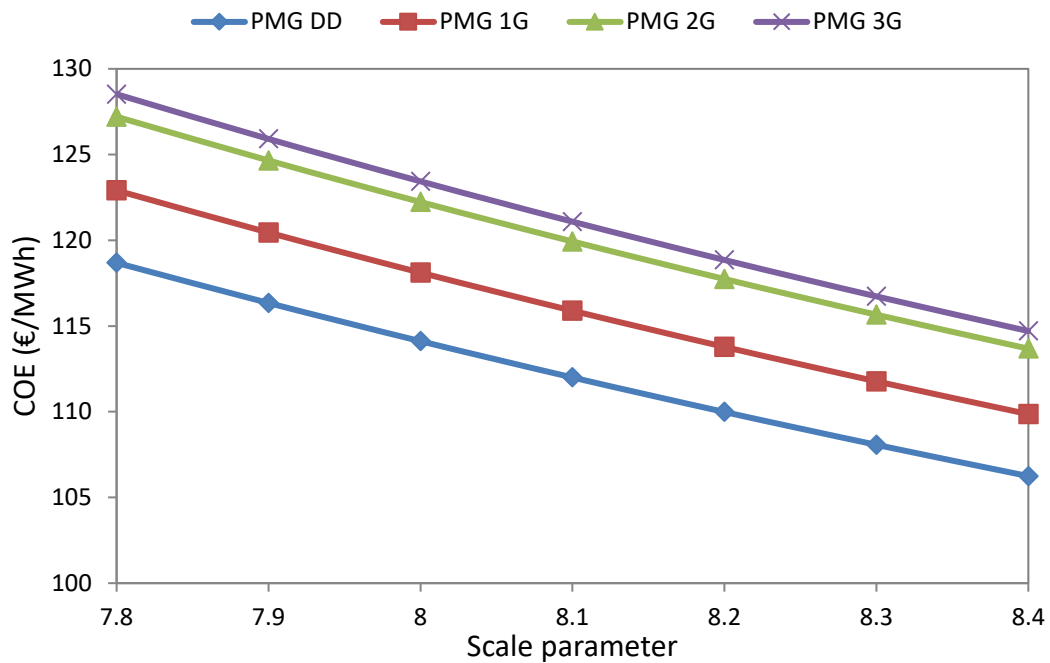
Figure 5.6 COE sensitivity to Weibull scale parameter for all 4 drive trains.

5.1.3 Reliability and generator replacement

One of the key aspects of the reliability analysis used in this thesis is that the PMGs do not have a major replacement throughout the project lifetime. This was based on limited data discussed in [1] that did not have any major replacements for permanent magnet generators. The technology is still considered to be in its infancy when regarding complete lifetime assessment, so a reasonable assumption could be that the complete generator system may require at least one full replacement over the 25 year operation. This section looks at the effects of having 1 generator replacement on top of the existing failures assumptions.

The O&M assumptions described in Chapter 3, were also applied to the generator replacement scenario such that the model calculates O&M costs that are inclusive of transport, technician and replacement parts cost, and also includes repair time and down time that used in the availability calculation. The COE of this scenario is directly compared to the results of Chapter 4.

|	PMG DD	PMG 1G	PMG 2G	PMG 3G
No replacement	109.99	113.78	117.74	118.85
1 replacement	111.61	114.75	118.45	119.37
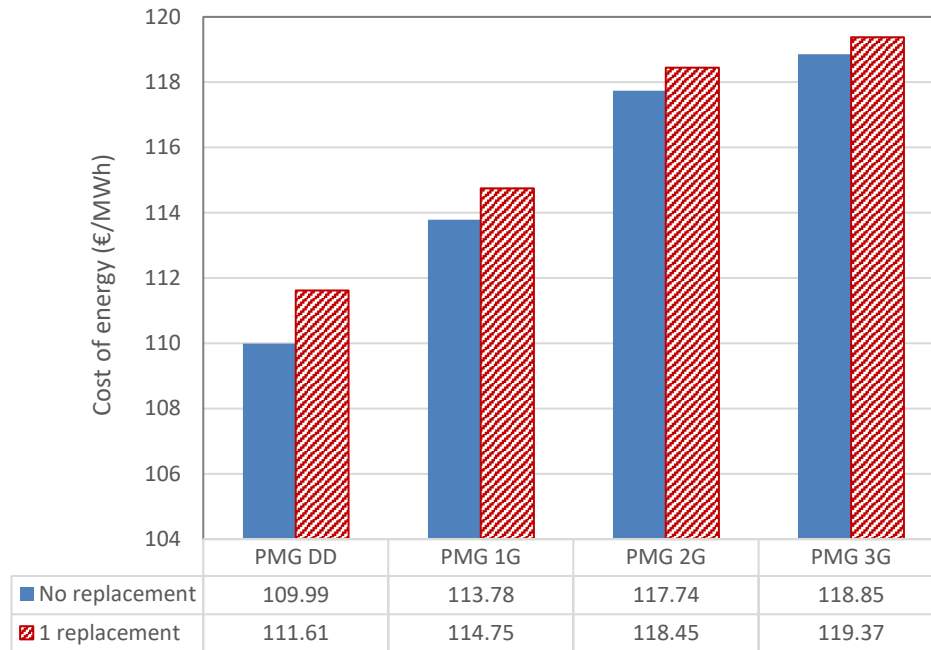
Figure 5.7 Cost of energy comparison for each drive train with and without a complete generator replacement over the lifetime of the wind turbine.

The effect on the COE when adding a complete generator replacement is shown in Figure 5.7. As expected with the larger sized generator of the PMG DD the COE increases by a greater value than the geared designs. The COE increases by 1.48%, 0.85%, 0.60% and 0.44% for the PMG DD, PMG 1G, PMG 2G and PMG 3G respectively. It is important to note that vessel requirements for generators are currently assumed to be uniform across all drive train type, but in reality, the PMG DD will have a much higher cost attributed to the use of a jack-up vessel and specialist equipment to remove and replace the generator. Therefore, the values will be higher than presented which creates an opportunity to develop the models as further work, but this is currently beyond the scope of this thesis.

Having access to lifetime data of permanent magnet generators will enable more accurate failure rates to be calculated and used in models similar to the ones presented in this thesis. The data at the moment does not yet exist and it will be a number of years before assumptions can be made with a higher degree of accuracy. If the minor and major repair categories are also impacted by higher failure rates than those assumed in this model, then the direct drive model will see a much more

significant increase in COE compared with the geared topologies. However, the motivation in using a direct drive configuration with a permanent magnet generator was to improve the reliability of the system. Therefore, assumptions in this case are reasonable to predict that there should not be a complete replacement required if the machine is correctly maintained and if a major replacement does occur it should only increase the COE by around 1.5 % for the PMG DD drive train.

	PMG DD	PMG 1G	PMG 2G	PMG 3G
■ No replacement	34.94	81.74	126.77	142.73
▨ 1 replacement	52.82	88.14	129.92	144.45
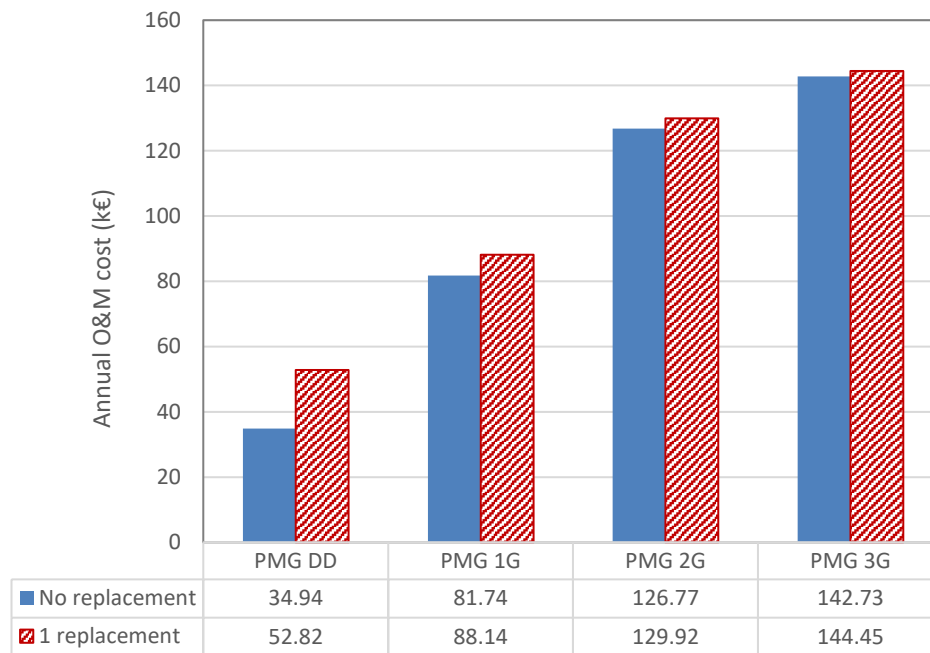
Figure 5.8 Annual O&M comparison for each drive train with and without a complete generator replacement over the lifetime of the wind turbine.

The annual operations and maintenance (AOM) cost changes as shown in Figure 5.8 when adding a complete generator replacement. As with the COE, the AOM increases most significantly for the PMG DD and has a diminishing effect as the generator size decreases when adding each extra gear stage. The AOM increases by 51.2%, 7.83%, 2.49%, and 1.2% respectively. Having over 50% increase in AOM for the direct drive design is a huge commitment to pay if the generator needs replacing. Although the direct drive O&M cost is still lower than the other drive trains, the current estimates for failure rates, repair times and repair costs may be higher than those used in this thesis (the values are outlined in Chapter 3). For example, if the base AOM for the PMG DD was €100k instead of the assumed €35k, a generator

replacement would force the AOM cost to €151k. This is a higher cost than the current values for the PMG 3G with a generator replacement. As a result, a major replacement for the PMG DD could have a significant impact on the maintenance aspect of the project, especially if vessel and repair costs increase over time. The price of the magnets is the most volatile material cost used the design. If the magnet prices were to increase vastly over the 25-year operation of the wind turbine, buying another generator to replace a broken one may be too costly for the project and perhaps an alternative drive train would have to be considered in such a case.

	PMG DD	PMG 1G	PMG 2G	PMG 3G
No replacement	95.49	94.45	93.83	93.43
1 replacement	94.88	93.92	93.41	93.09
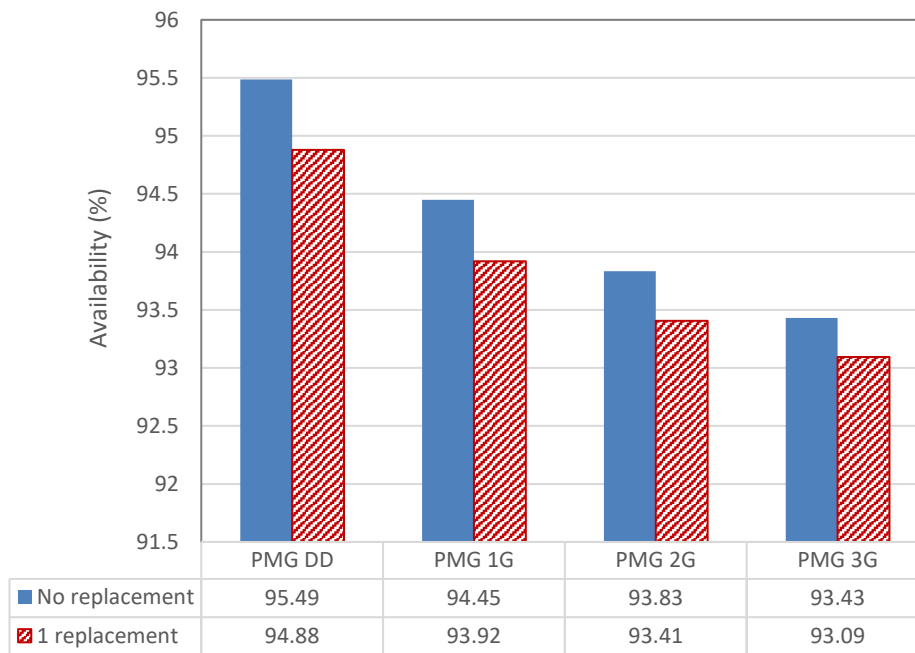
Figure 5.9 Availability comparison for each drive train with and without a complete generator replacement over the lifetime of the wind turbine.

The availability of the drive trains if a major generator replacement is required is shown in Figure 5.9. The direct drive option still maintains the best availability out of the 4 drive trains despite the long downtime associated with such a failure. This is due to the gearbox of the geared design carrying a significant contribution to down time. It can be suggested therefore, that the PMG DD drive train will offer the highest availability as long as major replacement of the generator does not exceed 1 over the lifetime of the project.

5.2 Basic Cost Sensitivity

The cost of the materials used to manufacture the drive train play a significant role in the ICC of the wind turbine. The first simple approach in the analysis the effect of changing material prices involved manually changing the cost and observing the effects on the optimised designs. Each material was independently varied in price and so the 4 designs were scrutinized for their key price sensitivities. The COE values were normalised to their original prices used in Chapter 2 and 3 so the relative changes against each drive train can be assessed.

5.2.1 Copper cost

Varying the cost of copper for each of the drive train allows the impact of the design dimensions to be assessed for price changes that affect the windings. The normalised COE values for each drive train through a copper cost range from 10 to 20 €/kg (based on historical maximum and minimum costs) are shown in Figure 5.10.
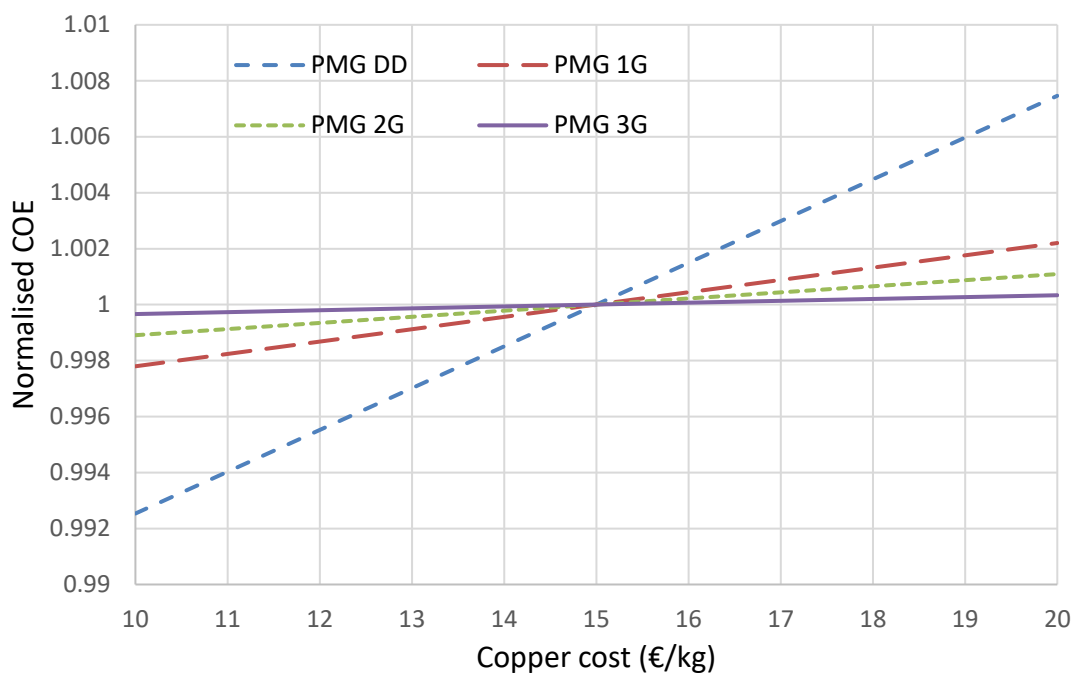
Figure 5.10 Normalised COE variations with increasing copper cost for all 4 drive trains.

The PMG DD is affected by the change in copper cost much more than the geared design due to the large volume of windings in the generator. As expected, as the generators get smaller as more gear stages are added, the effect of copper cost fluctuations are almost negligible in term of COE

5.2.2 Permanent magnet cost

This section looks at the effect of permanent magnet price rises for each drive train and the normalised COE values are presented in Figure 5.11.
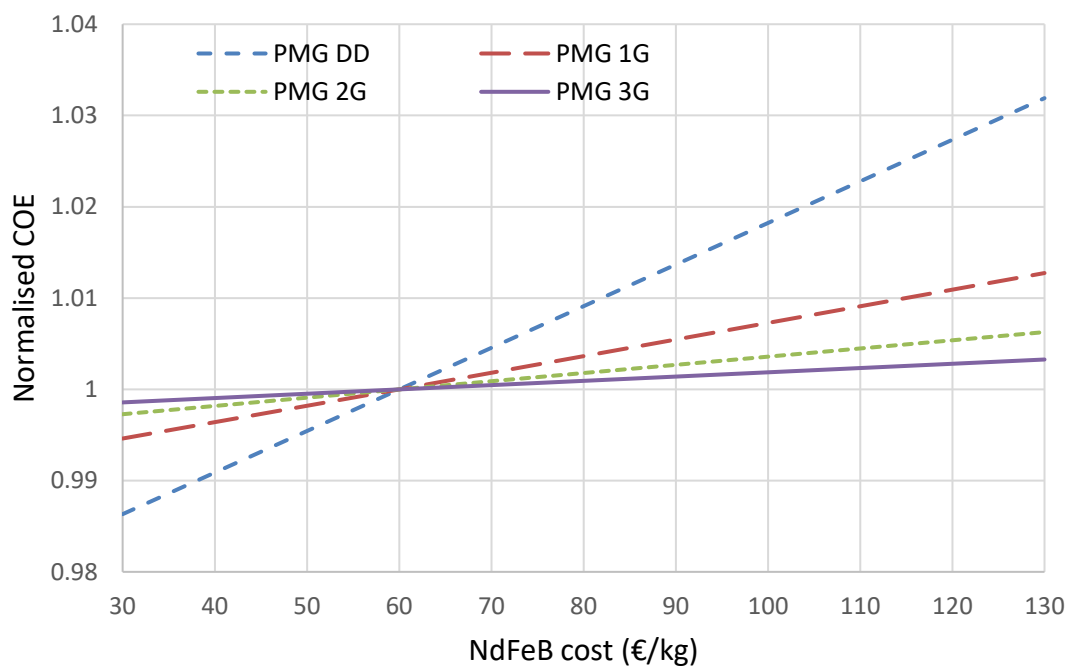
Figure 5.11 Normalised COE variations with increasing magnet cost for all 4 drive trains.

The change in magnet price has the most significant impact on PMG DD, as expected, due to the high price of rare earth materials. From Figure 5.11 the change in COE for the PMG DD reaches +3.7% compared with only +0.4% for the PMG 3G. It highlights the risk taken when using a high volume of magnets in large generators.

5.2.3 Steel cost

The impact of varying the cost of steel, which includes the iron laminations, structural steel and gearbox steel, is shown in Figure 5.12 as a normalised COE for each drive train. The range of steel cost represents a base steel price for the structural steel and parts of the gearbox. The iron laminations are assumed 1 €/kg higher to account for the processing and manufacturing of the sheets.
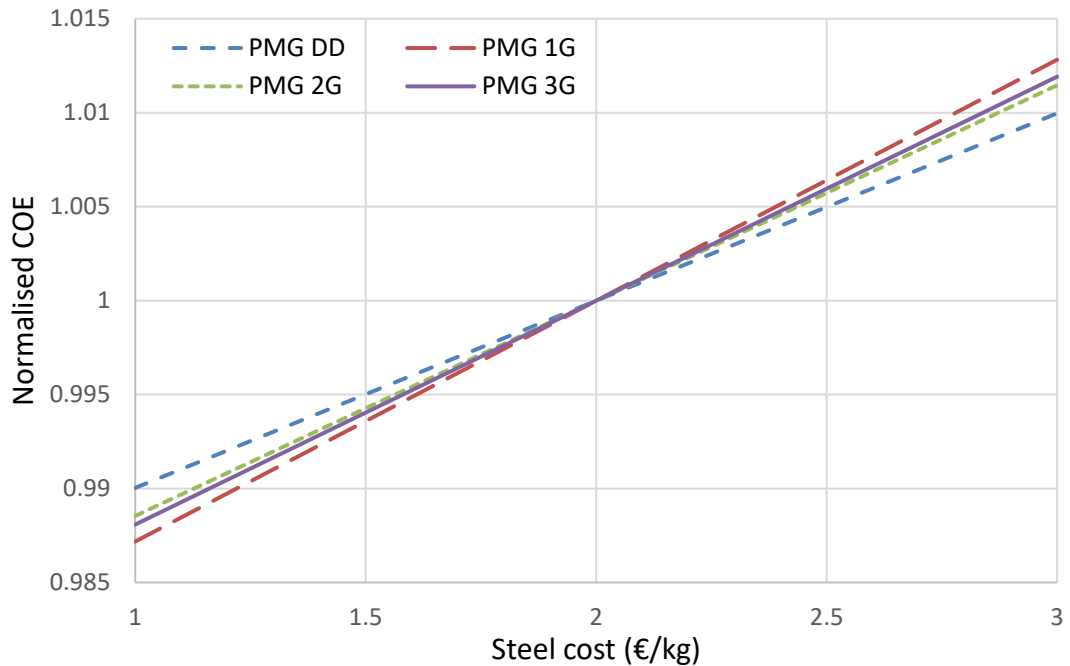
Figure 5.12 Normalised COE variations with increasing steel cost for all 4 drive trains.

When varying the price of steel, a different trend with each drive train is observed compared with the copper and magnet cost variations. Firstly, the DD PMG is least affected as the steel used in this layout only includes the generator laminations and structure. The PMG 2G and the PMG 3G are both equally affected in terms of COE when varying the price of steel. This is due the trade-off with larger generator size and low speed against having a high-speed gearbox and small generator. The total volume of steel used between gearbox and generator are similar and so for steel price fluctuations, either design will suit such conditions. The PMG 1G COE is moderately affected by the impact of fluctuations in steel price as the topology has both a large gearbox and sizable generator.

5.2.4 Summary of basic cost sensitivity

Fluctuations in magnet price are the most significant contribution to COE for all drive trains with the PMG DD being most affected as expected. The variation in copper price shows a similar trend to that shown for the magnet price fluctuations where the PMG DD has the higher COE increase, and the effect is reduced with the addition of each gear stage until a negligible change for the PMG 3G is observed. The steel cost variation has a different outcome for each design relative to one another, with the PMG 1G and PMG 3G being most affected and the PMG DD being the least. This is due to trade-off with having a generator and gearbox combination that each consist of steel through laminations, structure and gear sections.

The basic sensitivity study for each independent cost variable allowed a direct comparison between the relative impact of cost variations. It did not consider the probability of such costs and only presented the outcome if such cost were applied. Therefore, to understand how likely such variations are to occur in reality, a new probabilistic approached was developed and is outlined in the following sections.

5.3 Probabilistic Sensitivity Analysis

This section will look at sensitivity based on probability for each cost price. This will allow real historical material prices to influence the COE and identify the most likely cost scenarios and their impact on the project costs. This method expands the basic sensitivity study discussed in section 5.2 by adding a probability of cost fluctuations which would help distinguish between the designs that are most susceptible to the risks of price changes.

5.3.1 Cost Probability Density Functions

In order to obtain a reasonable set of cost assumptions, historical cost data for each of the materials used in the generator was used to create histograms of the costs. This allowed probability density functions to be created as normal distributions. Due to the data being based on extracting only a limited number of historical values and not having any certainty of future values, a normal distribution is a suitable fit for the

purposes of the model. The normal probability density function (PDF) is given by equation (5.1) where μ represents the mean of the function and σ is the standard deviation.

$$f(x|\mu,\sigma^2) = \frac{1}{\sqrt{2\pi\sigma^2}} e^{-\frac{(x-\mu)^2}{2\sigma^2}} \tag{5.1}$$

Each material cost is represented as a PDF so that each design can be evaluated against the most likely price scenarios. The variable costs considered in the model include copper, NdFeB magnets, electrical steel for the generator laminations, structural steel for other parts of the generator assembly and gearbox (if applicable). Aluminium can be added to structural sections of the generator to help reduce the structural mass, but it is not a significant contributor to the COE so in this case it is not used for the sensitivity analysis. The cost probability distribution of aluminium is included in this chapter for comparison purposes only. The costs are all scaled to represent suitable end-product/purchase values considering the cost of manufacture and processing of the material. This has been done primarily based on in-house knowledge and the processing costs are assumed to be a constant in addition to the baseline material prices.

5.3.1.1 Copper cost

The cost of copper was taken from a 10 year price history based on monthly prices from [2]. The values were scaled to assume an end-product/purchase cost and converted to €/kg. The time history is shown in Figure 5.13(a) and the corresponding histogram and fitted normal distribution Figure 5.13(b) and (c). The mean copper cost is €15.1 with a standard deviation of €1.1.
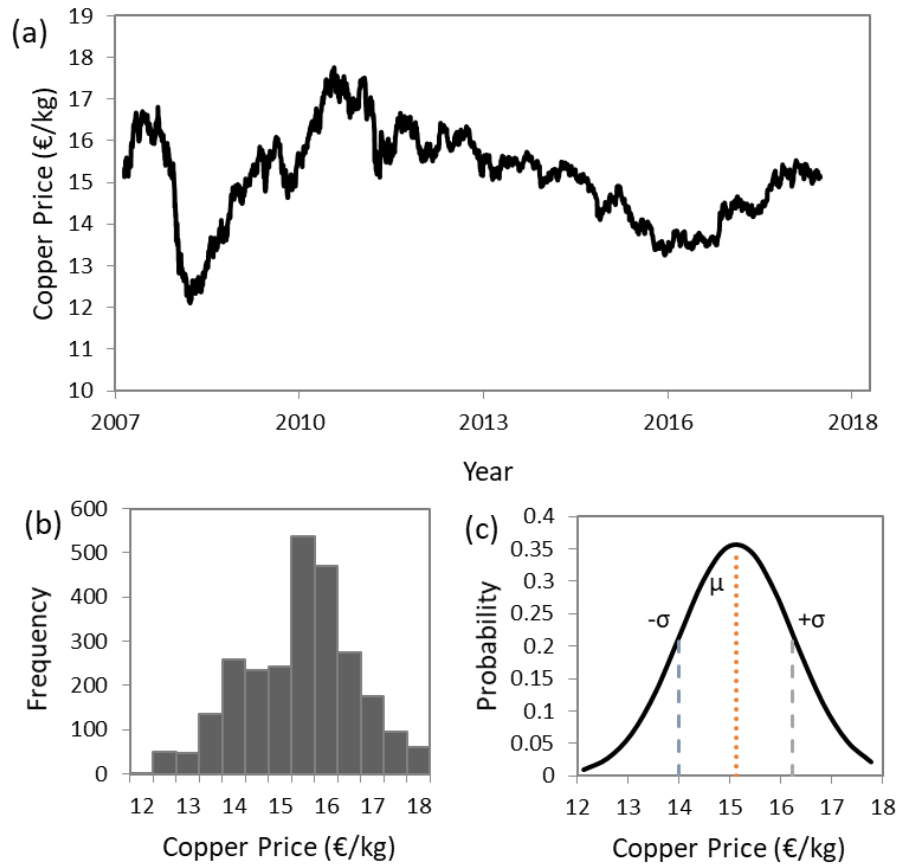
Figure 5.13 (a) Copper price history adapted from [2], (b) Histogram of the time series, and (c) PDF fitted to the histogram.

5.3.1.2 Permanent magnet cost

The exact make-up of the magnetic material used to create permanent magnets for PMGs (e.g. certain quantities of dysprosium) is not considered for the model as it would require much more specialist knowledge. However, a cost estimate based on Neodymium Iron Boron (NdFeB) has been made based on historical data and information from [3],[4] and [5] and converted to €/kg. The mean NdFeB cost is €72.8 with a standard deviation of €38 and the distributions are shown in Figure 5.14.
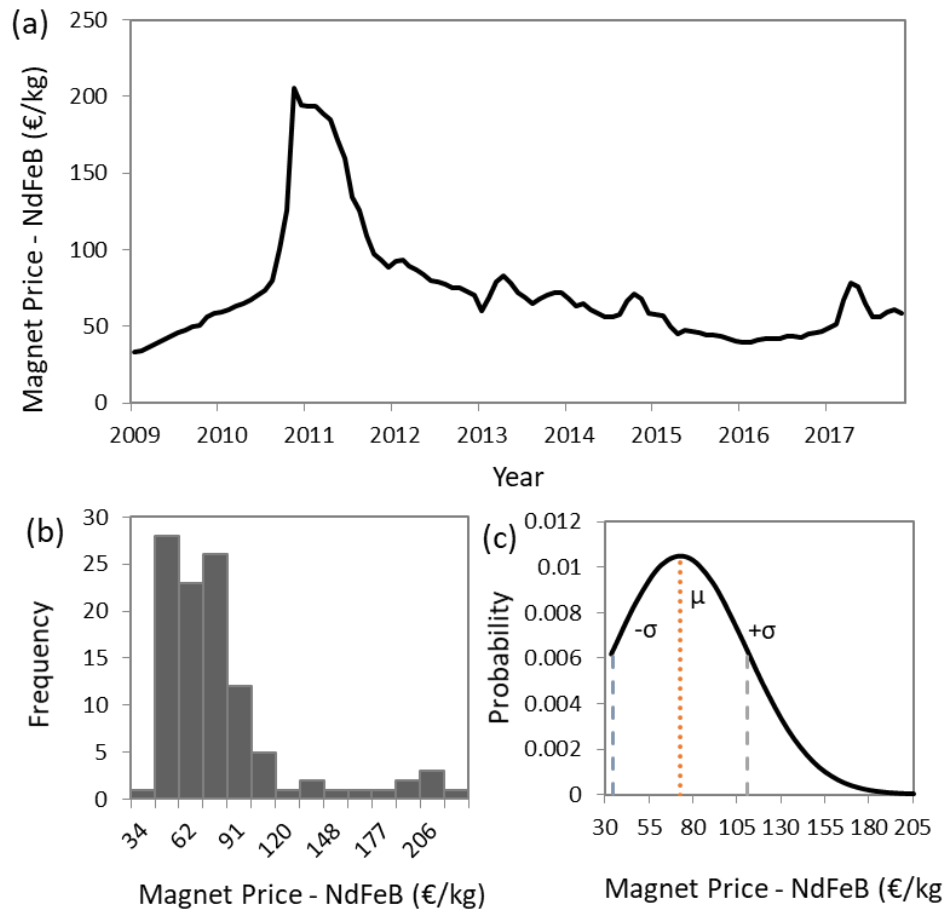
Figure 5.14 (a) NdFeB price history adapted from [3], (b) Histogram of the time series, and (c) PDF fitted to the histogram.

5.3.1.3 Electrical steel for iron laminations cost

The cost of the electrical steel for the generator's iron laminations was based on indexed values for "Cold rolled steel sheet and strip" from [6] which represented an appropriate material to estimate the cost of the end product. The indexed values were scaled to present estimated values used in other work such McDonald and Bhuiyan [7] and converted to €/kg. The mean electrical steel cost is €3.1 with a standard deviation of €0.14 and the distributions are shown in Figure 5.15.
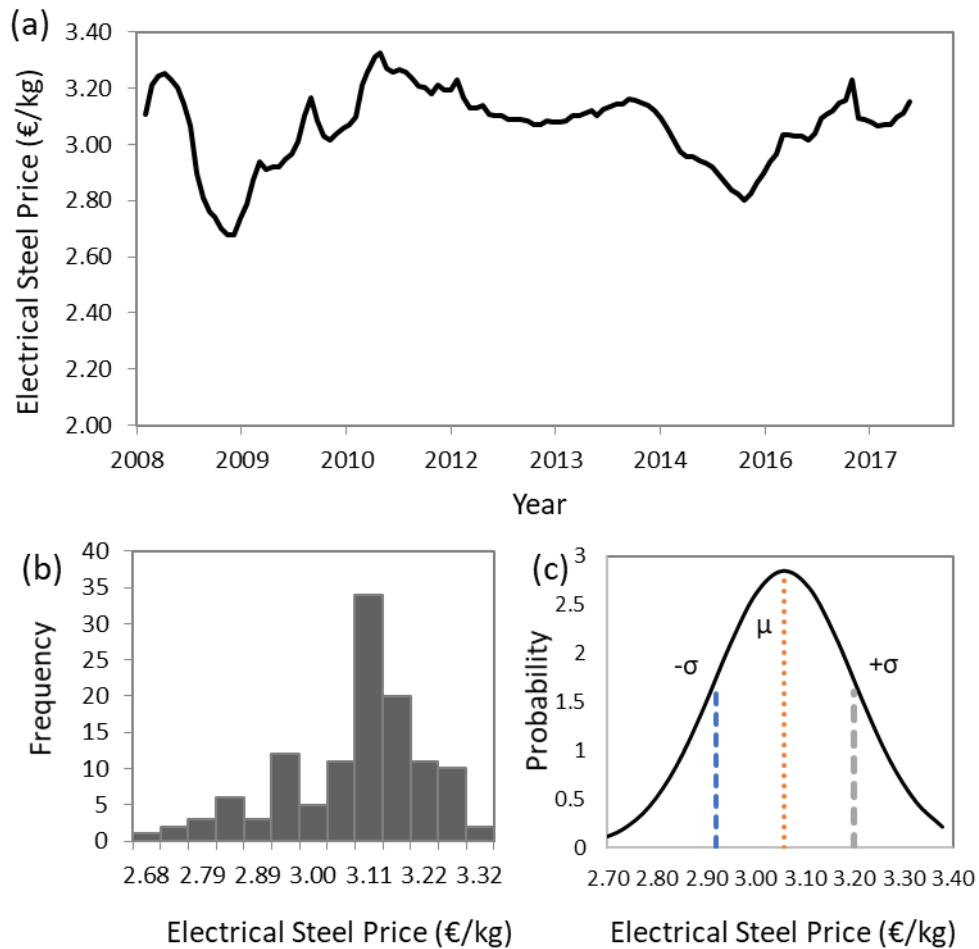
Figure 5.15 (a) Electrical steel price history adapted from [6], (b) Histogram of the time series, and (c) PDF fitted to the histogram.

5.3.1.4 Structural steel price

The generator supporting structure had a steel price based on historical indexed values for "Fabricated structural iron and steel" from [8]. As with the electrical steel price estimate, the structural steel was scaled to suitable values that represented the end-product and converted to €/kg. The mean structural steel cost is €2 with a standard deviation of €0.06 and the distributions are shown in Figure 5.16.
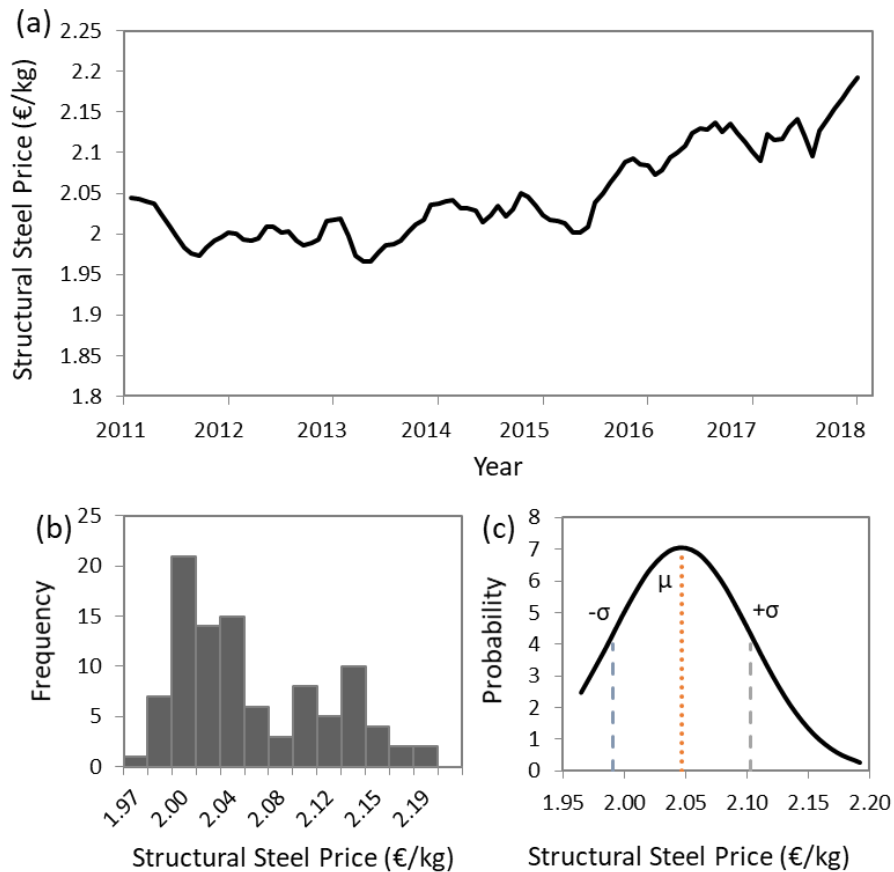
Figure 5.16 (a) Structural steel price history adapted from [8], (b) Histogram of the time series, and (c) PDF fitted to the histogram.

5.3.1.5 Aluminium price

Aluminium is used in part of the supporting structure and so a cost price was determined from historical data from [9] which were scaled and converted to €/kg. The mean aluminium cost is €6.8 with a standard deviation of €0.34 and the distributions are shown in Figure 5.17.
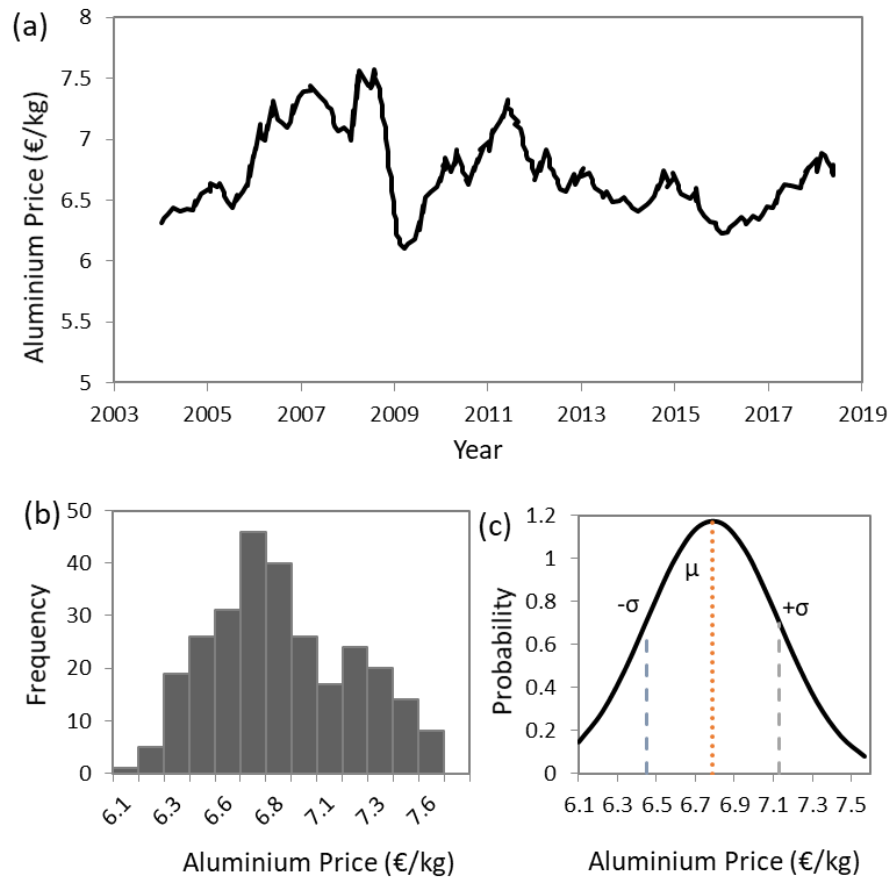
Figure 5.17 (a) Aluminium price history adapted from [9], (b) Histogram of the time series, and (c) PDF fitted to the histogram.

5.3.2 COE probability results

Similarly to the basic sensitivity analysis, the material cost were varied one at a time, but this time each has a probability density function to assess the likelihood of such cost scenarios arising. The results in this section are presented as probability distribution shapes of COE values of each drive train for different material price comparison purposes only and so they do not include individual probabilities for COE – this is explored in section 5.5 later in this chapter.

Figure 5.18 shows the COE probability distribution shapes (not inclusive of amplitude of probability) for each drive train when varying the cost of the NdFeB magnet material in accordance with its PDF in Figure 5.14. The straight vertical lines at the left hand side of each distribution represent the minimum price that is considered in this study.

Figure 5.19 and Figure 5.20 show the COE probabilities for varying the copper cost according to its PDF and the steel cost with its PDF respectively. As already shown and discussed in previous sections, the magnet price has the largest impact on the COE compared with the copper and steel cost price fluctuations. Having a probability associated with the costs allows the possible range of outcomes to be analysed. It is clear that the magnet price is highly uncertain and so produced a large range of COE probabilities indicated by the wide distributions of Figure 5.18, particularly for the PMG DD. The mean and standard deviation of the cost of energy for each drive train when applying the NdFeB price distributions are 110.67±1.82 €/MWh, 114.06±0.75 €/MWh, 117.89±0.39 €/MWh and 118.93±0.20 €/MWh for the PMG DD, PMG 1G, PMG 2G and PMG 3G respectively.
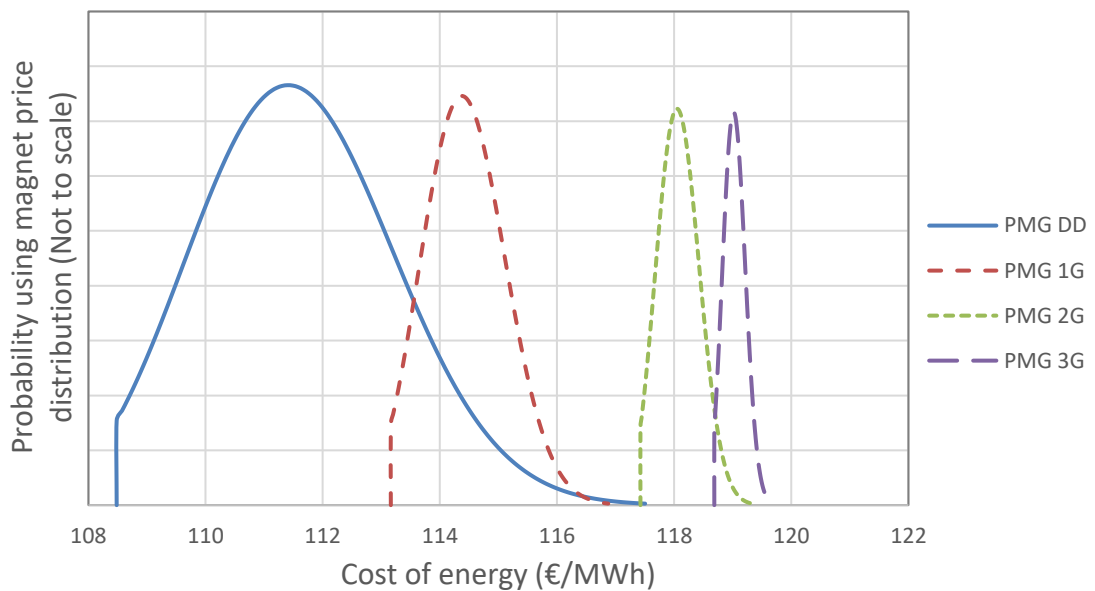
Figure 5.18 Cost of energy distributions illustration for each drive train with magnet price PDF as an input.

The copper price probability density function, when applied to the model, does not have a significant effect on the COE for any of the drive trains. Only the PMG DD has a small range of possible outcomes in terms of COE only spanning across a window of 1 €/MWh as shown in
Figure 5.19.
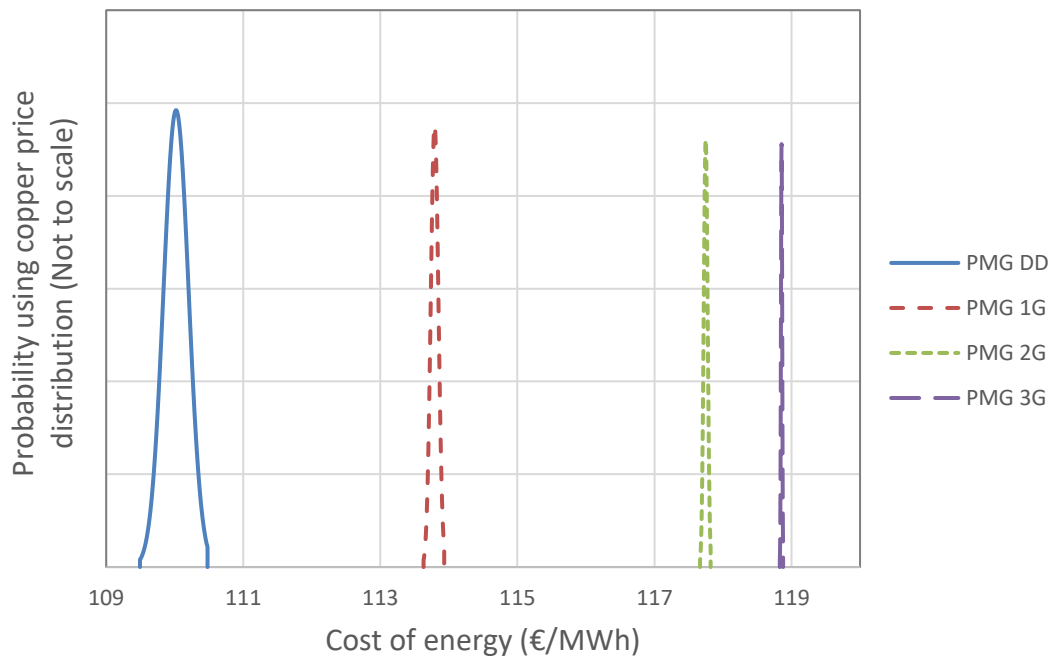
Figure 5.19 Cost of energy distribution illustration for each drive train with copper price PDF as an input.

The geared drive trains show almost no change in COE across the PDF range, implying that the effect of copper cost variations can be considered almost negligible for wind turbines has have gearboxes. The mean and standard deviation of the cost of energy for each drive train when applying the copper price distributions are 110.01±0.18 €/MWh, 113.79±0.05 €/MWh, 117.75±0.03 €/MWh and 118.85±0.01 €/MWh for the PMG DD, PMG 1G, PMG 2G and PMG 3G respectively.

The cost of steel also does not have much of an effect on the COE for the drive trains when its PDF is applied to the model. The mean and standard deviation of the cost of energy for each drive train when applying the steel price distributions are 110.04±0.13 €/MWh, 113.85±0.11 €/MWh, 117.80±0.1 €/MWh and 118.92±0.1 €/MWh for the PMG DD, PMG 1G, PMG 2G and PMG 3G respectively. From Figure 5.20, although the COE does not change by much, each drive train varies by almost identical amounts across the range. This reinforces that the trade-off when removing the gearbox to reduce the generator size and lower the mass of iron laminations, subsequently adds a volume of steel for the gearbox. Therefore, it can be concluded that the change in steel price may marginally alter the COE for all drive

trains which are equally affected by it and that drive train choice would not be a critical concern for steel price fluctuations.
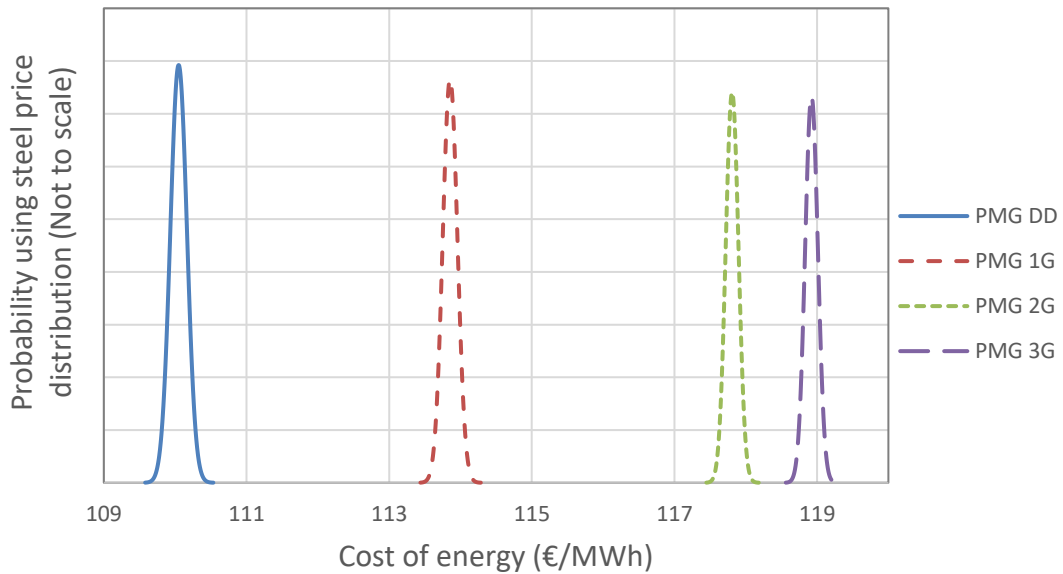
Figure 5.20 Cost of energy distributions illustration for each drive train with steel price PDF as an input.

5.3.3 Summary of the probabilistic sensitivity analysis

The optimised drive train solutions were subject to individual cost sensitivity analysis for each of the material price probability density functions. The COE distributions for all drive trains were highest when using the magnet PDF as the input. The copper distribution has a negligible effect on the geared designs in terms of COE probability distribution shape with varying copper cost. Finally, the steel cost variations had a modest effect on all drive trains, but carried no significance when considering drive train selections as reductions in generator iron laminations are counter balanced with the addition of gearbox steel when adding gear stages.

In reality, all materials are subject to price fluctuations and it would not be likely for only one price to change at a time as presented so far in this chapter. Therefore, the next step in understanding the drive train choice with material cost variations is to include a method of varying all costs together at the same time whist respecting their probability density functions.

5.4 Multi-Parameter Sensitivity Study

This section develops the probabilistic method outlined in section 5.3 to include all material cost variations simultaneously. This method looks at the complete range of probabilities for each unit cost and provides a sensitivity study of the optimised designs based on cost probabilities.

5.5 Monte Carlo Sampling

A Monte Carlo method of external sampling was used to obtain a range of solutions with probabilistic attributes. Monte Carlo methods [10][11] are effective tools for implementing random selections of parameters used in statistical analysis and provide useful analysis techniques for wind turbine cost [12]. For cases with probability distributions, such as those discussed in this thesis, the sampling method can include probability so that the outcomes are the most likely solutions.

Figure 5.21 illustrates the process used in this model for sampling all material prices simultaneously according to their individual probability distributions. Each material price is assigned its range of values and their corresponding probabilities where the model then selects at random, a price of each material. These prices are then used in the COE model to produce an output that carries probability.

Using the Monte Carlo sampling technique for all prices will allow the designs to undergo cost scrutiny in order to assess the combined impact of material price fluctuations.
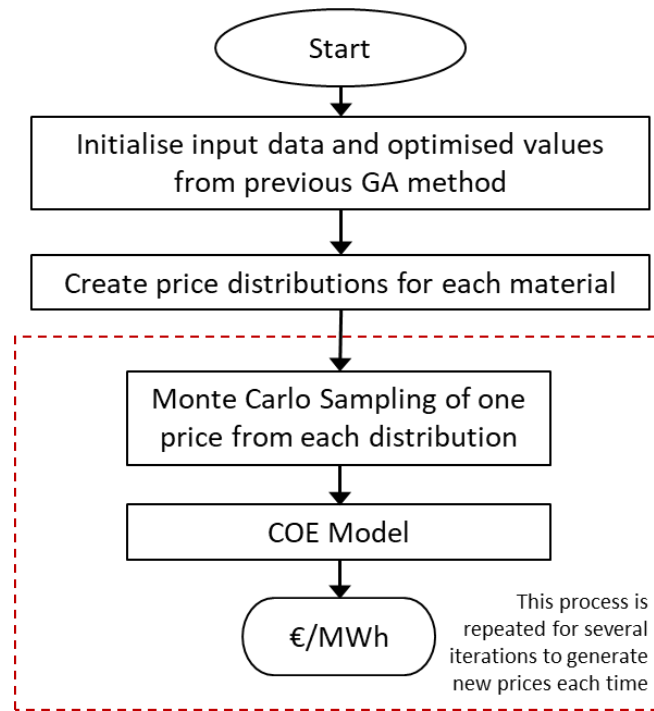
Figure 5.21 Flow chart of the Monte Carlo sampling method.

The following sections present the outcomes for each drive train that include the mean and standard deviation of the COE results. Although the effect of varying the price of aluminium in the previous section had a negligible effect on the COE, it is still included in the Monte Carlo Sampling method to reflect real-life fluctuations.

5.5.1 PMG DD Monte Carlo sampling

The optimised design for the direct drive case underwent the Monte Carlo sampling of material costs to observe the impact of all price fluctuations and their combine probabilities. The results are shown as a histogram in Figure 5.22. The mean COE was 111.28 €/MWh with a standard deviation of 1.63 €/MWh for the PMG DD. Although the data shows that some COE values reach above 116 €/MWh, 95% of the output values are below 113.91 €/MWh and so there would only be 5% chance of exceeding this cost. The standard deviation of the COE for the direct drive topology is quite significant for additional lifetime costs, but competitively it is still lower than the COE for the other drive trains.
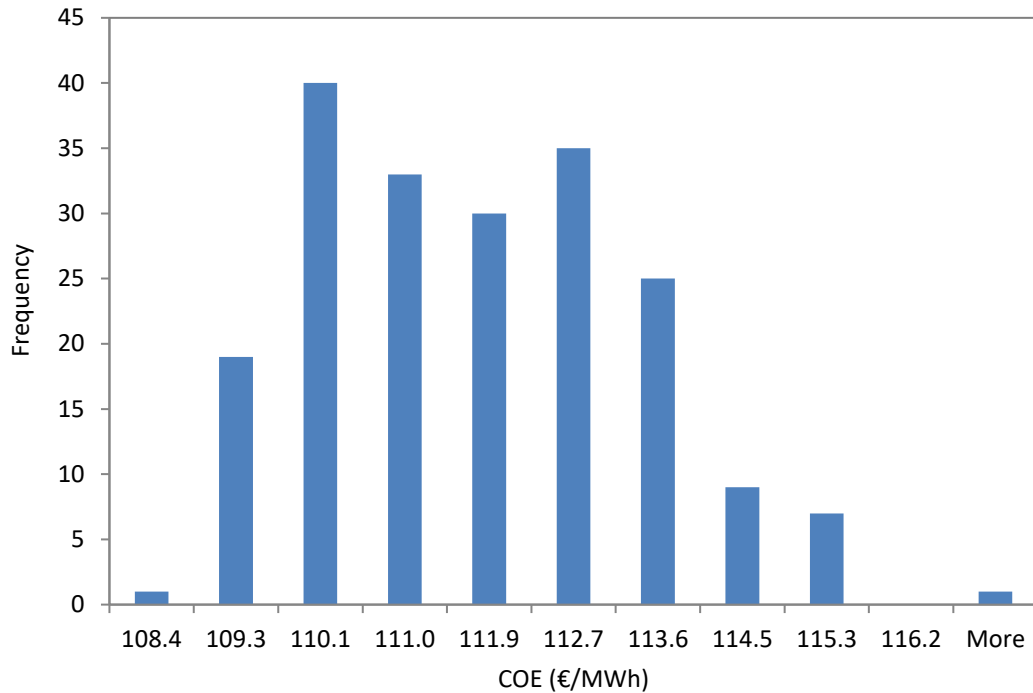
Figure 5.22 Histogram of COE based on Monte Carlo sampling of material costs for PMG DD.

5.5.2 PMG 1G Monte Carlo sampling

The mean COE was 114.31 €/MWh with a standard deviation of 0.68 €/MWh for the PMG 1G. The 95th percentile is 115.61 €/MWh and so only 5% of the output values would be above this number. Although the COE is higher than the PMG DD, the standard deviation is lower and so the range of outputs can be considered lower and that the design carries a reduced risk.
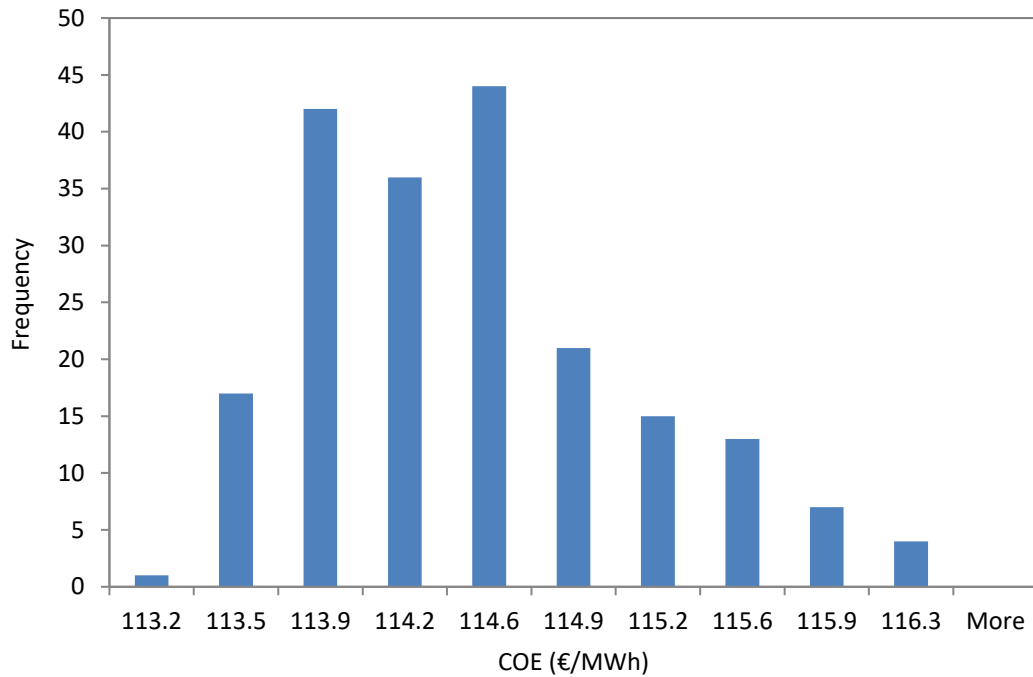
Figure 5.23 Histogram of COE based on Monte Carlo sampling of material costs for PMG 1G.

5.5.3 PMG 2G Monte Carlo sampling

The mean COE was 118.05 €/MWh with a standard deviation of 0.34 €/MWh for the PMG 2G and 95% of the COE results are below 18.76 €/MWh. The range of values produced is very small and so in terms of uncertainty and risk, the PMG 2G offers a design that will be largely unaffected by price fluctuations.
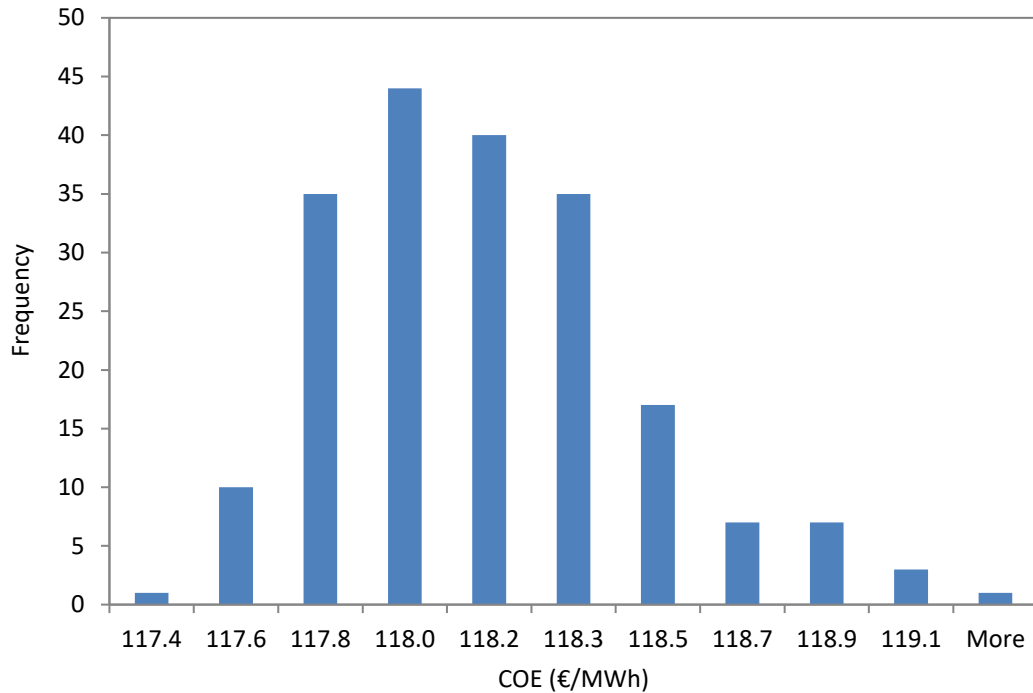
Figure 5.24 Histogram of COE based on Monte Carlo sampling of material costs for PMG 2G.

5.5.4 PMG 3G Monte Carlo sampling

The mean COE was 119.07 €/MWh with a standard deviation of 0.17 €/MWh for the PMG 3G and 95% of the output values are below 119.35 €/MWh. Out of all the optimised deigns, the PMG with 3-stage gearbox drive train varies the least over the price range of all the materials. In terms of material costs, this drive train offers the lowest risk for material price fluctuations. This is largely due to the low volume of magnets which dominate all of the designs. If the gearbox can be improved in terms of reliability and repair costs, having a geared wind turbine would provide the lowest risk for possible material price rises.
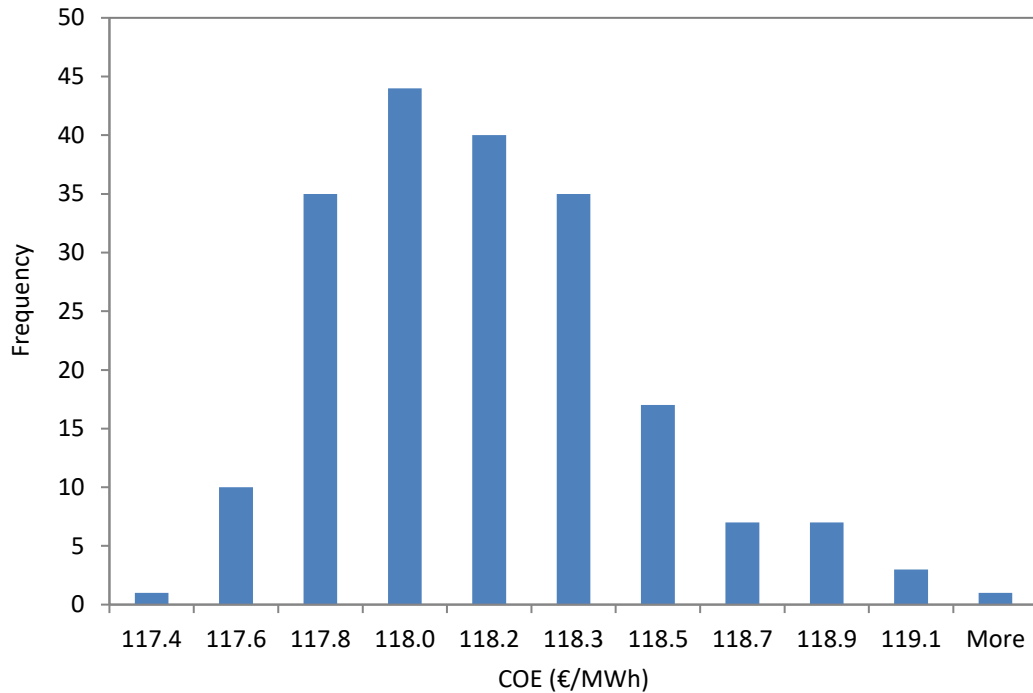
Figure 5.25 Histogram of COE based on Monte Carlo sampling of material costs for PMG 3G.

5.5.5 Comparison of drive trains with Monte Carlo sampling

The output histograms from sections 5.5.1 to 5.5.4 were fitted with normal distributions and plotted together in Figure 5.26. The range of distributions can be cleared compared between drive trains.

The wider the distribution, the most uncertain the mean value becomes. It can be seen that the widest distribution occurs with the PMG DD, closely followed by the PMG 1G, then the PMG 2G, and PMG 3G has the narrowest distribution. Simultaneously, the height of the distribution signifies the probability of attaining the mean value. The PMG 3G has the tallest distribution and so has the highest probability of achieving its mean value compared with the other 3 designs. In terms of planning and developing drive trains, having a reduced risk to cost price fluctuations brings many benefits to such designs. It means that perhaps alterations to the dimensions would not be necessary, even in worst case scenarios, as price rises would be almost inconsequential. However, the higher mean value for the PMG 3G would not instantly make this design the most appealing to manufacturers.
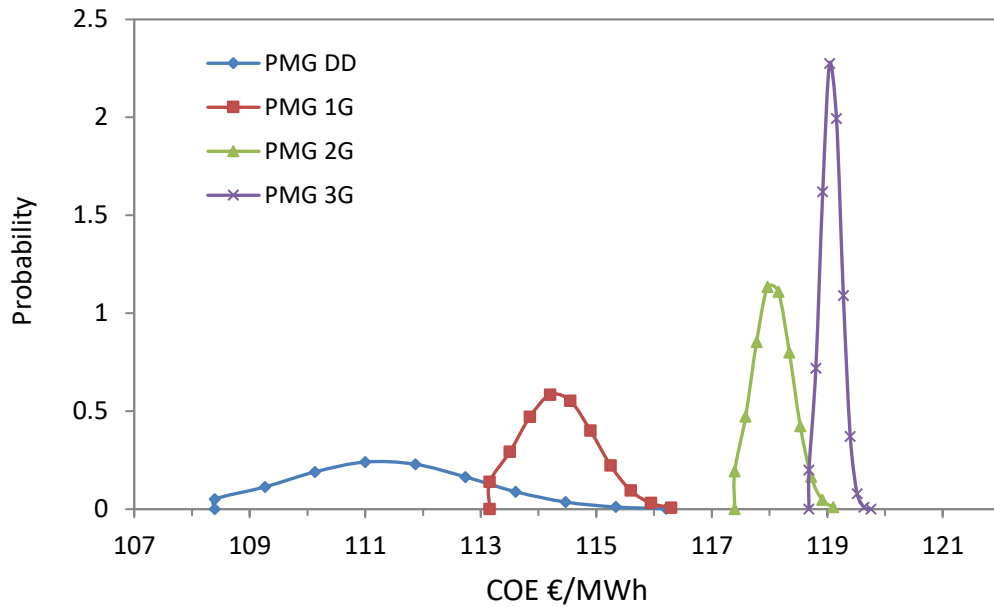
Figure 5.26 COE probability distribution comparison between the 4 drive trains.

For drive trains such as the PMG DD and PMG 1G that have broader ranges of COE probabilities, large price rises could have significant consequences for the topologies. They may need to be redesigned for the next generation of wind turbine installations to compensate for high material costs. This outcome would be expensive and time consuming and so carries a high level of risk when considering the raw material prices and their potential to increase.

5.6 Summary of Chapter 5

It was the purpose of this chapter to investigate the effects of varying a number of external conditions on the optimised designs that were produced in Chapter 4. These designs were subject to variations in the wind conditions, the generator reliability and the raw material prices.

The shape and scale parameters of the Weibull distribution for the wind profile were varied independently and the annual energy production and the cost of energy were compared with each drive train. It was concluded that relative to one another, the PMG 3G drive train would perform best in high variability winds. The PMG DD and the PMG 1G shared the same performance indicators and would be

suited to wind sites with higher shape parameters. All drive trains benefited from operating in high average wind speed sites, although it was acknowledged that additional design considerations would have to be included for operation in high load conditions such as blade and tower alterations. This was not within the scope of this thesis and was not considered as part of the sensitivity analysis.

When adding a major generator replacement into the failure rate for each drive train has the most significant impact on the PMG DD as expected due to its large size. The annual operations and maintenance costs subsequently increased by over 50% for the PMG DD. Depending on the base AOM cost assumptions, such an increase can potentially be very serious for such a design and so appropriate warranty and insurance considerations would be essential. The geared designs were much less affected by the addition of a generator replacement in the cost models.

With a basic linear cost sensitivity analysis, it was clear that fluctuations in the cost of the permanent magnets had the most significant impact on the COE for all drive trains. The copper cost fluctuations had a moderate effect on the COE for PMG DD and had a reduced impact on the geared designs with the lowest effect on the PMG 3G. Fluctuations in cost of steel presented a trade-off between the iron laminations and steel structure of the generator, and the gear steel used in the gearbox. It was concluded that the cost of steel presented no significant differences due the effect of this trade-off and so no drive train would be preferred over the other when considering steel price rises.

Probability distributions were applied to each material cost and the resulting COE outputs were compared with each drive train. Each material was assessed independently to compare the most significant effect on each drive train. A range of probabilistic outcomes were presented, and the permanent magnet cost distribution had the highest COE output compared with the distributions of the other material costs.

The final part of the chapter looked at combining all the cost probabilities simultaneously for each material and using a Monte Carlo method to produce a probabilistic COE for all drive trains. It was concluded that the PMG 3G carried the lowest risk is terms of material price rises as it was largely unaffected by the complete price range of materials. The PMG DD can be considered the most at risk

design for price fluctuations as it has a broader range of COE outcomes. Depending on future prices, it could be possible that the design presented in this thesis would no longer be a viable option and so redesign may be required to accommodate the new prices.

      The price uncertainty scenarios are summarised in Table 5.1 where the mean COE and standard deviation of each drive train are compared to the COE of the optimised results from Chapter 4. The effects of individual price uncertainty can be compared for each material and the combined effect of all price uncertainty can allow the most vulnerable designs to be determined.

Table 5.1 Comparison of COE values for

COE (€/MWh)	PMG DD mean	PMG DD mean difference	PMG DD stnd dev	PMG 1G mean	PMG 1G mean difference	PMG DD stnd dev	PMG 2G mean	PMG 2G mean difference	PMG 2G stnd dev	PMG 3G mean	PMG 3G mean difference	PMG 3G stnd dev
COE from Chapter 4	109.98			113.79			117.74			118.84		
With PM cost uncertainty	110.67	0.69	1.82	114.06	0.27	0.75	117.89	0.15	0.39	118.93	0.09	0.20
With copper cost uncertainty	110.01	0.03	0.18	113.79	0	0.05	117.75	0.01	0.03	118.85	0.01	0.01
With steel cost uncertainty	110.04	0.06	0.13	113.85	0.06	0.11	117.80	0.06	0.10	118.92	0.08	0.10
With multiple cost uncertainty	111.0	1.0	1.8	115.43	1.6	1.0	119.1	1.4	0.7	119.1	0.28	0.2

      For manufacturers, long term purchase agreements can help mitigate the risk of future price rises, but this all be dependent on the financial management of the project. If a company agrees on a contract to build a certain number of wind turbines, it could be beneficial to investigate the cost of the project for all price scenarios and make informed decisions based on the financial outlook for the supply chain. Alternatively, designs could potentially evolve with the cost of materials to either increase or reduce material volumes depending on their price and the design optimisation process. The designs presented in this thesis so have not been optimised to accommodate future price rises. Therefore, by altering the optimisation process to account for price fluctuations and uncertainty, more robust designs can be produced. Chapter 6 presents an optimisation under uncertainty method to mitigate some of the design risks from external factors such as material cost. This method will provide robust designs with reduced uncertainty for manufacturers and developers.

5.7 References for Chapter 5

[1]   J. Carroll, "Cost of energy modelling and reduction opportunities for offshore wind turbines," PhD Thesis, University of Strathclyde, 2016.

[2]   "InfoMine, accessed on 21/05/2018, Website address: http://www.infomine.com/investment/metal-prices/copper/." .

[3]   "Statista The Statistics Portal, Website accessed on 21/05/2018, address: https://www.statista.com/statistics/450152/global-reo-neodymium-oxide-price-forecast/." .

[4]   "Kitco, Strategic Metals, Accessed on 21/05/2018, Address: http://www.kitco.com/strategic-metals/." .

[5]   J. D. Widmer, R. Martin, and M. Kimiabeigi, "Electric vehicle traction motors without rare earth magnets," *Sustain. Mater. Technol.*, vol. 3, pp. 7–13, 2015.

[6]   "FRED Economic Data, St Louis FED, Website accessed on 21/05/2018, address: https://fred.stlouisfed.org/series/WPU101707." .

[7]   A. McDonald and N. Bhuiyan, "On the optimization of generators for offshore direct drive wind turbines," *IEEE Trans. Energy Convers.*, vol. 8969, no. c, pp. 1–1, 2016.

[8]   "FRED Economic Data, St Louis FED, Website accessed on 21/05/2018, address: https://fred.stlouisfed.org/series/WPU10740510." .

[9]   "InfoMine, Website accessed 21/05/2018, Address: http://www.infomine.com/investment/metal-prices/aluminum/." .

[10]   A. Shapiro, "Stochastic Programming," *Handbooks Oper. Res. Manag. Sci.*, vol. 10, pp. 353–425, 2003.

[11]   S. R. Arwade, M. A. Lackner, and M. D. Grigoriu, "Probabilistic Models for Wind Turbine and Wind Farm Performance," *J. Sol. Energy Eng.*, vol. 133, no. 4, p. 041006, 2011.

[12]   Y. Xu, Q. Hu, and F. Li, "Probabilistic model of payment cost minimization considering wind power and its uncertainty," *IEEE Trans. Sustain. Energy*, vol. 4, no. 3, pp. 716–724, 2013.

Chapter 6 Optimisation under Uncertainty and Robust Optimisation

A key issue with the COE optimisation process outlined in Chapter 4, it that the cost prices for the materials are fixed based on assumed current prices and do not consider price variability. Chapter 5 allowed the prices to change in accordance with real life historical data and probability, but the design was fixed and so only highlighted the key cost drivers for an existing design. The next step in creating a design methodology that includes cost uncertainty would be to identify how the designs from Chapter 4 are altered when optimised for higher prices.

A first simple approach would be to observe the individual impact of each material cost increase on the design optimisation outcome. This will allow the most significant material cost on the optimisation process to be identified. Further to the individual price increase effects, a combined increase of all materials will allow an alternative design to be explored for each drive train to conclude which are influenced the most when prices rise. A final step would be to allow the optimisation process to include probability density functions for the uncertain prices and to optimise based on this uncertainty. This chapter approaches the optimisation methodology with an aim to identify the highest impact of price uncertainty in the design process. During this chapter concepts based on *robust optimisation* and *optimisation under uncertainty* will be introduced and used.

Robust optimisation is a form of optimisation where the process must produce reliable outputs when faced with worst case input scenarios. The term "robust" can have several definitions when used in a design optimisation process such as those described in literature [1][2]. For the purposes of model usability as a design tool, constraints were used to achieve robust solutions within a given design space when the "worst-case" uncertain scenario is applied. For this process, the worst-case scenario is given by the highest assumed material prices for all inputs, but with additional design requirements (e.g. efficiency, mass) that must be met. This is detailed in section 6.1.3 where hypothetical design constraints are applied.

Optimisation under uncertainty (OUU) can be considered as a type of non-linear programming under uncertainty [3][4]. In this case our uncertain input parameters are characterised by their statistical probability density functions. The optimisation seeks to find an optimal solution that performs well across the range of scenarios and not just one set of inputs.

Three methods have been chosen to portray the issues faced with cost uncertainty and to produce suitable designs that fulfil criteria. The three methods used are outlined below:

1. Optimisation based on individual material price increases
2. Robust optimisation with additional design constraints
3. Optimisation under uncertainty based on Monte Carlo sampling of all material prices

The aim is to produce several viable designs and an optimum design solution when faced with price uncertainties for each of the drive trains. This will provide a useful insight into the crucial design considerations which will allow a cost-effective result to be obtained despite uncertainties. The results will also present a range of COE outcomes for each drive train such that they can be ranked from the highest to the lowest in term of risk-based material price uncertainty.

This chapter concludes with one final price comparison that investigates the use of a hypothetical magnet material used throughout this thesis. This is characterised by a higher mean cost, but lower variation in cost. The aim of using such an alternative would be to reduce the price uncertainty associate with volatile elements such as neodymium by using materials with easier worldwide availability albeit at a higher initial cost per kg.

6.1 Optimisation based on individual material price increases

By varying the material prices in a sensitivity analysis for set designs as shown in Chapter 5, the effect on the ICC of the drive train was determined but there were no redesign options to compensate for the increased cost. By allowing the model to optimise the designs based on higher assumed prices, any short-comings of designs can be identified and alternative designs suggested.

The prices of each of the 5 different materials were increased individually based on their probability distributions shown in Chapter 5 so that they are equal to their mean plus 1 standard deviation. This choice, when assuming a normal distribution means that 84% of the time, the cost will be less than or equal to that value. These prices, as shown in Figure 6.1 were used as cost inputs into the optimisation model and the COE was calculated for one material price change at a time. By changing only one single material cost at a time, the results allow a useful comparison between the key cost influencers for the designs in order to assess the impact of the most critical design material cost increases. By changing the prices individually for each of the materials used in the optimisation process, a direct comparison can be made between the designs produced in Chapter 4 that are subjected to material price increases and the new designs produced based on optimising with the increased prices.
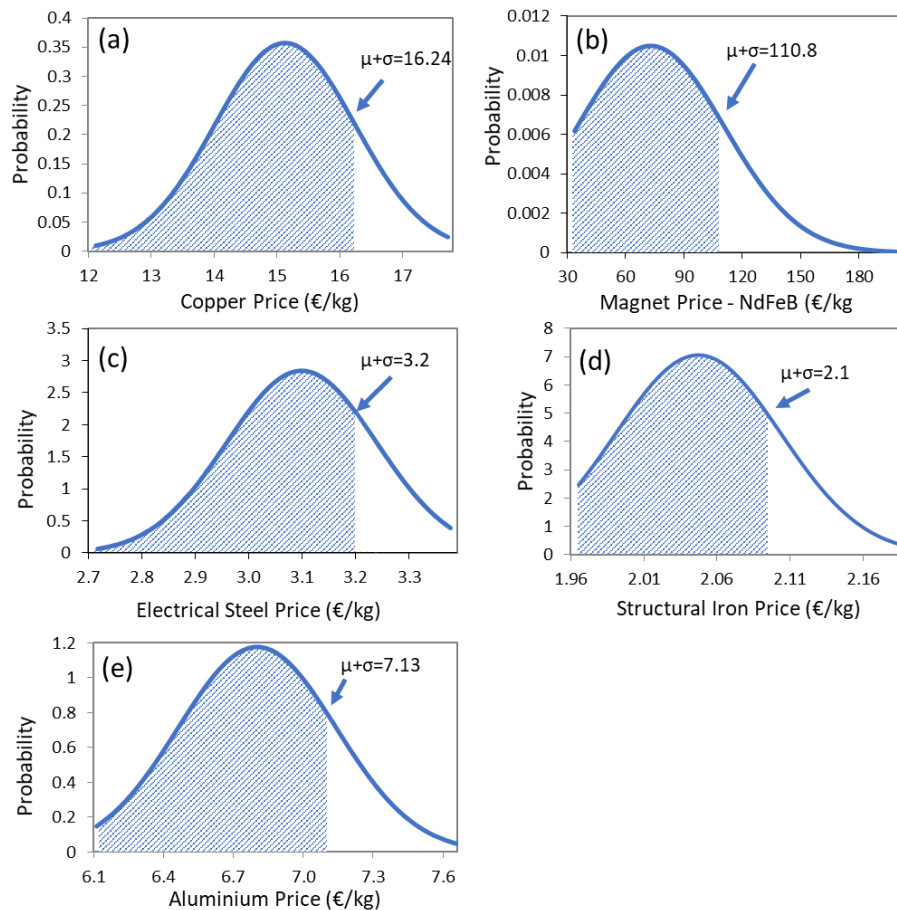
Figure 6.1 Mean plus 1 standard deviation for each material price. The shaded areas mean that for 84% of the time the price is less than or equal to mean plus one standard deviation value.

Figure 6.2 illustrates a flow chart of the process of optimising each drive train based on selecting one material price increase at a time. This method can use any time history and distribution for a particular distribution to observe the likely price fluctuations at a given time. The original prices that were chosen are based on present day (at the point of modelling) and are assumed to correspond to be the same for future values and used to re-optimise the designs.
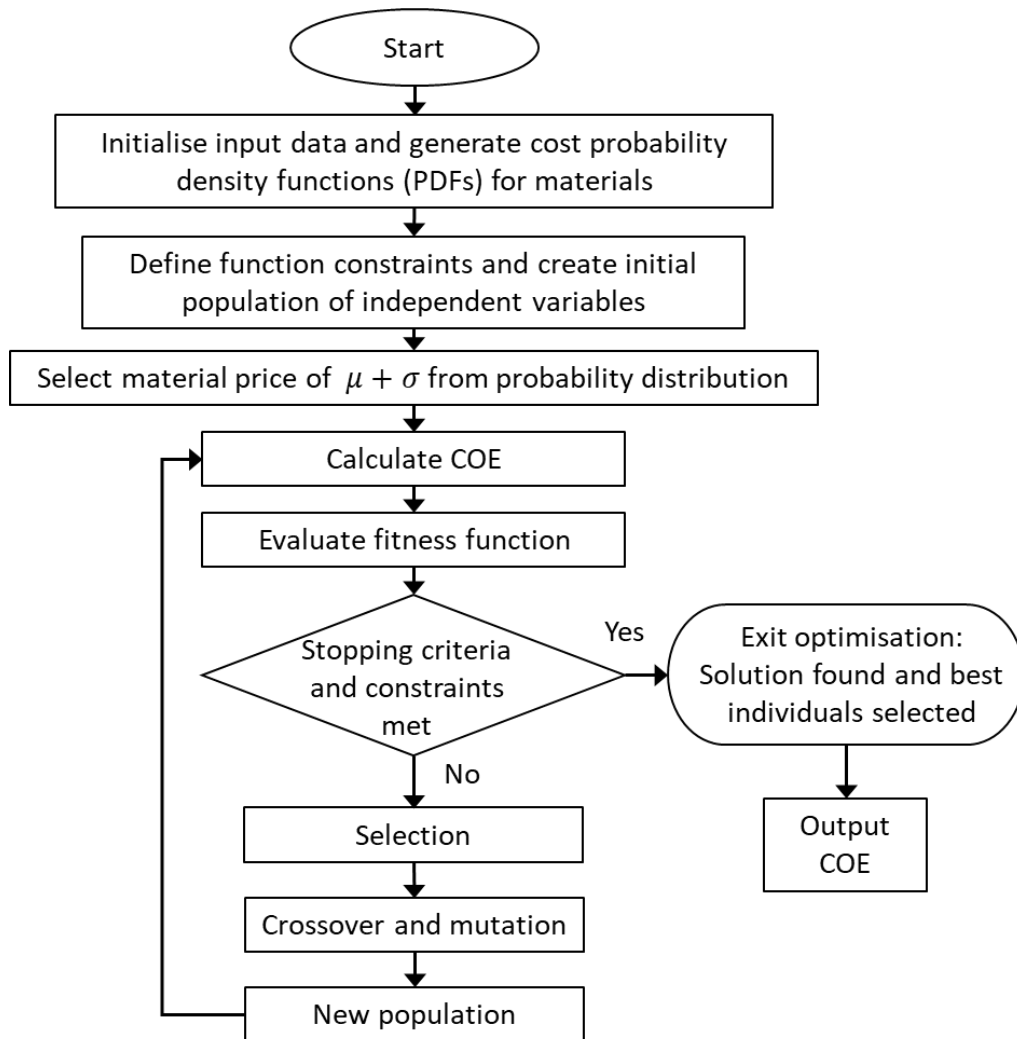
Figure 6.2 Flow chart of the process used for optimisation with individual price increases.

6.1.1 Drive train comparison for optimisation based on individual price increases

This section compares the optimised results for each drive train when the material prices are individually increased compared to the designs shown in Chapter 4 that have subjected to price increases. The motivation is to allow the design to be re-optimised based on higher assumed prices to identify COE and independent variable differences compared to simply applying a higher material cost to existing designs. Aluminium was not considered in this section as it has a negligible effect on the COE.

	% COE saving with copper price set to μ+σ compared against base design	% COE saving with magnet price set to μ+σ compared against base design	% COE saving with steel price set to μ+σ compared against base design
▦ PMG DD	2.11	0.37	2.12
▨ PMG 1G	1.08	0.40	0.83
▦ PMG 2G	0.60	0.32	0.62
■ PMG 3G	0.31	0.15	0.43

▦ PMG DD   ▨ PMG 1G   ▦ PMG 2G   ■ PMG 3G
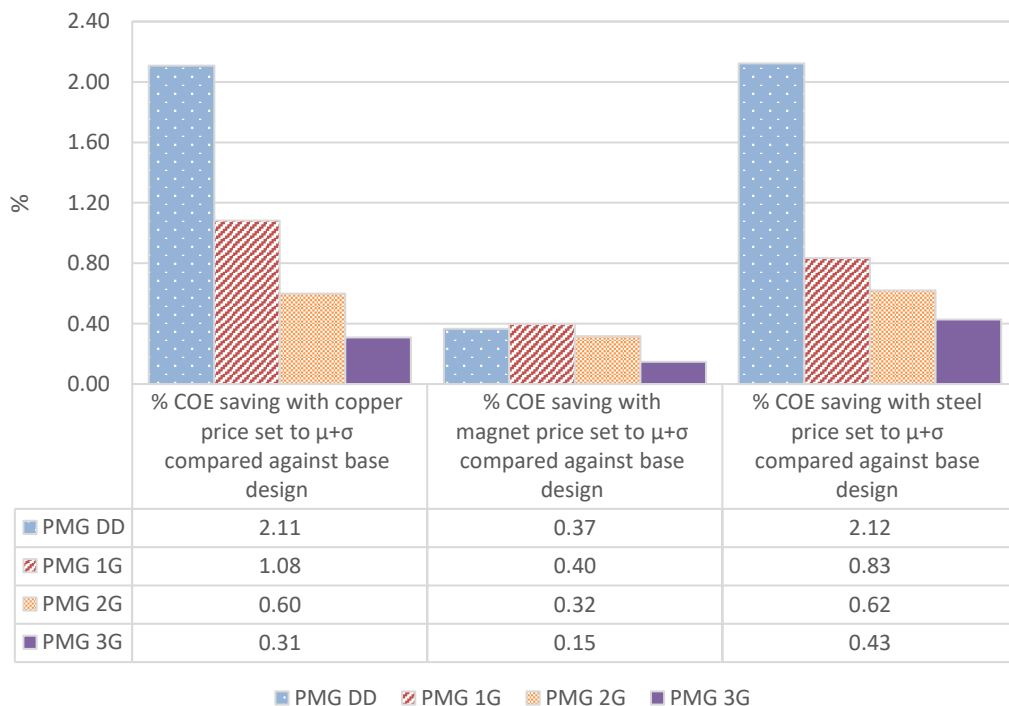
Figure 6.3 COE when optimising for increasing individual material prices compared with base case design from Chapter 4.

Figure 6.3 compares the evaluation of the designs from Chapter 4 with new material price points against newly optimised designs which assume the new material price points from the outset. A positive value of change means that the newly optimised drivetrains have a lower COE. This has been done for copper, magnet and steel costs and for the four different drive trains.

It can be seen in Figure 6.3 that the PMG DD can offer the highest saving in terms of COE when redesigned based on individually increased prices of copper and steel with over 2% lower COE compared with the original design from Chapter 4. The PMG 3G is least affected by individual price increases but does offer a saving nonetheless when redesigned. The radius and the stack length of the PMG DD are both reduced for all material price increase scenarios whilst the number of pole pairs increases (full details of the differences in variables are shown in the Appendix Tables A.1-A.3). Since there is no gearbox with the PMG DD, the options to alter the design to compensate for increased material prices are limited to the generator only, see Figure 6.4. There is a small saving of 0.37% optimising for the magnet price increase, as the optimisation process forces the design to have the lowest volume of magnets, but it also restricted by the magnetic circuit parameters.

	% Generator cost saving with copper price set to μ+σ compared against base design	% Generator cost saving with magnet price set to μ+σ compared against base design	% Generator cost saving with steel price set to μ+σ compared against base design
PMG DD	21.73	5.09	21.80
PMG 1G	28.64	17.46	32.10
PMG 2G	23.85	-0.92	17.10
PMG 3G	46.14	17.89	21.65
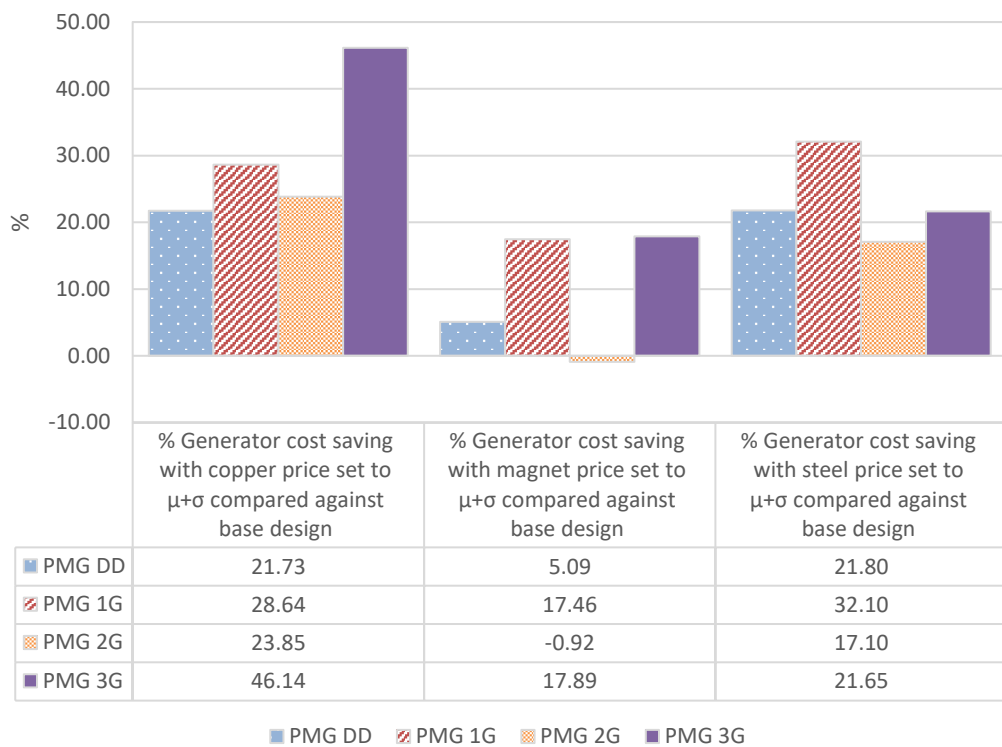
Figure 6.4 Generator cost when optimising for increasing individual material prices compared with base case design in Chapter 4.

The geared designs have diminishing achievable savings with each additional gear stage. This is due to the volume of materials in the generator decreasing (where

significant savings can be made) when each additional stage is added, and the designs become more dependent on the price of steel. The PMG 1G still has a large generator in comparison to the other geared drive trains and so has the most potential for redesign savings when magnet prices rise, as the gearbox arrangement can provide more operating possibilities and magnet volume reduction that the PMG DD. The PMG 2G and PMG 3G have much less magnet material and so magnet price increases would not have as significant effect on the COE as it does with the other 2 drive trains.

As previously discussed in Chapter 5, changes in the price of steel have an almost uniform effect on all the drive trains as both the generator and gearbox comprise of steel/iron. When adding a gear stage, the volume of steel that would have been in the generator is effectively replaced with the steel used in the gearbox. This effect can be seen in the comparing the savings in generator cost in Figure 6.4 to the more expensive cost of the gearbox in Figure 6.5 for the PMG 3G. Regardless of the material price increase, the PMG 3G will produce a more expensive gearbox compared to its base optimised design from Chapter 4.

	% Gearbox cost saving with copper price set to μ+σ compared against base design	% Gearbox cost saving with magnet price set to μ+σ compared against base design	% Gearbox cost saving with steel price set to μ+σ compared against base design
PMG DD	0.00	0.00	0.00
PMG 1G	0.35	0.62	-3.27
PMG 2G	4.52	18.31	13.24
PMG 3G	-12.30	-6.24	-7.90
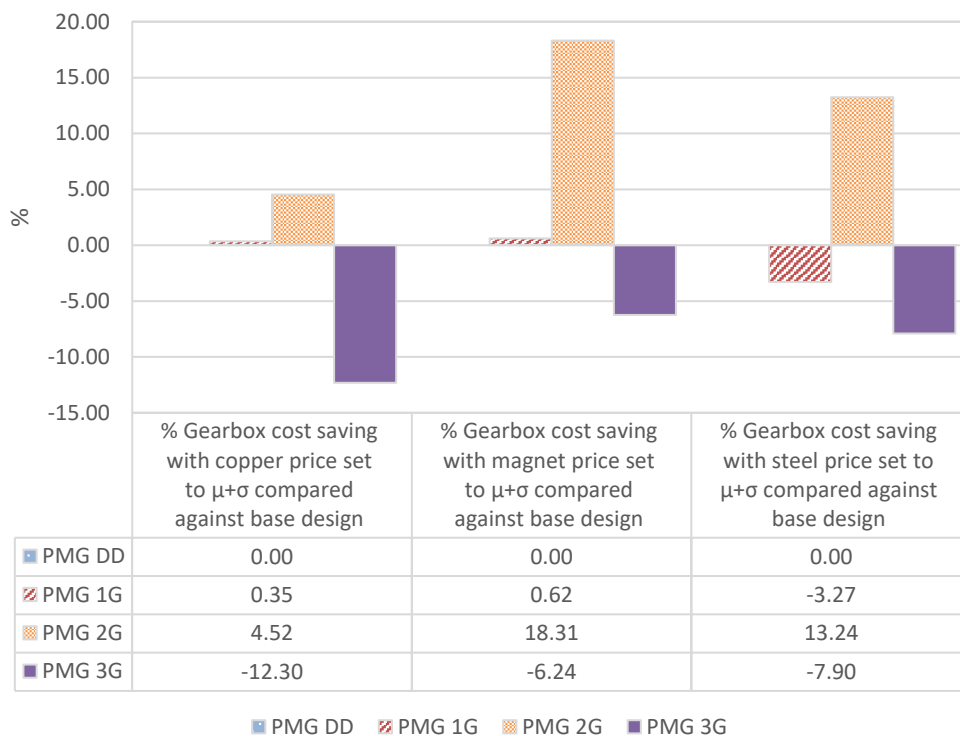
Figure 6.5 Gearbox cost when optimising for increasing individual material prices compared with base case design of Chapter 4.

6.1.2 Comparison of independent variable ranges based on individual price increases

Part of the motivation for allowing the model to create new designs with individual material price increases was to observe how it impacts the design variables output. The GA allows for multiple local minima to be identified and a variety of designs to be produced. These designs can have similar COE values but have completely different independent variable outputs. To observe the range of designs that are produced using the GA and how independent material price increases influence the designs, all the independent variable outputs were compared relative to each other by normalising the results and displaying side by side for a direct comparison. The cost inputs described in the previous section were used to produce 50 designs for each individual material price increase. The design output values were normalised to their average and the upper and lower values plotted together to observe the relative differences between each.

Depicted in Figure 6.6, are the normalised values for each independent variable based on their average across the 50 iterations for the PMG DD. These are all compared in groups of 4 corresponding to the material that was increased optimisation of the designs. So, for the left-hand sections of each variable, copper has been the material subjected to an increase in price during the optimisation. The next bar in the chart shows the results with optimising for an increase in magnet prices, followed by iron and aluminium at the right-hand side. The average of each lies along the value of 1, and the bars above and below represent 1 standard deviation from the mean in both directions. The maximum and minimum values are also shown as vertical lines. If we look at the values when optimising for the copper price fluctuations, the magnet height varies significantly compared with when optimising for the NdFeB magnet design point where it is very much restricted. This highlights how the model aims to maximum the efficiency of the generator depending on which material price impact is most dominant. It can also be seen that the ratio of slot width to pitch is not particularly affected by the optimisation based on distributions and so it is not a crucial design specification. Even though the cost of aluminium had a negligible influence on the

designs in terms of its cost increase, it was still subject to the GA output variation and so was included for the purposed of comparison and completeness.

Depicted in Figure 6.7, are the normalised values for each independent variable based on their average for the PMG 1G. Comparing directly to the direct drive wind turbine variables from Figure 6.6, there are significantly more variations across all 8 of the generator variables. This is due to the addition of 5 gearbox variables that allow more generator designs to be produced. The magnet height and number of pole pairs have a broad range of outputs regardless of which material price design point is set for the optimisation. This implies that despite using a large volume of magnets in the design (albeit lower that the direct drive wind turbine), the use of a gear stage can provide more options for designers in terms of magnet size and is a less restrictive design. The ratio of slot width to pitch also changes by about ±16 % and the height of the slot varies by about ±24 %.

Depicted in Figure 6.8, are the normalised values for each independent variable based on their average for the PMG 2G. The radius, which has been very restricted for the direct drive can be varied for the PMG 2G by ±20 % from its mean with a standard deviation in the region of ±10 %. Similarly, the gearbox independent variables can change by about ±20 % in contrast to the single stage geared design that was restricted to a 10% variation above and below its mean.

Depicted in Figure 6.9 are the normalised values for each independent variable based on their average for the PMG 3G. The magnet height can vary the most for this drive train compared with the other topologies. The 10 gearbox variables vary, on average, about 10 % above and below their mean values. The number of pole pairs has much larger values of standard deviation compared to the equivalent values from the single-stage gearbox design. This design has the most variation options due to the large range of gear ratios that can be produced and corresponding varying generator designs.
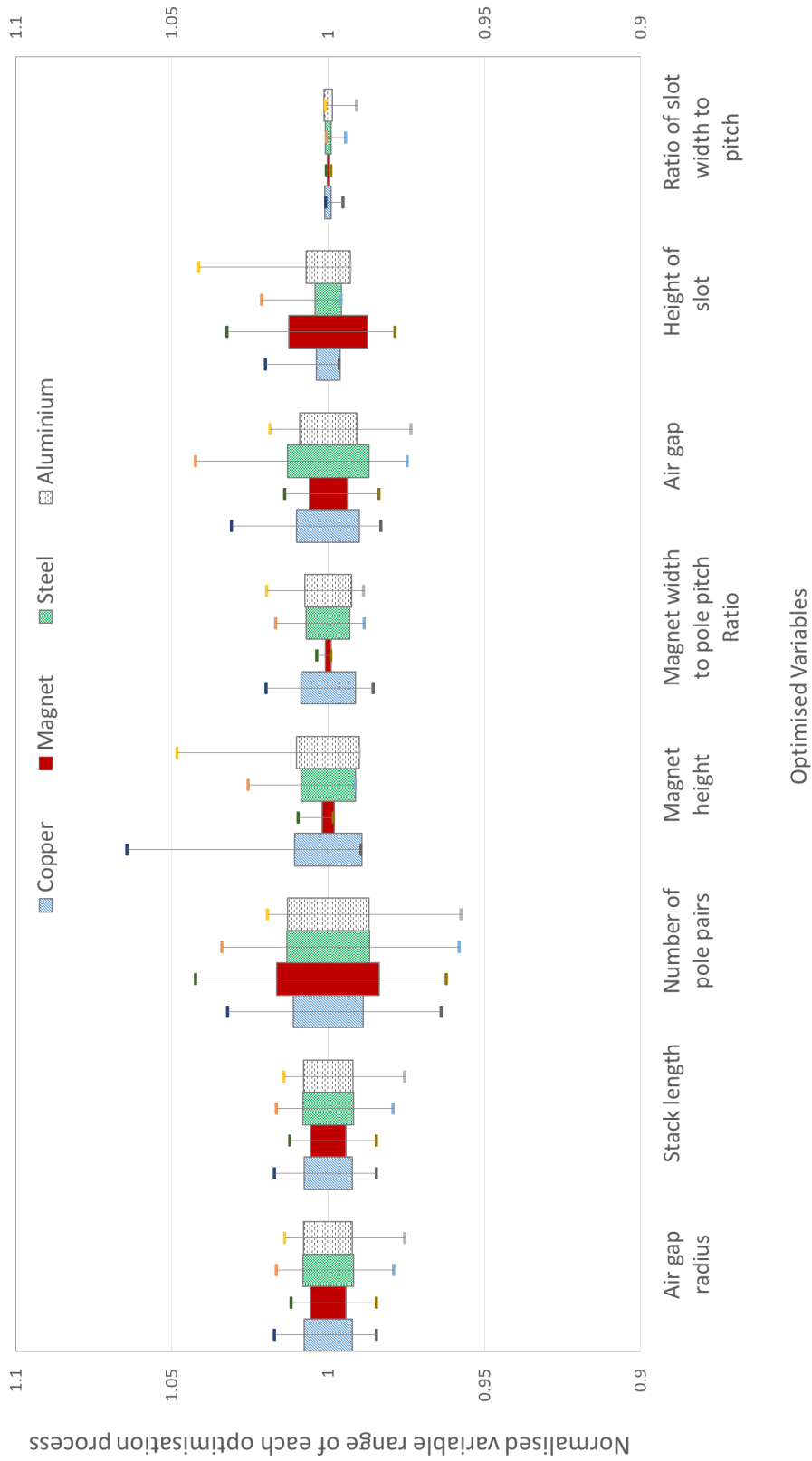
Figure 6.6 Comparison of each of the varied material prices and their effect on the independent variables after optimisation for PMG DD.
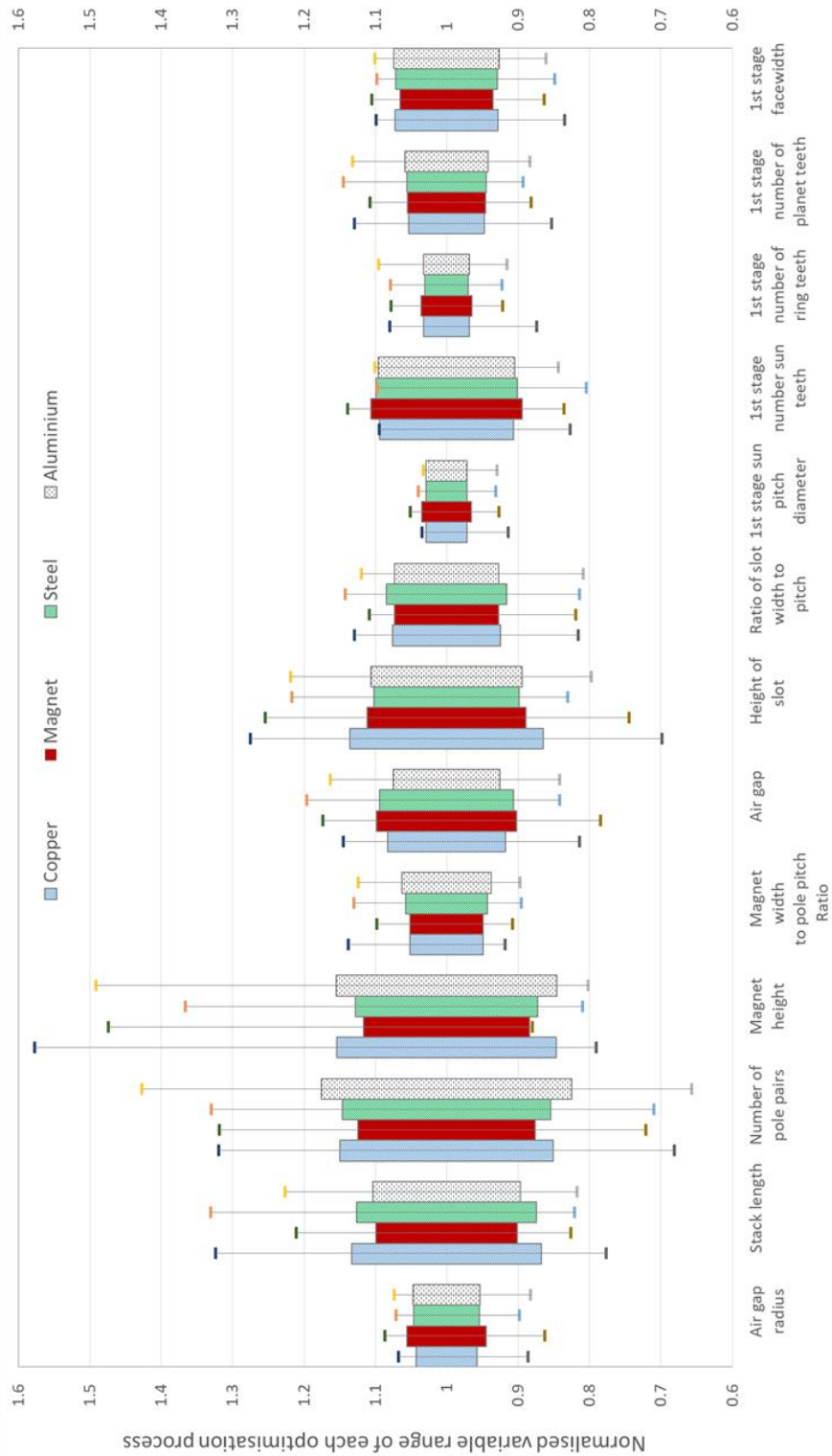
Figure 6.7 Comparison of each of the varied material prices and their effect on the independent variables after optimisation for PMG 1G.
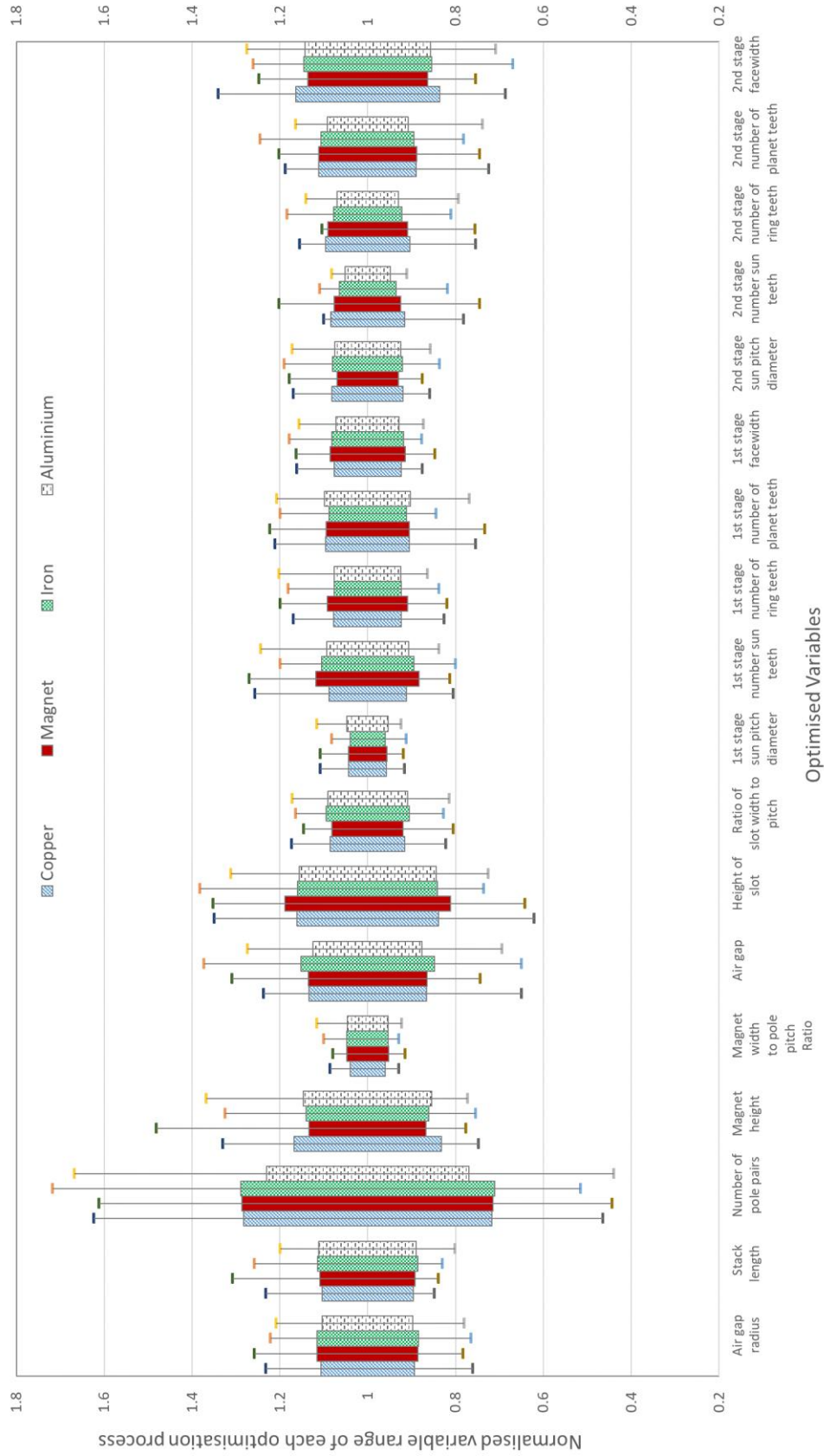
Figure 6.8 Comparison of each of the varied material prices and their effect on the independent variables after optimisation for PMG 2G.
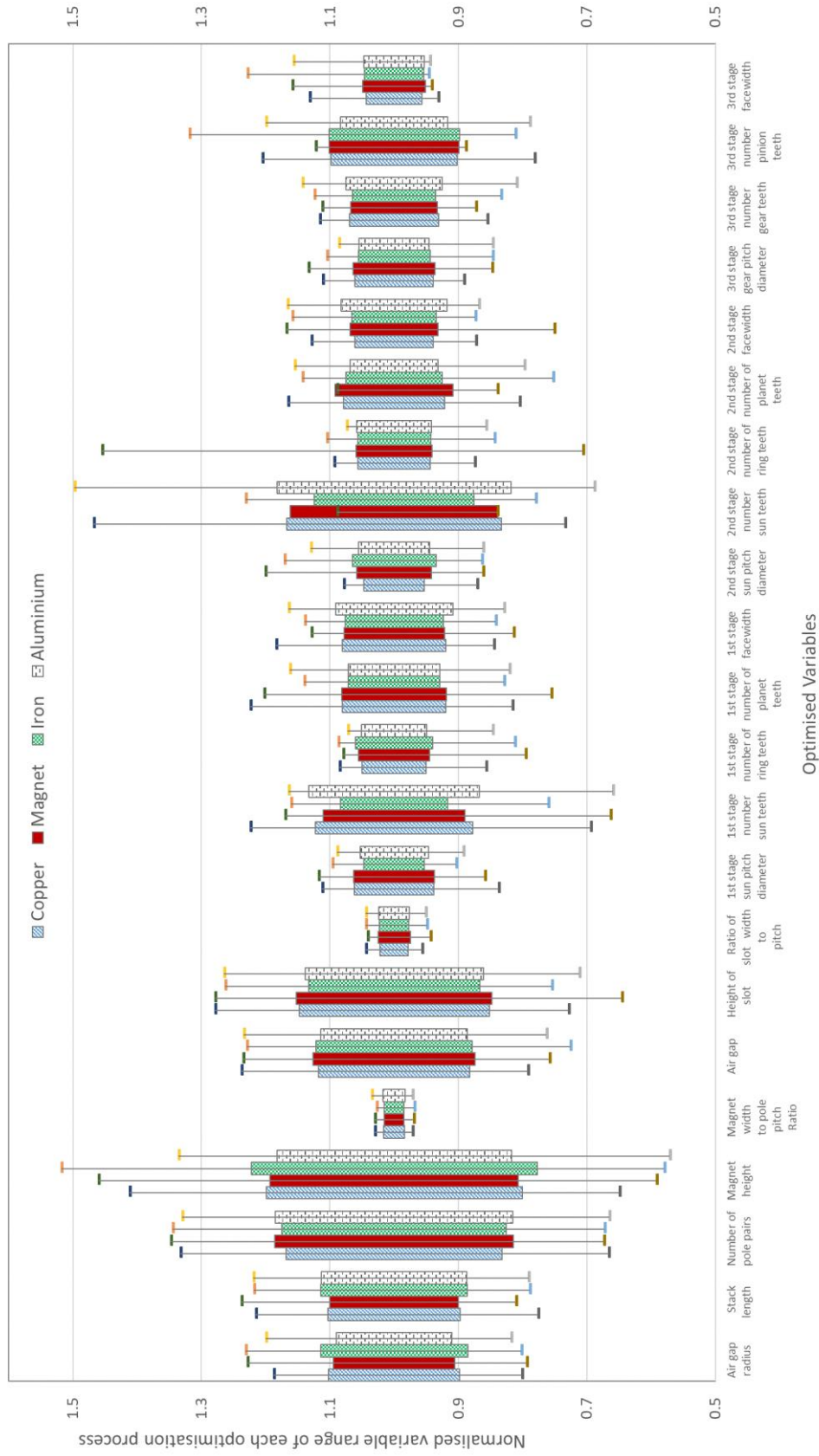
Figure 6.9 Comparison of each of the varied material prices and their effect on the independent variables after optimisation for PMG 3G.

6.1.3 Combined material cost increase comparison

After observing the effects of each individual price variation in section 6.1, the next step was to set all the prices to their mean plus 1 standard deviation values to allow the model to amend the original design from Chapter 4 to compensate for higher prices.

A complete comparison between the Chapter 4 designs and the new optimised designs when higher material costs are assumed for all materials (set at their mean values plus 1 standard deviation) is shown in the Appendix Table A.4. All designs offered lower COE values when re-optimised for higher material prices compared to the designs of Chapter 4.

6.1.4 Summary of optimisation based on material price increases

This study shows the effects of a drive train designer adopting a conservative view on future material prices, where the copper, magnet and steel prices are assumed to be at a price point of the historic mean plus standard deviation. It offers an insight into which design parameters ought to be varied to compensate for changes in those price points. Although the newly designed drivetrains are better than the Chapter 4 designs (in the scenario where material prices have increased), unsurprisingly they have a higher COE compared to the designs in Chapter 4 when the mean prices are used.

6.2 Optimisation for robust solutions with additional design constraints

This section looks at the effects of additional design constraints whilst applying worst case scenario conditions to identify robust solutions. Robust optimisation is a useful process in many fields from engineering to finance where worst case scenarios can be explored for probabilistic inputs and can have varieties of "hard" and "soft" conditions [1]. An example of this type of design method in a more extreme case, is designing a building or bridge to withstand extreme storm conditions. The robust designs would not collapse during such a storm, but these will have incurred more expensive materials and more complex construction procedures. A similar principle is used here for

hypothetical cases of design conditions on a more basic level. An example of the concept of robust optimisation is shown in Figure 6.10 where an initial design is altered based on the probabilities of its design variables and a constraint boundary. For this study, this process is replicated for material price probability and additional design requirements, such as maximum drive train mass, to represent the constraint boundary.
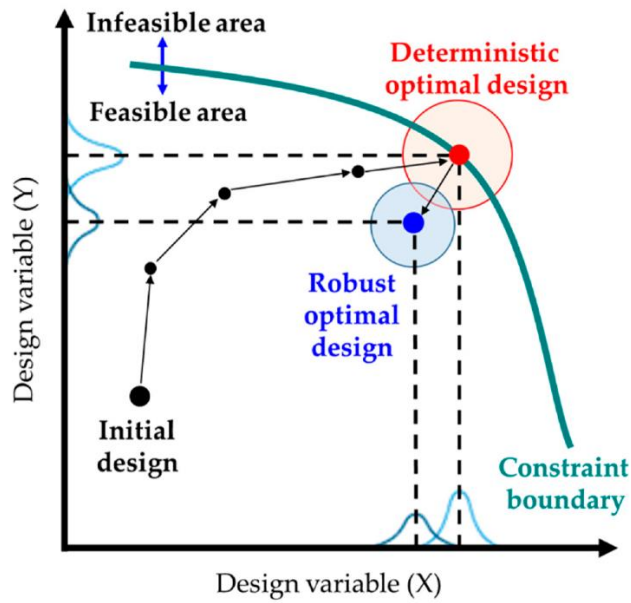
Figure 6.10 Illustration of robust optimisation and feasible design space. Taken from [5].

There are 4 scenarios considered in this section and each portrays a particular design limitation that could be imposed by the manufacturers or future owners. In addition, the worst-case scenario is more severe, as higher material costs are set at their mean plus 2 standard deviations to represent a situation where all costs are at the higher end of their probabilistic values. (Assuming that the material prices follow a normal distribution then the cost will be at these values or less for almost 98% of the time). The optimisation and selection process is shown in the following figure.
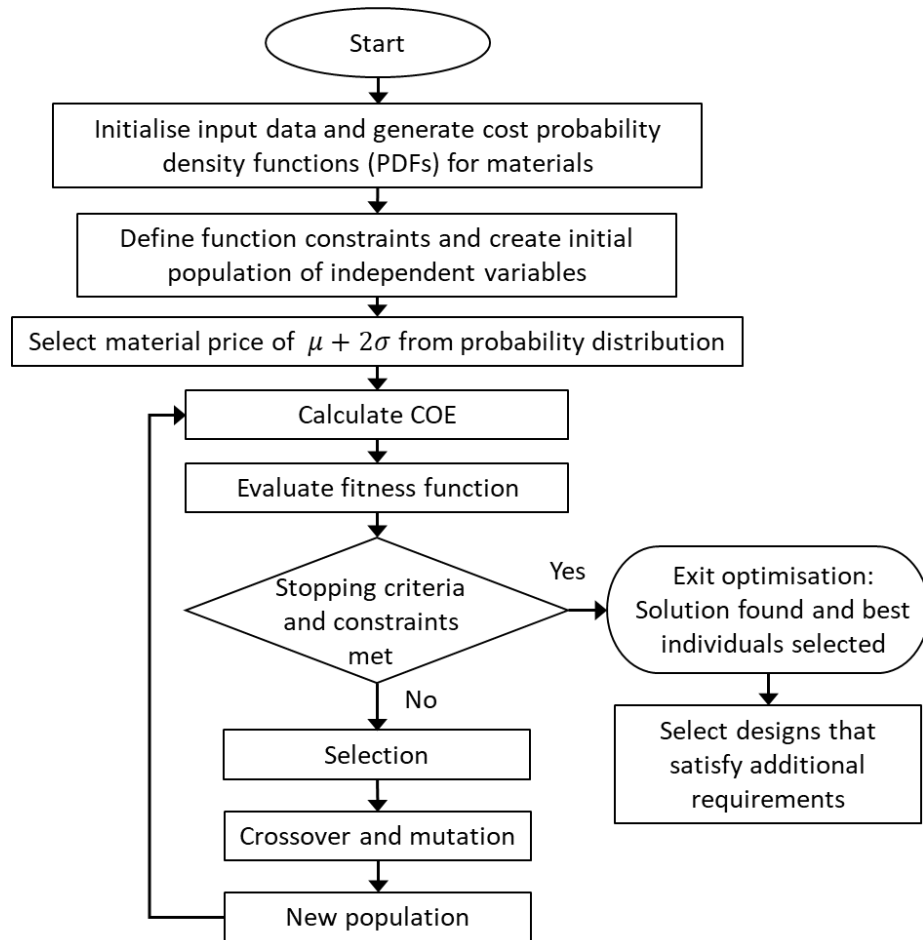
Figure 6.11 Flow chart of the process used for optimisation with additional requirements based on robust optimisation.

The new material prices are set as follows:

- Copper price, $\mu+2\sigma =$ €17.48/kg
- Magnet price, $\mu+2\sigma =$ €161.54/kg
- Electrical steel price, $\mu+2\sigma =$ €3.4/kg
- Structural steel price, $\mu+2\sigma =$ €2.2/kg
- Aluminium price, $\mu+2\sigma =$ €7.26/kg

These new values for material costs were used in the following cases:

1. The first scenario considered is for magnet mass to be limited to a maximum/fixed value. This represents a manufacturer's decision to limit the

volume of magnets in a generator because of concerns about the future availability of magnets.

2. The second scenario considered is a fixed maximum initial capital cost (ICC). This would represent a future owner's budget and can be a useful way of visualising how designs would change with such restrictions.

3. The third scenario is for a minimum system efficiency of the drive train to be met. Efficiency is often a selling point, and this is a useful way of attracting potential buyers.

4. The fourth scenario considered is for the generator and drive train mass to be limited to a maximum mass. This would represent craning limits and top head mass limits that restrict the designs.

The results from the optimisation process can be reviewed and ranked based on providing the lowest COE whilst satisfying additional design requirements to produce robust solutions when worst-case-scenarios are applied.

6.2.1 Magnet mass limitation scenario

Some of the considerations when building a permanent magnet generator are the availability of magnets, their cost and any overall mass limitations. The following figures compare all 4 drive train designs when considering limiting the mass of magnets and its effect on the COE. An arbitrary constraint on the magnet mass was applied to each drive train and is depicted by the solid vertical line in the following figures. This allows the designs that meet the additional requirements to be reviewed for the effect of the COE.
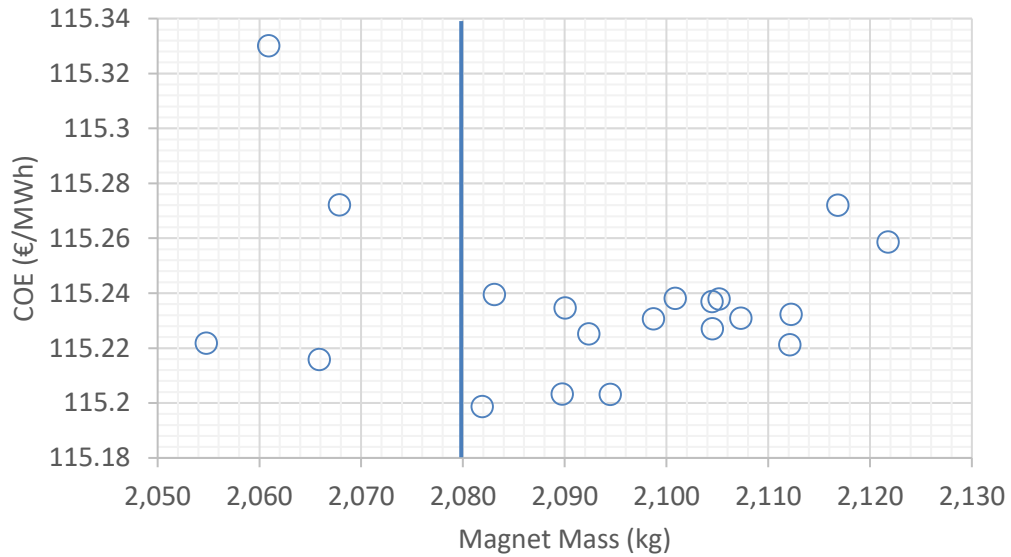
Figure 6.12 Magnet mass limitation for robust optimisation for PMG DD and its effect on COE with basic selection constraint shown as solid vertical line.

Figure 6.12 shows the variation of magnet mass and the effect on COE for the direct drive design. The cost of energy value does not change much, only ranging from around 115.2 to around 115.33 €/MWh. However, there is potential to save around 70 kg of magnet mass.
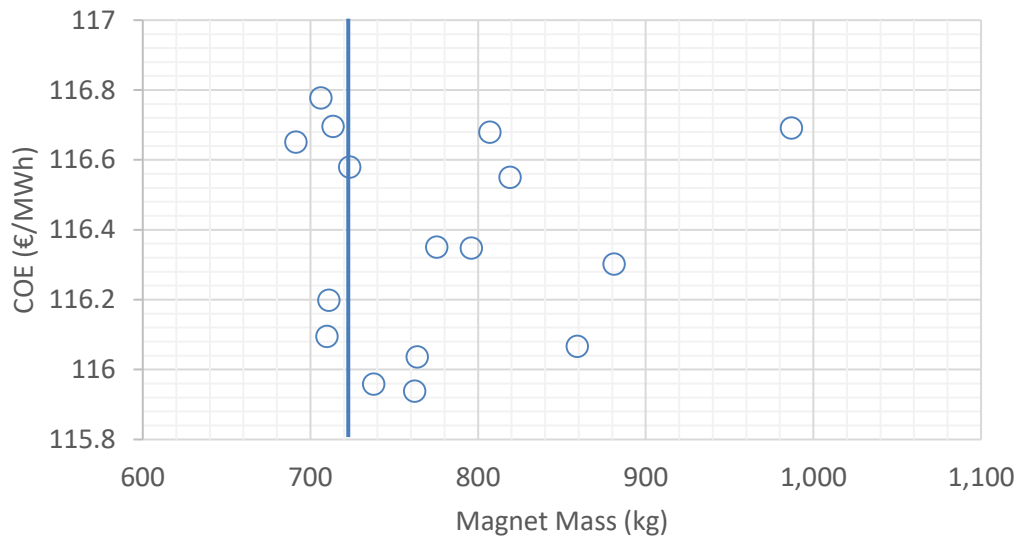
Figure 6.13 Magnet mass limitation for robust optimisation for PMG 1G and its effect on COE with basic selection constraint shown as solid vertical line.

The effect of magnet mass limitation as part of the robust optimisation process for a PMG with a single stage gearbox is shown in Figure 6.13. It can be observed that there is a range of magnet masses that provide the lowest COE. These values fall within 700 kg and 900 kg where COE is as low as 115.94 €/MWh. Masses above and below this range have larger COE values with the lowest mass of 690 kg having a COE of 116.65 €/MWh. Therefore, it can be argued that trying to limit magnet mass could cost an additional 0.7 €/MWh for the overall project. Likewise, using a high volume of magnets to increase the flux density in the airgap becomes too expensive to justify.
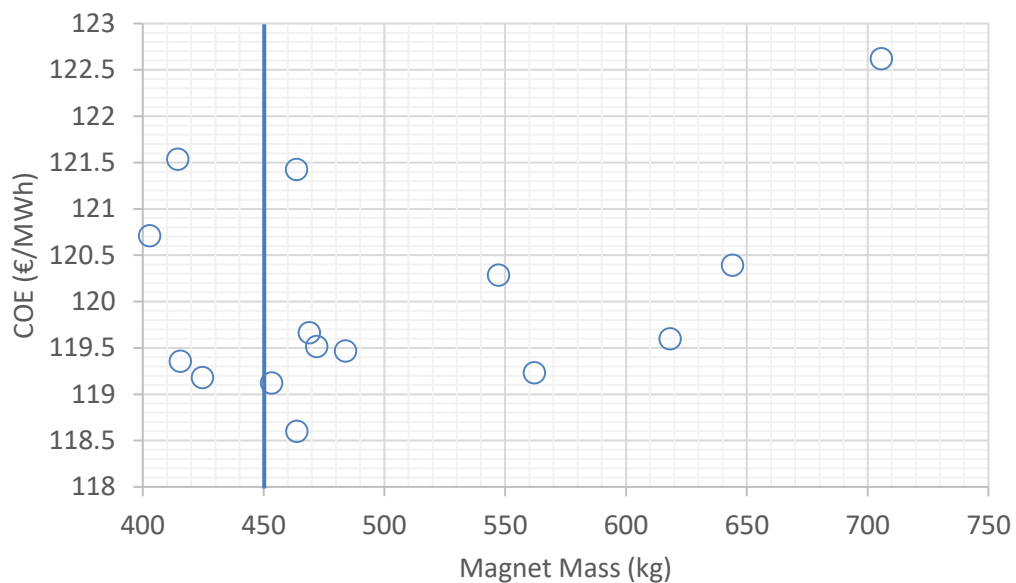
Figure 6.14 Magnet mass limitation for robust optimisation for PMG 2G and its effect on COE with basic selection constraint shown as solid vertical line.

The PMG with 2-stage gearbox was also optimised based on robustness for magnet mass and the results are shown in Figure 6.14. The cost of energy variation in this design spans from 118.5 to 122.5 €/MWh for a magnet mass range between 400 kg to 700 kg. The main reason for such a broad range of solutions lies within the implementation of the genetic algorithm which finds several local minima over the input range. To find a global minimum, more constraints on the input range would have to be applied along with some additional algorithm conditions, but this was not in the scope of this work as this study focuses primarily on comparison and providing

enough generations of results can allow the optimum to be identified. As with the single stage design, there appears to be an optimum range of magnet mass for the 2-stage design which lies between 450 and 500 kg. This produces a COE of around 119 €/MWh compared to an average of around 121 €/MWh when allowing the magnet mass to be higher or lower. Trying to minimise the volume of magnets would not produce an optimum design, and if a manufacturer was obligated to use a particularly low magnet mass, it could cost them an additional 2.0 €/MWh in terms of the overall project COE.
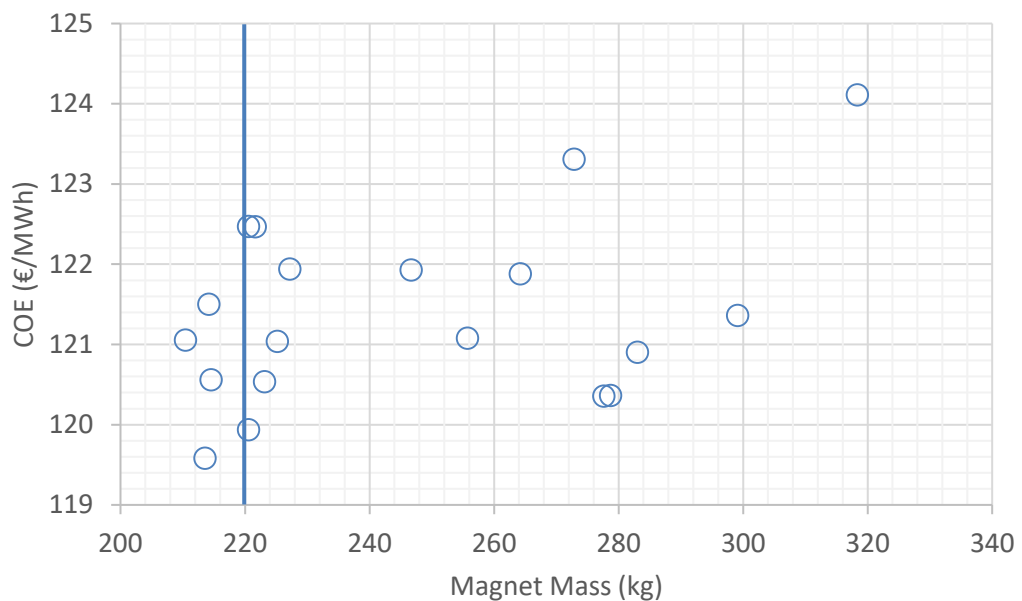
Figure 6.15 Magnet mass limitation for robust solutions with optimisation for PMG 3G and its effect on COE with basic selection constraint shown as solid vertical line.

The PMG with 3-stage gearbox was also optimised to limit the magnet mass and the results in terms of COE are shown in Figure 6.15. The general trend observed with reducing the magnet mass is that the COE can be reduced. There is a range of masses from about 210 to 280 kg there are similar values of COE which can be considered suitable designs regardless of the magnet mass. This is because variations of gearbox designs can be produced to maximise the output of a smaller generator. The lowest COE shown in Figure 6.15 was 119.58 €/MWh at a magnet mass of around 214 kg. The air gap in this design was optimised to 1 mm which is likely to be as low as

possible in terms of feasibility. Additional considerations would have to be taken into account when manufacturing with such a tight air gap tolerance. This reiterates that these design outputs are suggestive, and that expert opinion may rule out some options.

6.2.2 Fixed maximum ICC scenario

Fixing the maximum initial capital cost provides an insight into possible manufacture/developer incentives. Depending on budget and planning, upfront costs could take president over long term return on investment in some cases. The following results aim to portray the benefits/limitations of keeping the ICC low for each design.

Figure 6.16 ICC limitation for optimised robust solutions for PMG DD and its effect on COE with basic selection constraint shown as solid vertical line.

Limiting the ICC of the project for the PMG DD produces COE results as shown in Figure 6.16. Although there is very limited scope for ICC reduction for the DD design, it is apparent that reducing or increasing it beyond a point will only affect the COE marginally. It does not have a significant impact, increasing only by 0.04 €/MWh and so highlights the current issue direct dive designs being very expensive without room for cost reduction in terms of its efficiency and potential reliability.

The effect of restricting the ICC for the PMG with a single-stage gearbox on the COE is shown in Figure 6.17.
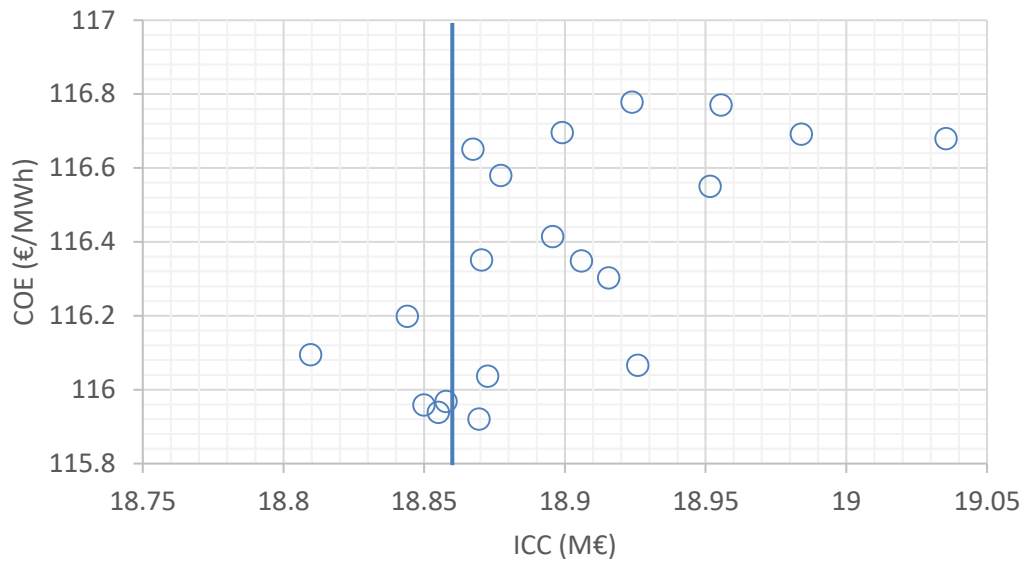
Figure 6.17 ICC limitation for robust optimisation for PMG 1G and its effect on COE with basic selection constraint shown as solid vertical line.

In contrast to the DD design, there is significant benefit to limiting the ICC of the PMG 1G. Reducing the ICC by €200,000, provides a COE saving of around 1 €/MWh. This suggests that with the addition of a gearbox and greater design variable flexibility, cheaper designs are possible and beneficial to the COE. There are several solutions that produce a COE around 116 €/MWh each with slightly different ICC values. This result shows that a PMG 1G can offer a number of benefits to manufacturers and developers as reduced upfront costs also provide benefits in terms of long-term cost. Due to the variety of options, it is a very effective drive train to consider for installation for offshore wind farms.

The COE when varying the ICC for the PMG 2G is shown in Figure 6.18. It offers a similar relationship to that observed in the PMG 1G where COE reduces with reducing ICC. It offers a COE minimum around €18.73M. This suggests that having a cheaper drive train outweighs the benefits of having an expensive drive train with higher efficiency as there is a certain point where those benefits are no longer cost effective. Careful consideration of the generator and gearbox as a combination that

needs to be optimised for uncertain costs could provide significant long-term cost reduction. The planning stages in terms of the drive train dimensions are crucial.
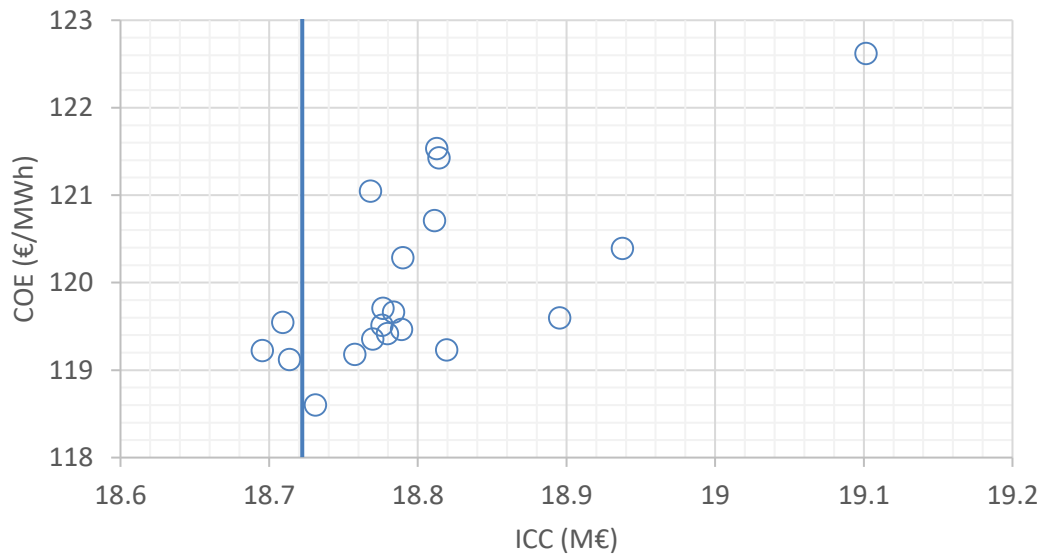
Figure 6.18 ICC limitation for robust optimisation for PMG 2G and its effect on COE with basic selection constraint shown as solid vertical line.

The ICC effect on the COE for the PMG 3G is shown in Figure 6.19, where the linear trend observed in the PMG 1G and PMG 2G cases is even more significant.
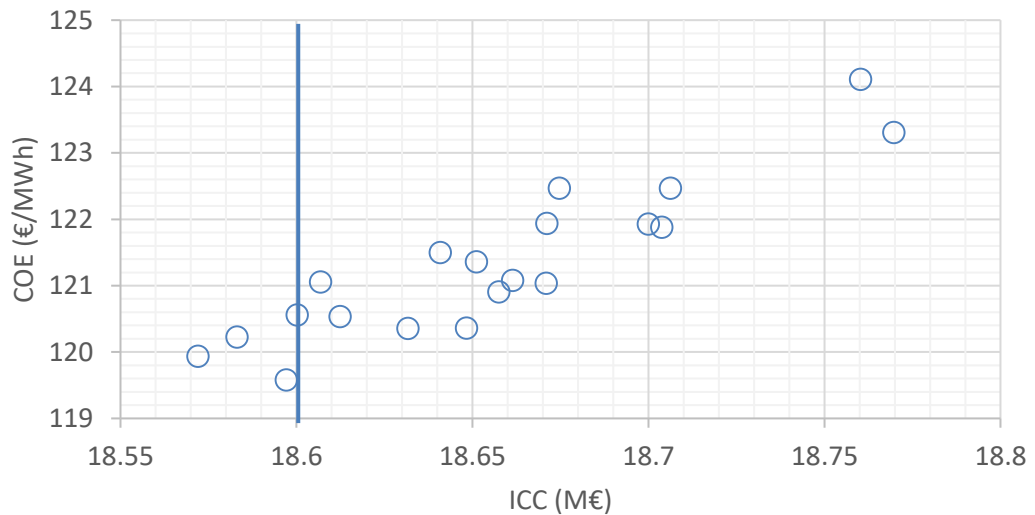
Figure 6.19 ICC limitation for robust optimisation for PMG 3G and its effect on COE with basic selection constraint shown as solid vertical line.

The design with the lowest value of COE has a gear ratio of 1:84.4 and the design with the highest COE in this sample has a gear ratio of 1:95.1. In this case, the reduction in cost is achieved by creating a lower speed generator and gearbox system. This also influences the annual operations and maintenance cost assumptions which are reduced by over 20% due to the smaller and more restricted gearbox and lower operating speed. It can be suggested that higher speed designs do not necessarily yield the best COE and that PMG drive trains with a 3-stage gearbox still have the potential to provide suitable turbines for offshore use when optimised appropriately.

6.2.3 Minimum system efficiency scenario

In certain cases, a minimum energy yield is a requirement for an offshore wind farm development. Optimisation based on uncertainty with robustness can be applied to the model to create a minimum total system efficiency. The following figures show the impact of applying a minimum total system efficiency constraint to the designs.
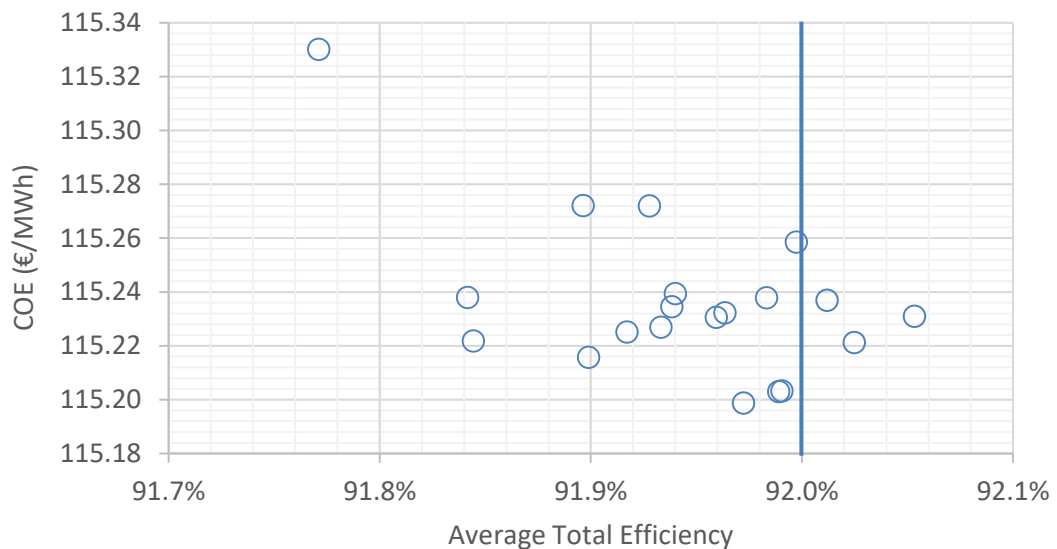
Figure 6.20 System efficiency for PMG DD and its effect on COE with basic selection constraint shown as solid vertical line.

From Figure 6.20, the COE generally decreases with increased system efficiency, but it is noted that at 91.97% there appears to be a minimum COE before increasing as the efficient tends towards 92.06%. The differences can be considered as very small and

that there is no significant benefit to design for as high an efficiency as possible when all other design considerations are taken into account.

Looking at the efficiency for a PMG 1G for various optimisation outcomes, it can be seen from Figure 6.21 that the COE has a minimum value of around 116.6 €/MWh at 93.57 % efficiency. To increase the efficiency to 93.93 %, it would cost an additional 0.75 €/MWh.
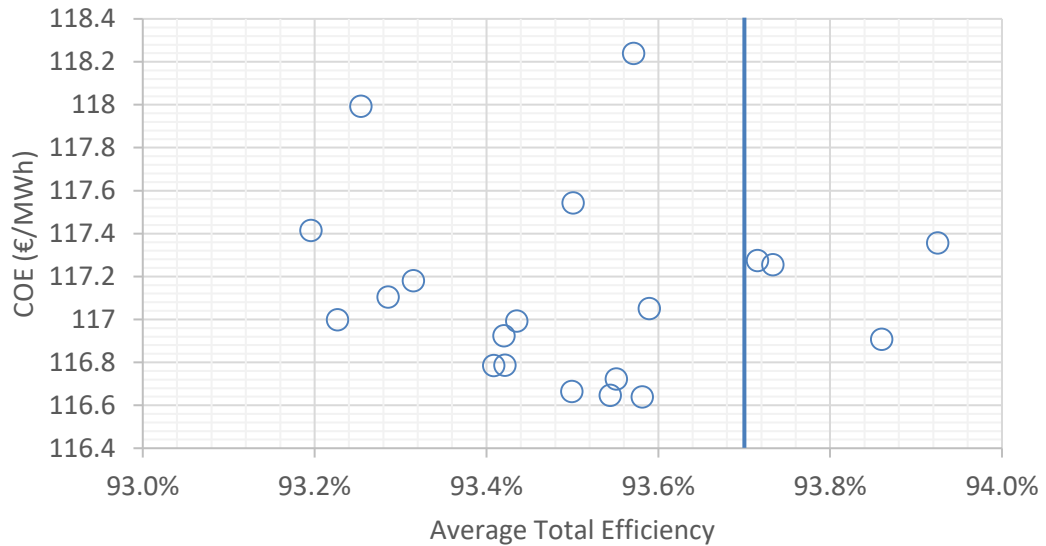
Figure 6.21 System efficiency for PMG 1G and its effect on COE with basic selection constraint shown as solid vertical line.

The main gain in efficiency comes from tweaking the generator parameters as it is still a large dimension generator and so influences the overall performance of the wind turbine significantly. The generator can be more efficient to meet requirements, but it will also increase the COE and so if developers are looking to pay more for higher efficiency levels, then the PMG 1G is a suitable option.

Looking at the PMG 2G in terms of robust optimisation based on maximum system efficiency, the COE results can be seen in Figure 6.22. There is a turning point in average efficiency at around 93.1% where the COE increases above and below this value. Even though the range of possible efficiencies is quite low, the best solutions in terms of COE are unaffected by the system efficiency.
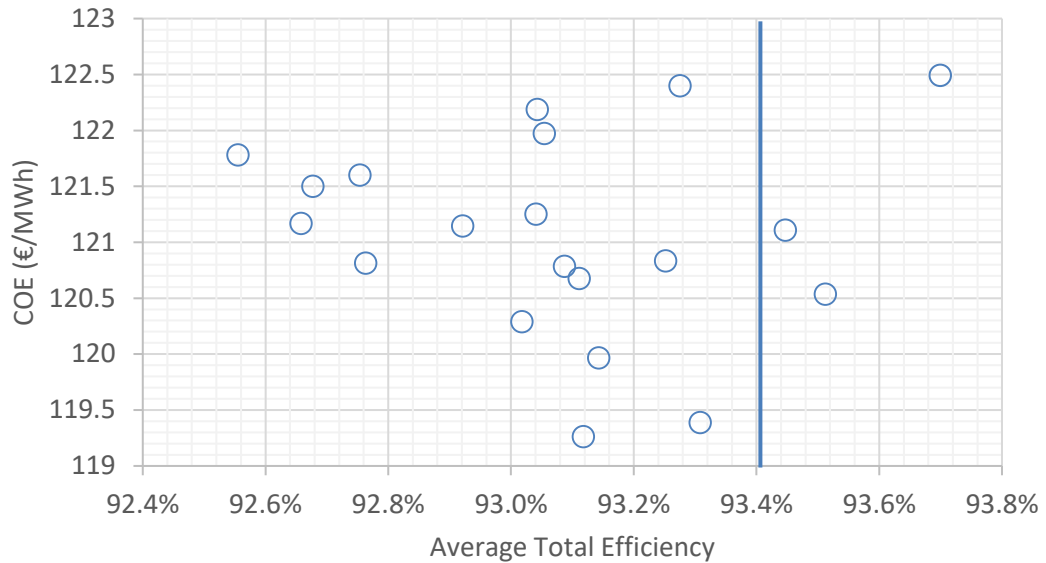
Figure 6.22 System efficiency for PMG 2G and its effect on COE with basic selection constraint shown as solid vertical line.

The PMG 3G COE when optimising for robustness with efficiency is shown in Figure 6.23. A minimum COE of 121.9 €/MWh is obtained at a system efficiency around 92.2 %. The highest system efficiency of 92.55 % produces a COE of 122.98 €/MWh, and so it cost 1.1 €/MWh to increase efficiency by 0.35 %. As a trade-off it appears to be an expensive method to increase efficiency.

The gearbox offers the largest scope for improving efficiency. This is because of the large variations of gearbox specifications that can be used in the design. There is incentive to have a high gearbox and generator efficiency for the drive train, but understanding when the cost benefit is limited will help developers and manufacturers during the design process.
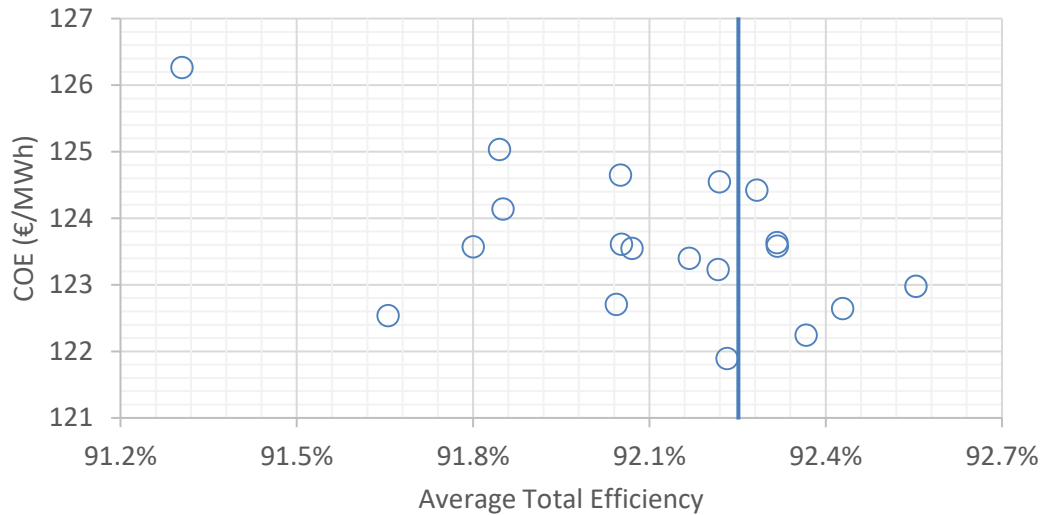
Figure 6.23 System efficiency for PMG 3G and its effect on COE with basic selection constraint shown as solid vertical line.

6.2.4 Maximum drive train mass scenario

Depending on the transport and lifting capabilities of the equipment used to install and service wind turbines as well as top head mass considerations, there may specific restrictions to the drive train mass. By applying a maximum drive train mass constraint to the optimisation under uncertainty process, robust solutions can be produced.

Figure 6.24 presents the COE variations in drive train mass of the PMG DD. Slightly lower COE values are obtained for higher drivetrain masses. This is directly linked to the use of permanent magnets and ties in with efficiency. The COE variations are still quite negligible as the direct drive design is a very restrictive design in term of its parameters and costs. Therefore, up to 2,000 kg of mass can be saved without significant impact on the COE and so if it comes to making a decision about maximum weight, the PMG DD offers a promising solution with minimal cost impact.
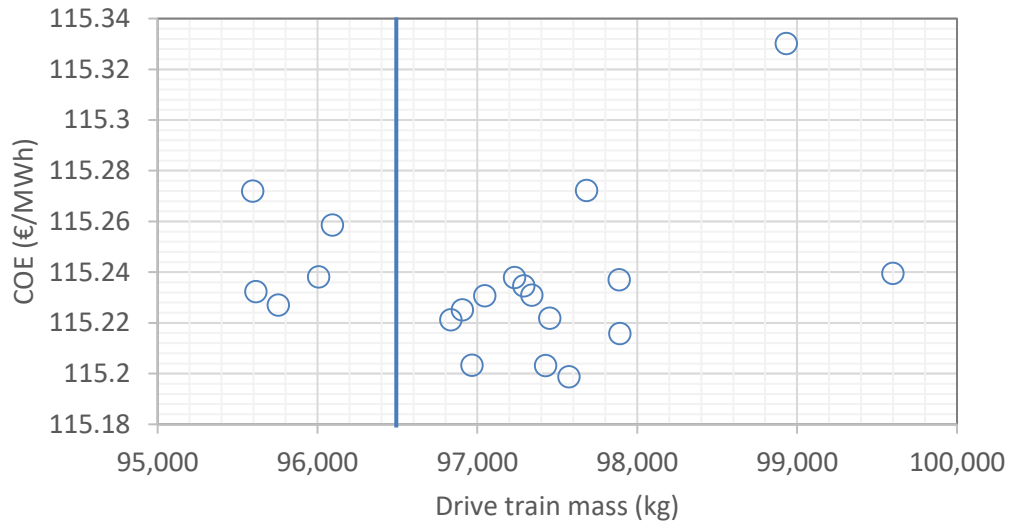
Figure 6.24 Drive train mass limitation for PMG DD and its effect on COE with basic selection constraint shown as solid vertical line.
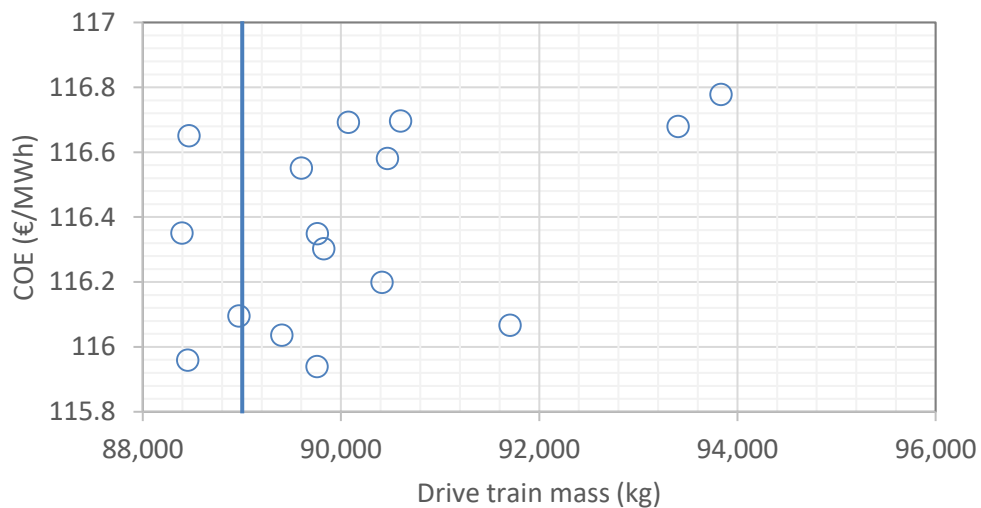
Figure 6.25 Drive train mass limitation for PMG 1G and its effect on COE with basic selection constraint shown as solid vertical line.

The effects on the COE when limiting the drive train mass for the PMG 1G are shown in Figure 6.25. In contrast to the direct drive design, the single stage gearbox design has its lowest COE when the drive train mass is lowest. This is very useful from a design point of view as not only can the material volume be minimised but the overall

cost will be reduced without compromising performance. A COE of 115.96 €/MWh can be achieved at a drive train mass of 88,400 kg.
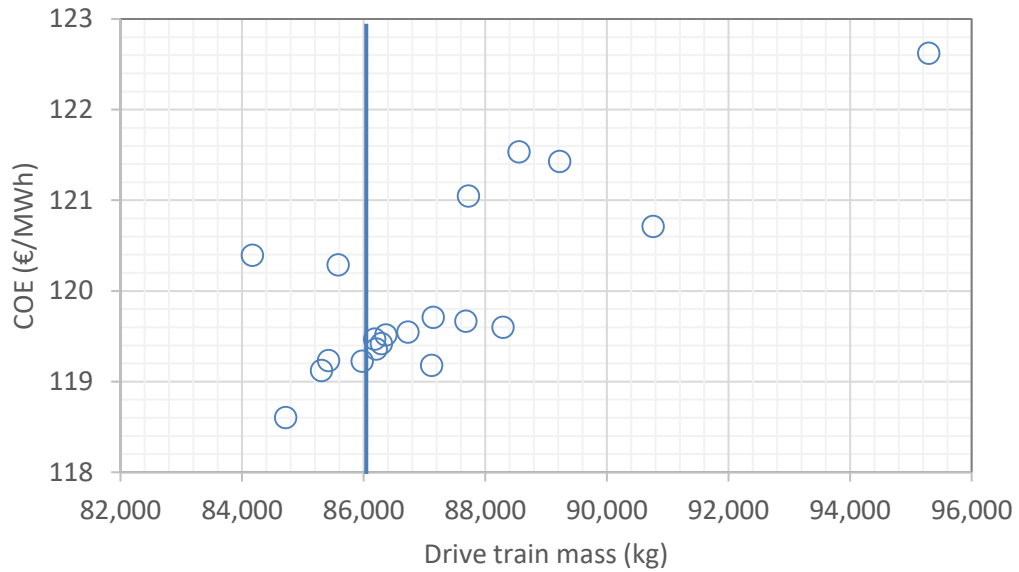
Figure 6.26 Drive train mass limitation for PMG 2G and its effect on COE with basic selection constraint shown as solid vertical line.

Limiting the drive train mass for the PMG 2G produces a range of COE results as shown in Figure 6.26. There as observed with the single stage design, the lowest values of drive train mass correspond with the lowest values of COE. The lowest COE in the sample is 118.6 €/MWh which is around 85,000 kg and above this mass, the COE increases.
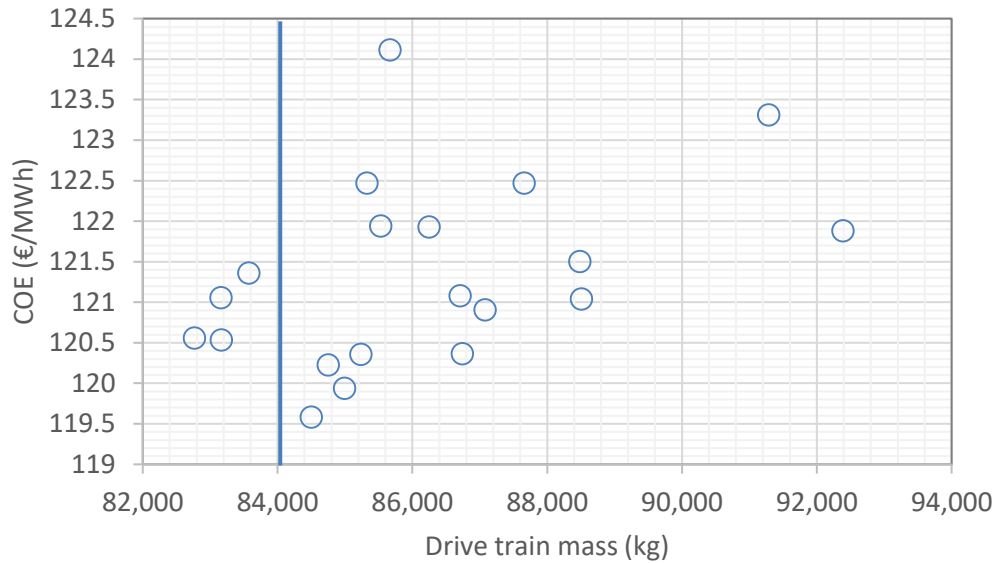
Figure 6.27 Drive train mass limitation for PMG 3G and its effect on COE with basic selection constraint shown as solid vertical line.

The effect of limiting the drive train mass on the COE for the PMG 3G is shown in Figure 6.27 where the COE has a minimum set of outcomes around 120 €/MWh and a drive train mass of 85,000 kg. This total mass of the drive train is almost identical to the total mass of the PMG 2G drive train. The trade-off with having an additional gear stage and smaller generator has minimal effect on the drive train mass going from 2 to 3 gear stages. The drive train can be minimised to 83,000 kg and so can be 5,000 kg lighter than a single stage equivalent. This could be a benefit to developers in terms of weight saving benefits if there is a restriction on the size of the generator or magnet use as the PMG 3G offers the lightest drive train out of the 4 designs.

6.2.5 Comparison between both price scenarios

A comparison of the optimised variables based on the assumed higher material prices of $\mu + 2\sigma$ of each price compared with the same higher material prices applied to the Chapter 4 designs is shown in the Appendix Table A.5.

6.2.6 Robust optimisation drive train summary

When optimising each drive train topology based on robust design considerations, each PMG type offered various compromises and trade-offs. The PMG DD provided the lowest COE designs, but the highest overall drivetrain mass. The efficiency improvement and mass reduction possibilities are very promising with the PMG 3G design and so when faced with magnet availability issues, it could be a suitable alternative to larger PMGs. When reducing the ICC of all drivetrains, there tends to be a point where the COE increases when ICC becomes too low. This shows that the model compromises system performance to keep the upfront costs low and although these differences are not significant, they should be considered to ensure the drive train design is optimised. All of the drive trains exhibit ranges of optimum system efficiency, particularly for the PMG 2G, where allowing the system to have a higher efficiency results in higher COE values and so can be considered diminishing returns. In the event of a minimum system efficiency being imposed on a project, all drive trains will incur higher overall costs, but it can be suggested that PMG 1G would offer the highest system efficiency configurations when material prices are high.

6.3 Optimisation under uncertainty based on Monte Carlo sampling of all material prices

Optimisation under uncertainty using Monte Carlo methods is a useful method of optimising a mathematical problem where inputs have statistical probability and is used in a number of design processes [6]. This method would allow the complete range of price probabilities to be taken into account during the optimisation process itself, and not just a sensitivity analysis as presented in Chapter 5. To create design solutions that accommodate price uncertainty, the objective function of the models was also altered to include a standard deviation from the mean of the probability density function. This method allows the optimisation process to assume a higher COE based on the standard deviation of the costs and not simply the average. The motivation of this approach is that the design parameters can be altered in accordance with higher

assumed prices that would reflect future price increases that may render an alternative design too expensive. The objective function in which to minimise is given by:

$$\min_{x \in \mathbb{R}}(\mu(x) + \sigma(x)) \qquad (6.1)$$

where x represents the independent variables that are optimised in the genetic algorithm, and $\mu(x)$ and $\sigma(x)$ are the mean and standard deviation of the COE which is linked to the material cost distributions. The use of standard deviation as a design consideration is an effect method to produce results that satisfy probabilities [7]. These processes are used in industry to assure that product and process characteristics are on target values and the variability around those targets is minimal [8].
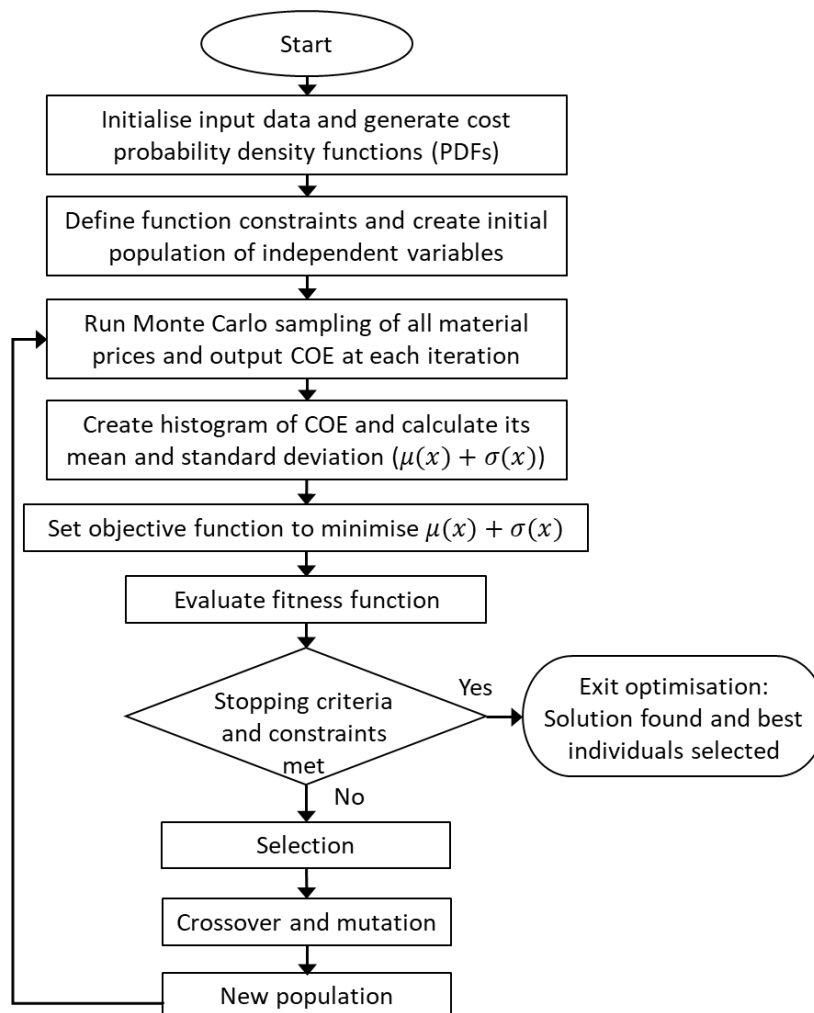
Figure 6.28 Flow chart of the Monte Carlo sampling technique used for optimisation under uncertainty.

The new objective in this optimisation problem is to minimise COE whilst also minimising the variation in potential COE. It implies that a reduction of 1 unit in the standard deviation is as valuable as 1 unit in the mean.

Figure 6.28 illustrates the procedure that uses Monte Carlo Sampling to select the price combinations based on their probabilities.

For each drivetrain type, the histogram produced a distribution of 50 values using a Monte Carlo based sampling method. Each selected cost for the materials carries its own probability and so combined with other probabilistic values, the most likely scenario can be investigated. The model optimises with its objective function set as the mean COE plus one standard deviation (equation (6.1)). 20 distributions were produced for each drive train and the total combined histogram output is shown in Figure 6.29.
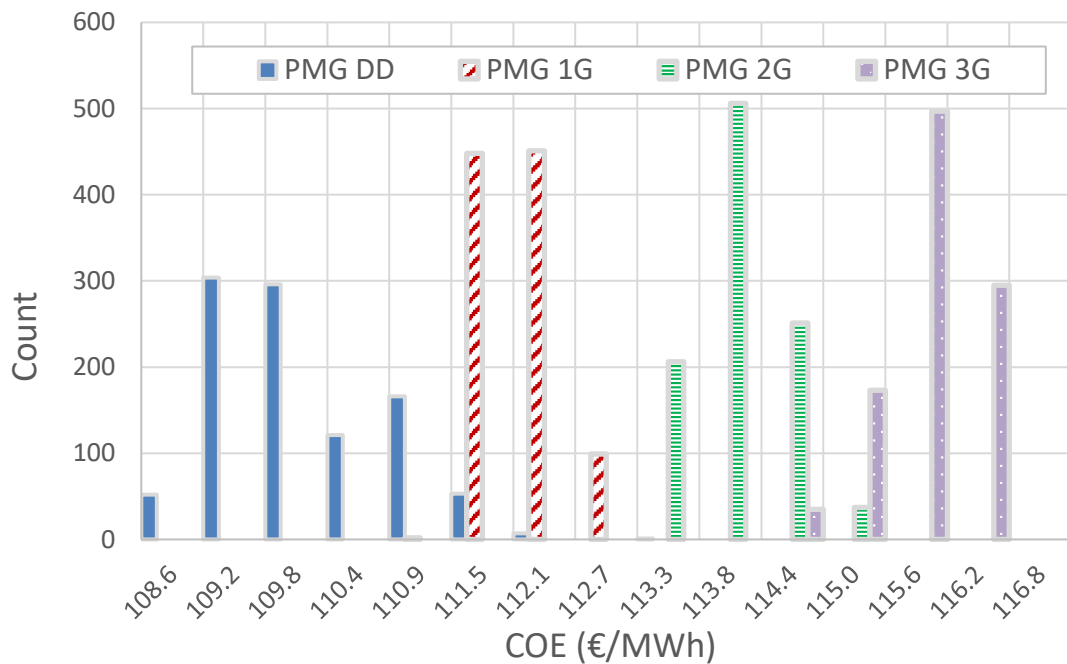
Figure 6.29 Histograms for each drive train subject to optimisation with Monte Carlo sampling.

6.3.1 Direct drive

The prices of all materials were varied based on their probability distributions using the Monte Carlo method and taking 50 values for each. The results were plotted as a

histogram and the subsequent normal distribution fitted to obtain the mean and standard deviation.

The COE of energy result for the 'best' direct drive topology was a mean value of 111.78 €/MWh and a standard deviation of 1.32 €/MWh, as shown in Figure 6.29.
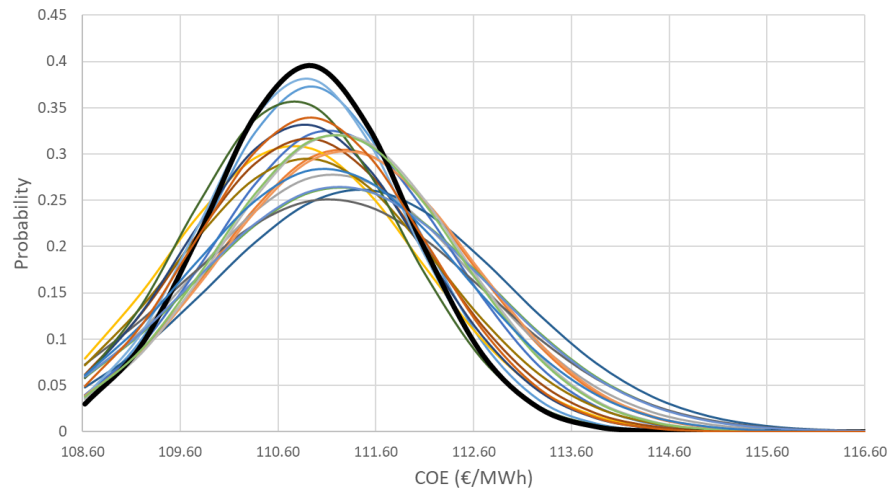
Figure 6.30 Fitted distributions of the COE optimisation results for candidates design results of PMG DD using Monte Carlo sampling of material prices. Each curve represents a design. 'Best' COE distribution shown as the black bold line.
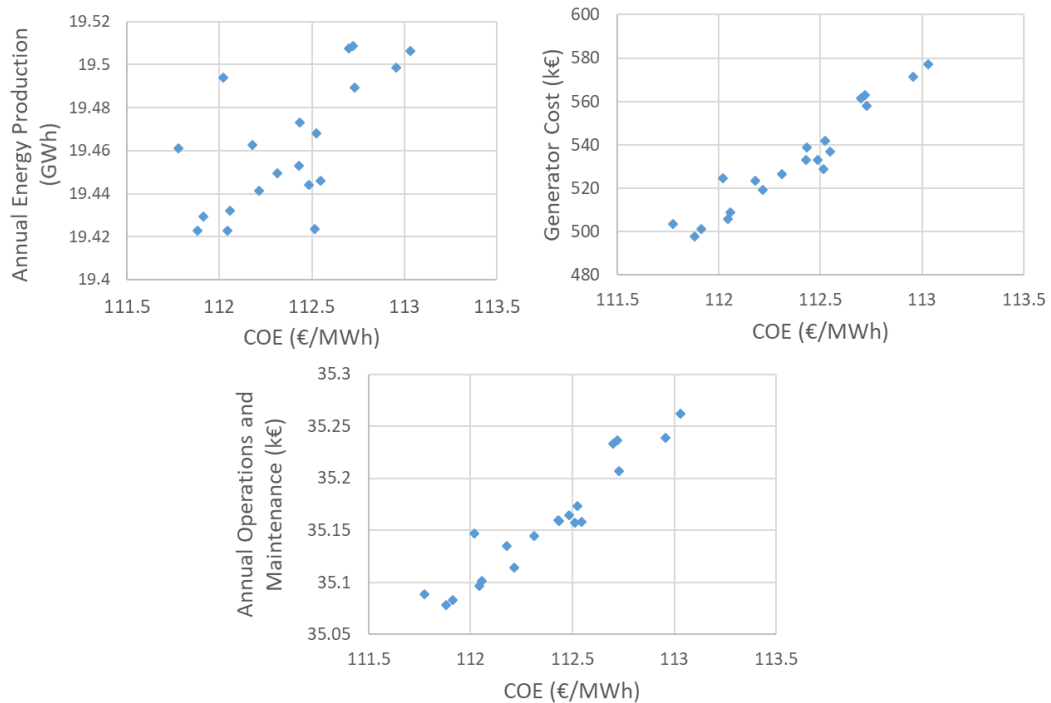
Figure 6.31 COE comparison of AEP, generator cost and AOM for the PMG DD.

6.3.2 PMG with 1-stage gearbox Monte Carlo method

The prices of all materials were varied based on their probability distributions using the Monte Carlo for the PMG with 1-stage gearbox. The COE results as fitted distributions based on their histogram are shown in Figure 6.32. The COE has a mean value of 114.64 €/MWh and a standard deviation of 0.56 €/MWh.
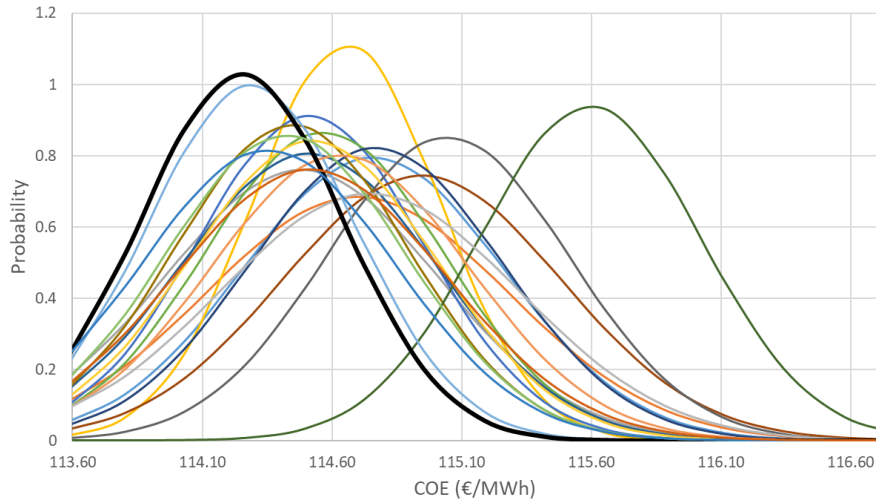
Figure 6.32 Fitted distributions of the COE optimisation for the PMG 1G using Monte Carlo sampling of material prices. 'Best' COE distribution shown as the black bold line.
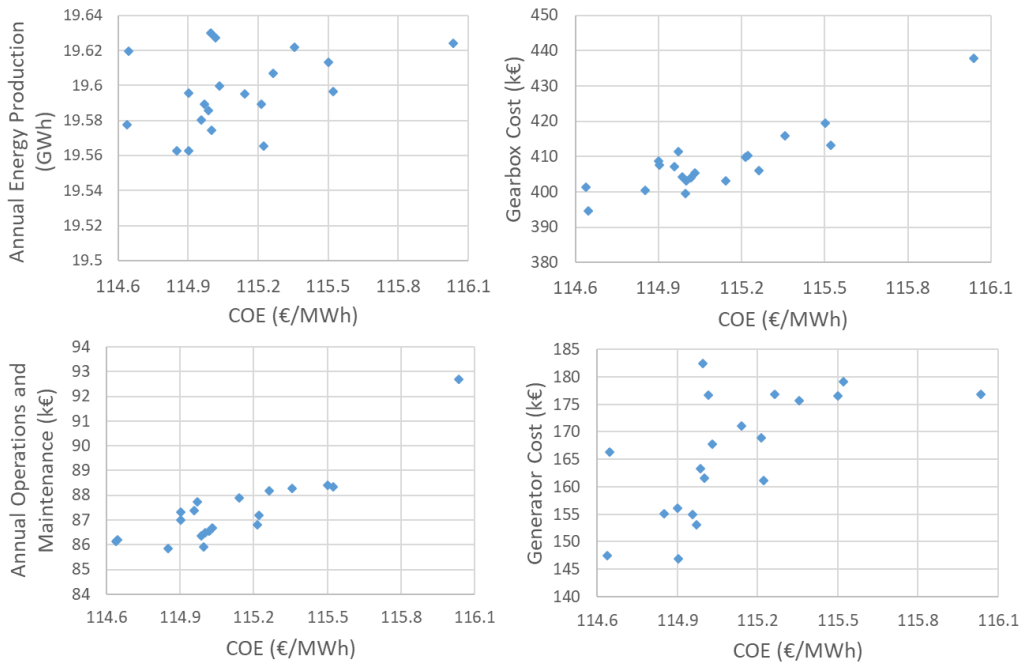
Figure 6.33 COE comparison of AEP, generator cost, AOM and gearbox cost for the PMG 1G.

6.3.3 PMG with 2-stage gearbox Monte Carlo method

The Monte Carlo sampling and optimisation process was repeated for the PMG with 2-stage gearbox and the 100 samples are shown as a histogram and fitted distribution in Figure 6.34. The mean COE is 117.73 €/MWh with a standard deviation of 0.61 €/MWh.
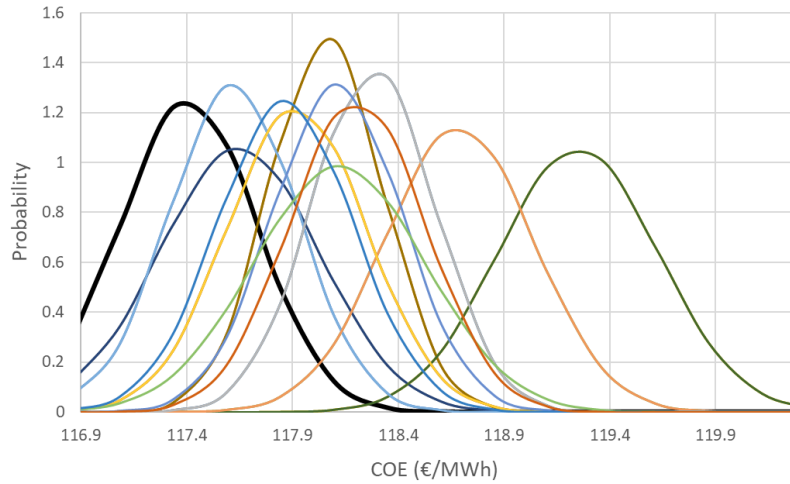
Figure 6.34 Fitted distributions of the COE optimisation for the PMG 2G using Monte Carlo sampling of material prices. 'Best' COE distribution shown as the black bold line.
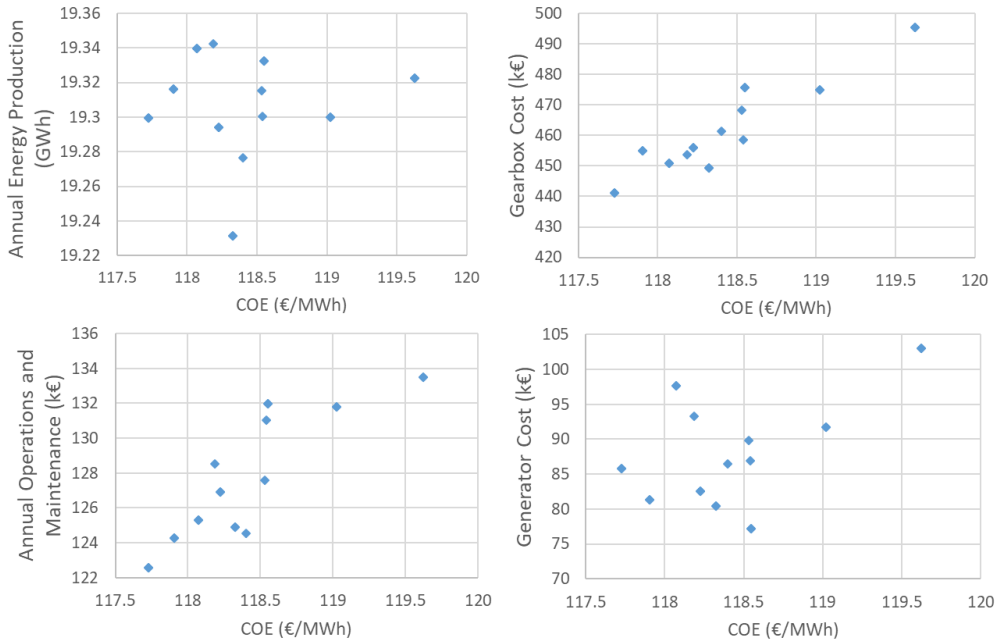
Figure 6.35 COE comparison of AEP, generator cost, AOM and gearbox cost for the PMG 2G.

6.3.4 PMG with 3-stage gearbox Monte Carlo method

The Monte Carlo sampling and optimisation process were finally used for the PMG with 3-stage gearbox and the results are shown in Figure 6.36. The mean COE is 119.57 €/MWh with a standard deviation of 0.67 €/MWh.
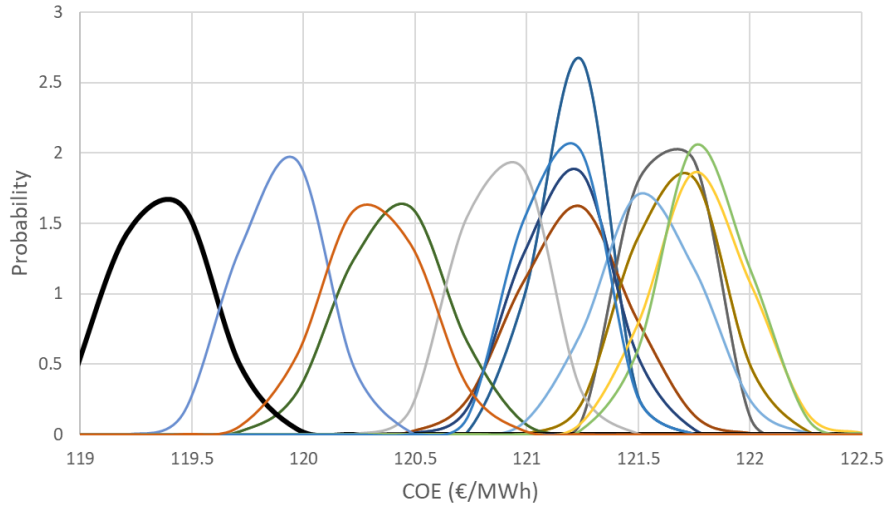
Figure 6.36 Histogram and fitted distribution of the COE for the PMG with 3-stage gearbox wind turbine with Monte Carlo sampling of material prices. 'Best' COE distribution shown as the black bold line.
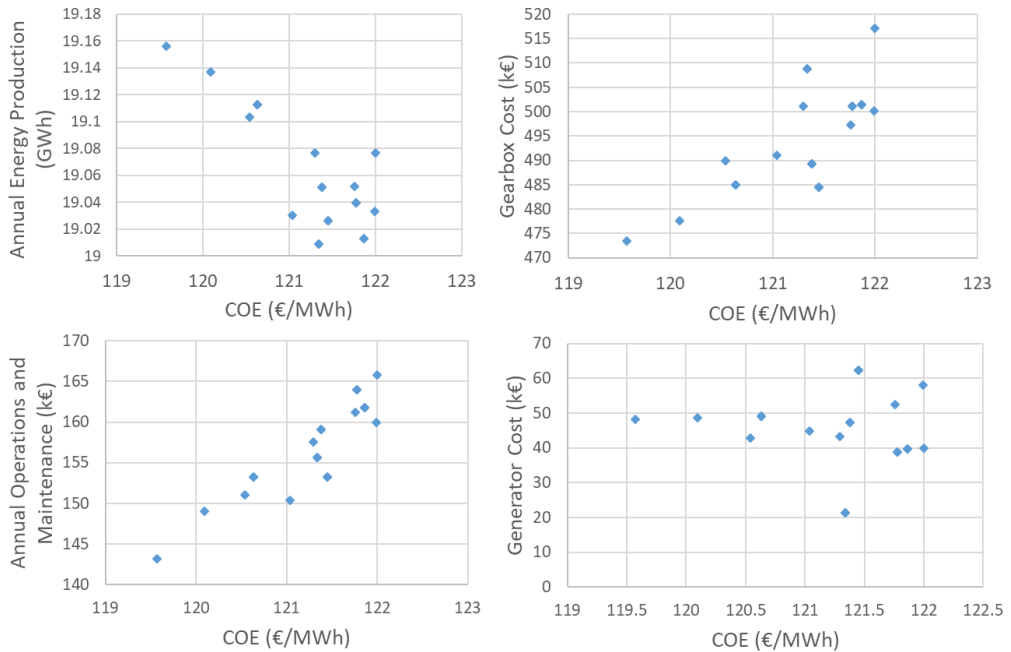
Figure 6.37 COE comparison of AEP, generator cost, AOM and gearbox cost for the PMG 3G.

6.3.5 Comparison of Monte Carlo based optimisation

Optimising the drive trains using Monte Carlo sampling of the material prices was an effective method of identifying the drive trains that are most impacted by price uncertainty and allowing the re-design of the original optimised designs from Chapter 4.

Table 6.1 below compares the results from optimisation under uncertainty with the original optimised results from Chapter 4. Looking at the results for the PMG DD, the COE increases by 1.8 €/MWh and all dimensions are slightly reduced. This new design considers the cost uncertainty of the materials in order to produce an outcome that will be optimised for assumed variable prices. It gives an indication of a probabilistic scenario for price rises and how at a design level, this can be overcome with appropriate dimensions and sizing of the generator. The magnet height is reduced by 13% to compensate for the uncertainty and allows the system to rely on a lower volume of magnets and still provide competitive results, and simultaneously the air gap is reduced to maintain the magnet circuit parameters. It is also observed that the design provides a slightly lower energy yield compared with the case of Chapter 4. Therefore, at uncertain material prices, lowering the system efficiency through dimension alterations could provide the best long-term solution.

The PMG 1G has a similar outcome with a cost increase of 0.85 €/MWh when designing for uncertainty. With the added uncertainty and higher cost price, the design results in a higher assumed AOM cost that is reflected as having a generator and gearbox combination that may result in higher failure rates. This shows that in order to optimise for uncertain prices the design produces a trade-off with reliability to keep overall lifetime costs low. The height of the magnet is significantly reduced (27%) in order to minimise the use of the NdFeB in the design.

The PMG 2G does not change in COE when designing with uncertainty and the slight decrease of 0.01 €/MWh is only representative of locating a different local minimum during the optimisation compared with Chapter 4. The PMG 2G is the only design that offers a decrease in AOM and an increase in number of pole pairs. This drive train has the most design flexibility when considering the uncertain cost of materials and can produce many designs, irrespective of price uncertainty, that result

in similar COE values. For a manufacture's perspective, having a geared arrangement with 2 stages could be the most stable arrangement in terms of price variability despite not being lowest COE option.

The PMG 3G shows an increase in COE of 0.73 €/MWh when optimised under uncertainty. This drive train is the only one to show an increase in the generator dimensions (radius and length) compared to the design of Chapter 4. The gearbox dimensions are reduced in this case to compensate for material price variability due to the high volume of steel used in this drive train. The magnet and copper prices have the lowest impact on the drive train and so the optimisation is weighted towards minimising the gear stage masses.

Table 6.1 Comparison between original optimisation method from Chapter 4 and the results from optimisation under uncertainty.

Optimisation output	Direct Drive		PMG with 1-stage GB		PMG with 2-stage GB		PMG with 3-stage GB	
	Chapter 4	Chapter 6	Chapter 4	Chapter 6	Chapter 4	Chapter 6	Chapter 4	Chapter 6
Cost of energy (€/MWh)	109.98	111.78	113.79	114.64	117.74	117.73	118.84	119.57
Standard deviation of COE (€/MWh)	-	1.32	-	0.56	-	0.61	-	0.67
Initial capital cost (k€)	18,219	18,482	18,580	18,637	18,563	18,562	18,448	18,544
Annual energy production (MWh)	19,500	19,461	19,626	19,578	19,335	19,300	19,177	19,156
Annual operations and maintenance (€)	34,935	35,089	81,750	86,127	126,771	122,594	142,727	143,131
Independent design variables								
Air gap radius (m)	4.04	4.01	2.61	2.59	1.19	1.16	0.43	0.47
Stack Length (m)	1.61	1.60	0.83	0.82	0.72	0.70	0.79	1.00
Number of pole pairs	183	181	86	84	27	35	10	9
Magnet height (mm)	12.36	10.75	17.12	12.43	25.40	22.10	28.81	25.60
Magnet width to pole pitch ratio	1.00	0.99	0.90	0.86	0.78	0.80	0.91	0.82
Air gap (mm)	6.47	5.18	5.25	4.12	2.26	1.68	0.93	0.94
Height of slot (mm)	66.33	64.76	55.03	59.19	64.84	66.26	55.09	52.32
Ratio of slot width to pitch	0.55	0.54	0.55	0.54	0.53	0.50	0.50	0.49
1st stage sun pitch diameter (mm)	-	-	908	931	1,046	1,035	1,093	1,049
Number of 1st stage sun teeth	-	-	44	44	35	39	46	42
Number of 1st stage ring teeth	-	-	176	176	106	118	140	141
Number of 1st stage planet teeth	-	-	61	61	33	36	43	46
Facewidth 1st stage (mm)	-	-	798	757	787	809	727	708
2nd stage sun pitch diameter (mm)	-	-	-	-	673	635	702	643
Number of 2nd stage sun teeth	-	-	-	-	38	43	37	38
Number of 2nd stage ring teeth	-	-	-	-	115	118	139	121
Number of 2nd stage planet teeth	-	-	-	-	37	35	47	38
Facewidth 2nd stage (mm)	-	-	-	-	510	586	381	461
3rd stage gear pitch diameter (mm)	-	-	-	-	-	-	1,473	1,524
Number of 3rd stage gear teeth	-	-	-	-	-	-	119	136
Number of 3rd stage pinion teeth	-	-	-	-	-	-	27	29
Facewidth 3rd stage (mm)	-	-	-	-	-	-	392	403

6.4 Magnetic material variation

It is clear that the volatility in rare earth material prices has a very significant impact on the COE for PMG based drive trains. Large price uncertainty arises particularly for direct drive options and so methods in which to improve confidence in future purchases of permanent magnets are key to enable effective project financing and projections. Altering the magnetic material composition to use less rare earth metals is a promising approach that would benefit manufacturers. This would represent current attempts to create substitute magnetic material that is less volatile than rare earths such as NdFeB [9]. It would help reduce the risks associated with the variable market price of elements such as neodymium and dysprosium. There is also an opportunity for machine designers to purchase NdFeB magnets on longer term basis, paying more on average but with less cost variability.
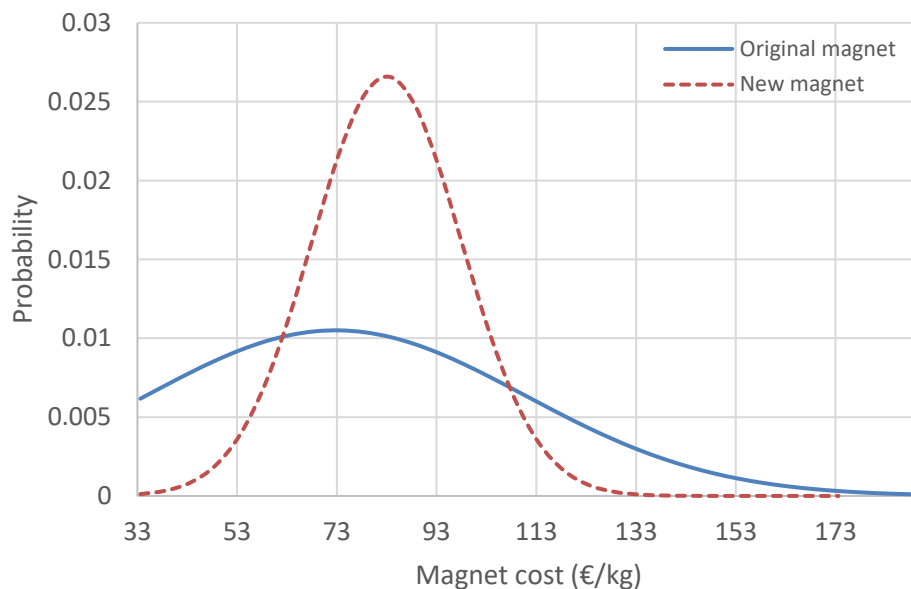
Figure 6.38 Original and new magnet material cost per kg probability distribution.

Figure 6.38 presents a comparison between the original magnet price distribution used throughout this thesis and a new magnet price distribution that corresponds to a hypothetical higher cost magnetic material with a reduced standard deviation. This would symbolise a more expensive magnet (assumed €10/kg higher average price), but with lower risk in terms of price fluctuations. The new magnet has a mean of

€83.0/kg and a standard deviation of €15.0/kg compared with €72.8/kg and €38/kg for the original NdFeB magnet.

The results are shown in the following figures and the COE and standard deviation comparison with the original NdFeB magnet are shown in Table 6.2.

The effect of using a hypothetical replacement magnetic material changes the COE as shown in Figure 6.39 for the PMG DD to produce a mean value of 112.25 €/MWh. The COE outputs variation shows an improvement in the standard deviation for the new material going from 1.32 to 0.73 €/MWh. This means that the despite the higher average cost per kg for the new magnet material, it produces a slightly higher mean cost of energy with a much higher probability and a much lower impact for price fluctuations and offers greater price stability.
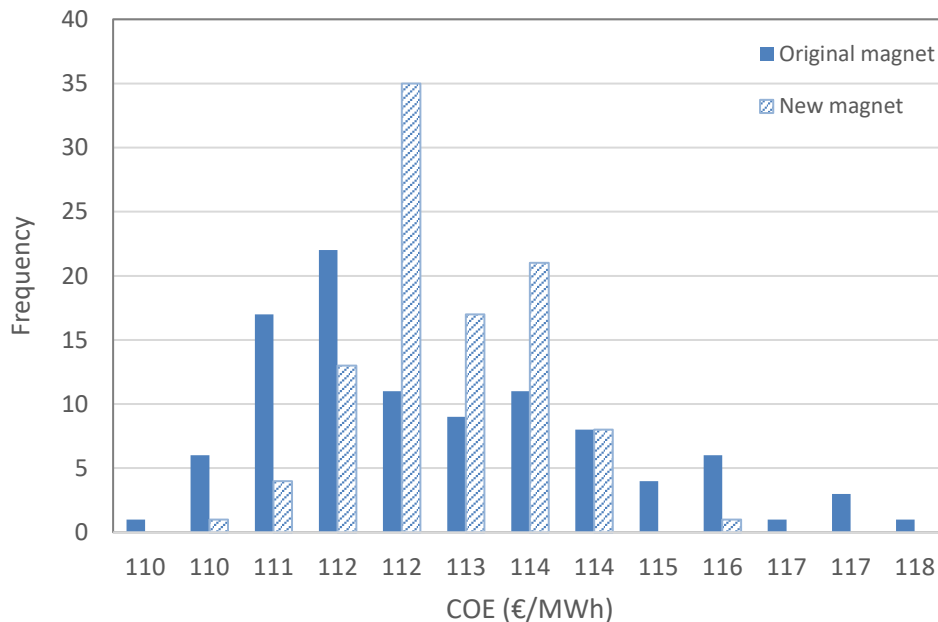
Figure 6.39 Comparison between COE sample distributions using the original and a new hypothetical magnetic material for the PMG DD.

From Figure 6.40 for the PMG 1G, the use of the alternative magnetic material produces a COE mean of 114.81 €/MWh and a standard deviation of 0.4 €/MWh. Comparing directly with the original NdFeB magnet which produced a standard deviation of 0.56 €/MWh, it offers a more predictable price outcome and stability against price rises.
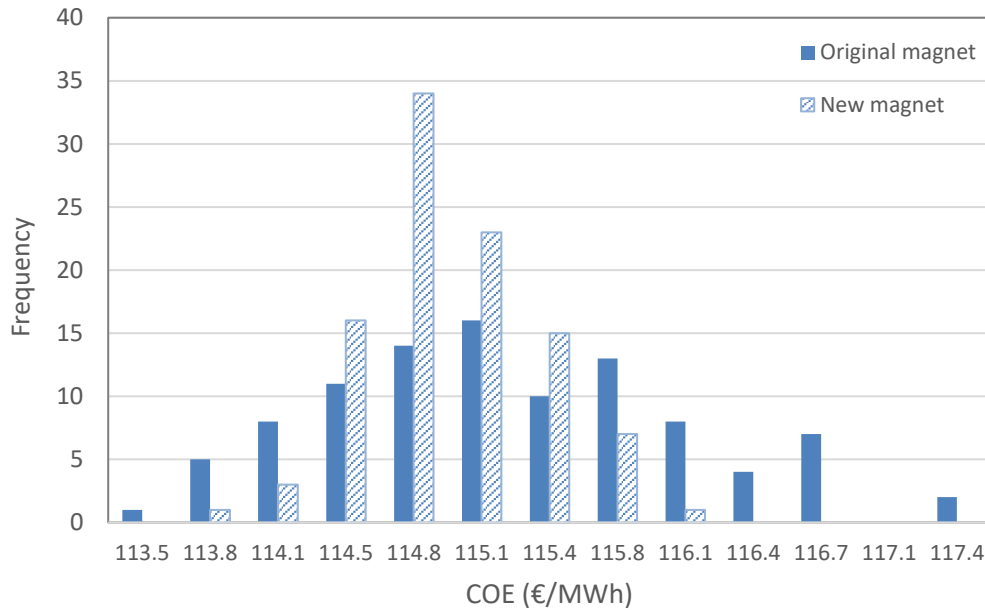
Figure 6.40 Comparison between COE sample distributions using the original and a new hypothetical magnetic material with the PMG 1G.

From Figure 6.41 for the PMG 2G, using the new magnetic material produced a COE mean of 117.96€/MWh and a standard deviation of 0.27. The original NdFeB magnet produced COE standard deviation of 0.61 €/MWh which shows a huge improvement as risk of COE variation is reduced by over half using the hypothetical magnet.

From Figure 6.42 the PMG 3G when optimised with the new magnetic material produced a COE mean of 119.93 €/MWh standard deviation of 0.14 €/MWh. The original NdFeB magnet produced a COE standard deviation of 0.67 €/MWh. By using an alternative and more expensive magnet in the PMG 3G drive train, the risk is reduced by almost a fifth for COE variations with price uncertainty.
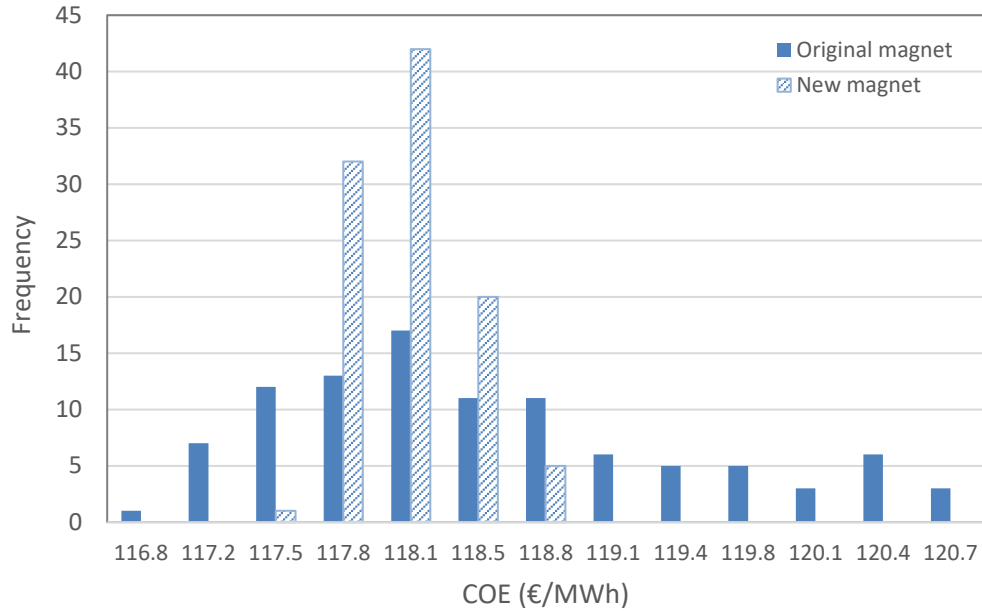
Figure 6.41 Comparison between COE sample distributions using the original and a new hypothetical magnetic material for the PMG 2G.
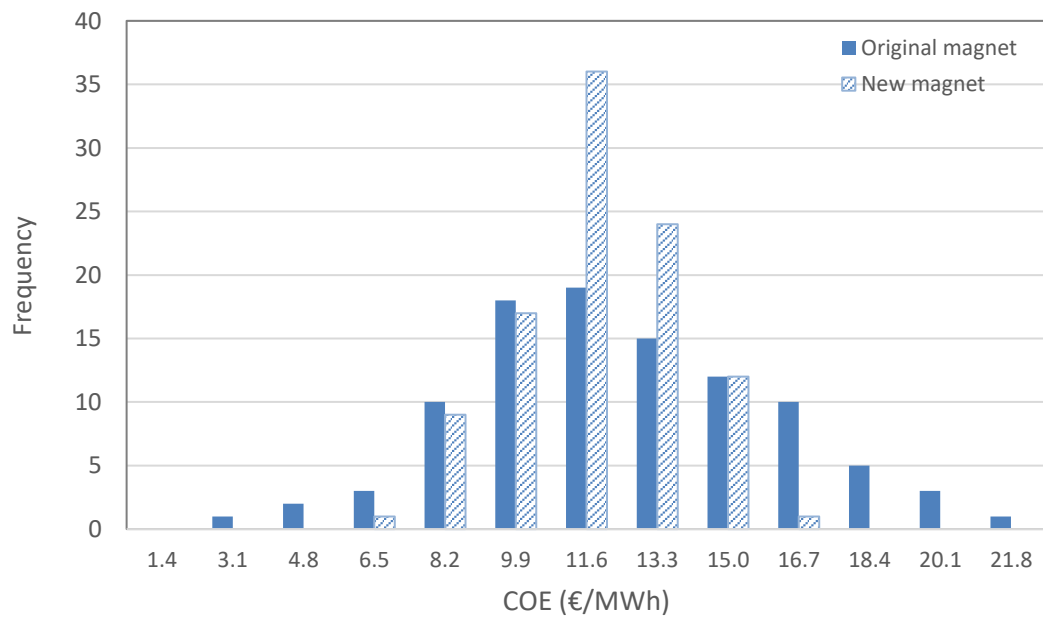
Figure 6.42 Comparison between COE sample distributions using the original and a new hypothetical magnetic material for the PMG 3G.

Trading off at higher mean prices with a lower variability helps reduce the risk of a high COE when prices rise. From Table 6.2, the use of a hypothetical magnet can offer a saving to all drive trains as the standard deviation of the designs is sufficiently

low enough to prevent the COE rising beyond the values obtained for the original magnet when its COE is set at its mean plus one standard deviation.

Table 6.2 Comparison between original NdFeB magnet and hypothetical magnet

	PMG DD		PMG 1G		PMG 2G		PMG 3G	
	NdFeb Magnet	Hypothetical Magnet	NdFeb Magnet	Hypothetical Magnet	NdFeb Magnet	Hypothetical Magnet	NdFeb Magnet	Hypothetical Magnet
COE Mean (€/MWh)	111.78	112.25	114.64	114.81	117.73	117.96	119.57	119.93
COE Standard Deviation (€/MWh)	1.32	0.73	0.56	0.40	0.61	0.27	0.67	0.14
COE Mean plus 1 Standard Deviation (€/MWh)	113.10	112.98	115.20	115.21	118.34	118.23	120.24	120.07

The use of an alternative magnetic compound for the generator poles to reduce the risk of price fluctuations associated with rare earth elements proved to be an effective method for all drive trains. The benefit of the original NdFeB magnets would be seen at a lower cost per kilogram where the new and more expensive magnet could not compete in terms of lower COE. However, ensuring the continued supply of magnetic material may prove more important for manufacturers compared to allowing their designs to be dependent on a volatile market, even if it does mean a higher capital cost.

6.5 Summary of Chapter 6

The first part of this chapter observed the individual impact of each material cost increase on the design optimisation outcome in comparison to the optimised designs of Chapter 4. Further to the individual price increase effects, a combined increase of all materials allowed alternative designs to be identified for each drive train for assumed higher material prices.

The next section of the chapter looked at robust optimisation, which is method of optimisation under uncertainty that includes additional requirements for a successful outcome. The examples explored in this chapter included a scenario for maximum magnet mass, a fixed maximum initial capital cost (ICC), a minimum system efficiency of the drive train and a maximum drive train mass. Each case was analysed for worst case scenario conditions which in this study was material prices set at their mean plus 2 standard deviations to represent very high costs for all materials

simultaneously. This method was extremely useful for comparing the impact of higher costs on the original optimised designs from Chapter 4 and offered an alternative design for all drive trains.

The chapter then explored a new objective function that is based on minimising the mean COE and simultaneously minimising the standard deviation for each material price probability density function independently. Combining this new objective function with Monte Carlo sampling of the material prices based on their probability distributions enabled the effects of each cost fluctuation to be taken into account during the planning process and limited the overall standard deviation of the COE for the new designs. The fluctuations in permanent magnet prices were the most significant for the designs and had the largest impact on the COE for all designs. The COE of energy result for the direct drive topology produced a mean value of 111.78 €/MWh and a standard deviation of 1.32 €/MWh. As with previous chapters the PMG DD outperformed the other drive trains in terms of providing a topology with the lowest COE. The poorest performing drive train was again the PMG 3G largely due to its reliability issues. The PMG 1G had its COE increased by 0.85 €/MWh when optimising under cost uncertainty but allowed the magnet mass to be significantly reduced. This could be a favourable choice if magnet mass is a restriction on the design. The PMG 2G showed no overall COE difference when optimising with the new objective function that includes standard deviation as the combinations of generator and gearbox topologies provides the most flexibility out of the 4 drive trains.

The chapter concluded with the introduction of an alternative magnetic material to address the key issues of magnet price volatility that is the most significant influence on the overall COE of the designs. Using an alternative magnetic material comprising of less volatile priced rare earth metals could potentially offer more robust designs to be created for each drive train as the risk of large price fluctuations would be significantly reduced, even if the material has a higher production cost. This might be more appealing from a design perspective to reduce the risk of a drive train topology of becoming unfeasibly expensive in the event of a rare earth price spike from economic uncertainty in the county of origin.

6.6 References for Chapter 6

[1]   E. Sandgren and T. M. Cameron, "Robust design optimization of structures through consideration of variation," *Comput. Struct.*, vol. 80, no. 20–21, pp. 1605–1613, 2002.

[2]   B. L. Gorissen, İ. Yanıkoğlu, and D. den Hertog, "A practical guide to robust optimization," *Omega*, vol. 53, pp. 124–137, Jun. 2015.

[3]   A. A. Giunta, M. S. Eldred, L. P. Swiler, T. G. Trucano, and S. F. Wojtkiewicz, "Perspective on Optimization Under Uncertainty: Algorithms and Applications," *Aiaa-2004-4451*, no. September, pp. 1–10, 2004.

[4]   W. B. Powell, *A Unified Framework for Optimization under Uncertainty*. 2016.

[5]   K.-Y. Yoon and S.-W. Baek, *Robust Design Optimization with Penalty Function for Electric Oil Pumps with BLDC Motors*, vol. 12, no. 1. 2019.

[6]   X. Hu, X. Chen, G. T. Parks, and W. Yao, "Review of improved Monte Carlo methods in uncertainty-based design optimization for aerospace vehicles," *Progress in Aerospace Sciences*. 2016.

[7]   N. COSTA, J. LOURENÇO, and Z. L. PEREIRA, "Optimization of the Mean and Standard Deviation of Multiple Responses," pp. 216–229, 2011.

[8]   N. R. P. Costa, "Simultaneous optimization of mean and standard deviation," *Qual. Eng.*, vol. 22, no. 3, pp. 140–149, 2010.

[9]   C. C. Pavel *et al.*, "Substitution strategies for reducing the use of rare earths in wind turbines," *Resour. Policy*, vol. 52, no. May, pp. 349–357, 2017.

Chapter 7 Discussion and Conclusion

This thesis presented the optimisation and cost of energy analysis for permanent magnet generators with various drive train configurations for offshore wind turbines. This chapter summarises the key findings and important issues discussed in the thesis and answers the original research question of "What is the best drive train design for a large offshore wind turbine with a permanent magnet generator in terms of cost of energy?".

7.1 Summary of the chapters

Chapters 1 and 2 introduced the challenge of reducing the cost of offshore wind energy and that drive train consideration could play a major role. The use of permanent magnet synchronous generators has many benefits such as increased efficiency and reliability, but with the volatile prices of rare earth metals causing uncertainty about the future costs, the design carries a high level of risk.

Chapter 3 described the cost of energy (COE) model used in this study and outlined various assumptions that contributed to the state of the art analysis conducted in this thesis. This chapter presented the four chosen drive train configurations to be modelled and illustrated base case COE results for each. The chosen drive trains were, PMG DD (direct drive permanent magnet synchronous generator), PMG 1G (permanent magnet synchronous with single-stage gearbox), PMG 2G (permanent magnet synchronous with 2-stage gearbox) and PMG 3G (permanent magnet synchronous with 3-stage gearbox). The results presented in Chapter 3 were not optimised for COE and this was especially clear for the PMG 3G that produced a COE in excess of 135 €/MWh which was significantly higher than the other 3 drive trains. The results therefore created a foundation on which to improve the design with a more reliable optimisation model which was the basis of Chapter 4.

Chapter 4 predominately focuses on an optimisation method using a genetic algorithm to allow the four drive trains described in Chapter 3 to be computationally optimised in terms of COE minimisation. This chapter included additional design

constraints and independent variables that were varied between upper and lower bounds to locate local optimum solutions. Chapter 4 also presented the model's sensitivity to the independent variables such as the air gap radius and also the effects of varying the gear ratio of the geared deigns. The sensitivity revealed where COE minimums lie when varying the air gap radius and designs above and below these values return more expensive overall costs for the project. The designs were all improved compared to the results presented in Chapter 3, especially for the PMG 3G where the COE was reduced by 17.04 €/MWh. The results indicated that the PMG DD can provide the lowest COE design and by adding a gear stage, and any subsequent gear stage progressively increases the COE. This was also observed in a sensitivity analysis of the gear ratio where all geared designs tend towards lower gear ratios, and ultimately towards 1:1 in an attempt to produce more cost-effective designs. This supports current industrial trends that see more and more direct drive wind turbines enter the offshore wind market.

Chapter 5 implements a sensitivity analysis of the optimised designs from Chapter 4. The performance of each drive train was scrutinised for various wind speed profiles and the effects of material price rises on the COE was observed. The cost of materials was based on real life historical data and an adapted probability density function. This chapter also provided a detailed insight to the cost impact on each design when a complete generator replacement was assumed to occur once in its lifetime (the base case assumed no major replacements occurred). As expected, the larger generator designs were affected the most, with the PMG DD having the highest impact at an increase in COE of 1.48% with a generator replacement. This chapter also introduced a Monte Carlo method of cost sampling to compare the most likely cost scenarios with the designs as the future of material prices remains uncertain. It was clear from all of the drive trains that the cost of the magnets played the most significant role in the COE variations observed when sampling the material cost prices.

Chapter 6 developed the optimisation models to include uncertainty and investigated the effects of design requirements for additional robustness. This approach allowed the output specifications to be defined whilst respecting cost uncertainty. The first sections of this chapter look at the effects of individual price

increases and how they would affect the optimisation process compared to the design from Chapter 4 being subjected to the same price rises. All of the drive trains produced designs with lower COE values when re-optimised for higher material costs. The geared designs provided the most varied options such as creating a more expensive gearbox to compensate for a reduction in generator dimensions.

The next part of Chapter 6 explored robust optimisation, which is method of optimisation that includes additional requirements for a successful outcome when a worst-case scenario is considered. The additional requirements included a maximum magnet mass constraint, a fixed maximum initial capital cost (ICC), a minimum system efficiency of the drive train and a maximum drive train mass. The results indicated the impact on COE when trying to obtain designs that satisfy the additional requirements. It is generally more expensive throughout the lifetime of the project to meet some of the requirements and depending on the needs of the developer, the PMG DD may not always be the dive train of choice e.g. if the drive train mass must be low, then the geared designs may offer the best solutions.

Chapter 6 also explored the use of a new objective function that is based on the mean COE plus one standard deviation for each material price probability density function independently. This method, combined with Monte Carlo sampling of material prices, enabled the uncertainty in the outcome to also be minimised creating designs that are less susceptible to COE fluctuations when prices vary over time. The permanent magnet cost fluctuations unsurprisingly forced the largest design changes and COE variations for all drive trains. Chapter 6 concluded with a comparison of the drive trains when using an alternative magnetic material compound in place of the NdFeB magnet assumed throughout the thesis. This presented the possibility of using a more expensive magnetic material to mitigate the high cost variability associated with economic uncertainty in the countries of origin of rare earth metals.

7.2 Contribution to knowledge

There are many studies that focus on COE modelling [1][2][3] and drive train design [4] [5]. However, these studies do not bring together dimensional details of the drive train components and failure rates linked to design specifications. This thesis offers a

framework for developing drive train optimisation models that encompass design specific failure rates and repair costs as well as improved loss calculations for gearboxes. This method will allow detailed design considerations to be understood during planning stages of wind turbine drive trains and offers long term analysis of component lifetimes and the impact on COE. This thesis focuses solely on permanent magnet generators as they offer significant reliability improvements over conventional electrically excited machines [6][7]. With limited data available in the public domain for offshore wind (and particularly PMGs), the failure rates were typically based on a study by Carroll [8] that looks at the effect of drive train selection on the COE for offshore wind. This thesis adds design specific details to this study and optimises these designs taking into account their topology effects on their reliability and repair requirements.

This thesis also considers the effects of price fluctuations and so offers an enhanced optimisation under uncertainty process that includes probability. With detailed design methodology and a process to optimise under uncertainty, the work undertaken in this thesis offers a new approach to COE minimisation for PMG offshore wind turbines. This valuable insight will also help re-design drive trains as projects evolve and the possibility of repowering a site or extending the life time of the wind farm becomes possible. As prices change, so can the designs to ensure the most cost-effective solution is implemented no matter what stage during the project. Not only can this methodology benefit manufacturers but can provide procurement decision support value for developers. The PMG DD was the best drive train throughout the study offering the lowest COE yet it is typically impacted the most from material cost uncertainty. As long as magnet prices do not increase significantly over the years, a direct drive topology can offer the most attractive option for offshore installations.

7.3 Further work

There are many simplified assumptions used in this thesis can be further developed to enhance the model capabilities and provide a higher degree of accuracy. One basic assumption is that the rest of the wind turbine has been assumed constant between all

the drive train topologies despite the design differences that could potentially arise between direct drive and geared topologies. For example, the "multibrid" design [9] offers a compact integrated drivetrain with reduced load path potential and so such considerations would improve the drive train selection process. The material cost prices only had an impact on the drive train design constituents despite the tower and support structure being comprised of steel and would result in significant price variation when steel prices change. As the study only reviewed the drive train, the changes in the rest of the wind turbine were not considered.

The failure rates of the design are linked directly to the surface area of the generator and gearbox (if applicable). This served as a basic yet effective method of failure rate based optimisation constraints as it was assumed that the larger the surface area, the higher the failure rate owing to the increased forces experienced by larger machines. To improve this assumption, more detailed failure rates of the windings, insulation, rotor, gearbox bearings, gear teeth etc. could allow very specific design considerations to be explored. For example, the length of the windings and the number of turns could be linked to failure rate such that the higher the number of turns, the higher the probability of end winding failures. Similarly with the gearbox, the higher the operating speed of the bearings, the possible increase in bearing failure rates. Data of this level of detail is not currently available in the public domain. If there was access to commercial data for particular topologies of drive trains, this approach could aid in the redesign of drive trains if components are proving to be unreliable.

The gearbox topologies remained constant for the geared designs such that the 3-stage gearbox comprised of 2 planetary gear stages and one parallel, the 2-stage had 2-planetary stages, and the single stage had 1 planetary stage. This was in keeping with current trends seen for large wind turbines, but was not altered for any other configuration of gearbox type. Innovations in gear technology could provide more reliable and cost effective methods of utilising high speed generator systems. Including new and innovative gear technology with the model could provide further scope for cost reduction.

The vessel cost assumptions for major replacements are assumed to be uniform regardless of the drive train type (a direct drive generator is assumed to have

the same vessel and lifting equipment as a high-speed generator for replacement works). In reality, the cost for a jack-up vessel and specialist equipment to lift a direct drive generator down from the nacelle and replace it is much more significant than a smaller high-speed generator which would not require a specialist jack-up vessel. Therefore, improvement should be made to this assumption when considering major replacements of the generator.

The model methodology in this thesis keeps the drive train optimisation process separate for each topology. That is that the PMG DD, the PMG 1G, the PMG 2G and the PMG 3G are all analysed separately and that the optimisation process does not simply produce one drive train result. The reason behind this choice of analysis was that not all manufacturers would be looking to build just one type of wind turbine. Some companies that specialise in high-speed designs may not consider the direct drive options. Having the design topologies independent of one another allows all aspects of their design to be compared directly with one another from the initial capital cost (ICC) and annual energy production (AEP) to the weight of the drive train. An alternative approach would be to conclude with an overall single drive train result directly from the model. Concluding from the results so far, this output would be almost entirely a direct drive topology, as the PMG DD outperformed all geared design throughout the thesis. Therefore, for the purposes of comparison and analysis, the design process was kept separate.

7.4 Concluding remarks

During this research project, four separate drive train topologies with permanent magnet generators were optimised for COE and throughout the study the direct drive PMG topology provided the lowest COE designs. Sensitivity to design parameters and material costs was a fundamental part of identifying the most vulnerable design considerations. The study also included additional requirements which included a maximum magnet mass constraint, a fixed maximum initial capital cost (ICC), a minimum system efficiency of the drive train and a maximum drive train mass.

The PMG DD offered the lowest COE throughout the study due to the increased reliability associated with the absence of a gearbox which for the geared

deigns increased both the AOM and downtime throughout the project. From the three geared designs, the PMG 1G was the most cost-effective solution due to only having one gear stage that was subject to lower levels of failure due to reduced operating speeds. The PMG 3G, albeit the most expensive drive train, was least affected by fluctuations in material prices (in particular the NdFeB magnet price) and so provided the lowest risk in terms of COE increase. The PMG 2G has potential for producing compact designs for ease of transport and installation, but in terms of COE only offered a slight reduction compared with the PMG 3G.

The variability in magnet price has the largest impact on the designs and the range of possible prices is much more significant and volatile compared to the other materials. To minimise the uncertainty in the optimisation process, a methodology was developed that included minimising the mean and standard deviation. This was an effective method for all drive trains, providing alternative designs that will not be as perturbed by increases in material prices.

7.5 References for Chapter 7

[1]   D.-M. Valcan, P. C. Kjar, L. Helle, S. Sahukari, M. Haj-Maharsi, and S. Singh, "Cost of energy assessment methodology for offshore AC and DC wind power plants," *2012 13th Int. Conf. Optim. Electr. Electron. Equip.*, pp. 919–928, May 2012.

[2]   K. Hart, A. McDonald, H. Polinder, E. Corr, and J. Carroll, "Improved cost of energy comparison of permanent magnet generators for large offshore wind turbines," *EWEA Conf. Proc.*, 2014.

[3]   S. Tegen, E. Lantz, M. Hand, B. Maples, A. Smith, and P. Schwabe, "2011 Cost of Wind Energy Review," 2013.

[4]   H. Polinder *et al.*, "Trends in Wind Turbine Generator Systems," vol. 1, no. 3, pp. 174–185, 2013.

[5]   H. Polinder, F. F. A. Van Der Pijl, G. J. De Vilder, and P. J. Tavner, "Comparison of direct-drive and geared generator concepts for wind turbines," *IEEE Trans. Energy Convers.*, vol. 21, no. 3, pp. 725–733, 2006.

[6]   Z. Wu, S. Member, W. Gao, S. Member, D. Yang, and Y. Shi,

"Comprehensive Modeling and Analysis of Permanent Magnet Synchronous Generator- Wind Turbine System with Enhanced Low Voltage Ride Through Capability," pp. 2091–2098, 2012.

[7]   H. Li and Z. Chen, "Design Optimization and Comparison of Large Direct-drive Permanent Magnet Wind Generator Systems," 2007.

[8]   J. Carroll, "Cost of energy modelling and reduction opportunities for offshore wind turbines," PhD Thesis, 2016.

[9]   H. Polinder, "Optimization of Multibrid Permanent-Magnet Wind Generator Systems," *IEEE Trans. Energy Convers.*, vol. 24, no. 1, pp. 82–92, Mar. 2009.

Appendix

Tables discussed in Chapter 6 are presented here.

Optimisation output	NdFeB price set at μ+σ							
	PMG DD from Chapter 4	PMG DD with optimisation	PMG 1G from Chapter 4	PMG 1G with optimisation	PMG 2G from Chapter 4	PMG 2G with optimisation	PMG 3G from Chapter 4	PMG 3G with optimisation
Cost of energy (€/MWh)	112.53	112.12	114.83	114.37	118.28	117.91	119.14	118.96
Initial capital cost (M€)	18.65	18.55	19.62	18.64	19.33	18.60	19.17	18.48
Annual energy production (GWh)	19.50	19.47	20.50	19.58	0.13	19.32	0.14	19.18
Annual operations and maintenance (k€)	35.22	35.13	81.84	80.91	126.82	124.39	142.75	141.50
Total wind turbine cost (M€)	6.15	6.12	6.19	6.15	6.16	6.14	6.10	6.10
Gear ratio	1	1	5	5.00	16.22	15.13	84.77	82.13
Gearbox cost (k€)	-	-	396.73	395.58	463.57	447.16	466.95	469.45
Generator copper mass (kg)	7,992	7,887	2,458	2,258	1,243	1,209	383	386
Generator magnet mass (kg)	2,440	2,031	1,011	771	512	529	268	203
Generator electrical steel mass (kg)	30,375	30,018	8,394	7,106	3,981	3,763	1,386	1,372
Independent design variables								
Air gap radius (m)	4.04	4.00	2.61	2.70	1.19	1.23	0.43	0.42
Stack length (m)	1.61	1.59	0.83	0.64	0.72	0.69	0.79	0.78
Number of pole pairs	183	187	86	88	27	33	10	10
Magnet height (mm)	12.36	10.50	17.10	16.43	25.40	26.95	28.80	22.07
Magnet width to pole pitch ratio	1.00	1.00	0.90	0.90	0.78	0.76	0.90	0.92
Air Gap (mm)	6.47	5.20	2.26	4.97	2.26	2.00	0.94	1.29
Height of slot (m)	0.07	0.07	0.06	0.06	0.06	0.06	0.06	0.06
Ratio of slot width to pitch	0.55	0.55	0.53	0.56	0.53	0.55	0.50	0.51
Sun pitch diameter (mm)				1029	1046	1021	1093	1036
1st stage number of sun teeth				44	35	41	46	43
1st stage number of ring teeth				176	106	127	140	143
1st stage number of planet teeth				61	33	40	43	46
1st stage facewidth (mm)				619	787	817	727	741
2nd stage sun pitch diameter (mm)					673	709	702	721
2nd stage number of sun teeth					38	39	37	42
2nd stage number of ring teeth					115	105	139	132
2nd stage number of planet teeth					37	31	47	43
2nd stage facewidth (mm)					510	465	381	373
3rd stage gear pitch diameter (mm)					-	-	1473	1521
3rd stage number of gear teeth					-	-	119	110
3rd stage number of pinion teeth					-	-	27	24
3rd stage facewidth (mm)					-	-	392	387

Table A.1 Comparison between the designs of Chapter 4 with magnet prices set at mean + 1 standard deviation and the re-optimised designs based on magnet prices set at mean + 1 standard deviation.

Optimisation output	Copper price set at μ+σ							
	PMG DD from Chapter 4	PMG DD with optimisation	PMG 1G from Chapter 4	PMG 1G with optimisation	PMG 2G from Chapter 4	PMG 2G with optimisation	PMG 3G from Chapter 4	PMG 3G with optimisation
Cost of energy (€/MWh)	110.19	110.16	113.84	113.59	117.77	117.57	118.86	118.77
Initial capital cost (M€)	18.25	18.23	19.62	18.57	19.33	18.57	19.17	18.45
Annual energy production (GWh)	19.50	19.48	20.68	19.64	0.13	19.34	0.14	19.17
Annual operations and maintenance (k€)	34.96	34.93	81.75	81.01	126.77	123.45	142.73	141.09
Total wind turbine cost (M€)	6.02	6.02	6.13	6.13	6.13	6.13	6.09	6.09
Gear ratio	1	1	5	5.00	16.22	16.33	84.77	85.25
Gearbox cost (k€)	-	-	396.73	396.08	463.57	459.52	466.95	471.88
Generator copper mass (kg)	7,992	7,614	2,458	2,301	1,243	1,209	383	311
Generator magnet mass (kg)	2,440	2,268	1,011	962	512	560	268	201
Generator electrical steel mass (kg)	30,375	29,093	8,394	7,183	3,981	4,213	1,386	1,314
Independent design variables								
Air gap radius (m)	4.04	4.03	2.61	2.62	1.19	1.24	0.43	0.45
Stack length (m)	1.61	1.60	0.83	0.63	0.72	0.72	0.79	0.71
Number of pole pairs	183	189	86	86	27	33	10	14
Magnet height (mm)	12.36	11.58	17.10	19.77	25.40	28.53	28.80	21.16
Magnet width to pole pitch ratio	1.00	1.00	0.90	0.98	0.78	0.73	0.90	0.99
Air Gap (mm)	6.47	5.75	2.26	4.61	2.26	2.54	0.94	0.89
Height of slot (m)	0.07	0.06	0.06	0.06	0.06	0.07	0.06	0.05
Ratio of slot width to pitch	0.55	0.55	0.53	0.56	0.53	0.51	0.50	0.46
Sun pitch diameter (mm)	-	-		970	1046	1099	1093	1061
1st stage number of sun teeth	-	-		44	35	36	46	41
1st stage number of ring teeth	-	-		176	106	110	140	129
1st stage number of planet teeth	-	-		61	33	34	43	41
1st stage facewidth (mm)	-	-		698	787	709	727	737
2nd stage sun pitch diameter (mm)	-	-		-	673	728	702	729
2nd stage number of sun teeth	-	-		-	38	38	37	38
2nd stage number of ring teeth	-	-		-	115	115	139	125
2nd stage number of planet teeth	-	-		-	37	38	47	40
2nd stage facewidth (mm)	-	-		-	510	424	381	380
3rd stage gear pitch diameter (mm)	-	-		-	-	-	1473	1599
3rd stage number of gear teeth	-	-		-	-	-	119	139
3rd stage number of pinion teeth	-	-		-	-	-	27	29
3rd stage facewidth (mm)	-	-		-	-	-	392	379

Table A.2 Comparison between the designs of Chapter 4 with copper prices set at mean + 1 standard deviation and the re-optimised designs based on copper prices set at mean + 1 standard deviation.

	Steel price set at μ+σ							
Optimisation output	PMG DD from Chapter 4	PMG DD with optimisation	PMG 1G from Chapter 4	PMG 1G with optimisation	PMG 2G from Chapter 4	PMG 2G with optimisation	PMG 3G from Chapter 4	PMG 3G with optimisation
Cost of energy (€/MWh)	110.16	110.14	113.95	113.87	117.89	117.55	119.00	118.63
Initial capital cost (M€)	18.25	18.23	19.62	18.57	19.33	18.56	19.17	18.47
Annual energy production (GWh)	19.50	19.49	20.66	19.60	0.13	19.35	0.14	19.21
Annual operations and maintenance (k€)	34.95	34.93	82.16	81.63	127.34	125.26	143.43	139.39
Total wind turbine cost (M€)	6.02	6.02	6.14	6.13	6.13	6.12	6.09	6.10
Gear ratio	1	1	5	5.00	16.22	15.03	84.77	80.44
Gearbox cost (k€)	-	-	401.92	402.82	468.47	451.71	472.08	470.11
Generator copper mass (kg)	7,992	7,789	2,458	2,153	1,243	1,466	383	505
Generator magnet mass (kg)	2,440	2,267	1,011	847	512	587	268	294
Generator electrical steel mass (kg)	30,375	29,655	8,394	6,872	3,981	4,524	1,386	1,735
Independent design variables								
Air gap radius (m)	4.04	4.02	2.61	2.72	1.19	1.20	0.43	0.44
Stack length (m)	1.61	1.60	0.83	0.61	0.72	0.74	0.79	0.84
Number of pole pairs	183	184	86	89	27	33	10	11
Magnet height (mm)	12.36	11.61	17.10	18.65	25.40	28.46	28.80	30.80
Magnet width to pole pitch ratio	1.00	1.00	0.90	0.90	0.78	0.77	0.90	0.85
Air Gap (mm)	6.47	5.84	2.26	4.04	2.26	2.03	0.94	0.98
Height of slot (m)	0.07	0.07	0.06	0.06	0.06	0.07	0.06	0.06
Ratio of slot width to pitch	0.55	0.55	0.53	0.55	0.53	0.56	0.50	0.53
Sun pitch diameter (mm)	-	-		1043	1046	1044	1093	1145
1st stage number of sun teeth				44	35	39	46	49
1st stage number of ring teeth				176	106	118	140	153
1st stage number of planet teeth				61	33	36	43	49
1st stage facewidth (mm)				606	787	795	727	646
2nd stage sun pitch diameter (mm)					673	694	702	669
2nd stage number of sun teeth					38	45	37	36
2nd stage number of ring teeth					115	123	139	113
2nd stage number of planet teeth					37	36	47	36
2nd stage facewidth (mm)					510	541	381	472
3rd stage gear pitch diameter (mm)					-	-	1473	1587
3rd stage number of gear teeth					-	-	119	132
3rd stage number of pinion teeth					-	-	27	28
3rd stage facewidth (mm)					-	-	392	391

Table A.3 Comparison between the designs of Chapter 4 with steel prices set at mean + 1 standard deviation and the re-optimised designs based on steel prices set at mean + 1 standard deviation.

Optimisation output	PMG DD from Chapter 4	PMG DD with optimisation	PMG 1G from Chapter 4	PMG 1G with optimisation	PMG 2G from Chapter 4	PMG 2G with optimisation	PMG 3G from Chapter 4	PMG 3G with optimisation
Cost of energy (€/MWh)	112.92	112.79	115.06	114.99	118.46	117.80	119.30	118.93
Initial capital cost (M€)	18.71	19.42	19.62	19.63	19.33	19.39	19.17	19.21
Annual energy production (GWh)	19.50	20.25	20.47	0.08	0.13	0.13	0.14	0.14
Annual operations and maintenance (k€)	35.27	35.12	82.26	82.17	127.38	128.00	143.45	138.85
Total wind turbine cost (M€)	6.17	6.14	6.20	6.20	6.16	6.14	6.11	6.12
Gear ratio	1	1	5	5.00	16.22	15.85	84.77	80.81
Gearbox cost (k€)	-	-	401.92	404.40	468.47	458.04	472.08	473.11
Generator copper mass (kg)	7,992	7,999	2,458	2,366	1,243	1,629	383	582
Generator magnet mass (kg)	2,440	2,260	1,011	926	512	376	268	258
Generator electrical steel mass (kg)	30,375	30,247	8,394	9,891	3,981	4,730	1,386	1,865
Independent design variables								
Air gap radius (m)	4.04	3.94	2.61	2.61	1.19	1.43	0.43	0.45
Stack length (m)	1.61	1.57	0.83	0.78	0.72	0.61	0.79	0.83
Number of pole pairs	183	178	86	87	27	39	10	9
Magnet height (mm)	12.36	12.04	17.10	16.06	25.40	16.33	28.80	28.15
Magnet width to pole pitch ratio	1.00	1.00	0.90	0.93	0.78	0.87	0.90	0.81
Air Gap (mm)	6.47	6.31	2.26	4.92	2.26	3.53	0.94	1.08
Height of slot (m)	0.07	0.07	0.06	0.06	0.06	0.08	0.06	0.07
Ratio of slot width to pitch	0.55	0.55	0.53	0.47	0.53	0.56	0.50	0.53
Sun pitch diameter (mm)	-	-		958	1046	1083	1093	1137
1st stage number of sun teeth	-	-		44	35	40	46	43
1st stage number of ring teeth	-	-		176	106	123	140	138
1st stage number of planet teeth	-	-		61	33	38	43	44
1st stage facewidth (mm)	-	-		721	787	726	727	638
2nd stage sun pitch diameter (mm)	-	-			673	655	702	675
2nd stage number of sun teeth	-	-			38	36	37	37
2nd stage number of ring teeth	-	-			115	104	139	124
2nd stage number of planet teeth	-	-			37	34	47	40
2nd stage facewidth (mm)	-	-			510	518	381	418
3rd stage gear pitch diameter (mm)	-	-			-	-	1473	1520
3rd stage number of gear teeth	-	-			-	-	119	150
3rd stage number of pinion teeth	-	-			-	-	27	34
3rd stage facewidth (mm)	-	-			-	-	392	366

Table A.4 Comparison between the designs of Chapter 4 with material prices set at mean + 1 standard deviation and the re-optimised designs based on material prices set at mean + 1 standard deviation.

Optimisation output	PMG DD from Chapter 4	PMG DD with optimisation	PMG 1G from Chapter 4	PMG 1G with optimisation	PMG 2G from Chapter 4	PMG 2G with optimisation	PMG 3G from Chapter 4	PMG 3G with optimisation
Cost of energy (€/MWh)	115.85	115.20	116.33	115.92	119.17	118.60	119.73	119.58
Initial capital cost (M€)	19.20	19.42	19.62	19.56	19.33	19.36	19.17	19.18
Annual energy production (GWh)	19.50	19.83	20.25	0.08	0.13	0.13	0.14	0.14
Annual operations and maintenance (k€)	35.60	35.27	82.76	82.70	127.96	126.68	144.13	140.08
Total wind turbine cost (M€)	6.34	6.27	6.27	6.23	6.20	6.18	6.13	6.14
Gear ratio	1	1	5	5.05	16.22	16.91	84.77	84.36
Gearbox cost (k€)	-	-	406.76	409.02	473.04	458.08	476.86	487.09
Generator copper mass (kg)	7,992	7,414	2,458	2,711	1,243	1,489	383	509
Generator magnet mass (kg)	2,440	2,082	1,011	732	512	464	268	214
Generator electrical steel mass (kg)	30,375	27,985	8,394	9,318	3,981	4,279	1,386	1,733
Independent design variables								
Air gap radius (m)	4.04	3.80	2.61	2.76	1.19	1.19	0.43	0.48
Stack length (m)	1.61	1.51	0.83	0.70	0.72	0.77	0.79	0.72
Number of pole pairs	183	172	86	87	27	30	10	12
Magnet height (mm)	12.36	12.01	17.10	15.49	25.40	21.87	28.80	25.38
Magnet width to pole pitch ratio	1.00	0.99	0.90	0.80	0.78	0.77	0.90	0.80
Air Gap (mm)	6.47	4.92	2.26	5.27	2.26	3.23	0.94	1.14
Height of slot (m)	0.07	0.07	0.06	0.07	0.06	0.07	0.06	0.07
Ratio of slot width to pitch	0.55	0.55	0.53	0.52	0.53	0.59	0.50	0.52
Sun pitch diameter (mm)	-	-		990	1046	1107	1093	1143
1st stage number of sun teeth				44	35	41	46	38
1st stage number of ring teeth				178	106	125	140	123
1st stage number of planet teeth				62	33	39	43	39
1st stage facewidth (mm)				661	787	700	727	624
2nd stage sun pitch diameter (mm)					673	583	702	719
2nd stage number of sun teeth					38	34	37	42
2nd stage number of ring teeth					115	108	139	130
2nd stage number of planet teeth					37	34	47	42
2nd stage facewidth (mm)					510	629	381	393
3rd stage gear pitch diameter (mm)					-	-	1473	1619
3rd stage number of gear teeth					-	-	119	141
3rd stage number of pinion teeth					-	-	27	29
3rd stage facewidth (mm)					-	-	392	391

Table A.5 Comparison between the design of Chapter 4 with material prices set at mean + 2 standard deviations and the re-optimised design based on material prices set at mean + 2 standard deviations.